

**POLYANILINE BASED METAL-ORGANIC FRAMEWORK  
COMPOSITES FOR HYDROGEN FUEL CELL**

**MSc (Chemistry)**

**K.E RAMOHLOLA**

**2017**

**POLYANILINE BASED METAL-ORGANIC FRAMEWORK COMPOSITES FOR  
HYDROGEN FUEL CELL**

By

KABELO EDMOND RAMOHLOLA

DISSERTATION

Submitted in fulfilment of the requirements for the degree of

MASTER OF SCIENCE

In

CHEMISTRY

In the

FACULTY OF SCIENCE AND AGRICULTURE

(School of Physical and Mineral Sciences)

At the

UNIVERSITY OF LIMPOPO

SUPERVISOR: DR K.D. MODIBANE

CO-SUPERVISORS: DR M.J. HATO

DR K.M. MOLAPO (UWC)

PROF. E.I. IWUOHA (UWC)

2017

## DEDICATION

---

TO MY PRECIOUS FAMILY

*Lucy, Prince, Thabo, Hlompho, Motshwana and Mathata Ramohlola*

## DECLARATION BY CANDIDATE

---

I declare that POLYANILINE BASED METAL ORGANIC FRAMEWORK COMPOSITES FOR HYDROGEN FUEL CELL is my own work and that all the sources that I have used or quoted have been indicated and acknowledged by means of complete references and that this work has not been submitted before for any other degree at any other institution.

.....  
Full Names

.....  
Date

## ACKNOWLEDGEMENTS

---

First of all, I would like to express my great Thanks and sincerest gratitude and appreciations to my Supervisor Dr K.D Modibane for his tremendous support and guidance throughout my postgraduate studies (Honours and Masters). Dr Modibane has given me a huge assistance in the designing of the research project and equipping me with problem solving skills and also being innovative, thinking beyond the scope. I really appreciate your precious time and valuable advices throughout the studies. I thank him not only providing me with lab facilities, but also for his extraordinary patience and consistent encouragements.

To my co-supervisors, thanks for helping, being there, offering both academically and social support throughout my studies. To Dr. Mpitloane Joseph Hato, you were with me during my initial postgraduate studies and you are still here assisting me day in and out. Your outstanding personality and wisdom has generated so big influence on me that it will be greatly beneficial to me for the future life. Thanks a lot to you. To Dr. Kerileng Molapo, thanks for helping us in understanding the electrochemistry part of this work and also for enriching the electrochemical knowledge to us. Massive Thanks to Prof. Iwouha for opening your SensorLab for us.

To my research mate Mr. Mdluli Siyabonga, thanks for your input in this study brother. Words cannot express how thankfully I am to you. May God Bless You and help you during you studies also man.

To University of Limpopo Nanotechnology Group, thanks for the enthusiasm and support you gave me. To Mr Monama Release, thanks a lot for helping me, encouraging me and standing by me always. You are indeed a great leader and a Good Brother to me, both academically and personally. Thanks to Daphney Makhafola, Thabiso Maponya, Thabo Pesha, Khuthadzo Mulaudzi, Thabang Somo, Gloria Mashao, Khutso Lekota, Bokome Shaku and Joseph Moropane for making lab a greatest place to be.

To University of Western Cape SensorLab students and staff led by Prof. Iwuoha and Prof. Baker, Thanks for opening your hands and welcomed me during my analysis

stay in your labs. You are the best and Thanks for making my time in UWC be memorable. Special gratitude to Dr M. Masikini for your guidance and mentorship role during my stay in UWC.

Special Thanks to the University of Limpopo, Department of Chemistry under the leadership of Dr. M.S Thomas (HOD) for giving me opportunity to study towards my postgraduate studies. The contribution done by various Department Staff members and postgraduate students which I could not name individually is much appreciated and Thanks for the support.

I would also like to thank the following people and institutions for offering with their characterisation instruments, without them it was going to be very difficult for this work to be completed successfully:

- ✓ University of Limpopo, School of Physical and Mineral Sciences, Geology Division for XRD analysis.
- ✓ Mr. Adrian Josephs and Ms. Natasha Peterson of University of the Western Cape Electron Microscopy Unit (EMU) for SEM and TEM analysis.
- ✓ Dr Waryo of University of Western Cape for supplying me with all necessity for electrochemical analysis.
- ✓ Mr Hillary Tanui of University of the Western Cape for sample preparation and helping me in running FTIR.
- ✓ Mr Yunus Kippie from School of Pharmacy of the University of the Western Cape for TGA analysis.

Special gratitude to Sasol Inzalo foundation and National Research Foundation of South Africa for Financial Assistance. Thanks a lot for settling all my fees, stipend as well as conferences expenses.

Without the support and encouragement of my family, I would not be where I am. Thanks to my single Mom for all the support. Indeed ***Bagologolo ba boletše ba re: 'Mosadi o tshwara thipa ka bogaleng'***. Thanks for continuous support and I REALLY LOVE YOU A LOT. To my uncle Mathata, Brothers Prince, Thabo and Hlompho and also my granny, Motshwana, Thanks for being there in difficult times and supplying a way out.

To all my friends who I cannot name individually, Thanks for always being there when I need you most. You made my stay in this world fun and continuous courage you give me to study is much appreciated.

Last but not least I would like to pass my sincere thanks to my good, precious friend of mine, Tebele Hanna for being there for me always. Thanks for constant support, unconditional love, understanding and encouragement.

Lastly I would like to thank God for life he enriched in me.

## ABSTRACT

---

In order to meet the great demand of energy supply globally, there must be a transition from dependency on fossil fuel as a primary energy source to renewable source. This can be attained by use of hydrogen gas as an energy carrier. In the context of hydrogen fuel cell economy, an effective hydrogen generation is of crucial significant. Hydrogen gas can be produced from different methods such as steam reforming of fossil fuels which emit greenhouse gases during production and from readily available and renewable resources in the process of water electrolysis. Hydrogen generated from water splitting using solar energy (photocatalysis) or electric energy (electrocatalysis) has attracted most researchers recently due to clean hydrogen (without emission of greenhouse gases) attained during hydrogen production. In comparison with photocatalytic water splitting directly using solar energy, which is ideal but the relevant technologies are not yet commercialized, electrolysis of water using catalyst is more practical at the current stage. The platinum group noble metals (PGMs) are the most effecting electrocatalysts for hydrogen evolution reactions (HER) but their scarcity and high cost limit their application. In this study, we presented the noble metal free organic-inorganic hybrid composites and their HER electrocatalysis performances were investigated. Polyaniline-metal organic framework (PANI/MOF) composite was prepared by chemical oxidation of aniline monomer in the presence of MOF content for hydrogen production. The properties of PANI, MOF and PANI/MOF composite were characterised for their structure and properties by X-ray diffraction (XRD), field-emission scanning electron microscopy (SEM), Fourier transform infrared (FTIR), thermogravimetric analysis (TGA), Raman, transmission electron microscopy (TEM), ultraviolet-visible spectroscopy (UV-vis), atomic absorption spectroscopy (AAS), square wave (SWV) and cyclic voltammetry (CV). There was a clear interaction of MOF on the backbone of the PANI matrix through electrostatic interaction as investigated by both Raman and FTIR. The MOF exhibited irregular crystals with further wrapping of MOF by PANI matrix as evidenced by both SEM and TEM analyses. The PANI composite exhibited some nanorods and microporous structure.



The determined energy band gap of the composite was in good agreement with previously reported catalysts for hydrogen evolution reaction (HER). The thermal stability of PANI increased upon addition of MOF. Experiments probing the electrochemical, HER and photophysical properties revealed that the composite was very stable and robust with significant improvement in properties. The resulting composite is a promising low-cost and environmentally friendly hydrogen production material. In this work we also reported about novel poly (3-aminobenzoic acid)-metal organic framework referred as PABA/MOF composite. Spectroscopic characterisations (UV-vis and FTIR) with support of XRD and TGA revealed a successful interaction between PABA and MOF. Morphological characterisation established that PABA is wrapping MOF and the amorphous nature of the materials were not affected. The catalytic effect of PABA and PABA/MOF composites on HER was studied using exchange current density and charge transfer coefficient determined by the Tafel slope method. A drastic increase in catalytic H<sub>2</sub> evolution was observed in PABA and composite. Moreover, they merely require overpotentials as low as  $\sim -0.405$  V to attain current densities of  $\sim 0.8$  and  $1.5 \text{ Am}^{-2}$  and show good long-term stability. We further demonstrated in the work the electrocatalytic hydrogen evolution reaction of MOF decorated with PABA. These novel MOF/PABA composites with different PABA loading were synthesised via in situ solvothermal synthesis of MOF in the presence of PABA. It was deduced that PABA with different loading amount have an influence on the morphologies, optical properties and thermal stabilities of MOF. Interestingly, the MOF/PABA composites exhibited the great significant on the HER performance and this is potentially useful in HER application for hydrogen fuel cell.

## RESEARCH OUTPUT FROM THE STUDY

---

### BOOK CHAPTER

1. **Kabelo E. Ramohlola**, Milua Masikini, Siyabonga B. Mdluli, Gobeng R. Monama, Mpitloane J. Hato\*, Kerileng M. Molapo, Emmanuel I. Iwuoha, Kwena D. Modibane\* “Electrocatalytic Hydrogen Production Properties of Polyaniline doped with Metal Organic Frameworks, Organic synthesis and carbon related materials: polymers, carbon nanocomposites, graphene” Book Chapter, *Springer* (**Accepted 13/03/2017**) (see Appendices 1(a) and (b)).

### PUBLICATIONS

1. **Kabelo Edmond Ramohlola**, Gobeng Release Monama, Kwena Desmond Modibane, Milua Masikini, Kerileng Mildred Molapo, Siyabonga Beizel Mdluli, Emmanuel Iwuoha, Mpitloane Joseph Hato, Polyaniline-metal organic framework nanocomposite as an efficient electrocatalyst for hydrogen evolution reaction, Revised Manuscript Submitted in *Composite Part B* (**Under Review**) (see Appendix 2 (a) and (b)).

2. **Kabelo E. Ramohlola**, Milua Masikini, Siyabonga B. Mdluli, Gobeng R. Monama, Mpitloane J. Hato, Kerileng M. Molapo, Emmanuel I. Iwuoha, Kwena D. Modibane, Electrocatalytic Hydrogen Production Properties of Poly(3-aminobenzoic acid) doped with Metal Organic Frameworks, *International Journal of Electrochemical Science* **12** (**2017**) 4392-4405 (see Appendix 3)

3. **Kabelo E. Ramohlola**, Milua Masikini, Siyabonga B. Mdluli, Gobeng R. Monama, Mpitloane J. Hato, Kerileng M. Molapo, Emmanuel I. Iwuoha, Kwena D. Modibane, Electrocatalytic Hydrogen Production Properties of Metal Organic Frameworks decorated with poly (3-aminobenzoic acid), Revised Manuscript Submitted in *Electrochimica Acta* (**Under Review**) (see Appendices 4 (a) and (b)).

## PRESENTATIONS

1. **Ramohlola K.E**, Mdluli S.B, Modibane K.D, Iwuoha I.E and Molapo K.M. Synthesis and Characterisations of Organometallic Composites for Catalytic Hydrogen Production. Faculty of Science and Agriculture Research Day, Bolivia Lodge, Polokwane, South Africa on the 1-2<sup>nd</sup> October 2015.
2. **Ramohlola K.E**, Mdluli S.B, Modibane K.D, Iwuoha I.E and Molapo K.M. Synthesis and Characterisations of Organometallic Composites for Catalytic Hydrogen Production. South African Chemical Institute (SACI) Northern Region Symposium, University of Venda, Thohoyandou, South Africa on the 20<sup>th</sup> November 2015.
3. **Ramohlola K.E**, Mdluli S.B, Modibane K.D, Iwuoha I.E and Molapo K.M. Synthesis and Characterisations of Organometallic Composites for Catalytic Hydrogen Production. SACI Young Chemist Symposium, University of South Africa, Florida, Roodepoort, South Africa on the 27<sup>th</sup> November 2015.
4. **Kabelo E. Ramohlola**, Milua Masikini, Mpitloane J. Hato, Kerileng M. Molapo, Emmanuel I. Iwuoha, Kwena D. Modibane. Electrocatalytic Hydrogen Production Properties of Poly(3-aminobenzoic acid)- doped With Metal Organic Frameworks. Faculty of Science and Agriculture Research Day, Bolivia Lodge, Polokwane, South Africa on the 24-25<sup>th</sup> October 2016.

## TABLE OF CONTENTS

---

DEDICATION .....	ii
DECLARATION BY CANDIDATE .....	iii
ACKNOWLEDGEMENTS .....	vi
ABSTRACT .....	ix
RESEARCH OUTPUT FROM THE STUDY .....	xi
BOOK CHAPTER .....	xi
PUBLICATIONS .....	xi
PRESENTATIONS .....	xii
TABLE OF CONTENTS .....	xiii
LIST OF FIGURES .....	xx
LIST OF SCHEMES .....	xxiv
LIST OF TABLES .....	xxv
LIST OF ABBREVIATIONS .....	xxvi
LIST OF SYMBOLS .....	xxviii
CHAPTER ONE .....	1
INTRODUCTION .....	1
1.1. BACKGROUND .....	1
1.2. PROBLEM STATEMENT .....	2
1.3. RATIONALE AND MOTIVATION .....	3
1.4. RESEARCH AIM AND OBJECTIVES .....	4
1.4.1. Research Aim .....	4
1.4.2. Objectives .....	4

1.5. DISSERTATION OUTLINE .....	5
1.6. REFERENCES.....	6
CHAPTER TWO.....	8
LITERATURE REVIEW .....	8
2.1. HYDROGEN TECHNOLOGY .....	8
2.1.1. Background of Hydrogen Technology .....	8
2.1.2. Hydrogen Production .....	9
2.1.2.1. Steam reforming of natural gases.....	9
2.1.2.2. Photoelectrochemical water splitting for hydrogen production.....	10
2.1.2.3. Other methods for hydrogen production .....	11
2.1.2.3.1. Biomass .....	11
2.1.2.3.2. Partial oxidation.....	12
2.1.3. Hydrogen Storage .....	12
2.1.3.1. Gaseous hydrogen storage .....	13
2.1.3.2. Liquid hydrogen storage .....	13
2.1.3.3. Solid hydrogen storage.....	14
2.2. HYDROGEN EVOLUTION REACTIONS (HER).....	14
2.2.1. Fundamentals and Mechanisms of HER .....	14
2.3. ELECTROCATALYSIS .....	16
2.3.1. The Concept of Catalysis .....	16
2.3.2. The Principle of Electrocatalysis .....	17
2.3.3. HER Electrocatalyst .....	18
2.4. POLYMERS.....	20
2.4.1. Background on Polymers .....	20
2.4.2. Conductive Polymers .....	21

2.5. POLYANILINE .....	23
2.5.1. History and Background of Polyaniline.....	23
2.5.2. Structure of Polyaniline .....	24
2.5.3. Synthesis of Polyaniline .....	27
2.5.3.1. Electrochemical polymerisation .....	27
2.5.3.2. Chemical polymerisation.....	27
2.5.4. Mechanism of Polymerisation .....	28
2.5.5. Modification of Polyaniline.....	30
2.5.6. Polyaniline Composites.....	31
2.6. METAL ORGANIC FRAMEWORKS .....	32
2.6.1. Background of Metal Organic Frameworks .....	32
2.6.2. Structure of a Metal Organic Framework.....	35
2.6.2.1. Metal ions/clusters .....	35
2.6.2.2. Organic linker .....	36
2.6.3. Design and Synthesis of Metal Organic Frameworks.....	39
2.6.3.1. Hydro/solvothermal method.....	39
2.6.3.2. Microwave assisted method .....	40
2.6.3.3. Microemulsion and reverse-phase microemulsion method.....	41
2.6.3.4. Electrochemical synthesis of MOF .....	43
2.6.3.5. Mechanochemical synthesis of MOF .....	44
2.7. ANALYTICAL TECHNIQUES .....	45
2.7.1. Spectroscopy .....	45
2.7.1.1. Ultraviolet-visible spectroscopy .....	45
2.7.1.2. Fourier transform infrared spectroscopy .....	48
2.7.1.3. Raman spectroscopy .....	49

2.7.1.4. Flame atomic absorption spectroscopy .....	49
2.7.2. Microscopy .....	51
2.7.2.1. Scanning electron microscopy .....	51
2.7.2.2. Transmission electron microscopy .....	52
2.7.3. Physical Methods .....	53
2.7.3.1. X-ray diffraction .....	53
2.7.3.2. Thermogravimetric analysis .....	54
2.7.4. Electroanalytical Methods .....	54
2.7.4.1. Cyclic voltammetry .....	55
2.7.4.2. Square wave voltammetry .....	56
2.8. CONCLUSIONS .....	57
2.9. REFERENCES .....	58
CHAPTER THREE .....	78
ABSTRACT .....	78
3.1. INTRODUCTION .....	80
3.2. EXPERIMENTAL SECTION .....	82
3.2.1. Materials .....	82
3.2.2. Synthesis of MOF, PANI and PANI/MOF composite .....	82
3.2.3. Materials characterisations .....	83
3.3. RESULTS AND DISCUSSION .....	84
3.3.1. Synthesis .....	84
3.3.2. Spectroscopic Characterisations .....	85
3.3.2.1. Fourier transform infrared (FTIR) and Raman spectroscopy .....	85
3.3.2.2. Ultraviolet-visible spectroscopy (UV-vis) .....	86
3.3.2.3. X-ray diffraction .....	88

3.3.3. Morphological Characterisations .....	89
3.3.4. Thermogravimetric analysis .....	93
3.3.5. Electrochemical Characterisations .....	95
3.3.6. Hydrogen Studies.....	98
3.4. CONCLUSIONS .....	105
3.5. REFERENCES .....	106
CHAPTER FOUR.....	113
ELECTROCATALYTIC HYDROGEN PRODUCTION PROPERTIES OF POLY(3-AMINOBENZOIC ACID) DOPED WITH METAL ORGANIC FRAMEWORKS .....	113
ABSTRACT .....	113
4.1. INTRODUCTION .....	115
4.2. EXPERIMENTAL SECTION .....	116
4.2.1. Materials.....	116
4.2.2. Synthesis of PABA, MOF and PABA/MOF Composite.....	116
4.2.3. Characterisation Techniques.....	117
4.3. RESULTS AND DISCUSSION .....	118
4.3.1. Synthesis.....	118
4.3.2. Spectroscopic Characterisations.....	119
4.3.3. Morphological Characterisations .....	121
4.3.4. Electrochemical Characterisations .....	124
4.3.5. Hydrogen Evolution Reaction.....	127
4.4. CONCLUSIONS .....	131
4.5. REFERENCES .....	133



CHAPTER FIVE .....	138
ELECTROCATALYTIC HYDROGEN EVOLUTION REACTION OF METAL ORGANIC FRAMEWORKS DECORATED WITH POLY (3-AMINO BENZOIC ACID) .....	138
ABSTRACT .....	138
5.1. INTRODUCTION .....	140
5.2. EXPERIMENTAL SECTION .....	141
5.2.1. Materials.....	141
5.2.2. Synthesis of PABA, MOF and MOF/PABA composite .....	141
5.2.3. Material Characterisations.....	142
5.3. RESULTS AND DISCUSSION .....	142
5.3.1. Spectroscopic Characterisations .....	142
5.3.2. Morphological Characterisations .....	145
5.3.3. Electrochemical Characterisations .....	148
5.3.4. Hydrogen Studies.....	150
5.4. CONCLUSIONS .....	154
5.5. REFERENCES .....	156
CHAPTER SIX: .....	161
GENERAL DISCUSSION, CONCLUSIONS AND RECOMMENDATIONS .....	161
6.1. GENERAL DISCUSSION AND CONCLUSIONS.....	161
6.2. RECOMMENDATIONS FOR FUTURE WORK .....	164
Appendix 1(a) .....	166
Appendix 1(b) .....	167
Appendix 2 (a) .....	168
Appendix 2 (b) .....	169

Appendix 3 .....	170
Appendix 4 (a) .....	171
Appendix 4 (b) .....	172

## LIST OF FIGURES

---

Figure 2.1: Energy diagram showing a reaction proceeding in the absence and presence of catalyst. ....	17
Figure 2.2: Trends in hydrogen evolution reaction activity. Experimental HER activity expressed as the exchange current density, $\log(i_0)$ , for different metal surfaces as a function of the calculated $^*H_{ad}$ chemisorption energy, $\Delta E_H$ . The result of a simple theoretical kinetic model is also shown as a dotted line. ....	20
Figure 2.3: Industrial applications of polyaniline. ....	24
Figure 2.4: The general structure of polyaniline, where $y = 1, 0.5$ and $0$ corresponding to fully reduced polyaniline (leucoemeraldine), the half oxidized polyaniline (emeraldine) and fully oxidized polyaniline (pernigraniline), respectively. ....	24
Figure 2.5: Structures of different forms of polyaniline. ....	25
Figure 2.6: Metal organic framework structure. ....	33
Figure 2.7: Year wise publication status from 2000 to 2015 of various aspects of MOFs (a) MOFs, (b) MOFs as luminescent materials, (c) MOFs for gas storage, (d) MOFs as magnets, (e) MOFs for drug delivery and (f) MOFs as catalyst [153]. ....	34
Figure 2.8: Coordination geometries of transition metal ions [153]. ....	36
Figure 2.9: Potential polytopic organic molecules (neutral, anionic and cationic) as linkers in MOFs. ....	38
Figure 2.10: Typical cyclic voltammogram showing the peak cathodic and anodic current respectively for a reversible reaction [209]. ....	56
Figure 3.1: (a) FTIR and (b) Raman spectra of MOF, PANI and PANI/MOF composite. ....	86
Figure 3.2: (a) Absorption spectra of MOF, PANI and the composite in DMSO as well as (b) absorption spectra of PANI/MOF composite measured at different concentrations. ....	87
Figure 3.3: Tauc plot of PANI and PANI/MOF composite for energy band gap determinations. ....	88
Figure 3.4: XRD patterns of MOF, PANI and PANI/MOF composite. ....	89

Figure 3.5: SEM images of (a) PANI, (c) MOF, (e) PANI/MOF composite and EDS spectra of (b) MOF, (d) PANI, (f) PANI/MOF composite. ....	91
Figure 3.6: TEM images (a) MOF (b) PANI (c) PANI/MOF composite and (d) EDX spectrum of PANI/MOF composite. Inset: SAED images of various samples. ....	93
Figure 3.7: TGA curves of MOF, PANI and PANI/MOF composite. ....	94
Figure 3.8: (a) CV and (b) SWV curves of MOF, PANI and PANI/MOF ( $\sim 3.0 \times 10^{-3}$ mol/L) in 0.1 M TBAP/DMSO electrolyte solution on Au electrode. ....	96
Figure 3.9: Voltammetric curves of (a) MOF (b) PANI (c) PANI/MOF composite ( $\sim 3.0 \times 10^{-3}$ mol/L) in 0.1 M TBAP/DMSO electrode system at different scan rate (0.02 – 0.10 $\text{Vs}^{-1}$ ) and (d) The log-log plot of the absolute value of the peak current vs scan rate of MOF, PANI and PANI/MOF composite. ....	97
Figure 3.10: Peak current as a function of square root of scan rate on Au in 0.1 M DMSO/TBAP electrode system at various scan rate (0.02 – 0.10 $\text{Vs}^{-1}$ ).....	98
Figure 3.11: (a) CV curves of PANI, MOF and PANI/MOF composite ( $\sim 2.0 \times 10^{-4}$ mol/L) at 0.10 $\text{Vs}^{-1}$ (b) CV curves of (b) MOF (c) PANI and (d) PANI/MOF composite in the presence 0.075 M $\text{H}_2\text{SO}_4$ at different scan rate on Au electrode in 0.1 M TBAP/DMSO electrode system. ....	100
Figure 3.12: CV curves of (a) MOF (b) PANI and (c) PANI/MOF composite ( $\sim 2.0 \times 10^{-4}$ mol/L) in the presence 0.033 to 0.45 M $\text{H}_2\text{SO}_4$ ; and (d) current as a function of $\text{H}_2\text{SO}_4$ concentration of the electrocatalyst in 0.1 M TBAP/DMSO electrolyte solution on gold electrode at 0.10 $\text{V} \cdot \text{s}^{-1}$ scan rate. Inset: Linear fitting at low concentration of composite. ....	101
Figure 3.13: Tafel plots of (a) blank, PANI, MOF and PANI/MOF composite ( $\sim 2.0 \times 10^{-4}$ mol/L) in the presence 0.075 M $\text{H}_2\text{SO}_4$ at 0.10 $\text{Vs}^{-1}$ (b) MOF (c) PANI and (d) PANI/MOF composite in different concentrations of $\text{H}_2\text{SO}_4$ and 0.10 $\text{Vs}^{-1}$ scan rate on Au electrode in 0.1 M TBAP/DMSO electrode system. ....	102
Figure 4.1: (a) FTIR, (b) UV-vis spectra of PABA, MOF and PABA/MOF in DMSO, (c) XRD and TGA analysis of MOF, PABA and PABA/MOF.....	120
Figure 4.2: SEM image of (a) MOF, (c) PABA, (e) PABA/MOF composite and EDS spectrum of (b) MOF, (d) PABA, (f) PABA/MOF composite.....	122

Figure 4.3: TEM images (a) MOF, (b) PABA, (c) PABA/MOF composite and (d) EDX spectrum of PABA/MOF composite. Inset: SAED image..... 123

Figure 4.4: (a) CV results of PABA and PABA/MOF at 0.1 Vs<sup>-1</sup>; (b) and (c) CV of PABA and PABA/MOF at different scan rates (0.02- 0.10 Vs<sup>-1</sup>); and (d) The log-log plot of the absolute value of the peak current vs scan rate for the PABA and PABA/MOF materials at 0.02 to 0.1 Vs<sup>-1</sup> in 0.1 M DMSO/TBAP electrolyte solution on gold electrode. ... 125

Figure 4.5: Peak current as a function of square root of scan rate on gold in 0.1 M DMSO/TBAP electrode system at different scan rate (0.02 – 0.10 Vs<sup>-1</sup>). ..... 126

Figure 4.6: (a) CV and (c) Tafel plots of PABA and PABA/MOF in the presence 0.15 M H<sub>2</sub>SO<sub>4</sub>; (b) CV and (d) Tafel plots of PABA/MOF at 0.10 Vs<sup>-1</sup> in the presence of different H<sub>2</sub>SO<sub>4</sub> concentration on gold electrode in 0.1 M DMSO/TBAP electrode system..... 127

Figure 5.1: (a) FTIR, (b) UV-vis spectra of MOF and MOF/PABA composites in DMSO, (c) XRD and (d) TGA analysis of MOF and MOF/PABA composites.....143

Figure 5.2: SEM image of (a) parent MOF, (c) MOF-3.6wt.-%-PABA (e) MOF-5wt.-%-PABA composites (inset : magnification on the crystal structure to view the surface of the crystal) and EDS spectrum of (b) MOF, (d) MOF-3.6wt.-%-PABA, (f) ) MOF-5wt.-%-PABA composites..... 146

Figure 5.3: TEM image of (a) parent MOF, (c) MOF-3.6wt.-%-PABA (e) MOF-5wt.-%-PABA composites (inset : SAED images) and EDX spectrum of (b) MOF, (d) MOF-3.6wt.-%-PABA, (f) ) MOF-5wt.-%-PABA composites..... 147

Figure 5.4: (a) CV results of blank, MOF and MOF-PABA at 0.1 Vs<sup>-1</sup>; (b) and (c) CV of MOF and MOF-3.6wt.-%-PABA and (d) MOF-5wt.-%-PABA at different scan rates (0.02- 0.10 Vs<sup>-1</sup>) in 0.1 M DMSO/TBAP electrolyte solution on gold electrode. .... 149

Figure 5.5: (a) The log-log plot of the absolute value of the peak current vs scan rate and (b) Peak current as a function of square root of scan rate for s<sup>-1</sup> for MOF, MOF-3.6wt.-%-PABA and MOF-5wt.-%-PABA composites in 0.1 M DMSO/TBAP electrode system at different scan rate (0.02 – 0.10 Vs<sup>-1</sup>)..... 150

Figure 5.6: (a) CV results of blank, MOF and MOF-PABA; and (b) MOF, (c) MOF-3.6wt.-%-PABA and (d) MOF-5wt.-%-PABA at 0.10 Vs<sup>-1</sup> in the presence of different H<sub>2</sub>SO<sub>4</sub> concentration on gold electrode in 0.1 M DMSO/TBAP electrode system. . 151

Figure 5.7: (a) Tafel plots of blank, MOF and MOF-PABA; and (b) MOF, (c) MOF-3.6wt%-PABA and (d) MOF-5wt%-PABA at  $0.10 \text{ Vs}^{-1}$  in the presence of different  $\text{H}_2\text{SO}_4$  concentration on gold electrode in 0.1 M DMSO/TBAP electrode system. . 152

## LIST OF SCHEMES

---

Scheme 2.1: Mechanisms of Hydrogen Evolution Reactions. ....	16
Scheme 2.2: Schematic diagram showing change in oxidation states of polyaniline upon doping. ....	26
Scheme 2.3: Oxidation of aniline monomer during polymerisation of aniline. ....	28
Scheme 2.4: Formation of a dimer. ....	29
Scheme 2.5: Formation of a trimer and polymer formation. ....	30
Scheme 2.6: Conventional solvothermal synthesis of MOF structures.....	40
Scheme 2.7: Microwave-assisted solvothermal synthesis of MOF structures .....	41
Scheme 2.8: General route to produce Gd MOF nanoparticles via a reverse microemulsion synthesis with a hydrotrope. Cetyltrimethylammonium bromide (CTAB) is employed as a surfactant and hexanol as a cosurfactant. Gadolinium(III) chloride and 1,4-benzenedicarboxylate (1,4-BDC) form the three-dimensional nanoscale metal organic framework.....	42
Scheme 2.9: Electrochemical synthesis of metal organic frameworks .....	43
Scheme 2.10: Mechanochemical synthesis of MOF structures.....	44
Scheme 2.11: Possible electronic transitions of $\pi$ , $\sigma$ , and n electrons. ....	46
Scheme 2.12: Basic components of FTIR.....	48
Scheme 2.13: Working principles and basic components of AA .....	50
Scheme 3.1: Schematic presentation of PANI/MOF composite through chemical oxidation polymerisation of aniline monomer in the presence of MOF.....	84
Scheme 4.1: Synthesis of poly(aminobenzoic acid) based MOF composites through oxidation polymerisation of aminobenzoic monomer in the presence of MOF material. ....	118

## LIST OF TABLES

---

Table 2.1: Table showing different intrinsically conducting polymers which have been studied mostly. ....	22
Table 3.1: Experimental values of Tafel slope, transfer coefficient $1-\alpha$ and exchange current $i_0$ , in the absence and presence of MOF, PANI and PANI/MOF composite. ....	104
Table 4. 1: Experimental values of Tafel slope, transfer coefficient $1-\alpha$ and exchange current $i_0$ , in the absence and presence of PABA and PABA/MOF composite. ....	131
Table 5. 1: Experimental values of Tafel slope, transfer coefficient $1-\alpha$ and exchange current $i_0$ , in the absence and presence of MOF and MOF/PABA composites. ....	154



## LIST OF ABBREVIATIONS

---

1,4-BDC	: 1,4-benzenedicarboxylate
ABA	: 3-aminobenzoic acid
ANI	: Aniline
APS	: Ammonium per sulfate
BASF	: Baden Aniline and Soda Factory
Cat	: Catalyst
CNTs	: Carbon nanotubes
CPs	: Coordination polymers
CTAB	: Cetyltrimethylammonium bromide
CV	: Cyclic voltammetry
DHTP	: 2,5-Dihydroxyterephthalic acid
DMSO	: Dimethyl sulfoxide
ECL	: Electrodeless discharge lamp
EDS, EDX	: Energy dispersive X-ray spectroscopy
EMU	: Electron microscope unit
FAAS	: Flame atomic absorption spectroscopy
FEG	: Field-emission gun
FESEM	: Field Emission Scanning Electron Microscope
FTIR	: Fourier transform infrared
GHG	: Greenhouse gases
GO	: Graphene oxide
H <sub>3</sub> BTC	: Trimesic acid, 1,3,5-benzenetricarboxylic acid
H <sub>ad</sub>	: Adsorbed hydrogen atom
HCL	: Hollow cathode lamp
HER	: Hydrogen evolution reaction
HFC	: Hydrogen fuel cell
HKUST-1	: Hong Kong University of Science and Technology-1
HRTEM	: High Resolution Transmittance Electron Microscope

ICPs	: Intrinsic conducting polymers
IR	: Infra-red
LMCT	: Ligand metal charge transfer
M	: Metal
MIL	: Materials of Institute Lavoisier
MOFs	: Metal organic frameworks
NMR	: Nuclear magnetic resonance
PA	: Polyacetylene
PABA	: Poly(3-aminobenzoic acid)
PADPA	: <i>p</i> -aminodiphenylamine
PANI	: Polyaniline
PEDOT	: Poly(3,4-ethylenedioxythiophene)
PGMs	: Platinum group metals
PPP	: Poly(para-phenylene)
PPV, PVP	: Poly(para-phenylene vinylene)
PPy	: Polypyrrole
PTh	: Polythiophene
rGO	: Reduced graphene oxide
SAED	: Selected area electron diffraction
SBU	: Secondary Building Units
SCE	: Saturated calomel electrode
SEM	: Scanning electron microscope
SWV	: Square Wave voltammetry
TBAP	: Tetrabutylammonium percholate
TEM	: Transmission electron microscope
TGA	: Thermogravimetric analysis
US DoE	: United State Department of Energy
UV	: Ultraviolet
UV-vis	: Ultraviolet visible
XRD	: Powder X-ray diffraction

## LIST OF SYMBOLS

---

$C$	: Concentration
$D$	: Diffusion coefficient
$E_{final}$	: Final potential
$E_{initial}$	: Initial potential
$E^{\circ'}$	: Formal electrode potential
$E_p$	: Peak potential
$E_{p,a}$	: Anodic peak potential
$E_{p,c}$	: Cathodic peak potential
$E_{RC_{cat}}$	: Fast catalytic reaction
$F$	: Faraday constant
$I$	: Current
$I_{p,c}$	: Current for the cathodic reaction
$I_{p,a}$	: Current for the anodic reaction
$I_p$	: Peak current
$I(t)$	: Impulse response function
$k$	: Average catalytic rate constant
$n$	: Number of electrons transferred
$Q$	: Charge
$R$	: Sample resistance
$v$	: Scan rate
$V$	: Applied voltage

## CHAPTER ONE

### INTRODUCTION

---

#### 1.1. BACKGROUND

Energy is the power derived from the utilisation of physical or chemical resources/matter in order to provide light and heat or to work machines. Since energy plays a core role in the above mentioned life processes, there is a need for sustaining both physical and chemical resources utilised for energy productions. One of the major contribution to the utility of energy is to closely look at the global population, thus energy supply must reach the demand of global population. The global population increases rapidly and it is expected to increase in the near future. So in this case, it means there will be a need of large supply of energy. The economic growth of the nation which is a key aspect in addressing the people's needs depends also on the energy. There is a need for a vast amount of energy to reach the target. With the mentioned global overpopulation growths, the resources which are used for energy generations will deplete, so there is also a need in ways which can help in sustaining the available resources. In sustaining the energy resources, there is a need in not to compromise the quality of the world we live in.

The primary energy source which is mainly used for energy productions and contribute 80% of the energy utilised globally comes from burning of fossil fuels which results in releasing greenhouse gases (GHG) which leads to unforeseen circumstances such as global warming [1, 2]. In this case, there is an essential for a new technology that can address the challenge of depletion of fossil fuels and at the same time countering the depletion of ozone (O<sub>3</sub>) layer which resulted from emission of GHG. Renewable energy technologies which is an alternative route for energy generations account for a little percentage in global energy supply [3-5]. The great advantage in utilising renewable resources (wind, hydrothermal, biomass and nuclear) is that they produce less or no waster products such as GHG or other chemical pollutants, so they have minimal

negative impacts on the environment [6]. Limitations of using renewable resources is that it is difficult to generate large quantity of energy and also the technologies have extremely large capital costs [4]. In this regard, there is a need to feasibly look at other technologies that can overcome the above mentioned challenges encountered by using non-renewable and renewable resources, thus (1) GHG emission, (2) little energy production and (3) large capital cost. Hydrogen gas can be regarded as a candidate to counter those limitations. Hydrogen as the most abundant element can serve the following advantages in the energy portfolio, (1) hydrogen gas is readily available (abundant), (2) no harmful emission during utility, (3) fuel efficient, thus hydrogen energy is very efficient fuel source and produce more energy (gasoline) and (4) it is renewable, it gives water as a by-product which can be split further into hydrogen and oxygen gas [7, 8].

## **1.2. PROBLEM STATEMENT**

It was stated previously that hydrogen gas can be used as an alternative energy carrier or source for utilisation in different energy sectors [7, 8], however, there is still a need to solve the challenges which are encountered in hydrogen technology. One of the key limitations for this technology lies in the hydrogen production components. Hydrogen production technologies mostly depends of fossil fuels [9]. Steam reforming of fossil fuels for generation of hydrogen still produces the GHG which will still have impacts on the environment [9, 10]. The new search for a feasible technology is underway and water splitting electrolysis is deemed as an alternative route for hydrogen production. Water splitting electrolysis gives off clean hydrogen, however since the process requires a lot of energy, the increase in electricity prices hindered the application of the process [11, 12]. The costness of the process can be due to the electrocatalyst which is utilise, thus there is a need of find a cheaper catalyst which can also meet the requirements of an electrocatalyst. Suitable electrocatalyst must have the following requirements [13]: (1) good processibility, (2) good conductivity, (3) mechanical and thermochemical stable, (4) large surface area and highly porous and (5) it must have

high current density at lower potentials. Intrinsic conducting polymers (ICPs) such as polyacetylene (PA), polypyrrole (PPy), polythiophene (PTh) polyaniline (PANI) and poly(p-phenylenevinylene) (PVP) have shown good conductive, optoelectrical, and luminescence properties and have been applied in most electrochemical applications [14]. Among all ICPs, PANI is found to be the most promising and studied mostly because of its ease of synthesis, low cost monomer, tunable properties, and better stability compared to other ICPs. The major drawback in utilising PANI and other intrinsic conducting polymers is poor processibility which is due to their insolubility in many organic solvents and also infusibility [15, 16].

### **1.3. RATIONALE AND MOTIVATION**

A possible solution for the use of polyaniline as an electrocatalyst is to counter the previously mentioned limitations. The poor processibility of polyaniline which was explained that it is due to low solubility of the material in many organic solvents can be addressed by introducing new functional groups in the polymer backbone. Since the benzene ring are unreactive, the additional functional groups can be introduced during polymerisation period whereby the starting reagent have that desired functional groups. The functional groups such as carboxylic acid and sulfonic acids have been reported and are able to enhance the solubility challenge of the polymer without alteration with the conductivity of the material [17]. To address the stability challenge of the material, it was reported that formation of composite of ICPs such as PANI and PTh with Ruthenium complexes improves the stability of the polymers as well as increasing the conductivity of the material [18]. Enhancement in the conductivity and the stability of the material can play a role in improving the catalytic efficiency of the material since there is additional functional groups and metal sites which can be used as a catalytic site. Porous materials such as zeolites, carbon nanotubes, graphene oxide and metal organic frameworks, can be easily incorporated to the polymer backbone through their ligands and also interaction of polymer precursor with the metal site of the materials. Among porous materials, metal organic frameworks

(MOFs) which have an open metal site and accessible organic linker can be used as a material that can be incorporated on polymer backbone in order to increase the stability of the polyaniline and also those additional groups which can serve as additional catalytic sites. The interaction between PANI and MOF can be due to  $\pi$ - $\pi$  stacking interaction on the benzene ring of PANI as well as aromatic rings of carboxylate organic linkers or electrostatic interactions between the oxygen atoms of organic linker of MOFs and nitrogen atom of polyaniline forming a new NO group on the composite.

## **1.4. RESEARCH AIM AND OBJECTIVES**

### **1.4.1. Research Aim**

The aim of this work is to synthesise and study the electrocatalytic hydrogen production properties of polyaniline/MOF, poly(3-aminobenzoic acid)/MOF and MOF decorated with poly(3-aminobenzoic acid) composites for hydrogen fuel cell applications

### **1.4.2. Objectives**

The objectives of this work are to:

- ✓ Synthesise polyaniline (PANI), poly(3-aminobenzoic acid) (PABA) and metal organic framework (MOF) using chemical polymerisation of aniline, 3-amino benzoic acid monomer and hydrothermal methods, respectively.
- ✓ Manufacture polyaniline (PANI/MOF) and poly(3-aminobenzoic acid) (PABA/MOF) doped with MOF using in-situ chemical polymerisation of aniline monomer/ 3-amino benzoic acid in the presence of MOF.
- ✓ Prepare metal organic frameworks in the presence of poly(3-aminobenzoic acid) (MOF/PABA) using hydrothermal methods

- ✓ Study optical, structural and morphological properties of the synthesised materials using Ultraviolet-visible spectroscopy (UV-vis), Fourier transform infrared spectroscopy (FTIR), X-ray diffraction (XRD), Thermogravimetric analysis (TGA), Scanning electron microscope (SEM), Transmission electron microscope (TEM), Energy dispersive X-ray spectroscopy (EDS, EDX), and Selected area electron diffraction (SAED).
- ✓ Investigate the electrocatalytic hydrogen evolution reaction of the synthesised materials using cyclic voltammetry and square wave voltammetry.

## 1.5. DISSERTATION OUTLINE

This dissertation attempts to tune the electrocatalytic properties of polyaniline and MOF composites. The outline of the remaining chapters in the dissertation are as follows:

- ✓ **Chapter two:** it focuses on the literature review, introducing the theoretical considerations of hydrogen technology, hydrogen evolution reaction, metal organic frameworks, polyaniline and characterisation methods.
- ✓ **Chapter three:** concentrate on the synthesis of polyaniline, metal organic frameworks and polyaniline-metal organic framework composite and their electrocatalytic properties.
- ✓ **Chapter four:** concentrate on the synthesis of poly(3-aminobenzoic acid) doped with MOF and their electrocatalytic hydrogen production.
- ✓ **Chapter five:** deals with synthesis and electrocatalytic hydrogen evolution reaction of metal organic frameworks decorated with poly(3-aminobenzoic acid) (MOF/PABA).
- ✓ **Chapter six:** summary of the main conclusions and the recommendations.



## 1.6. REFERENCES

- [1] Goldemberg, J. Ethanol for a sustainable energy future. *Science* 135 (2007) 808-810.
- [2] Lewis, N.S., Nocera, D.G. Powering the planet: Chemical challenges in energy utilisation. *Proceedings of the National Academy of Science of the United State of America* 103 (2006) 15729-15735.
- [3] Chow, J., Kopp, R.J., Portney, P.R. Energy resources and global development. *Science* 302 (2003) 1528-1531.
- [4] Panwar, N.L., Kaushik, S.C, Kothari, S. Role of renewable energy sources in environmental protection-A review. *Renewable and Sustainable Energy Reviews* 15 (2011) 1513-1524.
- [5] Demirbas, A. Potential applications of renewable energy sources, biomass combustion problems in boiler power systems and combustions related environmental issues. *Progress in Energy and Combustion Science* 31 (2005) 171-192.
- [6] Bazmi, A.A., Zahedi, G. Sustainable energy systems: Role of optimization modelling techniques in power generation-A review. *Renewable and Sustainable Energy Reviews* 15 (2011) 3480-3500.
- [7] Painuly, J.P. Barrier to renewable energy penetration; a framework of analysis. *Renewable Energy* 24 (2001) 73-89.
- [8] Turner, J.A. Sustainable hydrogen energy. *Science* 305 (2004) 972-974.
- [9] Edwards, P.P., Kuznetsov, V.L., David, W.I.F., Brandon, N.P. Hydrogen and fuel cells: Towards a sustainable energy future. *Energy Policy* 36 (2008) 4356-4362.
- [10] Koroneos, C., Dompos, A., Roumbas, G., Moussiopoulus, N. Life cycle assessment of hydrogen fuel production processes. *International Journal of Hydrogen Energy* 29 (2004) 1443-1450.
- [11] Carmo, M., Fritz, D.L., Mergel, J., Solten, D. A comprehensive review on PEM water electrolysis. *International Journal of Hydrogen Energy* 38 (2013) 4901-4934.

- [12] Barbir, F. PEM electrolysis for production of hydrogen from renewable energy sources. *Solar Energy* 78 (2005) 661-669.
- [13] Li, Y., Li, Y., Zhu, E., McLouth, T., Chiu, C.Y., Huang, X., Huang, Y. Stabilization of high-performance oxygen reduction reaction Pt electrocatalyst supported on reduced graphene oxide/carbon black composite. *Journal of American Chemical Society* 134 (2012) 12326-12329.
- [14] Pecher, J., Mecking, S. Nanoparticles of conjugated polymers. *Chemical Reviews* 110 (2010) 6260-6279.
- [15] Bhadra, S., Khastgir, D., Singha, N.K., Lee, J.H. Progress in preparation, processing and applications of polyaniline. *Progress in Polymer Science* 34 (2009) 783-810.
- [16] Jaymand, M. Recent progress in chemical modification of polyaniline. *Progress in Polymer Science* 38 (2013) 1287-1306.
- [17] Chen, X.P., Jiang, J.K., Liang, Q.H., Yang, N., Ye, H.Y., Cai, M., Shen, L., Yang, D.G., Ren, T.L. First principles study of the effect of functional groups on polymer backbone. *Scientific Reports* (2015) doi: 10.1038/srep16907.
- [18] Giri, S., Ghosh, D., Das, C.K. Effect of Ruthenium (III) incorporation in polyaniline backbone: Materials for supercapacitive energy storage application. *NANO: Brief Reports and Reviews* 8 (2013) doi: 10.1142/s1793292013500264.
- [19] Naqash, W., Majid, K. Synthesis, characterisation and study of effect of irradiation on electronic properties of polyaniline composite with metal complex of Co (III). *Material Research* 18 (2015) 1121-1127.

## CHAPTER TWO

### LITERATURE REVIEW

---

#### 2.1. HYDROGEN TECHNOLOGY

##### 2.1.1. Background of Hydrogen Technology

Hydrogen gas is emerging beyond its conventional role as an additive component for gasoline production, chemical and fertilizer manufacture and food production to become a promising alternate energy carrier for both mobile and stationary power [1-4]. As mentioned in Chapter one, hydrogen has unique characteristics that make it an ideal energy carrier which include the fact that: (1) it can be produced from and converted into electricity at relatively high efficiencies than the used traditional combustion of fossil fuels; (2) it can be produced from a readily, most abundant raw material, water (3) it is a completely renewable fuel; (4) it can be stored into three different forms, thus gaseous, liquid and solid state storage (5) it can be transported over large distances through pipelines or via tankers; (6) it can be converted into other forms of energy in more ways and more efficiently than any other fuel (such as catalytic combustion, electrochemical conversion, and hydriding); (7) it is environmentally compatible since its production, storage, transportation, and end use do not produce any pollutants (except for small amounts of nitrogen oxides), greenhouse gases, or any other harmful effects on the environment [5-7]. To utilise hydrogen gas as an energy source, there must be a technology that converts the chemical form of hydrogen to electrical energy. The convenient form of electrical energy conversions is through hydrogen fuel cell technology. Hydrogen fuel cell (HFC) generates electrical energy from an electrochemical processes and giving water as a by-product [8, 9]. This HFC are not just environmental friendly, but the energy efficiency is two times more than the traditional combustion technologies. A fuel cell consists of an electrolyte solution sandwiched between two electrodes (anode and cathode). Bipolar plates on

either sides of the cell help distribute gases and serve as a current collector. In principle, hydrogen gas flows through the channel of anode, where oxidation takes place. The oxidation process takes place when a catalyst usually platinum causes hydrogen molecule to separate into protons and electrons. The membrane which differ from fuel cell to fuel cell allows protons to pass through. Those protons will combine with oxidized air to form water. The electrons flow to the cathode to generate electricity or power [10-12]. However, the major limitation of commercializing the hydrogen fuel cell can be due to several factors. (1) The production cost of clean hydrogen (electrolysis process) is three times more than the one generated from fossil fuels, hence, there is a need of feasible accumulation of raw materials (hydrogen and oxygen) [13]. Oxygen can be easily obtained from air. The major challenge lies in the demand and supply of pure hydrogen gas. The three concepts which can really address this limitations (supply and demand of hydrogen) are covered in the concept of hydrogen technology, thus production, storage and utilisations. Several technologies or processes are currently employed to address this and they are fully discussed below.

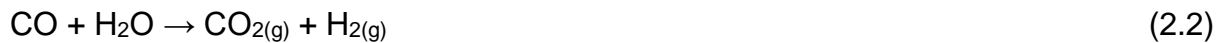
### **2.1.2. Hydrogen Production**

Hydrogen is the most abundant element in universe. It exists naturally in air but not in large quantities to be utilised industrially or for other uses. Mainly when it is produced, it has to be separated from other gases. Majority of the hydrogen today is produced from non-renewable resources such as steam reforming of natural gases or fossil fuels with minority coming from renewable electrolysis processes, partial oxidation and also from biomass [14, 15].

#### **2.1.2.1. Steam reforming of natural gases**

Steam reforming of natural gases such as methane and ethane is an important chemical process which is currently and mainly utilised to produce hydrogen gas. This

process is the most economic and convenient process since natural gases are readily available in large quantities [16, 17]. During the operation, this process utilises high energies and it gives synthetic gas (syngas) which is a mixture of hydrogen and carbon monoxide (H<sub>2</sub>/CO) as a product. The general equations for steam reforming of methane is given in Eq. 2.1 and 2.2 below:



In steam-methane reforming, methane reacts with steam under 3–25 bar pressure in the presence of a catalyst to produce hydrogen, and carbon monoxide. Steam reforming is endothermic reaction [18-20]. This is followed by water-gas shift reaction where carbon monoxide and steam are reacted using a catalyst to produce carbon dioxide and more hydrogen. In a final process step called "pressure-swing adsorption," carbon dioxide and other impurities are removed from the gas stream, leaving essentially pure hydrogen. Steam reforming can also be used to produce hydrogen from other fuels, such as ethanol, propane, or even gasoline.

#### **2.1.2.2. Photoelectrochemical water splitting for hydrogen production**

Photoelectrochemical water splitting is a green technology for hydrogen production which is based on the chemical principle similar to electrolysis. Semiconductor/catalysts are immersed into an electrolyte and irradiated by sunlight/electrical potential applied they release current that split water. Water molecule is split into hydrogen gas and oxygen using solar light or electric potential under the presence of a solid catalyst. This technology produces hydrogen gas without emission of carbons which can lead to environmental pollutants [21]. During water splitting hydrogen generation, when light with energy larger than the band gap is incident on the catalyst, electrons and holes are generated in the conduction and valence bands, respectively. The photo/electrogenerated electrons and holes cause

redox reactions similar to electrolysis. Water molecules are reduced by the electrons to form  $H_2$  and oxidized by the holes to form  $O_2$ ; leading to overall water splitting [22, 23]. Water splitting hydrogen production is influenced by factors such as charge separation, mobility, and lifetime of photo/electrogenerated electrons and holes also have an effect on the photocatalytic properties and there is a need for a material which can meet all photo-electrode materials requirements such as band gap, stability and electrical resistance [24]. Because this technology is deemed the future hydrogen production method, there is a need for intense study on it to find the best semiconductor/catalysts that can overcome the challenges imposed by this technology. The concept of electrocatalysis and hydrogen evolution reactions will be discussed in full detail in Section 2.2.

### **2.1.2.3. Other methods for hydrogen production**

Hydrogen can also be produced from biomass and partial oxidation (coal gasification) methods.

#### **2.1.2.3.1. Biomass**

Biomass is one of the most abundant renewable resources since it forms naturally by fixing carbon dioxide in the atmosphere during photosynthesis process in plant. Hydrogen in biomass can be produced through two processes, thus biomass gasification (in the presence of air) and pyrolysis (absence of air). In biomass gasification, biomass is gasified to produce charcoal in high temperature which can then processed to hydrogen gas. During pyrolysis, also the biomass is heated at high temperatures in absence of air and it gives hydrogen with mixture of other gases such as methane and carbon monoxide [25-27]. Methane and carbon monoxide can be further converted to hydrogen using steam reforming and water-gas shift processes, respectively (discussed above).

#### **2.1.2.3.2. Partial oxidation**

In the partial oxidation process which is mainly known as a gasification, hydrogen is produced from range of hydrocarbon fuels which include coal and oils. In gasification, coal is first reacted with oxygen and steam under high pressures and temperatures to form synthesis gas, a mixture consisting primarily of carbon monoxide and hydrogen [28]. The synthesis gas is cleaned of impurities and the carbon monoxide in the gas mixture is reacted with steam via the water-gas shift reaction to produce additional hydrogen and carbon dioxide. Hydrogen is removed by a separation system and the highly concentrated CO<sub>2</sub> stream can subsequently be captured and sequestered. The hydrogen can be used in a combustion turbine or solid oxide fuel cell to produce power, or utilised as a fuel or chemical feedstock [29, 30].

#### **2.1.3. Hydrogen Storage**

In order to commercialize hydrogen economy, the largest setback today does not lie on the production, but on the feasible method to store hydrogen since hydrogen is not a primary energy source like coal. Hydrogen can be stored in three different forms, thus (i) as a pressurized gas, (ii) as a cryogenic liquid and (iii) as a solid adsorbed on a surface of a material [31]. An effective storage method which reach the target set by US Department of Energy is required. They set a target that by 2015 and 2017 H<sub>2</sub> storage targets are 5.5 wt. % in gravimetric capacity, 40 g.L<sup>-1</sup> of volumetric capacity at an operating temperature of 40-60 °C under a maximum delivery pressure of 100 atm. [32, 33]. Six years and a year respectively of achieving anticipated target, all storage methods have failed then there is still a need to develop a method to reach that target or even higher than that. These target are based on storage systems including tank weight, pressure and temperature. Here, we will look at three different methods used for hydrogen storage, thus gaseous, liquefaction and solid hydrogen storage.

### **2.1.3.1. Gaseous hydrogen storage**

The most common method which is currently employed to store hydrogen is through compressed gas. Hydrogen is stored by means of compressing it at high pressure at room temperature and cryogenic conditions [34]. This method of storing hydrogen brings several advantages such as high H<sub>2</sub> fraction, rapid refuelling capability and excellent dormancy characteristics [35]. Their major challenge is the system volume which does not reach the target and an ideal cylinder which is cylindrical shape makes it difficult to conform storage to available space and the weight/energy penalties. The other inconvenient issue is the safety measures such as rapid loss of H<sub>2</sub> in an accident which can cause explosion [36]. Another gaseous hydrogen storage method is using glass microspheres which have more advantages than compression gaseous method. The process of storage occurs in three stages: charging, filling and discharging. In principle, hollow glass spheres are filled with hydrogen gas at high pressures and temperatures by permeation in high pressure vessels. After that process, the sphere is cooled to ambient temperatures and stored in vehicle tanks. Finally, the microspheres are heated to release hydrogen gas. The major setback in utilising this method are low volumetric density, high pressure needed for filling and high temperatures for releasing hydrogen [37].

### **2.1.3.2. Liquid hydrogen storage**

Hydrogen can also be stored in a liquid form via a process called liquefaction. During this process, hydrogen is cooled down to cryogenic temperatures (-253 °C) at 20 bar pressure and stored in a tank. The theoretical gravimetric density of liquid hydrogen is 100%, but only 20 wt.% of hydrogen is achieved on practical basis. On volumetric basis, the values are 80 kg/m<sup>3</sup> and 30 kg/m<sup>3</sup> respectively [38, 39]. This clearly means that liquid hydrogen has a much better energy density than the compressed gas since it can store high energy at low pressures. The main limitation with liquid hydrogen is that approximately 30-40% of hydrogen is lost and also the boil-off loss during



dormancy [40]. Hydrogen can also be stored in liquid form using the borane solutions and rechargeable organic liquids such as methyl cyclohexane and toluene.

### **2.1.3.3. Solid hydrogen storage**

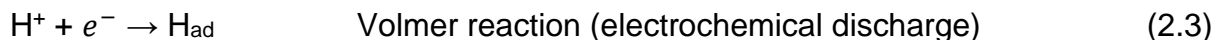
In solid materials, hydrogen can adsorb on the surface of the materials (adsorbent) and stored in a much convenient and safer way. The main advantage of adsorption over other physical storage (compressed gas and liquid hydrogen), it makes it possible to store large quantity of hydrogen at ambient temperatures) and adsorbed hydrogen does not chemically react during adsorption and therefore does not accumulate impurities which can poison operations of fuel cell [41, 42]. Hydrogen can bind/ interact with the adsorbent in two ways, i.e. chemisorption or physisorption. In chemisorption, hydrogen predominately bind stronger in an adsorbent and in physisorption, hydrogen bind via weak van der Waal forces. Physisorption has a great advantage to chemisorption since it has fast kinetics (during release of hydrogen) and it is fully reversible [43]. The problem with physisorption-based hydrogen storage is that, due to weak interaction between hydrogen and adsorbent the hydrogen density at ambient temperature is small [44].

## **2.2. HYDROGEN EVOLUTION REACTIONS (HER)**

### **2.2.1. Fundamentals and Mechanisms of HER**

The hydrogen evolution reaction (HER) is a central reaction in the renewable production and storage of hydrogen fuel from water, regardless of whether this process is driven directly by solar fuel production using photons harvested by semiconductors or indirectly by electrolysis of water powered by photovoltaics and is one of the most studied electrochemical reactions involved in electrolytic cells [45, 46]. The mechanism of the HER in aqueous acid or alkaline solutions proceeds in a series of three elementary reaction steps which comprises of two electrochemical steps and

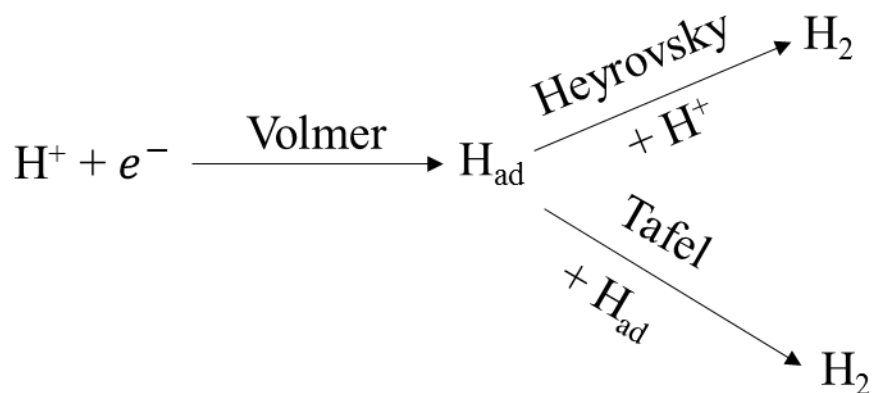
one chemical step [47-50]. The three elementary reaction steps in acidic medium give in Eq. 2.3-2.8:



and in alkaline solution are:



In an acidic solution, the first step (Eq. 2.3) is the Volmer reaction in which a proton receives an electron and generates an adsorbed hydrogen atom ( $\text{H}_{\text{ad}}$ ) at the active site as an intermediate [51, 52]. Then the second step can be Heyrovsky or Tafel reaction. In Volmer-Heyrovsky mechanism, a proton from a water layer reacts with one adsorbed hydrogen to form  $\text{H}_2$  as illustrated in Eq. 2.4. In the Volmer-Tafel mechanism, two adsorbed surface hydrogens next to each other react to form  $\text{H}_2$  molecule as illustrated in Eq. 2.5 [53]. Furthermore, Scheme 2.1 below shows two possible HER mechanism. The two steps of hydrogen adsorption and desorption on the catalyst surface are competitive in nature. A catalyst surface having too weak bonding strength with hydrogen atoms cannot efficiently adsorb the reactant to initiate the HER and a catalyst surface having too strong bonding strength would have a difficulty in releasing the product towards completion of the HER [54, 55]. Since, HER involves the adsorption and desorption of the hydrogen atoms on the surface of the catalyst, a suitable catalyst for HER should have a good balance between the two steps, thus the hydrogen evolution reactions depends on the electrocatalyst [56].



Scheme 2.1: Mechanisms of Hydrogen Evolution Reactions.

## 2.3. ELECTROCATALYSIS

### 2.3.1. The Concept of Catalysis

Catalyst from a definition is a substance that is used in a chemical reaction to accelerate the reaction without being consumed, thus catalyst does not form part of the product. The acceleration of the reaction is attained by lowering the activation energy ( $E_a$ ) which is the minimum energy required for reactants to be converted to products. Figure 2.1 below shows how catalyst plays a role in lowering the activation energy.

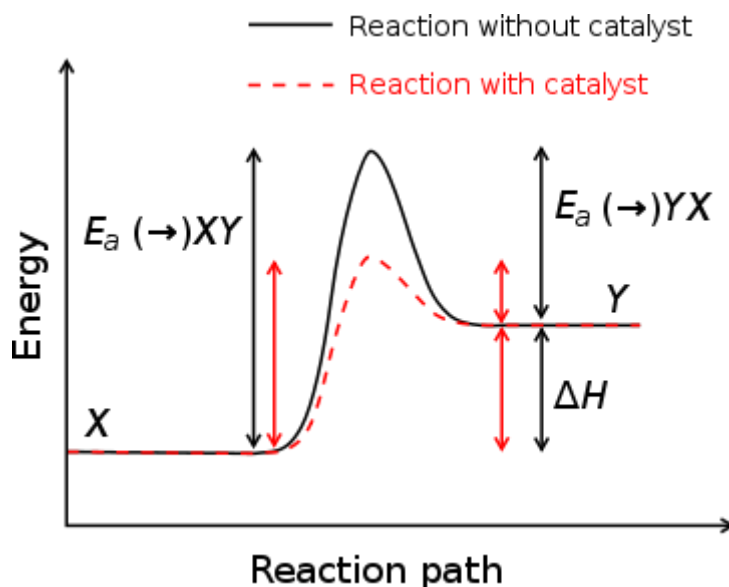


Figure 2.1: Energy diagram showing a reaction proceeding in the absence and presence of catalyst.

Catalysts can be in the same phase with the reactants or in the different phase known as homogeneous or heterogeneous catalyst, respectively. Most reactions take place using heterogeneous catalysts such as Haber process and also those which are involved in electrochemical reactions [57, 58]. The most important requisites of a catalyst are activity, stability, selectivity to the target reaction and cost [59, 60].

### 2.3.2. The Principle of Electrocatalysis

Electrocatalysis is the studying and realization of means for the acceleration of electrochemical reactions when an electrocatalyst is used as an electrode surface or when immersed in an electrolyte solution [61]. In other words, electrocatalyst enhances the electrode kinetics by minimizing the overpotential and also by lowering the excess energy consumed by the activation barriers of the redox reactions [62]. Overpotential is the extra potential over the equilibrium value that must be applied to cause an electrodic reaction at a certain rate [62]. An electrodic reaction may be anodic (oxidation) or cathodic (reduction) depending upon the direction of overpotential with

respect to the equilibrium potential of the electrode [63]. In addition, electrocatalyst assists in transferring electrons between the electrodes and reactants and this is facilitated by an intermediate chemical transformations described by half reactions [62]. In electrocatalysis, the high efficiency and catalytical activity of the electrode is the result of some combination of surface reactivity, electronic and ionic conductivity and electron hole pair separation and facile mass transport of molecules, which is furnished by the architectural design of both electrodes in the cell, i.e. the arrangement of materials in space [63]. In addition, the surface adsorption interactions between reactants or reaction products and electrode (electrocatalyst) is the most important factor affecting the electrochemical reaction rate and mechanism [61]. The composition, structure and dimension parameters determine the electron structure of the catalyst's active site, hence, the adsorption conditions and the reaction kinetic characteristics [61].

### **2.3.3. HER Electrocatalyst**

The efficient and commercialisation of HER depends mostly on the electrocatalyst, hence, most studies have been conducted in electrocatalysis with the great hope of finding a best suitable electrocatalyst for HER [64]. The advanced and ideally electrocatalyst should reduce the overpotential and increase the hydrogen production efficiency [65-67]. In addition, the efficient electrocatalyst must encounter different characteristics such as high thermal and mechanical stability as well as low cost [68, 69]. The HER activities of various catalysts can be summarized in the “Volcano plot” as shown in the Figure 2.2 below, where the exchange current density for different catalysts in acid are plotted as a function of the Gibbs free energy of adsorbed atomic hydrogen on catalyst [70]. Platinum group metals (PGMs) such as Pt, Pd, Ir and can be found on the apex of the Volcano plot and are the frequently used electrocatalysts for HER [71, 72]. PGMs especially Pt-based electrocatalysts meet various requirements for HER electrocatalyst as they exhibit low overpotential, high catalytic activity, fast kinetics and are most stable [73-75]. However, their extremely high cost

and limited abundance or scarcity are the major obstacles for industrial applications [76-78]. Thus, the important goal of the modern electrocatalysis is to completely replace PGM based electrocatalysts with low cost and catalytic active materials [79]. Although non-platinum active metals such as Fe, Ni, Mo or Co are considerably cheaper, they suffer from corrosion and passivation under reaction conditions [80]. Electrocatalysts based on conducting polymers (CPs) have been rarely investigated for HER. CPs such as polyaniline and polypyrrole have shown great environmental stability as well as low cost and have a great ranges of potentials windows [81, 82]. With this properties CPs can be used to replace the PGM-based electrocatalysts as well as corrosion prone earth-abundant Fe, Ni, Mo and Co. CPs such as polypyrrole (Ppy) and polyaniline have been greatly investigated as a catalytic support on earth-abundant metals such as Ni and also Pt for HER electrocatalysis [83, 84]. The main reason for incorporating the metal particle into polymer matrices is to disperse the former as to increase the specific surface area of these materials resulting in improved electrocatalytic efficiency [83].

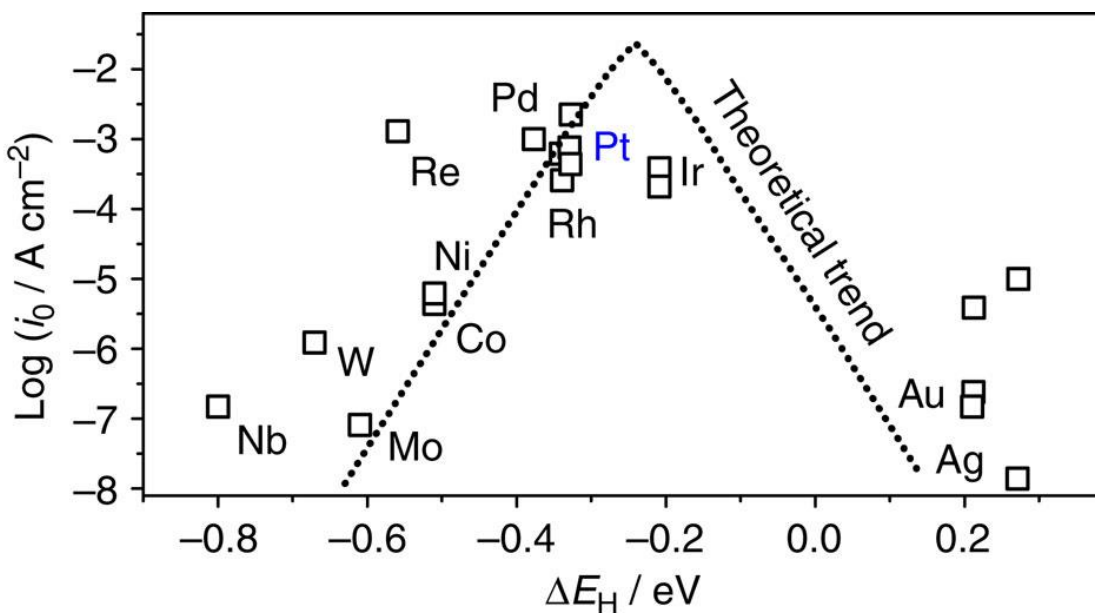


Figure 2.2: Trends in hydrogen evolution reaction activity. Experimental HER activity expressed as the exchange current density,  $\log(i_0)$ , for different metal surfaces as a function of the calculated  $^*H_{ad}$  chemisorption energy,  $\Delta E_H$ . The result of a simple theoretical kinetic model is also shown as a dotted line.

## 2.4. POLYMERS

### 2.4.1. Background on Polymers

Polymers are macromolecular substances that have high molar masses and are composed of a large number of repeating units which are called monomers. The monomers are held together by covalent bonds. There are both naturally occurring polymers which mostly are referred as biopolymers since they normally obtained from biological processes and synthetic polymers which are obtained from chemical reactions of monomers. Among naturally occurring polymers are proteins, starches, cellulose, and latex. Synthetic polymers are produced commercially on a very large scale and have a wide range of properties and applications/uses. The materials commonly called plastics are all synthetic polymers. The repeating unit of polymers are formed through a reactive intermediate which is a process in polymerisation.

Depending on the type of intermediate formed, polymerisation process can be categorized in the following:

- a) Radical Polymerisation where the initiator is a radical, and the propagating site of reactivity is a carbon radical.
- b) Cationic Polymerisation where the initiator is an acid, and the propagating site of reactivity is a carbocation.
- c) Anionic Polymerisation where the initiator is a nucleophile, and the propagating site of reactivity is a carbo-anion.
- d) Coordination Catalytic Polymerisation where the initiator is a transition metal complex, and the propagating site of reactivity is a terminal catalytic complex.

Traditionally, synthetic polymers are regarded as good insulator and semiconductors and have been widely applied in electronic applications.

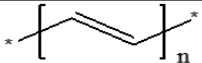
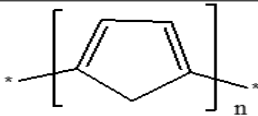
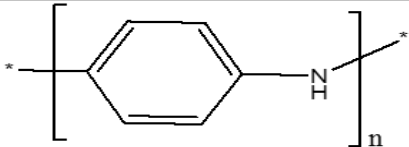
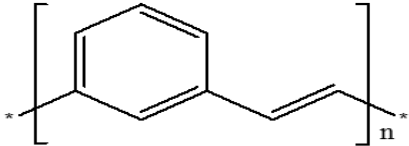
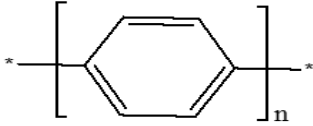
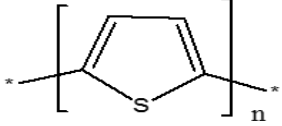
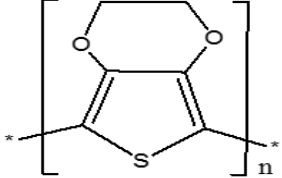
#### **2.4.2. Conductive Polymers**

ICPs are conjugated polymers possessing an extended  $\pi$ -electrons system and highly delocalized electronic states. The extended electron conjugation or delocalized is what gives rise to conductivity of polymers [86, 87]. These ICPs were discovered in the 1970s when conductivity of polyacetylene which are normally used as a semiconductor increases by 10 million-fold when polyacetylene was oxidized using iodine vapour [88-90]. The phenomenon was named doping which is essential for the conductivity of polymers. ICPs are amorphous and this makes its charge transport in this conducting polymers to be quite different from conventional polymers [91]. The chemical structures of conducting polymers are amenable to modification, and chemical modelling and synthesis which allows the alteration of their electrical and mechanical properties [92]. The alterations in both properties make the ICPs to merge the positive properties of metals and conventional polymers which enables the materials to conduct (charge transfer), have great electrical and optical properties with flexibility in processing and ease of synthesis. The conductivity of these polymers can be influenced by various factors, including polaron length, conjugation length, overall



polymer length and the charge transfer to adjacent molecule [93, 94]. There are many ICPs which have been investigated and they are summarized in the Table 2.1 below [95].

Table 2.1: Table showing different intrinsically conducting polymers which have been studied mostly.

NAME OF ICPs	CHEMICAL STRUCTURE
Poly(acetylene), PA	
Poly(pyrrole), PPy	
Poly(aniline), PANI	
Poly(para-phenylene vinylene), PPV	
Poly(para-phenylene), PPP	
Poly(thiophene), PT	
Poly(3,4-ethylenedioxythiophene), PEDOT	

## 2.5. POLYANILINE

### 2.5.1. History and Background of Polyaniline

PANI is one of the most investigated among polymer other ICPs because of its low cost, easy synthesis, environmental stability, unique doping/ de-doping property and relatively high conductivity [96-98] Based on this properties, PANI was studied for different applications such as capacitance, sensors, actuators and magnetism [99-102]. Polyaniline discovery can be dated back in the 1862 where it was formed by Letheby through oxidation of aniline under mild conditions [103, 104]. Anciently, it was known as 'aniline black' after black powder was obtained during oxidation and it was an important material for dyes and printings [105]. Attempt for control the synthesis conditions of polyaniline grew until in the 1910s when Green and Woodhead managed successfully to control the conditions [106]. This was followed by Jozefowic's group in the 1960s and 1970s for better understanding of the material [106]. After this, the study of polyaniline with other ICPs increased tremendously worldwide and were studied for different applications illustrated as shown in Figure 2.3 below.

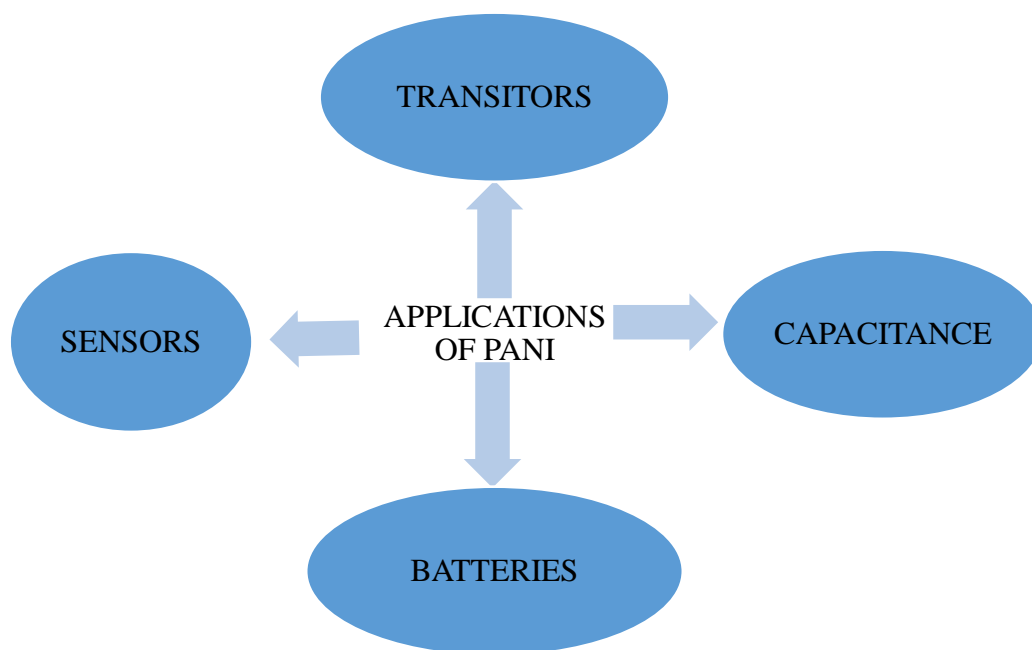


Figure 2.3: Industrial applications of polyaniline.

### 2.5.2. Structure of Polyaniline

Polyaniline have different chemical structures which is attributed to the oxidation state of the polymer backbone, hence it exists in different states [107, 108]. The general representation of the polyaniline structure can be described by the following molecular formula (Figure 2.4):

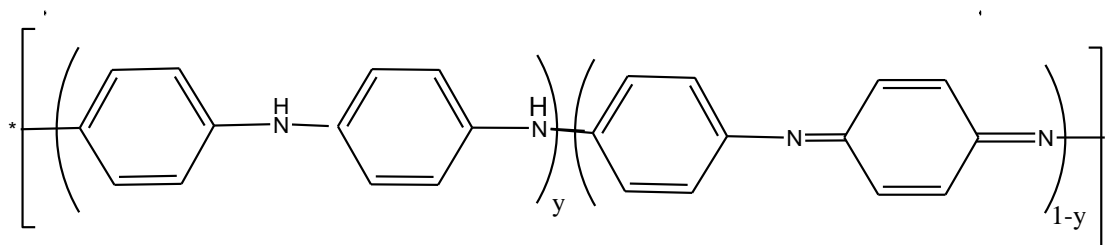


Figure 2.4: The general structure of polyaniline, where  $y = 1, 0.5$  and  $0$  corresponding to fully reduced polyaniline (leucoemeraldine), the half oxidized polyaniline (emeraldine) and fully oxidized polyaniline (pernigraniline), respectively.

The structure of three different oxidation states of polyaniline are shown in Figure 2.5 below.

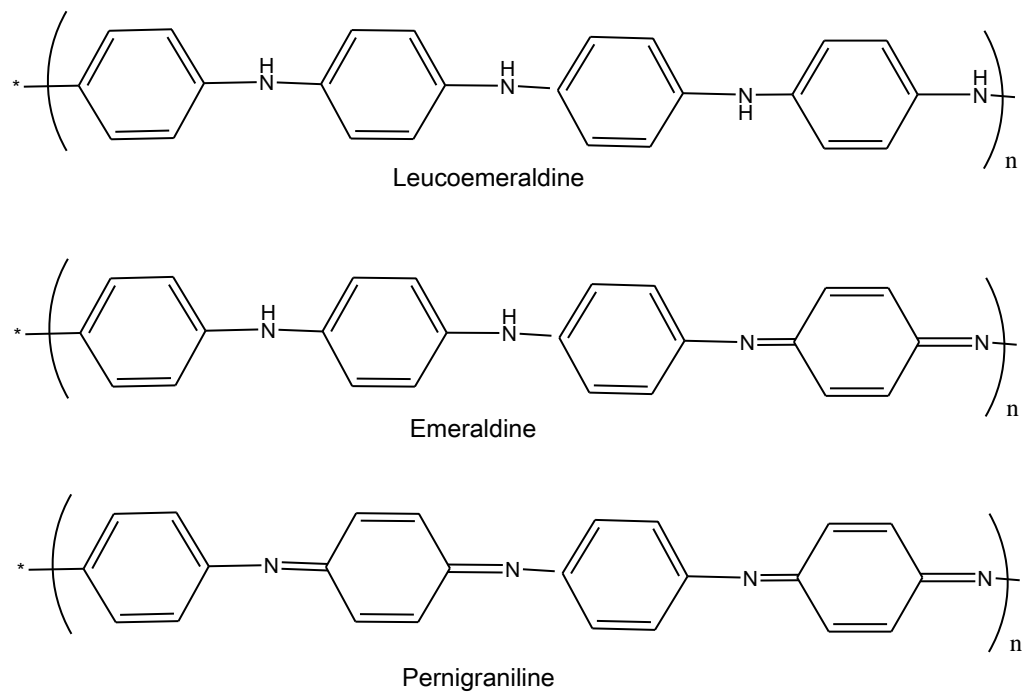
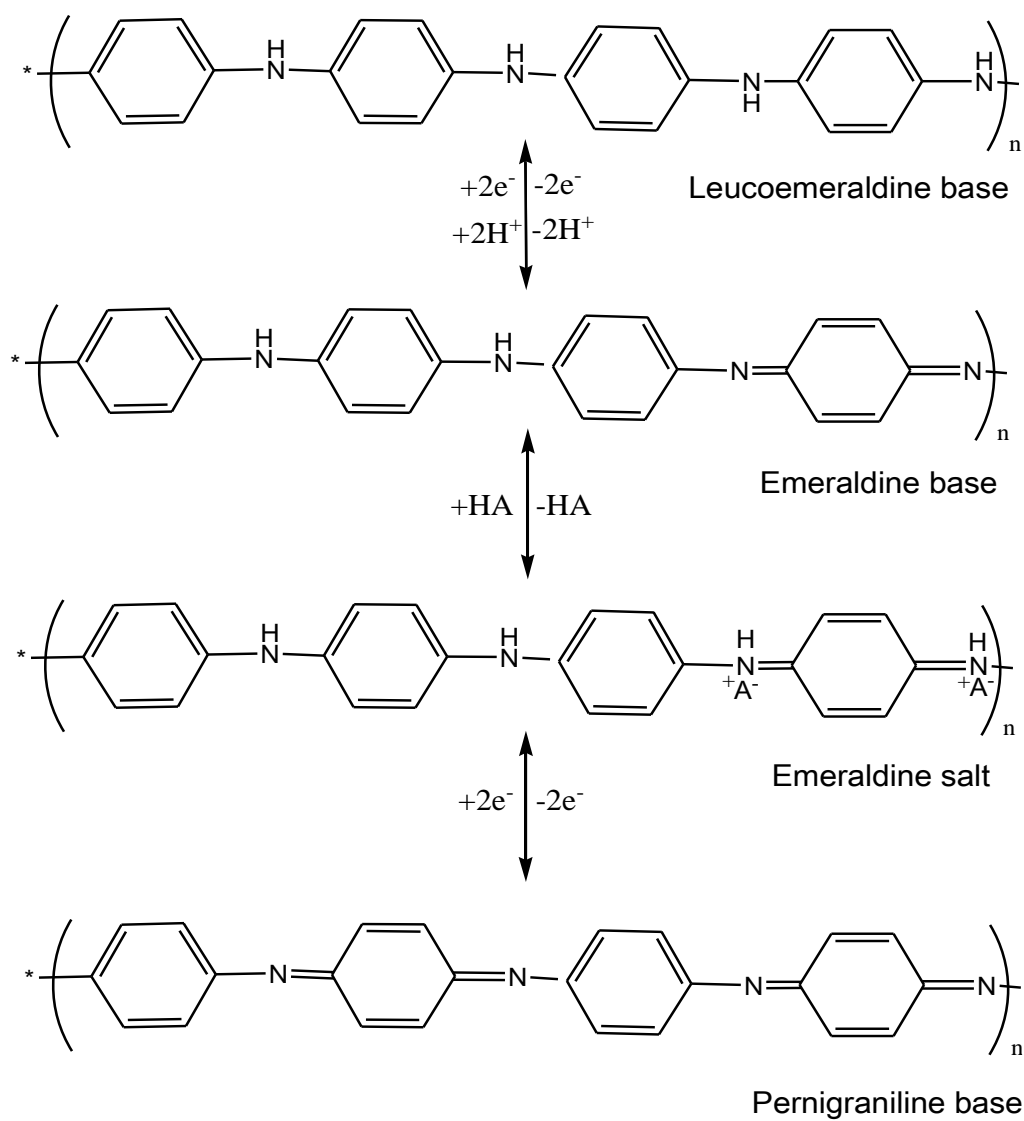


Figure 2.5: Structures of different forms of polyaniline.

Upon doping, polyaniline can be interconverted from one oxidation state to another [108]. The interconversions can be clearly deduced in Scheme 2.2 below.



Scheme 2.2: Schematic diagram showing change in oxidation states of polyaniline upon doping.

### **2.5.3. Synthesis of Polyaniline**

There are two general methods which are employed to synthesise conducting polymers; that is through electrochemical oxidation of the monomers or chemical oxidation of the monomers.

#### **2.5.3.1. Electrochemical polymerisation**

Electrochemical polymerisation or methods can be carried out by employing one of the three techniques. These is either by: (i) applying a constant current (galvanostatic), or (ii) applying a constant potential (potentiostatic), and lastly (iii) by applying a potential scanning/ cycling to the aqueous solution of aniline [109]. Electrochemical polymerisation of aniline is carried out in strongly acidic aqueous electrolyte using a radical polymerisation mechanism which allows a formation of anilinium radical cation by aniline oxidation on the electrode [110, 111]. Strongly, electrochemical polymerisations require the following factors:

- a) low pH which is needed for preparation of conductive polymeric materials,
- b) the dopant anion incorporated into polymer to determine the morphology, conductivity, rate of polymerisation growth and influences degradation process and
- c) inert electrode such as Pt, Au and graphite [112].

The electrochemical process is more advantageous since film properties such as thickness and conductivity can be controlled by the synthesis parameters, including the current density, substrate, pH, nature and concentration of electrolyte [113].

#### **2.5.3.2. Chemical polymerisation**

Like electrochemical polymerisation, chemical polymerisation is also carried out in an acidic medium such as hydrochloric acid (HCl) and formic acid which helps in giving unbranched polymer [114,115]. For chemical polymerisation to occur, a dopant is also

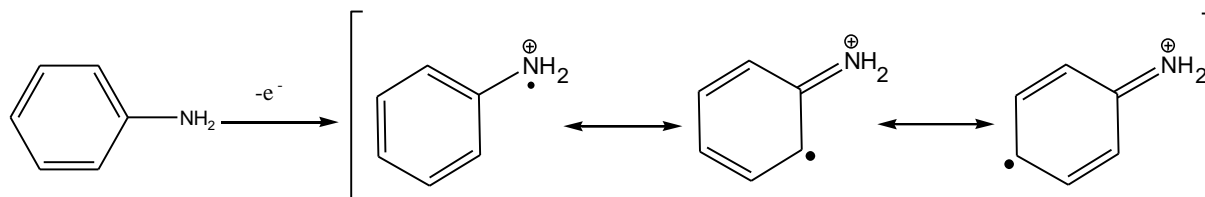
required. The dopant reagents used during this process are the oxidizing agents such as ammonium persulfate (APS), ferric chloride ( $\text{FeCl}_3$ ), hydrogen peroxide ( $\text{H}_2\text{O}_2$ ) and ceric nitrate and the principal function of the oxidant is to withdraw a proton from an aniline molecule, without forming a strong coordination bond either with the substrate intermediate or with the final product [116]. The mechanism taking place during polymerisation also is radical mechanism.

#### 2.5.4. Mechanism of Polymerisation

The general mechanism involved during polymerisation of aniline proceeds dominantly via radical mechanisms. Radical mechanisms can be subdivided into step such as initiation, chain propagation and termination step and in order to form stable intermediate, there must be resonance. The three different stages of polymerisation are illustrated below from Scheme 2.3- 2.5 below.

##### *Step 1: Initiation step (Oxidation of aniline monomer)*

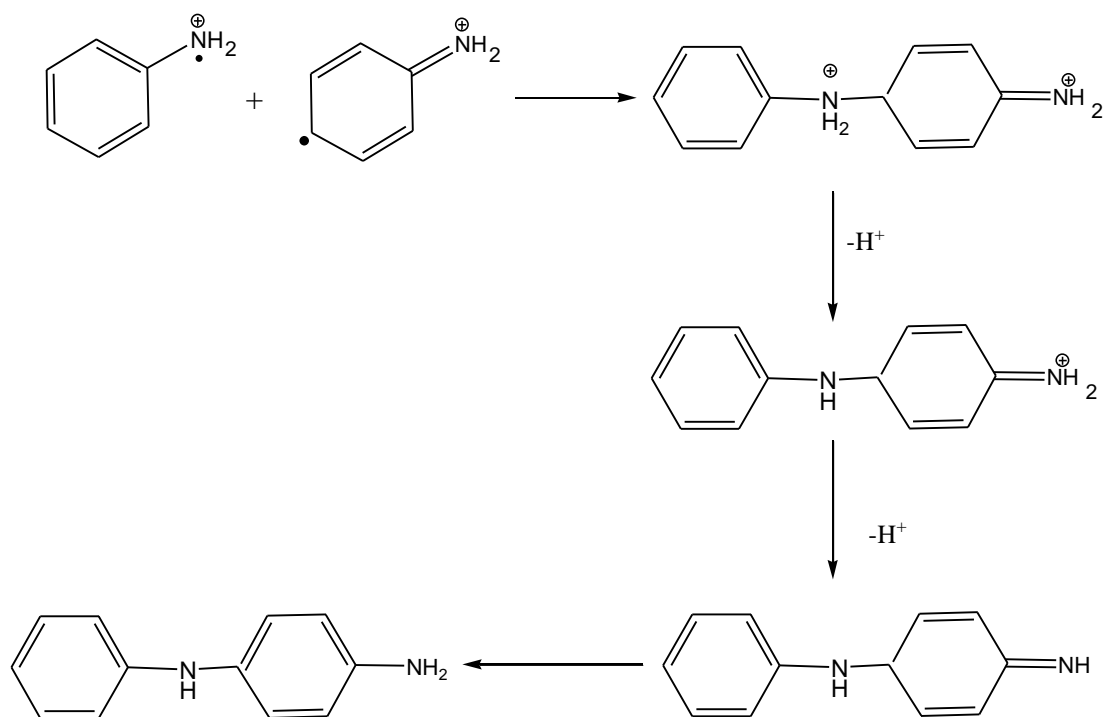
The initial step of aniline oxidative polymerisation is the generation of the aniline cation radical in the oxidation of aniline with an oxidant as shown in Scheme 2.3 below [117, 118]. The aniline cation radical undergoes resonance to attain the most stable and reactive radical cation which is free from steric hindrances [119]. This step is the slowest step in the reaction, hence it's deemed as the rate determining step in aniline polymerisation [120].



Scheme 2.3: Oxidation of aniline monomer during polymerisation of aniline.

### Step 2: Radical coupling and re-aromatisation

Head to tail coupling of the *N*- and *para*- radical cations (Scheme 2.4) takes place, yielding a dicationic dimer species. This dimer further undergoes the process of re-aromatisation which causes it to revert to its neutral state, yielding an intermediate referred to as *p*-aminodiphenylamine (PADPA) [121, 122]. These processes are also accompanied by the elimination of two protons.

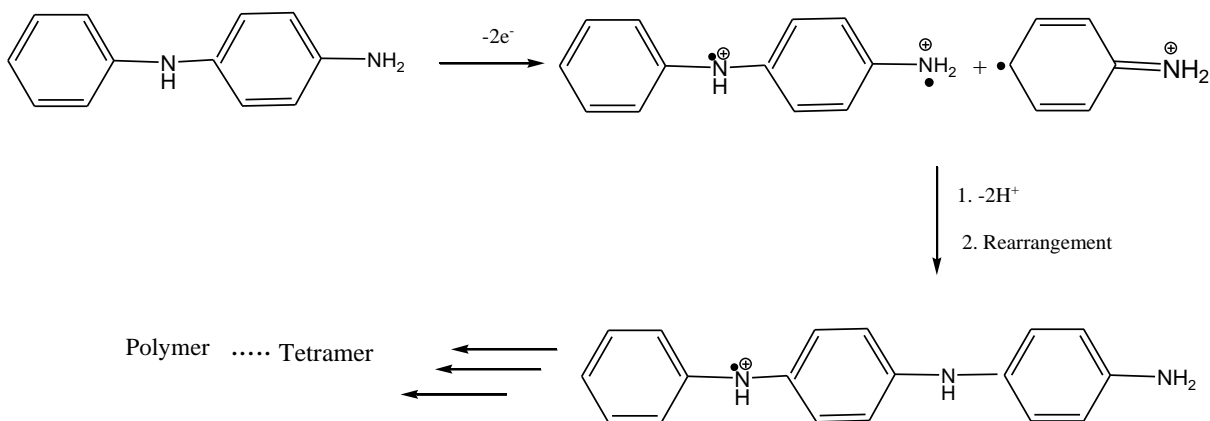


Scheme 2.4: Formation of a dimer.

### Step 3: Chain propagation

The dimers are immediately oxidized and then react with a stable aniline cation radical via an electrophilic aromatic substitution, followed by deprotonation and rearrangements to afford the trimer as seen in Scheme 2.5 [123]. The trimer further undergoes oxidation and reacts with aniline cation radical to form a tetramer and so on.





Scheme 2.5: Formation of a trimer and polymer formation.

### 2.5.5. Modification of Polyaniline

The study of polyaniline has become one of the most studied and reviewed conducting polymers followed by polypyrrole in the past decades [124]. PANI is highly conductive and has some other advantages. Firstly, the monomer aniline is very cheap as a basic industrial precursor to many chemicals and the synthesis of polyaniline is usually achieved through a very simple and inexpensive chemical or electrochemical oxidation processes. Secondly, polyaniline is environmentally stable and its thermal stabilities can reach up to 250 °C [125, 126]. However, the difficulties in processing of PANI and very low solubility in most of the available solvents, and its relatively poor mechanical properties decrease its performances and utilities in many applications [127]. Various methods have been used to address the processibility limitation of PANI. Those various methods includes:

- a) doping induced processibility of PANI using functionalized protonic acids,
- b) preparation of PANI composites with thermoplastic,
- c) homopolymerisation of aniline derivative e.g. ring or N-substituted anilines or their copolymers with aniline and
- d) incorporation of polar functional groups or electron withdrawing groups such as carboxyl, sulfo- and cyano- in the PANI backbone which tend to decrease

orbital overlap of the  $\pi$ -electrons and the nitrogen lone pair that may increase the solubility and readiness for processability [128].

Studies have been conducted whereby aniline derivative monomers such as sulfonated and carboxylated aniline have been used to form a substituted polyaniline to enhance the solubility properties of polymer backbone [129, 130].

### **2.5.6. Polyaniline Composites**

Organic–inorganic hybrid material remained an interesting area of research in the past due to its versatility in the range of applications and device performance. The properties of these hybrid materials are different from the organic part and corresponding inorganic nanoparticles depending on the type of bonding between them, but however capable of exhibiting the best properties of both the components [131, 132]. Polyaniline composites can be regarded as a material consisting of polyaniline and one or more components such as semiconductors, metal nanoparticle, organic compounds, inorganic compounds as well as biological and natural products in order to improve polymer backbone properties or extend its functionalities [133]. In order to prepare the composite materials successfully, several methods like physical mixing, sol–gel technique, *in situ* chemical polymerisation in the aqueous solution with the presence of polymer monomer and inorganic particles, emulsion technology, sonochemical process and irradiation technique are used [134]. Several studies reporting about the PANI and semiconductors as such ZnO and TiO<sub>2</sub> have been reported greatly for various applications mostly photocatalysis [135, 136]. The combination of nanocrystalline semiconductors such as TiO<sub>2</sub> and polyaniline is attractive because it gives a nanocomposite that exhibits excellent electrical, mechanical and optical properties such as surface hardness, modulus, strength, transparency and high refractive index [137]. In addition to polyaniline and semiconductor composite, a great attention was also paid on composite of polyaniline with graphene oxide and also carbon nanotubes (CNTs) [138, 139]. The general preparation of polyaniline-graphene composite involves two steps, i.e. polymerisation of aniline and reducing graphene

oxide (GO) to form reduced graphene oxide (rGO), then the composite can be prepared by chemical oxidative polymerisation of aniline in the presence of the rGO [140]. The interaction between PANI with GO/CNTs can be facilitated by several modes such as hydrogen bonding, ionic interactions and  $\pi$ - $\pi$  stacking interaction [141, 142]. Composites between polyaniline with inorganic porous materials such as metal organic frameworks have not studied intensively with only few reports on those composites. The polymer-metal containing dopant nanocomposites can provide highly porous structures together with large effective surface areas while some properties are highly dependent on the presence of additives [143, 144]. This study will provide also a platform on the novel synthesis of polyaniline with HKUST-1 (MOF-199) metal organic framework.

## **2.6. METAL ORGANIC FRAMEWORKS**

### **2.6.1. Background of Metal Organic Frameworks**

Metal organic frameworks (MOFs) or porous coordination networks/polymers are class of crystalline and porous compounds designed by employing a node (metal core/ion usually a transition metals) and multidentate/polytonic organic linker (usually connected through oxygen) resulting in a fascinating structural topology [145-147]. The combination of inorganic (metal ion/ cluster) and organic (linker) components provides endless possibilities. The sum of the physical and chemical properties as well as possible synergistic play between the two components provides exceptional properties of MOF [148]. Figure 2.6 below shows, the metal core or node serves as a connecting points and the organic linker serves as a bridging molecule to coordinatively connect metal -core resulting in the formation of a 3-D frameworks.

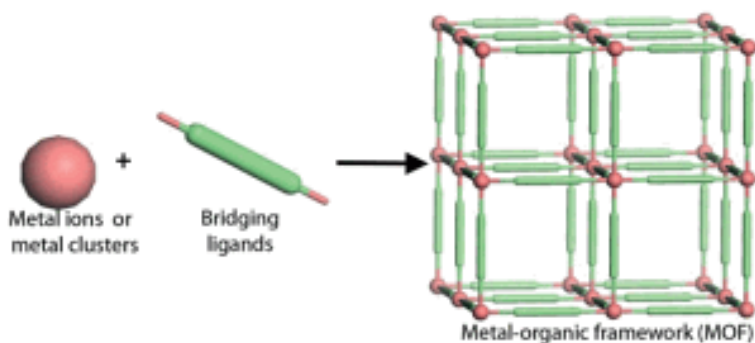


Figure 2.6: Metal organic framework structure.

Compared with other traditional porous materials such as zeolites and carbon materials, MOF are unique in terms of extraordinary porosities, tunable pores and diverse functional sites [149]. MOF materials are also characterised by having high surface area up to 5000 m<sup>2</sup>/g unlike other coordinated compounds such as zeolites and other inorganic-organic hybrids [150, 151]. The first MOF was reported by Yaghi and co-worker in 1995 for a newly synthesised copper-4,4'-bipyridyl complex that have the metal-organic interactions to become MOFs, these building units organise spatially in such a way that a crystalline porous regular size and shape on the nanometer scale are formed [152]. In the past decades, MOFs have gained a great attention with the number of MOF publications gradually increasing in different applications as illustrated in Figure 2.7 below [153]. The gradual increase in MOF research for different applications such as gas storage, luminescent, magnets, drug delivery and catalyst is because MOF have the characters of high stability and crystalline (ordered) structures, high surface area up to 5000 m<sup>2</sup>/g and porosities (pore volume of 1 g/cm<sup>3</sup>), excellent electrochemical, optical and electrical properties [154-157].

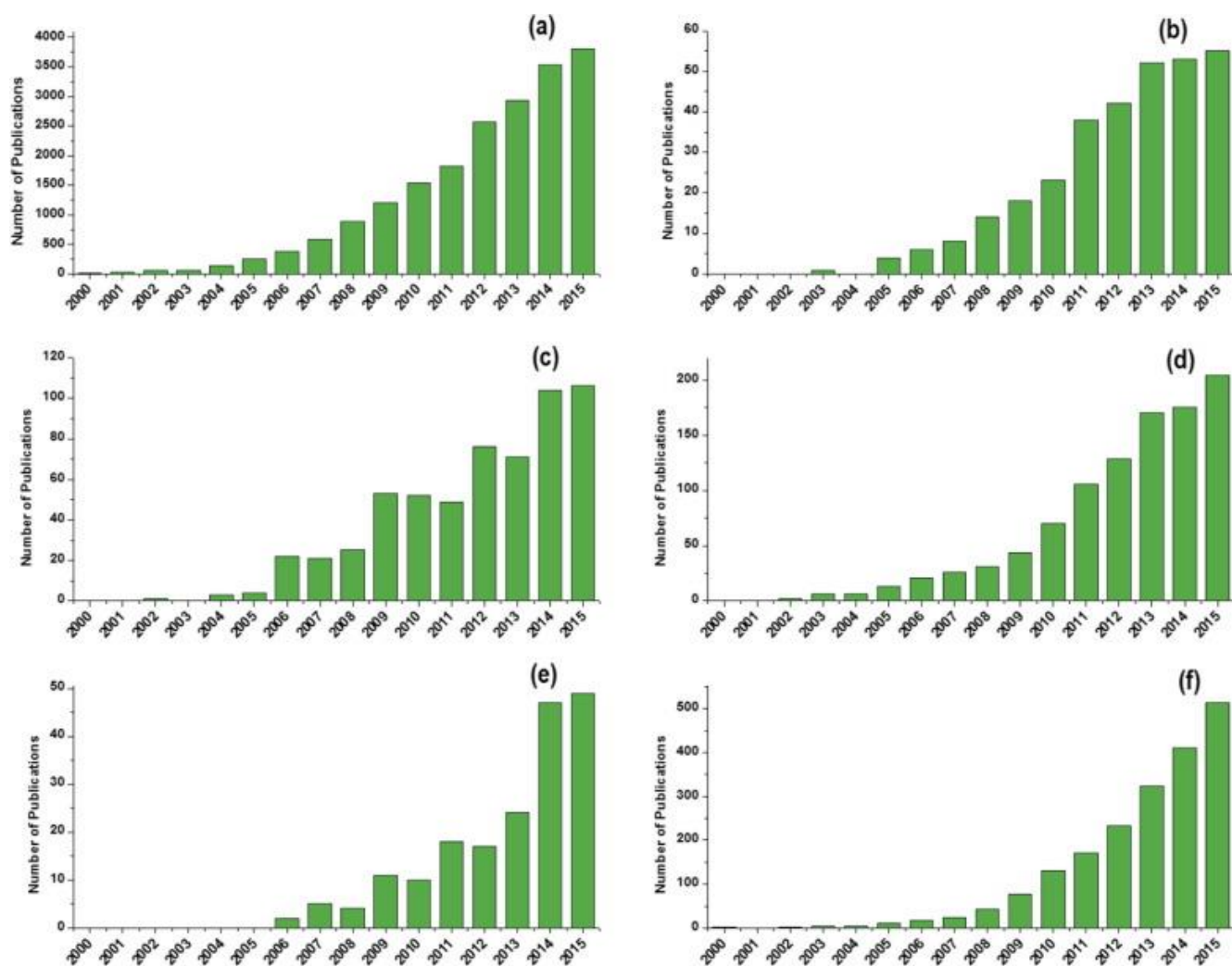


Figure 2.7: Year wise publication status from 2000 to 2015 of various aspects of MOFs (a) MOFs, (b) MOFs as luminescent materials, (c) MOFs for gas storage, (d) MOFs as magnets, (e) MOFs for drug delivery and (f) MOFs as catalyst [153].

## 2.6.2. Structure of a Metal Organic Framework

The two components that makes MOF structures are the secondary building units (SBUs), thus metal clusters or ions and organic molecule covalently linked to give a porous structure or framework. Different combination of the two components lead to an enormous number of MOFs with different geometries and coordination [158-160]. The choice of metal ions and organic linkers ultimately determines the coordination network to be attained, hence, below we look at metal ion and organic linker in details.

### 2.6.2.1. Metal ions/clusters

First row transitional metals are typically used as an inorganic component (metal core) of MOF materials. These transitional metals play a role in coordination sphere of the MOF material giving different geometries such as linear, T- or Y-shaped, tetrahedral, square-planar, square-pyramidal, trigonal-bipyramidal, octahedral, trigonal-prismatic, and pentagonal-bipyramidal as shown in Figure 2.8 below [153, 161, 162]. Different oxidation states of the metal result in different coordination numbers. For example, M (II), where M represent a transition metals of d electronic configurations, forms square-planar and tetrahedral geometries preferably, but it can also be found with other coordination numbers, depending on the organic linker used. Lanthanides-based MOFs are less reported in comparison with transition metal MOFS [163]. Lanthanide ions are also often used to generate new and unusual network topologies and flexible coordination geometries due to their large coordination numbers (usually from 7 to 10). These ions enables the formation of porous solids with Lewis centres and coordination unsaturated sites which can be advantageous during catalysis and luminescent applications [163, 164]. Alkali or s-block metal-based MOF are not extensively explored as compared to transition metals and lanthanide-based MOFs [165, 166].

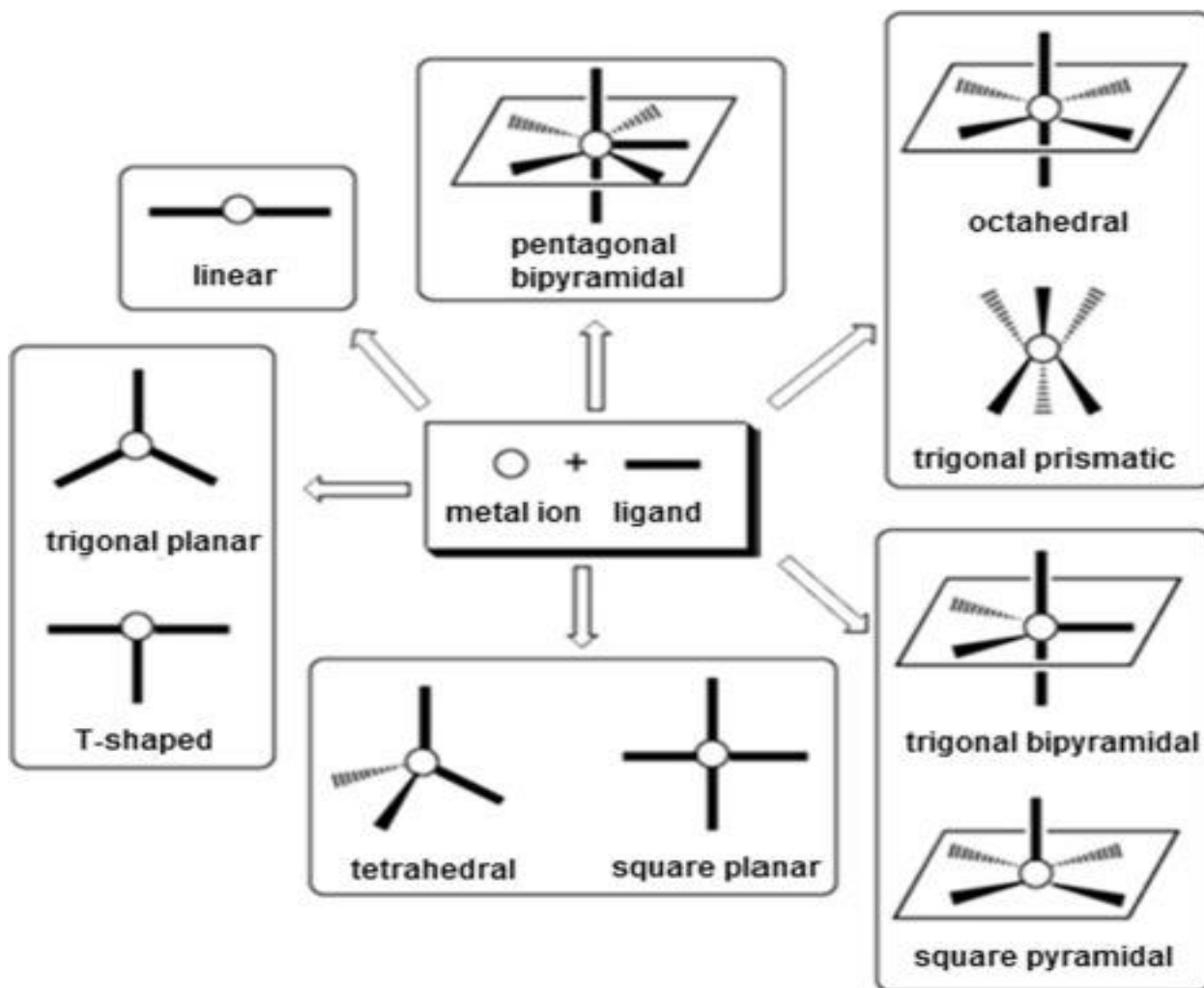


Figure 2.8: Coordination geometries of transition metal ions [153].

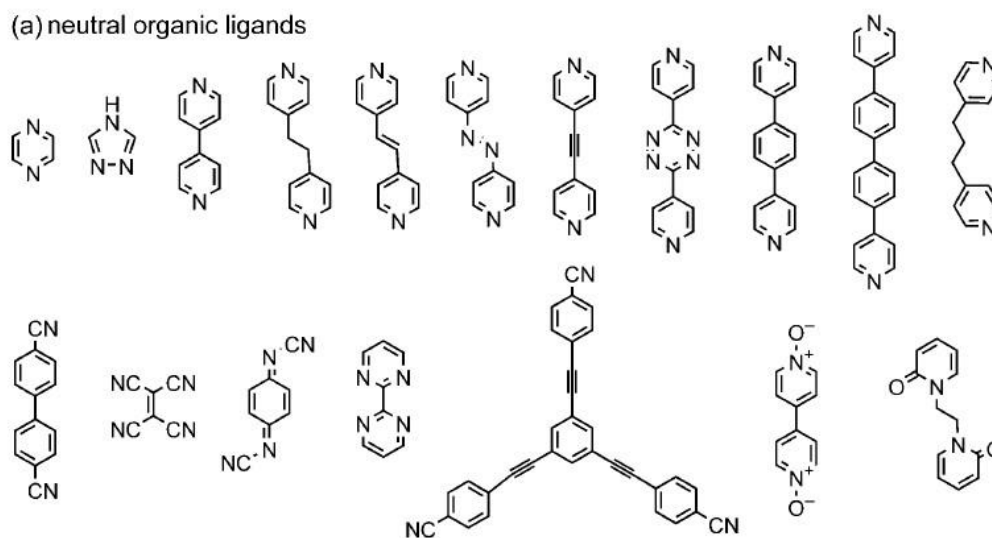
### 2.6.2.2. Organic linker

There are variety of choices to choose for organic linkers (Figure 2.9). The preferred organic linker is the one that will bring much stability to the MOF structure due to the rigidity of the backbone of the linker or ligand. The rigidity in backbone of the linker makes it easier to predict the network geometry and helps to sustain the open-pore structure after the removal of the included solvent. The organic linkers can be electrically neutral, anionic, or cationic. The most frequently used neutral organic linkers are pyrazine and 4,4' bipyridine (bpy) [163]. These linkers are especially useful

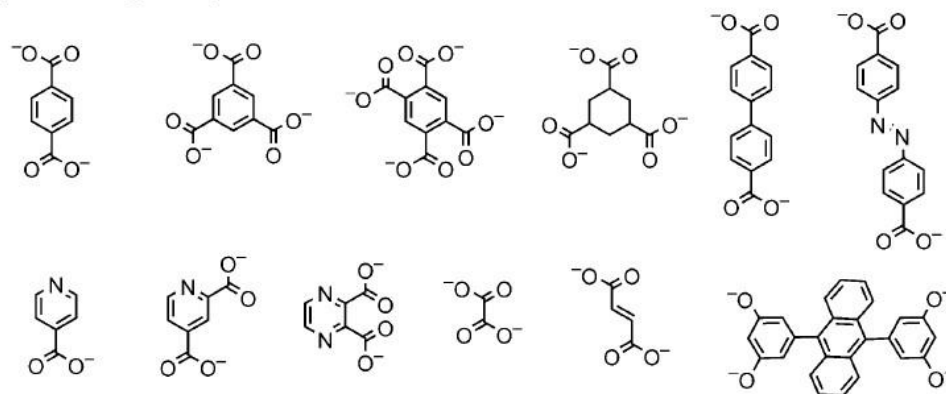
as pillars in the construction of pillared layer in 3D networks. The most widely used anionic linkers are carboxylates, because they have the ability to aggregate metal ions into clusters and thereby form more stable frameworks [161]. Cationic organic ligands are relatively little used, owing to their low affinities for cationic metal ions [165].



(a) neutral organic ligands



(b) anionic organic ligands



(c) cationic organic ligands

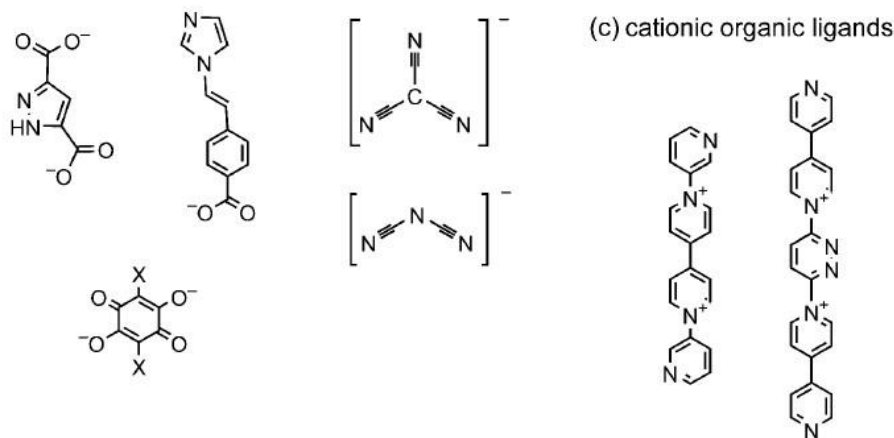


Figure 2.9: Potential polytopic organic molecules (neutral, anionic and cationic) as linkers in MOFs.

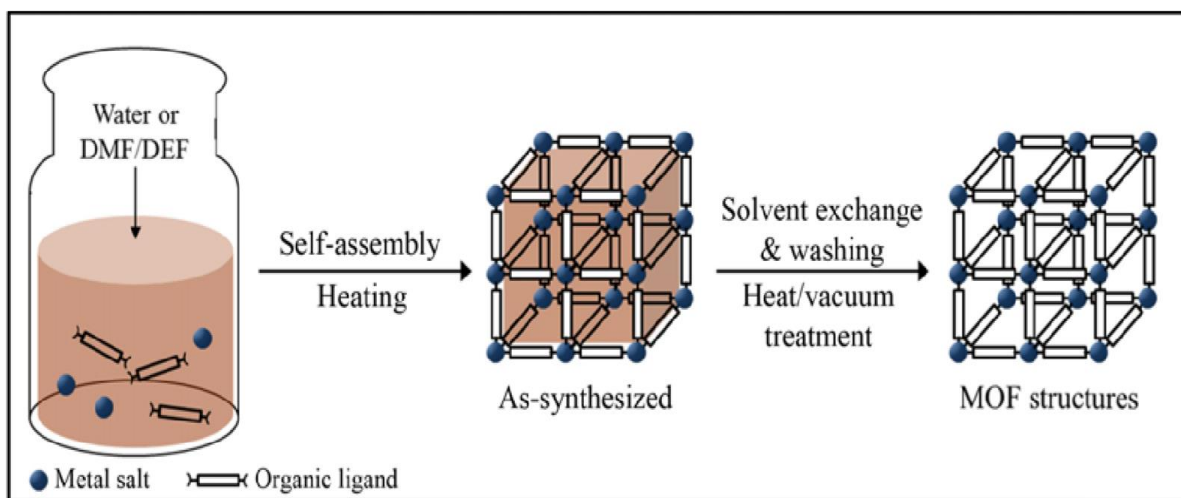
### **2.6.3. Design and Synthesis of Metal Organic Frameworks**

Methods of synthesis/design of MOFs lead to different topologies, morphologies and various physical properties. Facile synthesis of MOFs is very important not only for fundamental understanding but also viable for applications [167]. The main aspects of MOF synthesis is to establish synthetic conditions that can lead to a defined inorganic building blocks without decomposition of the organic linker. Simultaneously, the kinetics of the crystallization must be appropriate to allow nucleation and growth of the desired phase to take place [168]. Traditionally, MOFs have been generally prepared via hydrothermal or solvothermal synthesis routines by electrical heating in small scales, which take reaction time from several hours to days. Alternative synthesis methods were attempted afterward in an effort to shorten the synthesis time and to produce smaller and uniform crystals, such as microwave-assisted, microemulsion, electrochemical, and mechanochemical methods [169].

#### **2.6.3.1. Hydro/solvothermal method**

Hydro/solvothermal method is a method for preparing variety of materials such as metal, semiconductors, ceramics and polymers. In MOF, the reaction between the reagents usually metal core and organic linkers are dissolved in an organic solvent or water and the reaction proceeds by heating at temperatures above boiling point of solvent and pressure usually in an autoclave for hours or days to allow formation of desired MOF. When water is used as a solvent, the reaction is known as a hydrothermal. Despite the time drawback for this method, the reaction allows for the precise control over the size, shape distribution, well-crystallized solid on the nanoscale, efficient synthesis conditions and ability to control the morphology of material crystals [161, 170]. This is achieved by controlling the certain parameters during the reaction. The main parameters governing the solvothermal reaction are chemical and thermodynamical parameters [171]. Chemical parameters are the nature of the reagents and the selection of the solvents. The concentration and interaction of

the reagents play a role in controlling the shape of the nano-crystallites [172]. Solvents also play an important role in controlling the chemical mechanisms leading to the target MOF molecule. The thermodynamical parameters are the temperature, pressure and the reaction time. The temperature and pressure improve the solubility, the increase in these factors induces enhancement of the reagents-concentration into the solvent and then favours growing process in the formation of MOF [173-176]. The overall reaction for the synthesis of MOF using solvothermal process can be represented by the Scheme 2.6 below.

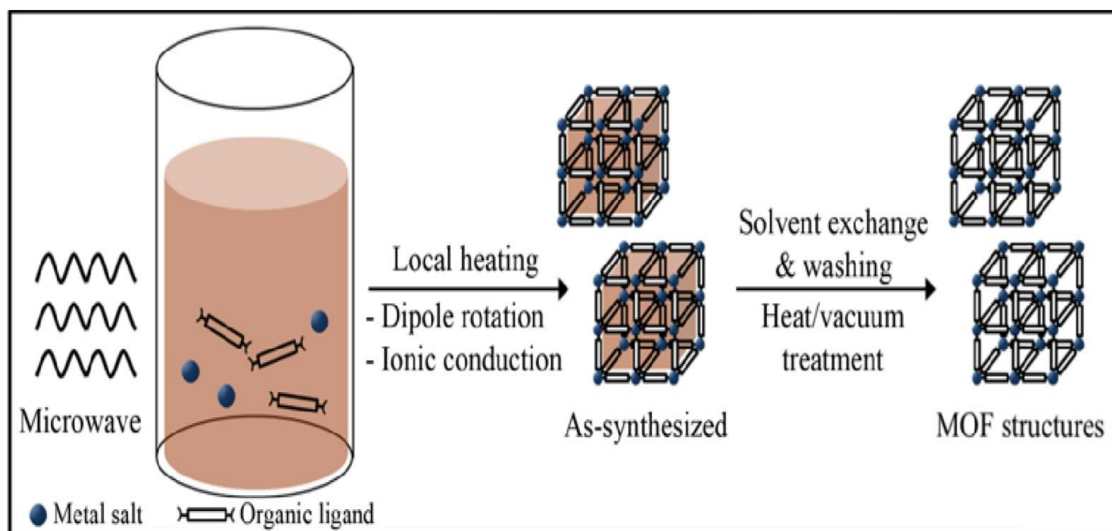


Scheme 2.6: Conventional solvothermal synthesis of MOF structures [169].

### 2.6.3.2. Microwave assisted method

Microwave assisted method is a rapid synthesis of nanoporous materials similar to synthesis of nanoporous materials under hydrothermal conditions. The synthesis (Scheme 2.7) involves placing the reagents in a suitable solvent and then transfers to the Teflon vessel, sealed and placed in microwave unit, and then subjected to heat for the appropriate time at a controlled temperature, thus it allows one to monitor temperature and pressure during synthesis. Microwave assisted synthesis relies on the interactions of electromagnetic waves with mobile electric charges such as polar solvent molecules or ions in the solution [177]. The synthesis has greater advantages than solvothermal synthesis as it accelerates the crystallization period, highly efficient,

have phase selectivity, narrow size particle and size distribution, and improves the purity of the product and facile morphology [177-179]. The quality of the crystals obtained by microwave assisted method is similar to those produced by regular solvothermal method [180-182]. Blanita and co-workers reported MOF-5 using both the solvothermal and microwave assisted methods, they observed similar XRD patterns [183]. The yield of MOF-5 using microwave assisted method and solvothermal method was 47% and 55% respectively. MOFs such as MIL-140(A) [184], Ni-DHTP [179] and MCF-23 [185] were also synthesised using microwave assisted method.

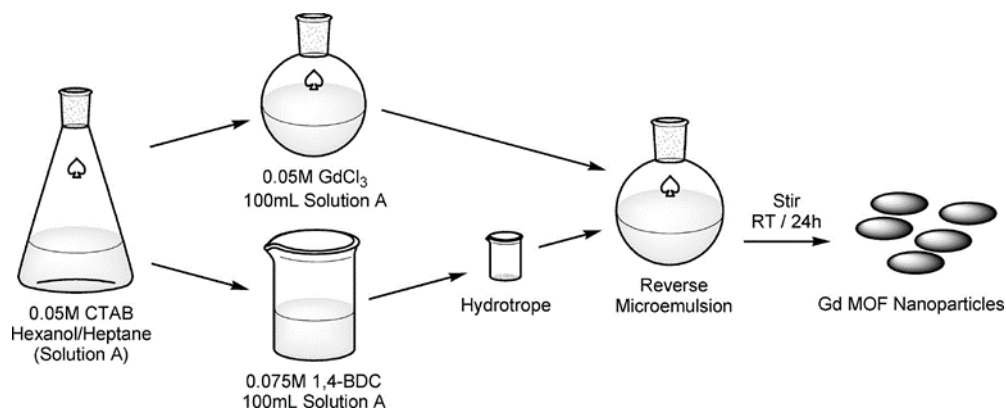


Scheme 2.7: Microwave-assisted solvothermal synthesis of MOF structures [169].

### 2.6.3.3. Microemulsion and reverse-phase microemulsion method

Microemulsion synthesis is a powerful method for obtaining ultrafine and nanometric particles taking advantages of the interfacial reactions providing shape control and confinement of the reaction zone at the same time [186]. The process is based on the use of microemulsions acting as chemical microreactors so as to control the particles size and shape. The use of a suitable emulsifier allows dispersing an aqueous solution

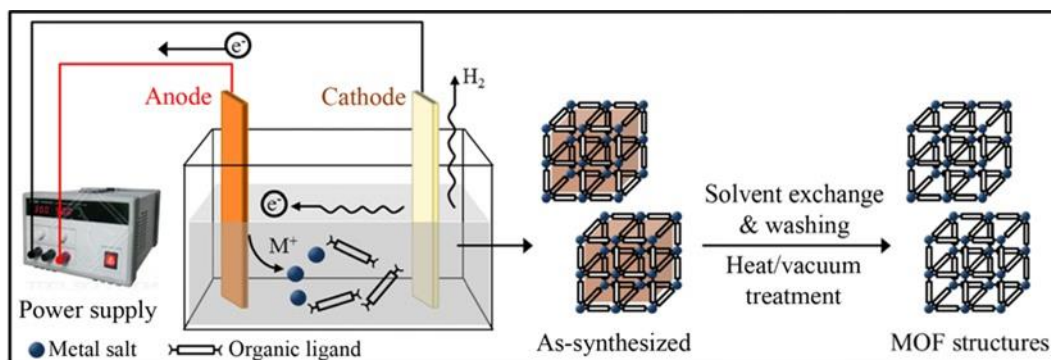
containing the metal precursor into the oil phase, forming nanosized droplets due to minimization of the surface energy [187]. Microemulsions are clear, thermodynamically stable, isotropic liquid mixtures of oil, water and surfactant, frequently in combination with a surfactant [188-190]. The use of surfactant as structure directing agent influence certain factors such as polydispersity of the particle, size and kind of size distribution [191]. The surfactants can be employed to stabilize oil- in-water dispersions through orientation of the molecules at the interface and significantly lowering interfacial free energy. Meanwhile, the interfacial free energy reduces according to the type and concentration of surfactant [192]. Figure 2.8 below shows route of synthesising Gadolinium-MOF nanoparticles via reverse-microemulsion method [193].



Scheme 2.8: General route to produce Gd MOF nanoparticles via a reverse microemulsion synthesis with a hydrotrope. Cetyltrimethylammonium bromide (CTAB) is employed as a surfactant and hexanol as a cosurfactant. Gadolinium(III) chloride and 1,4-benzenedicarboxylate (1,4-BDC) form the three-dimensional nanoscale metal organic framework [193].

#### 2.6.3.4. Electrochemical synthesis of MOF

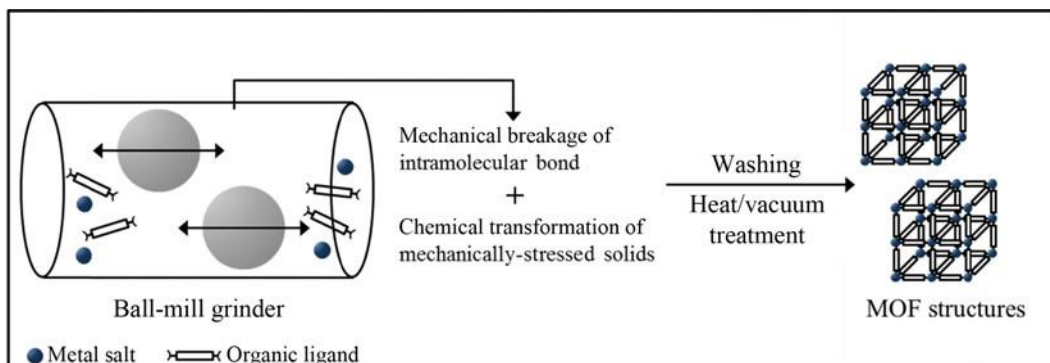
Electrochemical synthesis involves the use of electrochemical cell to prepare compounds. In order to synthesis, galvanic cell, potentiostat and two electrode set-up is required. Synthesis of MOF materials using this method is still a new topic and was first reported by researchers in BASF in 2005 [169]. Rather than adding metal salt during synthesis, the principle relies on supplying the metal ion by anodic dissolution to a synthesis mixture that contains the organic linker and an electrolyte [194]. Process such as metal deposition which can have an effect during synthesis of MOF is avoided by utilising protic solvent but it gives hydrogen gas [169]. Electrochemical methods have several advantages over traditional hydro/solvothermal and microwave-assisted methods that requires high temperature and long reaction time, such as, shorter synthesis times and milder synthesis conditions [169, 195, 196]. It also provides the possibility to influence the reaction directly in real-time, offering both more control and the ability to perform the synthesis in a continuous fashion. Furthermore, the localised nature of electrochemical methods allows the formation of directed thin films without the need to pre-treat the surface as is usually the case. The mild temperatures used during synthesis also reduce the effects of thermally induced film cracking, which is often a problem with hydrothermal methods [196]. The scheme 2.9 below shows the electrochemical synthesis of MOFs.



Scheme 2.9: Electrochemical synthesis of metal organic frameworks [169].

### 2.6.3.5. Mechanochemical synthesis of MOF

In mechanochemical synthesis, there is a mechanical breakage of intramolecular bonds followed by a chemical transformation [169, 197]. The mechanisms of mechanochemical transformations are often complex and different from usual thermal or photochemical mechanisms. The method of ball milling which allows substantial improvement in energy efficiency as compared to conventional methods is widely used process in which mechanical force is used to achieve chemical processing and transformations [158, 198]. The advantages of mechanochemical synthesis is that reactions can be carried out at room temperature under solvent free conditions, which is especially advantageous when organic solvents can be avoided. Short reaction times, normally in the range of 10-60 min, can lead to quantitative yields and higher surface areas, and generally products containing small particles are obtained [153, 199, 200]. Moreover, in some cases metal salts can be replaced by metal oxides as a starting material, which results in the formation of water as the only side product. Scheme 2.10 below shows mechanochemical synthesis of MOF structures [169].



Scheme 2.10: Mechanochemical synthesis of MOF structures [169].

## 2.7. ANALYTICAL TECHNIQUES

Analytical methods are set of techniques which are used to determine the chemical, physical or optical nature of a material and also quantify certain species within the material. This analytical technique can be separated into different categories such as spectroscopy, microscopy, physical and electroanalytical methods.

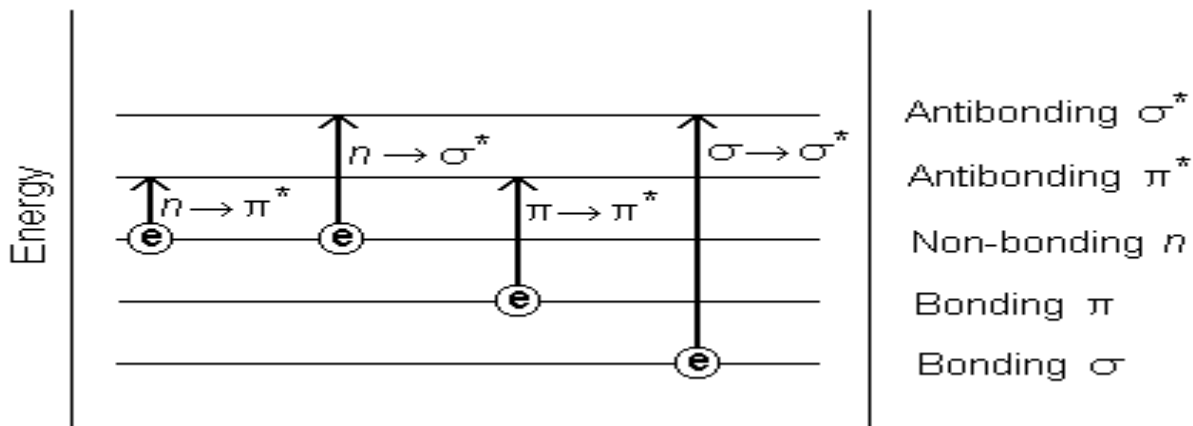
### 2.7.1. Spectroscopy

Spectroscopy is the study of the interaction of electromagnetic radiation in all its forms with matter which can be used for both quantitative and qualitative analysis. The interaction might give rise to electronic excitations, (UV), molecular vibrations (IR) or nuclear spin orientations (NMR).

#### 2.7.1.1. Ultraviolet-visible spectroscopy

Ultraviolet-visible (UV-vis) spectroscopy refers to absorption or reflectance spectroscopy which uses light in the ultraviolet-visible region. This means it uses light in the visible and adjacent (near-UV and near-infrared) ranges. Basically, it is used to study the electronic transitions that molecules undergo. In principle, a light is irradiated on a molecule. The  $\pi$  electrons or non-bonding electrons absorb the energy in the form of ultraviolet or visible light and excited from ground state to higher energy state [201-203]. The transitions are summarised in the Scheme 2.11 below.





Scheme 2.11: Possible electronic transitions of  $\pi$ ,  $\sigma$ , and  $n$  electrons.

The energy of the ultra-violet radiation that are absorbed is equal to the energy difference between the ground state and higher energy states and are given by the following equation [204]:

$$E = h\nu \quad (2.9)$$

where,  $E$  is the energy,  $h$  is the Planck constant and  $\nu$  is the frequency. Since the study of spectroscopy deals with energy coming from light and also the molecules in question absorb light at a certain wavelength, equation one can be arranged to [204]:

$$E = \frac{hc}{\lambda} \quad (2.10)$$

where  $c$  is the speed of light and  $\lambda$  is the wavelength the molecules or compound absorbs maximally at it. The reading the spectrometer which is an instrument used to measure the intensity of light absorbed is called absorbance denoted by  $A$ , which can be related by the amount of light transmitted and be given by the following equation [204]:

$$A = -\log T \quad (2.11)$$

where T represent transmittance of light. It is routinely used in analytical chemistry for qualitative and quantitative analysis. Quantitative information of materials can be determined in relation to Beer's law which state that: *when a beam of monochromatic light is passed through a solution of an absorbing substance, the rate of decrease of intensity of radiation with thickness of the absorbing solution is proportional to the incident radiation as well as the concentration of the solution.* The mathematical expression of the law is given by [204]:

$$A = abc \quad (2.12)$$

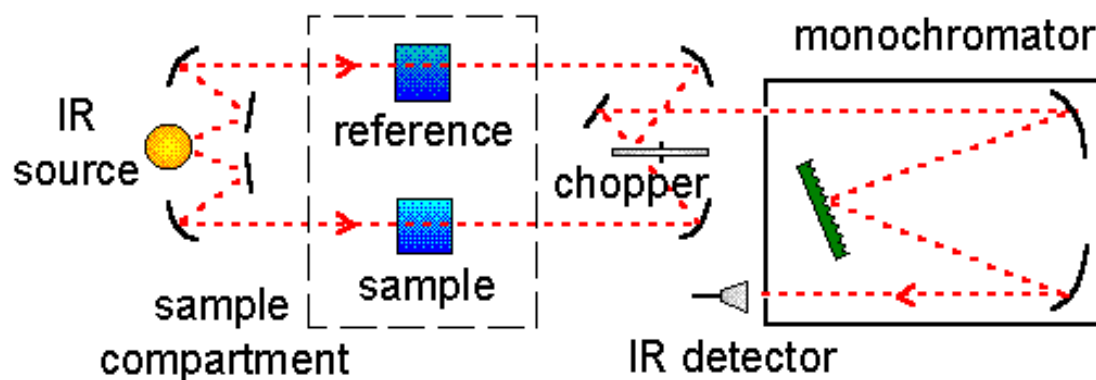
where A is the absorbance, a is the absorptivity constant, b is the path length of a cell and c is the concentration of analyte. Since the concentration of the analyte is commonly measured in molarity, M (moles per litre), the Beer's law can be written as follows [204]:

$$A = \epsilon bc \quad (2.13)$$

where  $\epsilon$  the molar absorptivity of the material which can be used to determine the conductivity of the materials. In this research the UV/VIS spectroscopy was used to determine the optical properties of the materials and also band gab of the materials. Formation of composite was monitored by examining the types of effects such as bathochromic effect (red shift), hypsochromic (blue shift), hyperchromic and hypochromic effect.

### 2.7.1.2. Fourier transform infrared spectroscopy

Fourier transform infrared spectroscopy (FTIR) is a technique which is used to obtain an infrared spectrum of absorption or emission of a solid, liquid, or a gas. FTIR relies on the fact that the most molecules absorb light in the infra-red region of the electromagnetic spectrum [203, 204]. This absorption corresponds specifically to the bonds present in the molecule. The frequency range are measured as wave numbers typically over the range  $4000 - 400 \text{ cm}^{-1}$ . The background emission spectrum of the IR source is first recorded which will be used to correct the spectra reading of analyte, followed by the emission spectrum of the IR source with the sample in place [202]. The ratio of the sample spectrum to the background spectrum is directly related to the sample's absorption spectrum. The resultant absorption spectrum from the bond natural vibration frequencies indicates the presence of various chemical bonds and functional groups present in the sample. Scheme 2.12 shows representation of the basic components of FTIR.



Scheme 2.12: Basic components of FTIR [205].

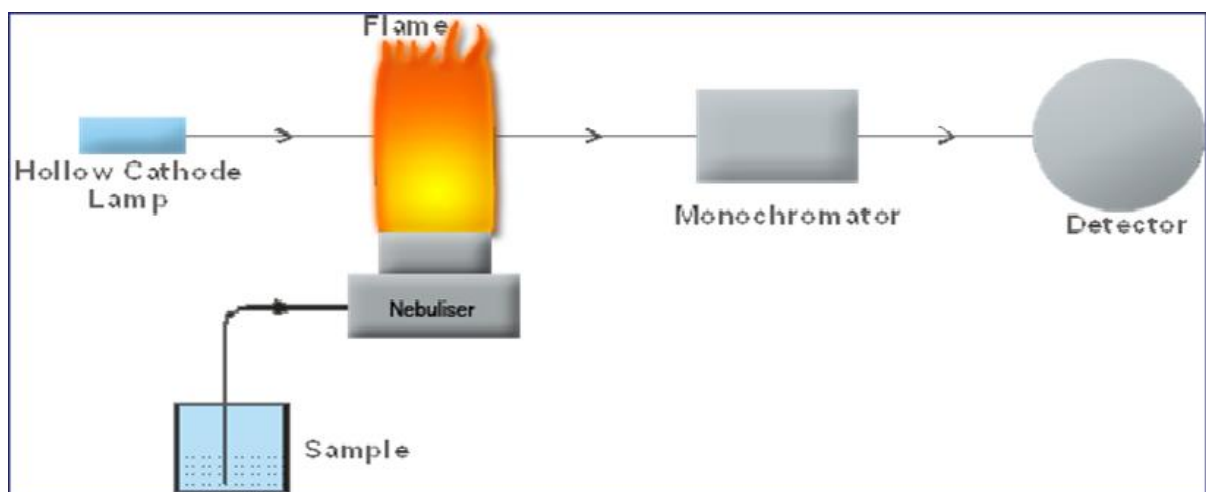
FTIR is mainly used for qualitative analysis in which the functional groups of the sample is determined. In this work FTIR was used to observe functional groups present in the polyaniline, metal organic framework and mainly overlaps and appearance of new vibrations during composite formations.

### **2.7.1.3. Raman spectroscopy**

Raman spectroscopy is a spectroscopic technique used to observe vibrational, rotational, and other low-frequency modes in a system which mostly appears in the fingerprint regions of FTIR [201]. IR inactive molecules such as metal oxides vibrations can also be determined using this type of spectroscopy. It is mostly employed in chemistry to provide a fingerprint by which molecules can be identified. This technique offers several advantages for microscopic analysis. Since, it is a scattering technique, specimens do not need to be fixed and that its spectra can be collected from a very small volume ( $<1\mu\text{m}$  in diameter) [204]. However, it faces difficulties when separating the weak inelastic scattered light from the intense Rayleigh scattered laser light. It is most applicable in chemistry since vibrational information is specific to the chemical bonds and symmetry of molecules. In this work it was used to determine the vibrations of Cu-O vibration during composite formations.

### **2.7.1.4. Flame atomic absorption spectroscopy**

Atomic absorption spectroscopy (AA) is a spectroanalytical procedure for the quantitative determination of chemical elements using the absorption of optical radiation (light) by free atoms in the gaseous state [201]. In principle, the analyte interact with flame which converts the aerosol from nebuliser (sample injection system) into an atomic vapour. The ground state atom absorbs light of a specific wavelength from hollow cathode lamp (HCL) or electrodeless discharge lamp (ECL) as it enters excited state [201, 202]. Quantitative analysis is done by measuring the amount of light absorbed. The Scheme below shows the working principle and instrumental components of AAS using HCL.



Scheme 2.13: Working principles and basic components of AA [206].

In analytical chemistry the technique is used for determining the concentration of a particular element (analyte) in a sample to be analysed. It requires standards with known analyte to establish the relation between the measured absorbance and the analyte concentration and it strictly adheres to the Beer-Lambert Law [201]. It has many uses in different areas of chemistry such as clinical analysis, water analysis, and pharmaceuticals. It possesses great advantages such as having high sample throughput, easy to use, has high precision, and is inexpensive. Its main disadvantages are that it analyses only solutions, one element at time, less sensitive, and requires large sample quantities (1-3 ml) [201, 204]. In this work, it was used for elemental analysis of Cu metal in MOF and composites.

## **2.7.2. Microscopy**

Microscopic techniques are set of methods which are used to view objects that cannot be detected by naked eye or simple spectroscopic techniques such as UV-vis or IR.

Microscopy can be categorized into three sections, namely:

- a) optical microscopy which uses visible light to produce enlarged images,
- b) scanning probe microscopy that involves using a probe to scan object and
- c) electron microscopy that uses an electron beams to create an image of an object.

The next section focuses on the electron microscopy which have been used in this work.

### **2.7.2.1. Scanning electron microscopy**

Scanning electron microscopy (SEM) is a powerful method that utilises focused beam of electrons for high-resolution imaging of surfaces of the materials. The basic principle is that a beam of electrons is generated by a suitable source, typically a tungsten filament or a field emission gun. The electron beam is accelerated through a high voltage (e.g.: 20 kV) and pass through a system of apertures and electromagnetic lenses to produce a thin beam of electrons [204, 207]. The beam scans the surface of the specimen by means of scan coils. Electrons are emitted from the specimen by the action of the scanning beam and collected by a suitably-positioned detector [204]. In this study, the SEM technique was employed for investigation of the morphology of the synthesised materials.

### **2.7.2.2. Transmission electron microscopy**

Transmission electron microscopy (TEM) is a very powerful tool for material science. A high energy beam of electrons is shone through a very thin sample, and the interactions between the electrons and the atoms can be used to observe features such as the crystal structure and features in the structure like dislocations and grain boundaries [204]. TEM can be used to study the growth of layers, their composition and defects in semiconductors. High resolution can be used to analyse the quality, shape, size and density of quantum wells, wires and dots. In principle, the electrons pass through multiple electromagnetic lenses. These solenoids are tubes with coil wrapped around them. The beam passes through the solenoids, down the column, makes contact with the screen where the electrons are converted to light and form an image. The image can be manipulated by adjusting the voltage of the gun to accelerate or decrease the speed of electrons as well as changing the electromagnetic wavelength via the solenoids [205]. The coils focus images onto a screen or photographic plate. During transmission, the speed of electrons directly correlates to electron wavelength; the faster electrons move, the shorter wavelength and the greater the quality and detail of the image. The lighter areas of the image represent the places where a greater number of electrons were able to pass through the sample and the darker areas reflect the dense areas of the object. These differences provide information on the structure, texture, shape and size of the sample [203, 204, 207]. To obtain a TEM analysis, samples need to have certain properties. They need to be sliced thin enough for electrons to pass through, a property known as electron transparency. Samples need to be able to withstand the vacuum chamber and often require special preparation before viewing. In this study, TEM was used for internal morphological studies of the materials.

### 2.7.3. Physical Methods

Physical methods are techniques which are used to determine the physical properties of the materials or compounds. This technique helps in determining the crystallinity of the compounds, surface area and also the mechanical and thermal stability of the materials. In principles this method uses the spectroscopy and microscopy techniques.

#### 2.7.3.1. X-ray diffraction

X-ray diffraction (XRD) is an analytical technique that is used primarily for phase identification of a crystalline material and can provide information on unit cell dimensions. This technique is based on constructive interference of monochromatic X-rays and a crystalline sample of which interaction of the incident rays with the sample induces constructive interference such that Bragg's law is satisfied which is given by [202]:

$$n\lambda = 2d\sin\theta \quad (2.14)$$

where  $\lambda$  designates the wavelength of the radiation beam,  $d$  is the interplanar spacing between two diffracting lines,  $\theta$  is the diffraction angle, and  $n$  is an interger usually equal to 1. XRD is most widely used for identification of unknown crystalline materials such as minerals and inorganic compounds, measurements of sample purity, characterisation of crystalline materials, and determination of unit cell dimensions [204]. The technique possesses numerous advantages such as being powerful and rapid (<20 min) for identification of unknown materials and data interpretation is relatively straight forward. However, its disadvantage is that peak overlay may occur and worsens for high angle reflections and that for fixed materials, detection limit is ~2% of sample [207]. In this study, XRD was used to fingerprint the materials using the known reference spectra and also monitor the composite formation.



### **2.7.3.2. Thermogravimetric analysis**

Thermogravimetric analysis (TGA) is a method of thermal analysis in which changes in physical and chemical properties of materials are measured as a function of increasing temperature (with constant heating rate). It reveals information about physical phenomena such as vaporization, sublimation, adsorption, and desorption. Likewise it also reveals information about chemical phenomena such as chemisorption, desolvation, and decomposition [202]. TGA is commonly used to determine selected characteristics of materials that exhibit either mass loss or gain due to decomposition, oxidation, or loss of volatiles (such as moisture). Its common applications are (i) determination of organic content in a sample, and (ii) studies of degradation mechanisms and reaction kinetics [202]. Again TGA can be used to evaluate the thermal stability of a material. In simple terms, if a species is thermally stable, there will be no observed mass change. Advantages of this method are that it provides very little room for instrumental error and does not require a series of standards for calculation of an unknown. Its disadvantage is that it only provides for the analysis of a single element, or a limited group of elements at a time. It was used to estimate the thermal stability of the materials.

### **2.7.4. Electroanalytical Methods**

Electroanalytical methods are a class of techniques in analytical chemistry which study an analyte by measuring the potential (volts) and/or current (amperes) in an electrochemical cell containing the analyte. These methods can be broken down into several categories depending on which aspects of the cell are controlled and which are measured. The three main categories are potentiometry (the difference in electrode potentials is measured), coulometry (the cell's current is measured over time), and voltammetry (the cell's current is measured while actively altering the cell's potential) [202, 204]. Electroanalytical techniques follow the basics of electrochemistry whereby redox reactions occurs during operations and uses the electrochemical cell

principles. This means that there is an electron loss and gain between the species in question. The simplest electrochemical cell will consist of two electrodes immersed in an electrolyte solution which can be separated by a salt bridge. Chemical reactions mostly occur on the surface of the electrodes giving several half reactions. Mostly three compartment electrodes are used which are placed in an electrolytic solution in a glass [207, 208]. The reactions occur on the surface of the working electrode. There are several types of working electrode which are commonly used, thus glassy carbon, gold and mercury working electrodes. During operations, there must be a standardization process which occurs in reference electrode. The potential in reference electrode is fixed and the potential change is monitored on working electrode. The most commonly used reference electrode are saturated calomel electrode (SCE) and silver/silver chloride (Ag/AgCl) electrode. Then lastly there is an auxiliary electrode which is known as counter electrode. It serves as a sink for electrons so that the current can be passed from the external circuit. The electroanalytical technique used in this work is voltammetry, so next sections will review types of voltammetry methods used in study.

#### **2.7.4.1. Cyclic voltammetry**

Cyclic voltammetry (CV) is an electrochemical technique which measures the current that develops in an electrochemical cell under conditions where voltage is in excess of that predicted by the Nernst equation [204, 207, 208]. The CV (Figure 2.10) is performed by cycling the potential of a working electrode, and measuring the resulting current. In this technique it is compulsory to have a working, reference, and counter electrode, and an electrolytic solution to be added to the sample solution to ensure sufficient conductivity [208]. It is often used to study a variety of redox processes, to determine the stability of reaction products, the presence of intermediates in redox reactions, reaction and electron transfer kinetics and the reversibility of a reaction [207]. The CV was used to evaluate the electrochemical properties of the materials as well as the hydrogen evolution reaction for hydrogen production.

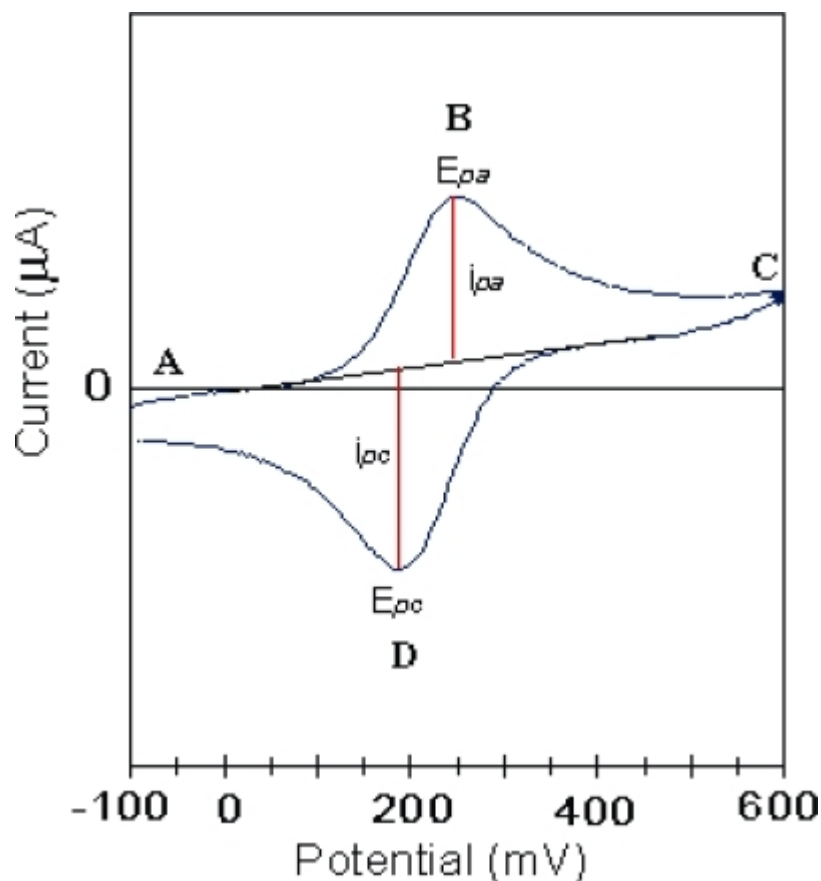


Figure 2.10: Typical cyclic voltammogram showing the peak cathodic and anodic current respectively for a reversible reaction [209].

#### 2.7.4.2. Square wave voltammetry

Square wave voltammetry (SWV) is a form of linear potential sweep voltammetry which has found numerous applications in various fields. In SWV experiments the current at a working electrode is measured while the potential between the working electrode and a reference electrode is swept linearly in time. Its advantage is that it can be used to perform an experiment much faster than the other electrochemical techniques [208]. SWV suppresses background currents much more effectively than cyclic voltammetry. The SWV was used in this work to support the CV analysis for

investigation of electrochemical properties of the materials as well as the hydrogen evolution reaction for hydrogen production.

## **2.8. CONCLUSIONS**

In summary, this chapter presented a review of literature related on hydrogen fuel cell. The chapter introduced basic concepts of hydrogen fuel cell technology, it also highlighted the pathways and mechanisms involved in production of hydrogen. Hydrogen gas offers a great advantage in transforming from fossil fuel energy dependency to a much feasible energy sources. However, the future utilisation of hydrogen as an alternative energy carrier, there is a need to solve key challenges encountered in hydrogen economy, thus hydrogen production and storage. Hydrogen can be stored in three forms/ states, gaseous, liquid and solid storage. Electrocatalysis exhibits several advantages over other hydrogen production methods; hence, strategies of enhancing hydrogen evolution reaction using a conduction polymer or metal organic framework are also discussed. From the literature that has been surveyed, it is evident that HER is powerful tool and has hydrogen production applications. No known attempts were made to study the interaction of MOF to the backbone of polyaniline for HER productivity. The electrocatalyst modification technology on the basis of MOF offers the ability to enhance HER generation for hydrogen fuel cell applications. In-depth experimental studies of performance of these electrocatalysts will lead to deeper understand of hydrogen evolution reaction mechanism, in turn, to develop the novel HER catalysts. The literature review also presented that electrochemistry and photophysical properties of the HER material can be evaluated using CV, SWV, UV-vis, FTIR, Raman, XRD, SEM, TEM and TGA.

## 2.9. REFERENCES

- [1] Sakintunaa, B., Lamari-Darkrimb, F., Hirscher, M. Metal hydride materials for solid hydrogen storage: A review. *International Journal of Hydrogen Energy* 32 (2007) 1121 – 1140.
- [2] Dutta, S. A review on production, storage of hydrogen and its utilisation as an energy resource. *Journal of Industrial and Engineering Chemistry* 20 (2014) 1148–1156.
- [3] Cipriani, G., Dio, V.D., Genduso, F., La Cascia, D., Liga, R., Miceli, R., Galluzzo, G.R. Perspective on hydrogen energy carrier and its automotive applications. *International Journal of Hydrogen Energy* 39 (2014) 8482-8494.
- [4] Stojic, D.L., Marceta, M.P., Sovili, S.P., Miljanic, S.S. Hydrogen generation from water electrolysis—possibilities of energy saving. *Journal of Power Sources* 118 (2003) 315–319.
- [5] Sherif, S.A., Barbir, F., Veziroglu, T.N. Towards a Hydrogen Economy. *The Electricity Journal* 18 (2005) 62–76.
- [6] Mazloomi, K., Chandima Gomes, C. Hydrogen as an energy carrier: Prospects and challenges. *Renewable and Sustainable Energy Reviews* 16 (2012) 3024–3033.
- [7] Midilli, A., Ay, M., Dincer, I., Rosen, M.A. On hydrogen and hydrogen energy strategies I: current status and needs. *Renewable and Sustainable Energy Reviews* 9 (2005) 255–271.
- [8] Ross, D.K. Hydrogen storage: The major technological barrier to the development of hydrogen fuel cell cars. *Vacuum* 80 (2006) 1084–1089.
- [9] Yilanci, A., Dincer, I., Ozturk, H.K. A review on solar-hydrogen/fuel cell hybrid energy systems for stationary applications. *Progress in Energy and Combustion Science* 35 (2009) 231–244.
- [10] Haile, S.M. Fuel cell materials and components. *Acta Materialia* 51 (2003) 5981–6000.
- [11] Steele, B.C.H., Heinzel, A. Materials for fuel-cell technologies. *Nature* 414 (2001) 345-352.

- [12] Fayaz, H., Saidur, R., Razali, N., Anuar, F.S., Saleman, A.R., Islam, M.R. An overview of hydrogen as a vehicle fuel. *Renewable and Sustainable Energy Reviews* 16 (2012) 5511–5528.
- [13] Balat, M. Potential importance of hydrogen as a future solution to environmental and transportation problems. *International Journal of Hydrogen Energy* 33 (2008) 4013–4029
- [14] Momirlana, M., Veziroglu, T.N. The properties of hydrogen as fuel tomorrow in sustainable energy system for a cleaner planet. *International Journal of Hydrogen Energy* 30 (2005) 795 – 802.
- [15] Haryanto, A., Fernando, S., Murali, N., Adhikari, S. Current status of hydrogen production techniques by steam reforming of ethanol: A Review. *Energy Fuels* 19 (2005) 2098-2106.
- [16] Choudhary, T.V., Goodman, D.W. Co-free production of hydrogen via stepwise steam reforming of methane. *Journal of Catalysis* 192 (2000) 316-321.
- [17] Heinzl, A., Vogel, B., Hübner, P. Reforming of natural gas—hydrogen generation for small scale stationary fuel cell systems. *Journal of Power Sources* 105 (2002) 202-207.
- [18] Barelli, L., Bidini, G., Gallorini, F., Servili, S. Hydrogen production through sorption-enhanced steam methane reforming and membrane technology: A review. *Energy* 33 (2008) 554–570.
- [19] Simpson, A.P., Lutz, A.E. Exergy analysis of hydrogen production via steam methane reforming. *International Journal of Hydrogen Energy* 32 (2007) 4811 – 4820.
- [20] Minggu, L.R., Daud, W.R.W., Kassim, M.B. An overview of photocells and photoreactors for photoelectrochemical water splitting. *International Journal of Hydrogen energy* 35 (2010) 5233-5244.
- [21] Bak, T., Nowotny, J., Rekas, M., Sorrell, C.C. Photo-electrochemical hydrogen generation from water using solar energy. Materials-related aspects. *International Journal of Hydrogen Energy* 27 (2002) 991 – 1022.
- [22] Momirlana, M., Veziroglu, T.N. Current status of hydrogen energy. *Renewable and Sustainable Energy Reviews* 6 (2002) 141–179.

- [23] Nowotny, J., Sorrell, C.C., Sheppard, L.R., Bak, T. Solar-hydrogen: Environmentally safe fuel for the future. *International Journal of Hydrogen Energy* 30 (2005) 521 – 544.
- [24] Demirbas, A. Biomass resource facilities and biomass conversion processing for fuels and chemicals. *Energy Conversion and Management* 42 (2001) 1357–1378.
- [25] McKendry, P. Energy production from biomass (Part 3): Gasification technologies. *Bioresource Technology* 83 (2002) 55-63.
- [26] Florin, N., Harris, A. Hydrogen production from biomass. *Environmentalist* 27 (2007) 207-215.
- [27] Brown, R.C., Qin Liua, Q., Norton, G. Catalytic effects observed during the co-gasification of coal and switchgrass. *Biomass and Bioenergy* 18 (2000) 499-506.
- [28] Gemmen, R.S., Tremblay, J. On the mechanisms and behavior of coal syngas transport and reaction within the anode of a solid oxide fuel cell. *Journal of Power Sources* 161 (2006) 1084-1095.
- [29] Burnette, D.D., Kremer, G.G., Bayless, D.J. The use of hydrogen-depleted coal syngas in solid oxide fuel cells. *Journal of Power Sources* 182 (2008) 329-333.
- [30] Sakintunaa, B., Lamari-Darkrimb, F., Hirscher, M. Metal hydride materials for solid hydrogen storage: A review. *International Journal of Hydrogen Energy* 32 (2007) 1121-1140.
- [31] Suh, M.P., Park, H.J., Prasad, T.K., Lim, D.W. Hydrogen Storage in Metal Organic Frameworks. *Chemical Reviews* 112 (2012) 782–835.
- [32] Attia, F., Geckeler, K. E. Polyaniline as a material for hydrogen storage applications. *Macromolecular Rapid Communications* 34 (2013) 1043-1055.
- [33] Durbin, D.J., Malardier-Jugroot, C. Review of hydrogen storage techniques for on board vehicle applications. *International Journal of Hydrogen Energy* 38 (2013) 14595-14617.
- [34] Hadjipaschalis, I., Poullikkas, A., Efthimiou, V. Overview of current and future energy storage technologies for electric power applications. *Renewable and Sustainable Energy Reviews* 13 (2009) 1513–1522.

- [35] Schlapbach, L., Züttel, A. Hydrogen-storage materials for mobile applications. *Nature* 414 (2001) 353-358.
- [36] Brow, R.K., Schmitt, M.L. A survey of energy and environmental applications of glass. *Journal of the European Ceramic Society* 29 (2009) 1193–1201.
- [37] Ahluwalia, R.K., Hua, T.Q., Peng, J.K., Lasher, S., McKenney, K., Sinha, J., Gardiner, M. Technical assessment of cryo-compressed hydrogen storage tank systems for automotive applications. *International Journal of Hydrogen Energy* 35 (2010) 4171–4184.
- [38] Aceves, S.M., Espinosa-Loza, F., Ledesma-Orozco, E., Ross, T.O., Weisberg, A.H., Brunner, T.C., Kircher, O. High-density automotive hydrogen storage with cryogenic capable pressure vessels. *International Journal of Hydrogen Energy* 35 (2010) 1219–1226.
- [39] Zuttel, A. Materials for hydrogen storage. *Materials Today* 6 (2003) 24-33.
- [40] Jena, P. Materials for Hydrogen Storage: Past, Present, and Future. *Journal of Physical Chemistry Letters* 2 (2011) 206–211.
- [41] Xiao, B., Yuan, Q. Nanoporous metal organic framework materials for hydrogen storage. *Particuology* 7 (2009) 129–140.
- [42] Langmi, H.W., Rena, J., North, B., Mathe, M., Bessarabov, D. Hydrogen Storage in Metal-Organic Frameworks: A Review. *Electrochimica Acta* 128 (2014) 368–392.
- [43] Broom, D.P., Webb, C.J., Hurst, K.E., Parilla, P.A., Gennett, T., Brown, C.M., Zacharia, R., Tylianakis, E., Klontzas, E., Froudakis, G.E., Steriotis, T.A., Trikalitis, P.N., Anton, D.L., Hardy, B., Tamburello, D., Corgnale, C., van Hassel, B.A., Cossement, D., Chahine, R., Hirscher, M. Outlook and challenges for hydrogen storage in nanoporous materials. *Applied Physics A* 151 (2016). doi :10.1007/s00339-016-9651-4.
- [44] Cao, B., Veith, G.M, Neufeind, J.C., Adzic, R.R., Khalifah, P.G. Mixed close-packed cobalt molybdenum nitrides as on-noble metal electrocatalysts for the hydrogen evolution reaction. *Journal of the American Chemical Society* 135 (2013) 19186-19192.



- [45] Rosalbino, F., Borzone, G., Angelini, E., Raggio, R. Hydrogen evolution reaction on Ni-RE (RE=rare earth) crystalline alloys. *Electrochimica Acta* 48 (2003) 3939-3944.
- [46] Conway, B.E. Electrochemical proton transfer and cathodic hydrogen evolution. *Science Progress* 71 (1987) 479-509.
- [47] Zheng, Y., Jiao, Y., Jaroniec, M, Qiao, S.Z. Advancing the electrochemistry of the hydrogen-evolution reaction through combining experiment and theory. *Angewandte Chemie International Edition* 54 (2015) 52-65.
- [48] Rosalbino, F., Delsante, S., Borzone, G., Angelini, E. Electrocatalytic behaviour of Co-Ni-R (R=rare earth metal) crystalline alloys as electrode materials for hydrogen evolution reaction in alkaline medium. *International Journal of Hydrogen Energy* 33 (2008) 6696-6703.
- [49] Bocutti, R., Saeki, M.J., Florentino, A.O., Oliveira, C.L.F. Angelo, A.C.D. The hydrogen evolution reaction on codeposited Ni-hydrogen storage intermetallic particles I alkaline medium. *International Journal of Hydrogen Energy* 25 (2000) 1051-1058.
- [50] Azizi, O., Jafarian, M., Gobal, F., Heli, H., Mahjani, M.G. The investigation of the kinetics and mechanism of hydrogen evolution reaction on tin. *International Journal of Hydrogen Energy* 32 (2007) 1755 – 1761.
- [51] Gu, C., Norris, B.C., Fan, F.R., Bielawski, C.W., Bard, A.J. Is base-inhibited vapor phase polymerized PEDOT an electrocatalyst for the hydrogen evolution reaction? Exploring substrate effects, including Pt contaminated Au. *ACS Catalysis* 2 (2012) 746–750.
- [52] Tang, Q., Jiang, D. Mechanism of hydrogen evolution reaction on 1T-MoS<sub>2</sub> from first principle. *ACS Catalysis* 6 (2016) 4953-4961.
- [53] Laursen, A.B., Varela, A.S., Dionigi, F., Fanchiu, H., Miller, C., Trinhammer, O.L., Rossmeisl, J., Dahl, S. Electrochemical Hydrogen Evolution: Sabatier's Principle and the Volcano Plot. *Journal of Chemical Education* 89 (2012) 1595-1599.

- [54] Benck, J.D., Hellstern, T.R., Kibsgaard, J., Chakthranont, P., Jaramillo, T.F. Catalyzing the hydrogen evolution reaction (HER) with molybdenum sulphide nanomaterials. *ACS Catalysis* 4 (2014) 3957-3971.
- [55] Zhang, L., Chang, Q., Chen, H., Shao, M. Recent advances in palladium-based electrocatalysts for fuel cell reactions and hydrogen evolution reactions. *Nano Energy* (2016) 198-219.
- [56] Costentin, C., Robert, M., Saveant, J.M. Catalysis of the electrochemical reduction of carbon dioxide. *Chemical Society Reviews* 42 (2013) 2423-2436.
- [57] Thomas, J.M., Thomas, W.J. Principles and practice of heterogeneous catalysis. 2<sup>nd</sup> Edition. Wiley-VCH (2015)
- [58] Fachete, I., Wang, Y., Vedrine, J.C. The past, present and future of heterogeneous catalysis. *Catalysis Today* 189 (2012) 2-27.
- [59] Blaser, H.U. Heterogeneous catalysis for fine chemicals production. *Catalysis Today* 60 (2000) 161-165.
- [60] Tarasevich, M.R., Korchagin, Electrochemicals and pH (A review). *Russian Journal of Electrochemistry* 49 (2013) 600-618.
- [61] Rao, G.R., Justin, P., Meher, S.K. Metal oxide promoted electrocatalysts for methanol oxidation. *Catalysis Survey from Asia* 15 (2011) 221-229.
- [62] Arvia, A.J., Salvarezza, R.C., Triaca, W.E. Noble metal surfaces and electrocatalysis: Review and perspectives. *Journal of New Materials for Electrochemical Systems* 7 (2004) 133-143.
- [63] Lin, Y., Yu, H., Chen, S., Zhao, H., Zhang, Y. Efficient and durable hydrogen evolution electrocatalyst based on non-metallic nitrogen doped hexagonal carbon. *Scientific Reports* 4 (2014) doi: 10.1038/srep06843.
- [64] Li, Y., Wang, H., Xie, L., Liang, Y., Hong, G., Dai, H. MoS<sub>2</sub> nanoparticles grown on graphene: An advanced catalysis for the hydrogen evolution reaction. *Journal of the American Chemical Society* 133 (2011) 7296-7299.
- [65] Cui, W., Liu, Q., Xing, Z., Asiri, A.M., Alamry, K.A. MoP nanosheets supported on biomass-derived carbon flake: One-step facile preparation and application as a novel high-active electrocatalyst toward hydrogen evolution reaction. *Applied Catalysis B: Environmental* 164 (2015) 144-150.

- [66] Tian, J., Liu, Q., Asiri, A.M., Sun, X. Self-supported nanoporous cobalt phosphide nanowire arrays: an efficient 3d hydrogen-evolving cathode over the wide range of pH 0–14. *Journal of the American Chemical Society* 136 (2014) 7587–7590.
- [67] Vesborg, P.C.K., Seger, B, Chorkendorff, I. Recent development in hydrogen evolution reaction catalysts and their practical implementation. *The Journal of Physical Chemistry Letters* 6 (2015) 951-957.
- [68] Safizadeh, F., Ghali, E., Houlachi, G. Electrocatalysis developments for hydrogen evolution reaction in alkaline solutions – A Review. *International Journal of Hydrogen Energy* 40 (2015) 256-274.
- [69] Conway, B.E., Jerkiewicz, G. Relation of energies and coverages of underpotential and overpotential deposited H at Pt and other metals to the ‘volcano curve’ for cathodic H<sub>2</sub> evolution kinetics. *Electrochimica Acta* 45 (2000) 4075–4083.
- [70] Zeng, M., Li, Y. Recent advances in heterogeneous electrocatalysts for the hydrogen evolution reaction. *Journal of Materials Chemistry A* 3 (2015) 14942-14962.
- [71] Conway, B.E., Jerkiewicz, G. Nature of electrosorbed H and its relation to metal dependence of catalysis in cathodic H<sub>2</sub> evolution. *Solid State Ionics* 150 (2002) 93 – 103.
- [72] Zhou, J., Caban-Acevedo, M., Liang, H., Samad, L., Ding, Q., Fu, Y., Li, M., Jin, S. High-performance electrocatalysis for hydrogen evolution reaction using Se-doped pyrite-phase nickel diphosphide nanostructures. *ACS Catalysis* 5 (2015) 6355-6361.
- [73] Zheng, Y., Jiao, Y., Li, L.H., Xing, T., Chen, Y., Jaroniec, M., Qiao, S.Z. Toward design of synergistically active carbon-based catalysts for electrocatalytic hydrogen evolution. *ACS Nano* 8 (2014) 5290–5296.
- [74] Liu, Q., Tian, J., Cui, W., Jiang, P., Cheng, N., Asiri, A.M., Sun, X. Carbon nanotubes decorated with CoP nanocrystals: A highly active non-noble-metal nanohybrid electrocatalyst for hydrogen evolution. *Angewandte Chemie* 126 (2014) 6828-6832.

- [75] Popczun, E.J., Read, C.G., Roske, C.W., Lewis, N.S., Schaak, R.E. Highly activity electrocatalysis of the hydrogen evolution bu cobalt phosphide nanoparticles. *Angewandte Chemie* 126 (2014) 5531-5534.
- [76] Wua, Z., Fang, B., Bonakdarpour, A., Suna, A., Wilkinsonb, D.P., Wang , D. WS<sub>2</sub> nanosheets as a highly efficient electrocatalyst for hydrogen evolution reaction. *Applied Catalysis B: Environmental* 125 (2012) 59–66.
- [77] Kong, D., Wang, H., Lu, Z., Cui, Y. CoSe<sub>2</sub> nanoparticles grown on carbon fiber paper: An efficient and stable electrocatalyst for hydrogen evolution reaction. *Journal of the American Chemical Society* 136 (2014) 4897-4900.
- [78] Skulason, E., Tripkovic, V., Bjorketun, M.E., Gudmundsdottir, S., Karlberg, G., Rossmeisl, J., Bligaard, T., Jonsson, H., Norskov, J.K. Modeling the electrochemical hydrogen oxidation and evolution reactions on the basis of Density Functional Theory calculations. *Journal of Physical Chemistry* 114 (2010) 18182-18197.
- [79] Zheng, Y., Jiao, Y., Zhu, Y., Li, L.H., Han, Y., Chen, Y., Du, A., Jaroniec, M., Qiao, S.Z. Hydrogen evolution by a metal-free electrocatalyst. *Nature Communications* (2014) doi: 10.1038/ncomms4783.
- [80] Aydin, R., Koleli, F. Hydrogen evolution on conducting polymer electrode in acidic medium. *Progress in Organic Coating* 56 (2006) 76-80.
- [81] Orinakova, R., Filkusova, M. Hydrogen evolution on microstructured polypyrrole films with nickel. *Synthetic Metals* 160 (2010) 927-931.
- [82] Corte, D.A.D., Torres, C., Correa, P.S.C., Rieder, E.S., Malfatti, C.F. The hydrogen evolution reaction on nickel-polyaniline composite electrodes. *International Journal of Hydrogen energy* 37 (2012) 3025-3032
- [83] Navarro-Flores, E., Omanovic, S. Hydrogen evolution on nickel incorporated in three-dimensional conducting polymer layers. *Journal of Molecular Catalysis A: Chemical* 242 (2005) 182–194.
- [84] Trueba, M., Trasatti, S.P., Trasatti, S. Electrocatalytic activity for hydrogen evolution of polypyrrole films modified with nobel metal particles. *Material Chemistry and Physics* 98 (2006) 165-171.

- [85] Seeber, R., Terzi, F., Zanardi, C. Functional Materials in Amperometric Sensing. Chapter 2: Intrinsically conducting polymers. Springer. (2014) 23-57.
- [86] Freund, M.S., Deore, B. Self-doped conducting polymer. John Wiley Sons. (2007) 3-4.
- [87] Guimard, N.K., Gomez, N., Schmidt, C.E. Conducting polymers in biomedical engineering. *Progress in Polymer Science* 32 (2007) 876-921.
- [88] Kumar, S. Conducting polymers and their characterisation. *International Research Journal of Engineering and Technology* 3 (2016) 479-482.
- [89] Balint, R., Cassidy, N.J., Cartmell, S.H. Conductive polymers: Towards a smart biomaterial for tissue engineering. *Acta Biomaterialia* 10 (2014) 2341–2353.
- [90] Alemayehu, T., Himariam, B. Synthesis and characterisation of conducting polymers: A review paper. *International Journal of Recent Research in Physics and Chemical Sciences* 1 (2014) 24-28.
- [91] Brito-Madurro, A.G., Ferreira, L.F., Vieira, S.N., Ariza, R.G., Filho, L.R.G., Madurro, J.M. Immobilization of purine bases on a poly-4-aminophenol matrix. *Journal of Material Sciences* 42 (2007) 3238-3243.
- [92] Gerard, M., Chaubey, A., Malhotra, B.D. Application of conducting polymers to biosensors. *Biosensors Bioelectronics* 17 (2002) 345-359.
- [93] Harima, Y., Jiang, X., Kunugi, Y., Yamashita, K., Naka, A., Lee, K.K., Ishikawa, M. Influence of  $\pi$ -conjugation length on mobilities of charge carriers in conducting polymers. *Journal of Materials Chemistry* 13 (2003) 1298-1305.
- [94] Bai, H., Shi, G. Gas sensors based on conducting polymers. *Sensors* 7 (2007) 267-307.
- [95] Ciric-Marjanovic, G., Dragicevic, L., Milojevic, M., Mojovic, M., Mentus, S., Dojcinovic, B., Marjanovic, B., Stejskal, J. Synthesis and characterisation of self-assembled polyaniline nanotubes/silica nanocomposites. *The Journal of Physical Chemistry B* 113 (2009) 7116–7127.
- [96] Du, X.S., Xiao, M., Meng, Y.Z. Facile synthesis of highly conductive polyaniline/graphite nanocomposites. *European Polymer Journal* 40 (2004) 1489–1493.

- [97] Dong, H., Prasad, S., Nyame, V., Jones, W.E. Submicrometer conducting polyaniline tubes prepared from polymer fiber templates. *Chemistry of Materials* 16 (2004) 371-373.
- [98] Li, H., Wang, J., Chub, Q., Wang, Z., Zhanga, F., Wang, S. Theoretical and experimental specific capacitance of polyaniline in sulfuric acid. *Journal of Power Sources* 190 (2009) 578–586.
- [99] Huang, J., Virji, S., Weiller, B.H., Kaner, R.B. Polyaniline nanofibers: facile synthesis and chemical sensors. *Journal of American Chemical Society* 125 (2003) 314-315.
- [100] Lu, W., Smela, E., Adams, P., Zuccarello, G., Mattes, B.R. Development of solid-in-hollow electrochemical linear actuators using highly conductive polyaniline. *Chemistry of Materials* 16 (2004) 1615-1621.
- [101] Lv, R., Tang, R., Kan, J. Effect of magnetic field on properties of polyaniline doped with dysprosium chloride. *Materials Chemistry and Physics* 95 (2006) 294–299.
- [102] Ciric-Marjanovic, G. Recent advances in polyaniline research: Polymerisation, structural aspects, properties and applications. *Synthetic Metals* 177 (2013) 1-47.
- [103] Trajanowicz, M. Application of conducting polymers in chemical analysis. *Microchimica Acta* 143 (2003) 75-91.
- [104] Li, D., Huang, J., Kamer, R.B. Polyaniline nanofibers: A unique polymer nanostructure for versatile applications. *Accounts of Chemical Research* 42 (2009) 135-145.
- [105] Kang, E.T., Neoh, K.G., Tang, K.L. Polyaniline: A polymer with many interesting intrinsic redox states. *Progress in Polymer Science* 23 (1998) 277-324.
- [106] Zeng, X.R., Ko, T.M. Structures and properties of chemically reduced polyanilines. *Polymer* 39 (1998) 1187-1195.
- [107] Sattari, S., Reyhani, A., Khanlari, M.R., Khabazian, M., Heydari, H. Synthesis of polyaniline-multi walled carbon nanotubes composite on the glass and silicon substrates and methane gas sensing behaviour of them at room temperature. *Journal of Industrial and Engineering Chemistry* 20 (2014) 1761-1764.

- [108] Bhadra, S., Khastgir, D., Singha, N.K., Lee, J.H. Progress in preparation, processing and applications of polyaniline. *Progress in Polymer Science* 34 (2009) 783-810.
- [109] Liu, X.X., Zhang, L., Li, Y.B., Su, Z., Zhang, L.J. Electropolymerisation of aniline in aqueous solutions at pH 2 to 12. *Journal of Materials Science* 40 (2005) 4511-4515.
- [110] Gurunathan, K., Murugan, A.V., Marimuthu, R., Mulik, U.P., Amalnerkar, D.P. Electrochemically synthesised conducting polymeric materials for optoelectronics and energy storage devices. *Materials Chemistry and Physics* 61 (1999) 173-191.
- [111] Gvozdenovic, M.M., Jugovic, B.Z., Stevanovic, J.S., Grgur, B.N. Electrochemical synthesis of electroconducting polymers. *Hemijaska Industrija* 68 (2014) 673-684.
- [112] Jaymand, M. Recent progress in chemical modification of polyaniline. *Progress in Polymer Science* 38 (2013) 1287-1306.
- [113] Toshima, N., Hara, S. Direct synthesis of conducting polymers from simple monomers. *Progress in Polymer Science* 20 (1995) 155-183.
- [114] Jangid, N.K., Chauhan, N.P.S., Mengwal, K., Ameta, R., Punjabi, P.B. A review: Conducting polymers and their applications. *Research Journal of Pharmaceutical, Biological and Chemical Sciences* 5 (2014) 383-412.
- [115] Campos, T.L.A., Kersting, D.F., Ferreira, C.A. Chemical synthesis of polyaniline using sulphanic acid as dopant agent into the reactional medium. *Surface and Coatings Technology* 122 (1999) 3-5.
- [116] Ciric-Marjanovic, G., Konyushenko, E.N., Trchova, M., Stejskal, J. Chemical oxidative polymerisation of anilinium sulfate vs aniline: Theory and experimental. *Synthetic Metals* 158 (2008) 200-211.
- [117] Mazur, M., Michota-Kaminska, A., Bukowska, J. Surface-catalyzed growth of poly (2-methoxyaniline) on gold. *Electrochimica Acta* 52 (2007) 5669-5676.
- [118] Nicolas- Debarnot., Poncin- Epailard, F. Polyaniline as a new sensitive layer for gas sensors. *Analytica Chimica Acta* 475 (2003) 1-15.

- [119] Cordeiro, M.A.M., Goncalvel, D., Bulhoes, L.O.S., Cordeiro, J.M.M. Synthesis and characterisation of poly-o-toluidine: Kinetic and structural aspects. *Medical Research* 8 (2005) 5-10.
- [120] Sapurina, I.Y., Stejskal, J. The effect of pH on the oxidative polymerisation of aniline and the morphology and properties of products. *Russian Chemical Reviews* 79 (2010) 1123-1143.
- [121] Molapo, K.M., Ndangili, P.M., Ajayi, R.F., Mbambisa, G., Mailu, S.M., Njomo, N., Masikini, M., Baker, P., Iwouha, E.I. Electronics of Conjugated Polymers (I): Polyaniline. *International Journal of Electrochemical Science* 7 (2012) 11859-11875.
- [122] Ahmed, S.M. Mechanistic investigation of the oxidative polymerisation of aniline hydrochloride in different media. *Polymer Degradation and Stability* 85 (2004) 605-614.
- [123] Song, E.T., Choi, J.W. Conducting polyaniline nanowire and its applications in chemiresistive sensing. *Nanomaterials* 3 (2013) 498-523.
- [124] Abu- Thabit, N.Y. Chemical oxidative polymerisation of polyaniline: A practical approach for preparation of smart conductive textiles. *Journal of Chemical Education* 93 (2016) 1606-1611.
- [125] Luong, N.D., Korhonen, J.T., Soininen, A.J., Ruokolainen, J., Johansson, L.S., Seppala, J. Processable polyaniline suspensions through in situ polymerisation onto cellulose. *European Polymer Journal* 49 (2013) 335-344.
- [126] Silva, R.C., Sarmenti, M.V., Faez, R., Mortimer, R.J., Ribeiro, A.S. Electrochromic properties of polyaniline-based hybrid organic/inorganic materials. *Journal of Brazilian Chemical Society* 27 (2016) 1847-1857.
- [127] Nabid, M.R., Taheri, S.S., Sedghi, R., Entezami, A.A. Chemical synthesis and characterisation of water-soluble, conducting poly(N-phenylglycine). *Iranian Polymer Journal* 17 (2008) 365-371.
- [128] Sophia, I.A., Gopu, G., Vedhi, C. Synthesis and characterisation of poly anthranilic acid metal nanocomposites. *Open Journal of Synthesis Theory and Applications* 1 (2012) 1-8.



- [129] Benyoucef, A., Boussalem, S., Belbachir, M. Electrochemical synthesis of poly(*o*-aminobenzoic acid) and poly(*o*-amiobenzoic acid-co-aniline): Electrochemical and in-situ FTIRs characterisation. *World Journal of Chemistry* 4 (2009) 171-177.
- [130] Bian, C., Yu, Y., Xue, G. Synthesis of conducting polyaniline/TiO<sub>2</sub> composite nanofibers by one-step in situ polymerisation method. *Journal of Applied Polymer Science* 104 (2007) 21-26.
- [131] Raman, N., Pothiraj, S.S.K. Synthesis and structural reactivity of inorganic-organic hybrid nanocomposites-A review. *Journal of Saudi Chemical Society* 16 (2012) 339-352.
- [132] Hatchett, D.W., Josowicz, M. Composites of intrinsically conducting polymers as sensing materials. *Chemical Reviews* 108 (2008) 746-769.
- [133] Karim, M.R., Lim, K.T., Lee, M.S., Kim, K., Yeum, J.H. Sulfonated polyaniline-titanium dioxide nanocomposites synthesised by one-pot UV-curable polymerisation method. *Synthetic Metals* 159 (2009) 209-213.
- [134] Schnitzler, D.C., Meruvia, M.S., Hummelgen, I.A., Zarbin, A.J.G. Preparation and characterisation of novel hybrid materials formed from (Ti, Sn)O<sub>2</sub> nanoparticles and polyaniline. *Chemistry of Materials* 15 (2003) 4658-4665.
- [135] Mostafaei, A., Zolriasatein, A. Synthesis and characterisation of conducting polyaniline nanocomposites containing ZnO nanorods. *Progress in Natural Science: Materials International* 22 (2012) 273-280.
- [136] Parveen, A., Roy, A.S. Effects of morphology on thermal stability of core-shell polyaniline/TiO<sub>2</sub> nanocomposites. *Advanced Materials Letters* 4 (2013) 696-701.
- [137] Kumar, N.A., Choi, H.J., Shin, Y.R., Chang, D.W., Dai, L., Baek, J.B. Polyaniline-grafted reduced graphene oxide for efficient electrochemical supercapacitors. *ACS Nano* 6 (2012) 1715-1723.
- [138] Oueing, C., Berlioz, S., Perrin, F.X. Carbon nanotube-polyaniline composites. *Progress in Polymer Science* 39 (2014) 707-748.
- [139] Lou, J., Zhong, W., Zou, Y., Xiong, C., Yang, W. Preparation of morphology-controllable polyaniline and polyaniline/graphene hydrogels for high

- performance binder-free supercapacitor electrodes. *Journal of Power Source* 319 (2013) 73-81.
- [140] Radtke, M., McMillan, D.G.G., Schroter, B., Hoppener, S., Dietzek, B., Schubert, U.S., Ignaszak, A. The effect of 3-amino benzoic acid linker and the reversal of donor-acceptor pairs on the electrochemical performance and stability of covalently bonded poly(pyrrole) nanotubes. *Polymer* 77 (2015) 289-296.
- [141] Zhao, Y., Tang, G.S., Yu, Z.Z., Qi, J.S. The effect of graphite oxide on the thermoelectric properties of polyaniline. *Carbon* 50 (2012) 3064-3073.
- [142] Bagheri, H., Javanmardi, H., Abbasi, A., Banihashemi, S. A metal organic framework-polyaniline nanocomposite as a fiber coating for solid phase microextraction. *Journal of Chromatography A* 1431 (2016) 27-35.
- [143] Guo, S.N., Zhu, Y., Yan, Y.Y., Min, Y.L., Fan, J.C., Xu, Q.J., Yun, H. (Metal-organic framework)-polyaniline sandwich structure composites as novel hybrid electrode materials for high-performance supercapacitor. *Journal of Power Sources* 316 (2016) 176-182.
- [144] Kuppler, R.J., Timmons, D.J., Fang, Q.R., Li, J.R., Makal, T.A., Young, M.D., Yuan, D., Zhao, D., Zhuang, W., Zhou, H.C. Potential applications of metal-organic frameworks. *Coordination Chemistry Reviews* 253 (2009) 3042-3066.
- [145] Srimuk, P., Luanwuthu, S., Krittayavathanon, A., Sawangphruk, M. Solid-type supercapacitor of reduced graphene oxide-metal organic framework composite coated on carbon fibre paper. *Electrochimica Acta* 157 (2015) 69-77.
- [146] Xamena, F.X.L., Corma, A., Garcia, H. Applications of metal-organic frameworks (MOFs) as quantum dot semiconductors. *Journal of Physical Chemistry C* 111 (2007) 80-85.
- [147] Zhou, H.C., Long, J.R., Yaghi, O.M. Introduction to metal-organic frameworks. *Chemical Reviews* 112 (2012) 673-674.
- [148] Cui, Y., Li, B., He, H., Zhou, W., Chen, B., Qian, G. Metal-organic frameworks as platforms for functional materials. *Accounts of Chemical Research* 49 (2016) 483-493.

- [149] Salunke-Gawali, S., Kathawate, L., Puranik, V.G. MOF with hydroxynaphthoquinone as organic linker: Molecular structure of [Zn (Chlorolawsone)<sub>2</sub>(H<sub>2</sub>O)<sub>2</sub>] and thermogravimetric studies. *Journal of Molecular Structure* 1022 (2012) 189-196.
- [150] Kreno, L.E., Leong, K., Farha, O.K., Allendorf, M., Van Duyne, P.R., Hupp, J.T. Metal-organic framework materials as chemical sensors. *Chemical Reviews* 112 (2012) 1105-1125.
- [151] Rowsell, J.L.C., Yaghi, O.M. Metal-organic frameworks: a new class of porous materials. *Microporous and Mesoporous Materials* 73 (2004) 3-14.
- [152] Gangu, K.K., Maddila, S., Mukkamala, S.B., Jonnalagadda, S.B. A review on contemporary metal-organic framework materials. *Inorganica Chimica Acta* 446 (2016) 61-74.
- [153] Sun, L.B., Li, J.R., Park, J., Zhou, H.C. Cooperative template-directed assembly of mesoporous metal-organic frameworks. *Journal of the American Chemical Society* 134 (2012) 126-129.
- [154] Dikio, E.D., Farah, A.M. Synthesis, characterisation and comparative study of copper and zinc metal organic frameworks. *Chemical Science Transactions* 2 (2013) 1386-1394.
- [155] Kurmoo, M. Magnetic metal-organic frameworks. *Chemical Society Reviews* 38 (2009) 1353-1379.
- [156] Yu, Y., Ren, Y., Shen, W., Deng, H and Gao, Z. Applications of metal-organic frameworks as stationary phases in chromatography. *Trends in Analytical chemistry* 50 (2013) 50, 33-41.
- [157] Butova, V.V., Soldatov, M.A., Guda, A.A., Lomachenko, K.A., Lamberti, C. Metal-organic frameworks: Structure, properties, methods of synthesis and characterisation. *Russian Chemical Reviews* 85 (2016) 280-307.
- [158] Schoedel, A., Li, M., Li, D., O’Keeffe, M., Yaghi, O.M. Structures of metal-organic frameworks with rod secondary building units. *Chemical Reviews* 116 (2016) 12466-12535.

- [159] Qiu, S., Zhu, G. Molecular engineering for synthesising novel structures of metal-organic frameworks with multifunctional properties. *Coordination Chemical Reviews* 235 (2009) 2891-2911.
- [160] Alhamami, M., Doan, H., Cheng, C.H. A review on breathing behaviour of metal-organic frameworks (MOFs) for gas adsorption. *Materials* 7 (2014) 3198-3250.
- [161] Furukawa, H., Cordova, K.E., O’Keeffe, M., Yaghi, O.M. The chemistry and applications of metal-organic frameworks. *Science* 341 (2013) 1-12.
- [162] Pagis, C., Ferbinteanu, M., Rothenberg, G., Tenase, S. Lanthanide-based metal organic frameworks: Synthetic strategies and catalytic applications. *ACS Catalysis* 6 (2016) 6063-6072.
- [163] Cui, Y., Chen, B., Qian, G. Lanthanide metal-organic frameworks for luminescent sensing and light-emitting applications. *Coordination Chemistry Reviews* 273-274 (2014) 76-86.
- [164] Abdelbaky, M.S., Amghouz, Z., Garcia-Granda, S., Garcia, J.R. Synthesis, structures and luminescence properties of metal-organic frameworks based lithium-lanthanide and terephthalate. *Polymer* 8 (2016) 86-100.
- [165] Raja, D.S., Luo, J.H., Wu, C.Y., Cheng, Y.J., Yeh, C.T., Chen, Y.T., Lo, S.H., Lai, Y.L., Li, C.H. Solvothermal synthesis, structural diversity, and properties of alkali metal-organic frameworks based on V-shaped ligands. *Crystal Growth & Design* 13 (2013) 3785-3793.
- [166] Ahmed, I., Jeon, J., Khan, N.A., Jhung, S.H. Synthesis of a metal-organic framework, iron-benzenetricarboxylate, from dry gels in the absence of acid and salt. *Crystal Growth & Design* 12 (2012) 5878-5881.
- [167] Stock, N., Biswas, S. Synthesis of metal-organic frameworks (MOFs): Route to various MOF topologies, morphologies, and composites. *Chemical Reviews* 112 (2012) 933-969.
- [168] Lee, Y.R., Kim, J., Ahn, W.S. Synthesis of metal-organic frameworks: A mini review. *Korean Journal of Chemical Engineering* 30 (2013) 1667-1680.

- [169] Yuan, Z., Zhang, J., Liu, G. Synthesis of O<sub>3</sub> nanocrystals via hydro/solvothermal route and their photoluminescence properties. *International Journal of Electrochemical Science* 8 (2013) 1794 – 1801.
- [170] Song, Y.S., Yan, B., Chen, Z.X. Hydrothermal synthesis, crystal structure and luminescence of four novel metal–organic frameworks. *Journal of Solid State Chemistry* 179 (2006) 4037-4046.
- [171] Hayashi, H., Hakuta, Y. Hydrothermal synthesis of metal oxide nanoparticles in supercritical water. *Materials* 3 (2010) 3794-3817.
- [172] Soultanidis, N.S., Zhou, W., Kiely, C.J, Wong, M.S. Solvothermal synthesis of ultrasmall tungsten oxide nanoparticles. *Langmuir* 28 (2012) 28, 17771–17777.
- [173] Zhu, M., Wang, Y., Meng, D., Qin, X and Diao, G. Hydrothermal synthesis of hematite nanoparticles and their electrochemical properties. *The Journal of Physical Chemistry: C* 116 (2012) 16276–16285.
- [174] Carpenter, M.K., Moylan, T.E., Kukreja, R.S., Atwan, M.H., Tessema, M.M. Solvothermal synthesis of platinum alloy nanoparticles for oxygen reduction electrocatalysis. *Journal of American Chemical Society* 134 (2012) 8535–8542.
- [175] Haw, C.Y., Mohamed, F., Chia, C.H., Radiman. S., Zakaria, S., Huang, M.N., Lim, H.N. Hydrothermal synthesis of magnetite nanoparticles as MRI contrast agents. *Ceramics International* 36 (2010) 1417-1422.
- [176] Sun, Y., Zhou, H.C. Recent progress in the synthesis of metal-organic frameworks. *Science and Technology of Advanced Materials* 16 (2015) doi:10.1088/1468-6996/16/5/054202.
- [177] Seo, Y.K., Hundal, G., Jang, I.T., Hwany, Y.K., Jun, C.N., Chang J-S. Microwave synthesis of hybrid inorganic–organic materials including porous Cu<sub>3</sub>(BTC)<sub>2</sub> from Cu(II)-trimesate mixture. *Microporous and Mesoporous Materials* 119 (2009) 331-337.
- [178] Lee, J.S., Halligudi, S.B., Nak Han Jang, N.H., Hwang, D.W., Chang, J.S., Hwang, Y.K. Microwave synthesis of a porous metal-organic framework, Nickel(II) dihydroxyterephthalate and its catalytic properties in

- oxidation of cyclohexene. *Bulletin of the Korean Chemical Society* 31 (2010) 1489-1495.
- [179] Lin, Z.J., Yang, Z., Liu, T.F., Huang, Y.B., Cao, R. Microwave-assisted synthesis of a series of lanthanide metal-organic frameworks and gas sorption properties. *Inorganic Chemistry* 51 (2012) 1813-1820.
- [180] Choi, T.Y., Kim, J., Jhung S.H., Kim, H.K., Cheng, J.S., Chae, H.K. Microwave synthesis of a porous metal-organic framework, zinc terephthalate MOF-5. *Bulletin of the Korean Chemical Society* 27 (2006) 1523-1524.
- [181] Liu, W., Lihau, Y., Liu, X., Yuan, L., Lu, X., Jiay, J. Rapid synthesis of a novel cadmium imidazole-4,5-dicarboxylate metal-organic framework under microwave-assisted solvothermal condition. *Inorganic Chemistry Communications* 11 (2003) 1250-1252.
- [182] Blanita, G., Ardelean, O., Lupu, D., Borodi, G., Mihet, M., Coros, M., Vlassa, M., Misan, I., Coldea, I., Popenecin, G. Microwave assisted synthesis of MOF-5 at atmospheric pressure. *Revue Roumaine de Chimie* 56 (2011) 583-588.
- [183] Liang, W., Babarao, R and D'Alessandro, D.M. Microwave-assisted solvothermal synthesis and optical properties of tagged MIL-140a metal-organic framework. *Inorganic Chemistry* 52 (2013) 12878-12880.
- [184] Wang, X.F., Zhang, Y.B., Huang, H., Zang, J.P., Chen, X.M. Microwave-assisted solvothermal synthesis of a dynamic porous metal-carboxylate framework. *Crystal Growth & Design* 8 (2008) 4559-4563.
- [185] Flugel, E.A., Ranft, A., Haase, F., Lotsch, B.V. Synthetic routes toward MOF nanomorphologies. *Journal of Materials Chemistry* 22 (2012) 10119-10133.
- [186] Chen, D.H., Wu, S.H. Synthesis of nickel nanoparticles in water-in-oil microemulsions. *Chemical Materials* 12 (2000) 1354-1360.
- [187] Solanki, J.N., Murthy, Z.V.P. Controlled size silver nanoparticles synthesis with water-in-oil microemulsion method: a topical review. *Industrial & Engineering Chemistry Research* 50 (2011) 12311-12323.
- [188] Basheer, H.S., Noordin, M.I., Ghareeb, M.M. Characterisation of microemulsions prepared using isopropyl palmitate with various surfactants

- and cosurfactants *Tropical Journal of Pharmaceutical Research* 12 (2013) 305-310.
- [189] Zori, H.M. Synthesis of TiO<sub>2</sub> nanoparticles by microemulsion/heat treated method and photodegradation of methylene blue. *Journal of Inorganic Organometallic Polymers and Materials* 21 (2011) 81–90.
- [190] Seoane, B., Dikhtiarenko, A., Mayoral, A., Tellez, C., Coronas, J., Kapteijn, F., Gascon, J. Metal organic framework synthesis in the presence of surfactants: towards hierarchical MOFs? *Crystal Engineering Communications* 17 (2015) 1693-1700.
- [191] Tojo, C., de Dios, M., Barroso, F. Surfactant effects on microemulsion-based nanoparticle synthesis. *Materials* 4 (2011) 55-72.
- [192] Hatakeyama, W., Sanchez, T.J., Rowe, M.D., Serkova, N.J., Liberatore, M.W., Boyes, S.G. Synthesis of gadolinium nanoscale metal–organic framework with hydrotropes: manipulation of particle size and magnetic resonance imaging capability. *ACS Applied Materials & Interfaces* 3 (2011) 1502-1510.
- [193] Joaristi, A.M., Juan-Alcaniz, J., Serra-Crespo, P., Kapteijn, F., Gascon, J. Electrochemical synthesis of some archetypical Zn<sup>2+</sup>, Cu<sup>2+</sup>, and Al<sup>3+</sup> metal organic frameworks. *Crystal Growth & Design* 12 (2012) 3489-3498.
- [194] Yang, H., Du, H., Zhang, L., Liang, Zli, W. Electrosynthesis and electrochemical mechanism of Zn-based metal-organic frameworks. *International Journal of Electrochemical Science* 10 (2015) 1420-1433.
- [195] Al-Kutubi, A.H., Gascon, J., Sudholter, E.J.R., Rassaie, L. Electrosynthesis of metal-organic framework: Challenges and Opportunities. *ChemElectroChem* 2 (2015) 462-474.
- [196] Seetharaj, R., Vandana, P.V., Arya, P., Mathew, S. Dependence of solvents, pH, molar ratio and temperature in tuning metal organic framework architecture. *Arabian Journal of Chemistry* (2016) doi.org/10.1016/j.arabjc.2016.01.003.
- [197] Friscic, T., Halasz, I., Strukil, V., Eckert-Maksic, M., Dinnebier, R.E. Clean and efficient synthesis using mechanochemistry: coordination polymers, metal-organic frameworks and metallodrugs. *Croatica Chemica Acta* 85 (2012) 367–378.

- [198] Klimakow, M., Klobes, P., Thunemann, A.F., Rademann, K., Emmerling, F. Mechanochemical synthesis of metal-organic frameworks: a fast and facile approach toward quantitative yields and high specific surface areas. *Chemistry of Materials* 22 (2010) 5216-5221.
- [199] Yang, H., Orefuwa, S., Goudy, A. Study of mechanochemical synthesis in the formation of the metal-organic framework  $\text{Cu}_3(\text{BTC})_2$  for hydrogen storage. *Microporous and Mesoporous Materials* 143 (2011) 37-45.
- [200] Atkins, P., Overton, T., Rourke, J., Weller, M., Armstrong, F. Shriver & Atkins Inorganic Chemistry, 5<sup>th</sup> Edition, Oxford University Press (2010).
- [201] Clugston, M., Flemming, R., Vogt, D. Chemistry: An introduction for southern African students, 1<sup>st</sup> Edition, Oxford University Press (2002)
- [202] McMurry, J. Organic Chemistry, 7<sup>th</sup> Edition Brooks/Cole, Thomson Learning, Inc (2008).
- [203] Skoog, D.A., West, D.M., Holler, F.J. Fundamentals of Analytical Chemistry, 8<sup>th</sup> Edition, Saunders College Publishing (1992).
- [204] <http://www.chemicool.com/img1/graphics/ir.gi>.
- [205] <http://lab-training.com/wp-content/uploads/2013/03/AAS-Diagram.png>.
- [206] Kenkel, J. Analytical Chemistry for Technicians, Lewis Publishers (1994).
- [207] Bard, A.J., Faulkner, L.R. In: Electrochemical Methods: Fundamentals and applications. 2nd edition, John Wiley & Sons Inc (2001).
- [208] [https://openi.nlm.nih.gov/imgs/512/389/2871148/PMC2871148\\_ijms-11-01956f1.png](https://openi.nlm.nih.gov/imgs/512/389/2871148/PMC2871148_ijms-11-01956f1.png).



## CHAPTER THREE

### POLYANILINE-METAL ORGANIC FRAMEWORK NANOCOMPOSITE AS AN EFFICIENT ELECTROCATALYST FOR HYDROGEN EVOLUTION REACTION

---

*This chapter has been submitted for publication:*

**Kabelo Edmond Ramohlola**, Gobeng Release Monama, Mpitloane Joseph Hato, Kwena Desmond Modibane, Milua Masikini, Siyabonga B. Mdluli, Kerileng M. Molapo, Emmanuel I. Iwuoha. *Polyaniline-metal organic framework nanocomposite as an efficient electrocatalyst for hydrogen evolution reaction. Composites Part B.*

#### ABSTRACT

Polyaniline-metal organic framework (PANI/MOF) composite was prepared by chemical oxidation of aniline monomer in the presence of 3.6 wt.% MOF content for hydrogen evolution reaction (HER). The structure, morphology and properties of the fabricated composite were investigated. There was a clear interaction of MOF on the backbone of the PANI matrix through electrostatic interaction as investigated by both Raman and Fourier transform infrared analyses. The MOF exhibited irregular crystals with further wrapping of MOF by PANI matrix as evidenced by both scanning electron microscopy and transmission electron microscopy studies. The PANI composite showed some nanorods and microporous structure. The energy band gap values of PANI and its composite were found to be 1.50 and 1.35 eV, respectively. The thermal stability of the neat PANI increased upon composite formation, which was due to a stabilizing effect of MOF and a change in morphology of the composite. The catalytic effect of MOF, PANI and PANI/MOF composite on HER was studied using exchange current density ( $i_0$ ) and charge transfer coefficient determined by the Tafel slope method. A drastic increase in catalytic H<sub>2</sub> evolution was observed in the composite. It was also observed that Tafel slope values of PANI and the composite decreased with increasing the concentration of the acid, suggesting the Volmer reaction coupled with

either Heyrovsky or Tafel reaction. The  $i_0$  increased with increasing the acid concentration and in an order of PANI/MOF > MOF > PANI at various concentrations.

**Keywords:** Polyaniline, Metal organic frameworks, Polymer-matrix composites (PMCs), Hydrogen evolution reaction.

### 3.1. INTRODUCTION

Today, fossil fuels are known as the main energy sources with their disadvantages such as limited resources, global warming and the environmental pollution. Numerous efforts are being considered to use other energy sources instead of fossil fuels to overcome these disadvantages. Nowadays, hydrogen fuel cell technology is considered as one of the most promising energy sources for sustainable energy applications owing to its numerous advantages including recyclability, pollution-free and fuel efficiency [1-4]. Nonetheless, the major challenge of using hydrogen as energy carrier is the need to produce hydrogen with high purity. Toward this end, electrochemical reduction of water is considered an effective and alternative route to produce hydrogen with high purity and in large quantity because of its simplicity and economical way [1]. This method needs an efficient electrocatalyst for hydrogen evolution reaction (HER) to reduce the over potential during HER process and achieve large exchange current density [5,6]. Up to date, platinum (Pt)-based electrocatalysts have been known as efficient catalysts for hydrogen generation [7]. Nonetheless, their widespread application has been restricted by their high cost and low-earth abundance. In this context, it is therefore necessary to synthesize material suitable for electrochemical studies as an alternative to Pt.

As previously mentioned in Chapter 2, conducting polymers such as polypyrrole, polythiophene and polyaniline (PANI), etc., have been considered as potential candidates for electrochemical HER due to their impressive structural and physical properties as well as the ability to catalyse electrode reactions. In particular, PANI is promising to be used as a suitable electrocatalyst due to its high conductivity, environmental stability, has good photo- and chemical-physical properties, ease of synthesis, synthesised from cheap monomers, and the different redox states [8-10]. Recently, PANI and other conducting polymers were used as a support for metal electrocatalysts in order to improve their utilisation, enhance the conductivity, activity and stability [11]. Unfortunately, structural decomposition of PANI may occur if it is used under harsh environmental conditions for hydrogen production [10, 12]. For this reason, incorporation of different materials such as zeolites, metal, metal sulfide,

carbon nanotubes, and metal organic frameworks (MOFs) to the polymer backbone have been developed to prepare polymer-based composite with improved thermal stability, mechanical properties and some more functional sites on the polymer backbone [13-16]. For example, Corte *et al.* [17] reported the HER behaviour of nickel-PANI composite and observed that the presence of polymer matrix enhanced the catalytic activity on the electrode. Ding and co-workers [18] also reported a novel molybdenum ( $\text{MoS}_2$ )-disulfide nanosheets-decorated on the PANI matrix as HER electrocatalysts. The  $\text{MoS}_2$ /PANI nanocomposites exhibited higher catalytic activity and lower Tafel slopes for HER in  $\text{H}_2\text{SO}_4$  solution [18]. In addition, MOFs have shown great interest in various applications such as catalysis, magnetism, sensors as well as drug delivery owing to their high surface area and adjustable pore size [19]. Guo *et. al* [20] and reported the preparation of carbonized Zn-MOF/PANI composite by in situ chemical polymerisation. In another study, MOFs/PANI were synthesized by electrochemical polymerisation of aniline in the presence of different materials ( $[\text{NH}_2(\text{CH}_3)_2]_2[\text{Zn}_3(4,4\text{-biphenyldicarboxylate})_4]_5\text{DMF}$  (MOF1),  $[\text{Cd}(2,6\text{-naphthalene dicarboxylate})(\text{DMF})]$  (MOF2) and  $[\text{NH}_2(\text{CH}_3)_2]_2\text{Zn}_3(1,4\text{-benzenedicarboxylate})_4\text{DMF}\cdot\text{H}_2\text{O}$  (MOF3) [21]. In these studies, it was found that MOF/PANI composites showed superior activities as compared to neat PANI matrix as an electrode material for high performance supercapacitor and as a fiber coating for solid phase microextraction, respectively. In the current study, a PANI/MOF composite was prepared through in situ chemical polymerisation of aniline in the presence of MOF (HKUST-1). To the best of our knowledge, there are no reports on the synthesis of PANI based MOF (HKUST-1) composite for HER. The MOF (HKUST-1) was prepared via hydrothermal method, which allows precise control over the size, shape distribution, well-crystallised solid on the nanoscale, efficient synthetic conditions and ability to control the morphology of material crystals [22, 23]. The resulting PANI/MOF composite showed excellent structural and thermal properties as well as significant activity as an electrocatalyst for HER.

## 3.2. EXPERIMENTAL SECTION

### 3.2.1. Materials

Aniline (ANI) monomer, copper nitrate trihydrate ( $\text{Cu}(\text{NO}_3)_2 \cdot 3\text{H}_2\text{O}$ ), trimesic acid ( $\text{H}_3\text{BTC}$ ) and tetrabutylammonium perchlorate (TBAP) were purchased from Sigma Aldrich, South Africa. Ammonium per sulfate (APS) and iron chloride ( $\text{FeCl}_3$ ) were purchased from Riedel-de Haen and Educhem, respectively. Absolute ethanol was purchased at Merck, South Africa and hydrochloric acid (HCl), dimethyl sulfoxide (DMSO) and sulphuric acid ( $\text{H}_2\text{SO}_4$ ) were procured from Rochelle Chemicals. Aniline was distilled before use and the rest of the reagents were used without any further purification.  $\text{H}_2\text{SO}_4$  standard solutions were made in DMSO solution with 0.1 M TBAP as a supporting electrolyte system unless otherwise stated. All measurements were carried out at  $22 \pm 2$  °C maintained using water bath.

### 3.2.2. Synthesis of MOF, PANI and PANI/MOF composite

PANI was prepared by chemical oxidation polymerisation of aniline according to a previously reported method [24]. Cu-trimesic MOF (HKUST-1) was synthesized by following a hydrothermal procedure reported by Ke et al. [25]. PANI/MOF composite was synthesized as shown in Fig. 1. Briefly, 1 ml of the distilled aniline monomer and 3.6 wt.% MOF were dissolved in a solution of 10 ml HCl/100 ml distilled water in a 250 ml round-bottom flask. The solution was stirred for 30 min kept at 50 °C. About 2.40 g of  $(\text{NH}_4)_2\text{S}_2\text{O}_8$ , and 1.88 g of  $\text{FeCl}_3$  were added in the solution. The reaction mixture was stirred for another 3 hrs at the same temperature. The mixture was placed in an oven for overnight to evaporate the solvents and remaining content was washed with ethanol several times and re-dried at 50 °C.

### 3.2.3. Materials characterisations

The formation of the composite was confirmed by Cary 600 series Fourier transform infrared (FTIR) spectrometer (Agilent Technologies). The spectra were obtained in the wavenumber range between 500 and 4500  $\text{cm}^{-1}$  at room temperature. A minimum of 32 scans were collected at a resolution of 4  $\text{cm}^{-1}$ . The Raman spectra were recorded on a Horiba Jobin-Yvon Labram HR 2000 confocal Raman microscope with a wavelength of 514 nm.

Optical absorption spectra were recorded at room temperature in the wavelength region 200 nm – 800 nm using a Varian Cary 300 UV-Vis-NIR spectrophotometer. The structure of PANI, MOF and PANI/MOF composite was analyzed using X-ray diffraction (XRD Phillips PW 1830,  $\text{CuK}\alpha$  radiation,  $\lambda = 1.5406 \text{ \AA}$ ).

The surface morphology was performed using Auriga field-emission scanning electron microscope (SEM) coupled with EDS. The internal morphology was carried out using a FEI Tecnai G2 20 transmission electron microscope (TEM) coupled with EDX, operated at an accelerating voltage of 200 kV. The elemental analysis was determined using Varian SpectrAA 110 atomic absorption spectrometer (AAS).

The thermal stability was performed using a Perkin-Elmer STA 6000 instrument connected to a PolyScience digital temperature controller under  $\text{N}_2$  gas purged at a flow rate of 20 ml/min. The calibration of the instrument was performed using indium (melting point = 156.6  $^\circ\text{C}$ ) and aluminium (melting point = 660  $^\circ\text{C}$ ). Samples ranging between 1–4 mg were heated from 30–500  $^\circ\text{C}$  at a constant heating rate of 20  $^\circ\text{C}/\text{min}$ . The data was collected and analyzed using Pyris software®.

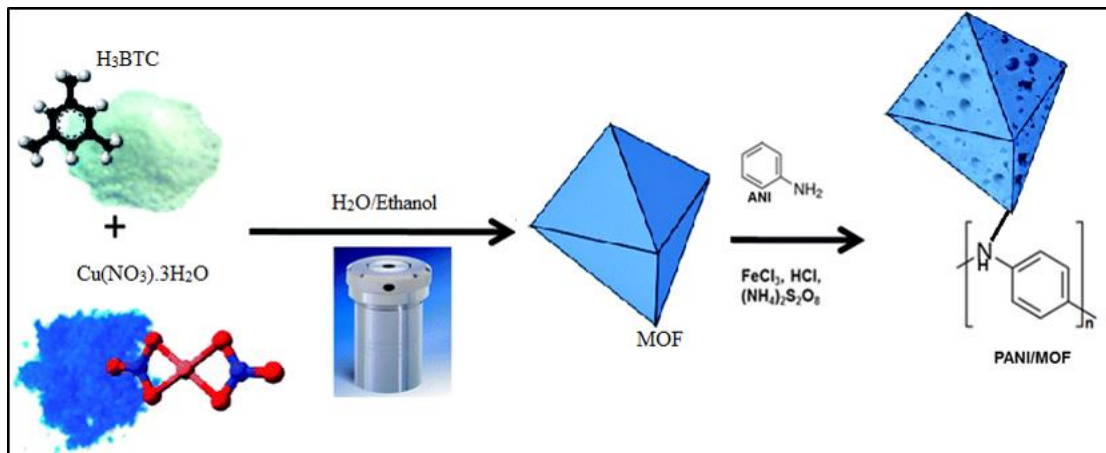
Electrochemical measurements were carried out using EPSILON electrochemical workstation. The data was collected using a conventional three-electrode set-up with gold electrode (3 mm diameter, 0.071  $\text{cm}^2$  area) as a working electrode, Pt wire as a counter electrode and Ag/AgCl wire as a reference electrode. Repetitive scanning of MOF, PANI and PANI/MOF composite ( $\sim 3.0 \times 10^{-3} \text{ mol/L}$ ) was measured from -2.0 to 1.25 V at the scan rate of 0.02 - 0.10  $\text{Vs}^{-1}$ . Electrochemical experiments were performed in 10 ml of 0.1 M TBAP/DMSO electrolytic system. HER studies were done using various concentrations of 0.03–0.45 M  $\text{H}_2\text{SO}_4$  as hydrogen source in 0.1 M

TBAP/DMSO system and  $\sim 2.0 \times 10^{-4}$  mol/L of MOF, PANI AND PANI/MOF as electrocatalysts.

### 3.3. RESULTS AND DISCUSSION

#### 3.3.1. Synthesis

The synthesis of polyaniline doped with metal organic framework composite referred as PANI/MOF was prepared by in situ chemical oxidative polymerisation of aniline monomer in presence of MOF, using ammonium persulfate as an oxidant. The integrated preparation process is depicted in Scheme 3.1. Initially, prior to in situ polymerisation, MOF material was prepared from hydrothermal conditions using Cu-metal salt and trimesic acid ( $H_3BTC$ ) as a carboxylate organic linker to yield pure, highly crystalline MOF. Subsequently, for comparison, pure polyaniline was prepared in absence of MOF for comparison. The mechanism of oxidative polymerisation of aniline in the presence of ammonium persulfate oxidant was explained in details in Scheme 2.3-2.5. The process of composite formation undergoes similar mechanism of polyaniline and MOF materials interacting with polymer using different interaction processes as explained. The resultant PANI/MOF gave similar dark blue powder of as-prepared polyaniline.



Scheme 3.1: Schematic presentation of PANI/MOF composite through chemical oxidation polymerisation of aniline monomer in the presence of MOF.

### 3.3.2. Spectroscopic Characterisations

#### 3.3.2.1. Fourier transform infrared (FTIR) and Raman spectroscopy

To examine the polymerisation process and recognition of any changes on the PANI after being embedded by MOF, FTIR analysis was employed in the region 500-4500  $\text{cm}^{-1}$  and the results are presented in Figure 3.1(a). For the neat PANI, the existence of the absorption band at 806  $\text{cm}^{-1}$  relates to C-H out of plane deformation bending of the benzene ring [21]. The absorption band at 1138  $\text{cm}^{-1}$  was due to the vibration mode of the  $-\text{NH}^+=$ . The band at 1493  $\text{cm}^{-1}$  corresponds to C=N stretching vibration, while the peak at 1575  $\text{cm}^{-1}$  is associated to C=C stretching vibration, showing the deformation of the benzenoid and quinoid rings [26]. The peaks between 2500 and 3500  $\text{cm}^{-1}$  are due to =N-H stretching vibration [27, 28]. The observed absorption bands are characteristics of PANI, confirming its successful synthesis. Furthermore, all these bands suggest that this type of polymer is similar to that of an emeraldine base [29]. It is also noteworthy to mention that the absorption band at 1575  $\text{cm}^{-1}$  in the case of MOF disappeared in the composite indicating a successful synthesis of PANI/MOF composite.

The Raman analysis was performed to confirm the interaction between MOF and PANI. Figure 3.1(b) presents Raman spectra of PANI, MOF and PANI/MOF composite. The Raman spectra of MOF exhibit the weak and strong bands at  $\sim 1000$  and  $\sim 1520$   $\text{cm}^{-1}$ , which are due to  $\nu(\text{C}=\text{C})$  modes of benzene ring on organic linker. There are observable bands at  $\sim 710$  and  $\sim 810$   $\text{cm}^{-1}$  ascribed to out of phase ring C-H bending vibrations. The bands at lower frequencies are due to Cu-O stretch and this is in accordance with the work reported in the literature [30, 31]. The Raman spectrum of PANI showed vibrations at  $\sim 1197$ , 1220, 1500 and 1610  $\text{cm}^{-1}$  which are associated to C-H in-plane bending vibration of benzenoid ring, C-N bonding modes of benzenoids ring, C=N stretching vibrations of unprotonated quinoid ring and C-C stretching of emeraldine salt, respectively [32, 33]. To elucidate the character of the interaction between PANI and MOF, we discuss the changes of the spectrum of pure



PANI and MOF. This interactions can be deduced by the appearance of new bands or disappearance. It can be seen that the spectrum of the composite shows four bands at  $\sim 683, 956, 1110 \text{ cm}^{-1}$ . These peaks are assigned to in plane C-H bending of quinoid, benzoid symmetry ring stretching and ring deformation of semiquinoid, respectively. There is an observable peak at  $1345 \text{ cm}^{-1}$  which is attributable to electrostatic interactions between the partially negative charge of organic linker on MOF and partially positive nitrogen of PANI [34]. In addition, the peak associated with MOF also shifted from  $605$  to  $728 \text{ cm}^{-1}$  in the composite. These obvious changes suggested the existence of an interaction between MOF and PANI since the transition metal Cu has a tendency to form coordination compound with the nitrogen atom in PANI [35].

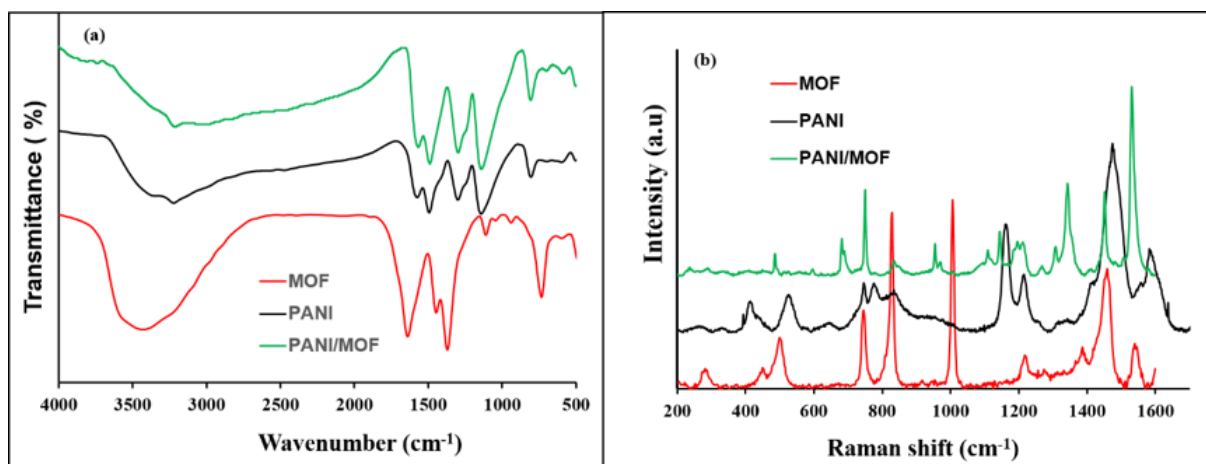


Figure 3.1: (a) FTIR and (b) Raman spectra of MOF, PANI and PANI/MOF composite.

### 3.3.2.2. Ultraviolet-visible spectroscopy (UV-vis)

The absorption spectra of neat PANI, MOF and its composite dissolved in DMSO are shown in parts a and b of Figure 3.2(a). The neat PANI shows two absorption peaks at 353 and 552 nm. The band at 353 nm corresponds to the  $\pi - \pi^*$  transitions of the benzoid structure, while the absorption at 552 nm is associated to exciton formation in the quinoid rings as well as partially oxidised absorption peak of conducting PANI [36, 37]. Nevertheless, there is a slight shift in the absorption peak at a lower wavenumber

upon composite formation to 357 nm. The shift in the peaks is attributed to the increase in the  $\pi$  conjugation in the PANI backbone [37]. The obvious shift in the peak suggested a possible interaction between PANI and MOF as conferred by FTIR. Figure 3.2(b) shows the concentration dependent studies of the PANI/MOF composite. The Beer-Lambert assumption was obeyed with an increase in the concentration of the composite, whereby the conduction band on the material did not change. Nonetheless, there is an increase in the absorbance of the PANI composite. The inset in Figure 3.2(b) shows the plot of absorbance versus concentration which was used to determine the molar extinction coefficient of PANI and its composite. The molar extinction coefficient was found to be  $4 \times 10^{-3}$  and  $4.2 \times 10^{-3} \text{ cm}^{-1} \text{ ppm}^{-1}$  for PANI and PANI/MOF composite, respectively.

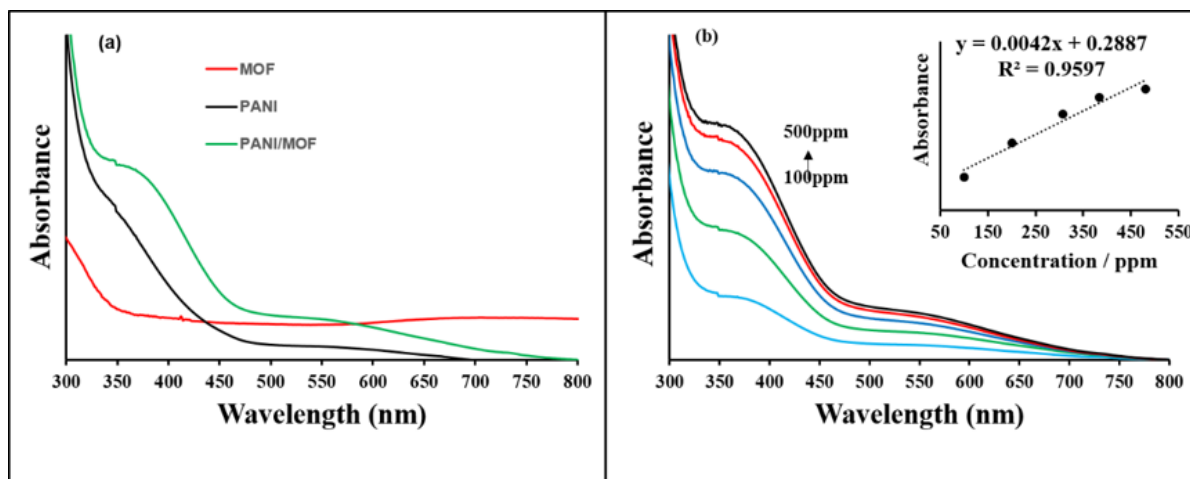


Figure 3.2: (a) Absorption spectra of MOF, PANI and the composite in DMSO as well as (b) absorption spectra of PANI/MOF composite measured at different concentrations.

Figure 3.3 presents Tauc plot variation  $(\alpha h\nu)^2$  that was employed to calculate the energy band gap of PANI and its composite [38]. The energy band gap was calculated by a linear extrapolation of the Tauc curve when it cuts the x-axis. The energy band gap values of the neat PANI and PANI/MOF composite were found to be 1.50 and 1.35 eV, respectively. The reduction in the optical band gap in the case of the

composite was due to a rise in the electron density of the composite as compared to the neat PANI. This observation showed our samples can be suitable for catalytic applications [39]. From the AAS results, it was found that the amount of Cu present in MOF and PANI/MOF composite was 23.99 and 0.05 wt. %, respectively, further confirming the presence of MOF in the composite.

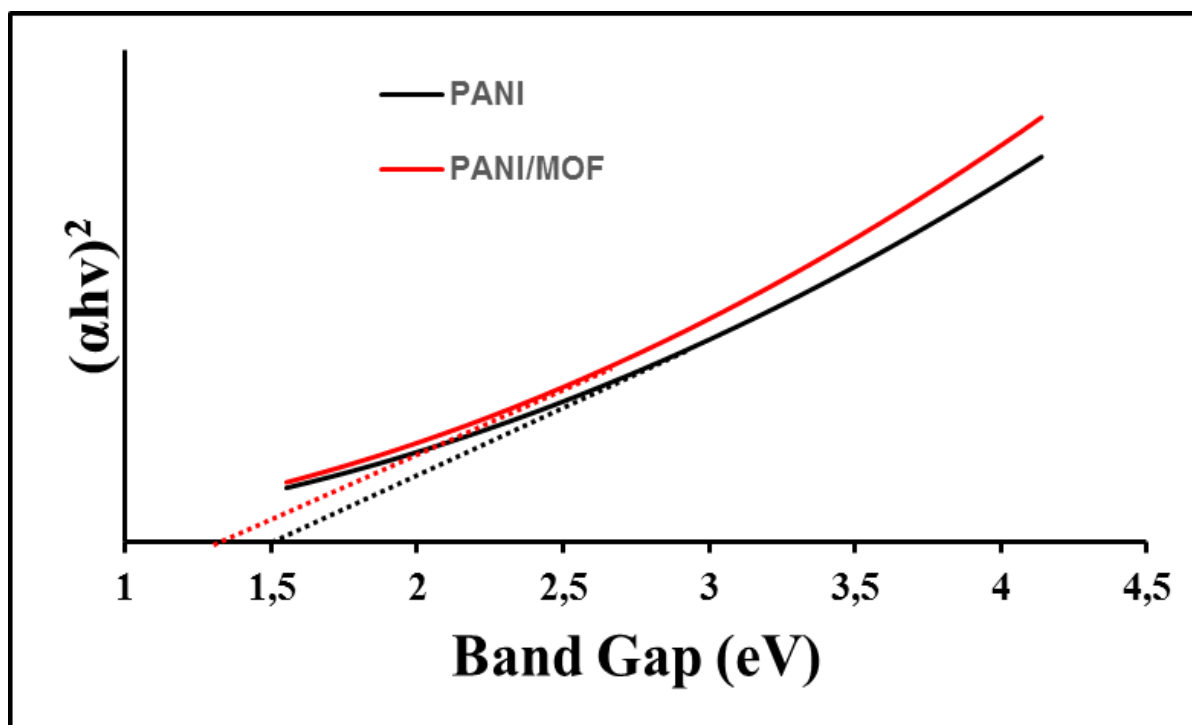


Figure 3.3: Tauc plot of PANI and PANI/MOF composite for energy band gap determinations.

### 3.3.2.3. X-ray diffraction

In order to substantiate the purity of the synthetic MOF, XRD analysis was performed. The XRD patterns of MOF, PANI and PANI/MOF composite are depicted in Figure 3.4. It can be noticed that MOF exhibits cubic crystal structure diffraction patterns identical to those of the simulated one (MOF CSID), indicating that the structure of HKUST-1 was well preserved and the MOF was a pure powder [40]. In addition, the well-defined sharp peaks were observed for MOF, indicating a highly crystalline microporous

structure [27]. The neat PANI exhibits some sharp and two broad diffraction peaks at  $2\theta = 21$  and  $26^\circ$  corresponding to (100), and (200) planes, respectively [41, 42]. The sharp peaks indicate some degree of crystallinity [43]. The PANI/MOF composite shows similar diffraction peaks to the neat PANI, and no obvious diffraction peaks of MOF appeared. This observation suggested that the amorphous structure of PANI was maintained upon composite formation with MOF.

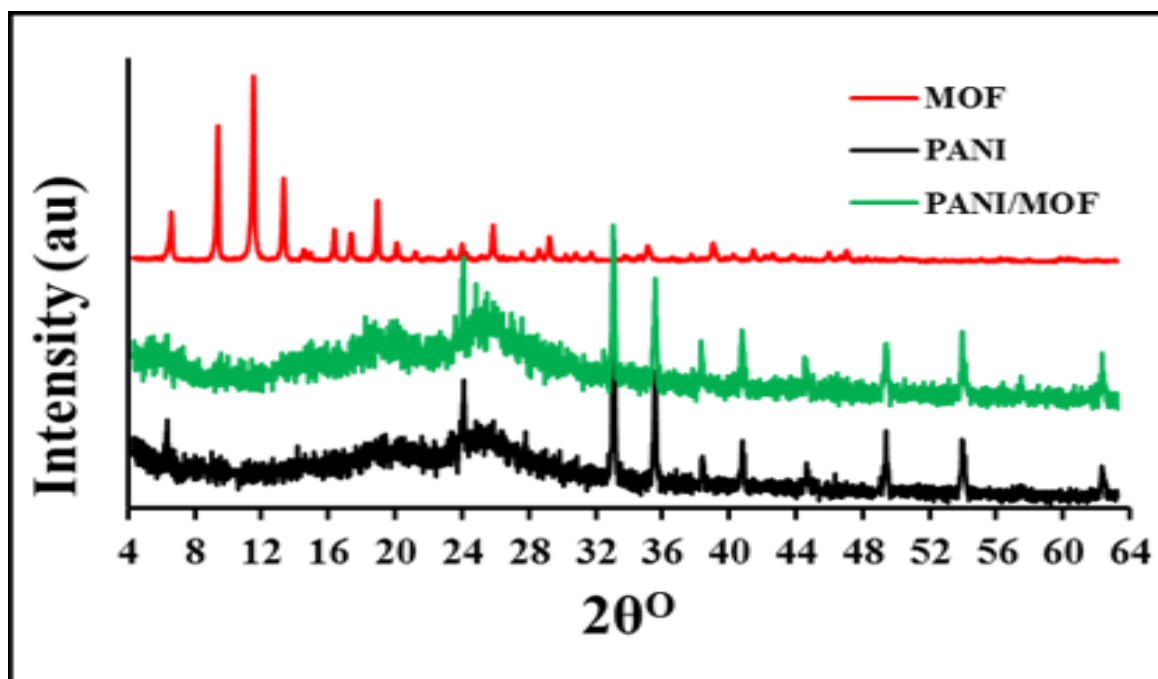


Figure 3.4: XRD patterns of MOF, PANI and PANI/MOF composite.

### 3.3.3. Morphological Characterisations

The morphologies of PANI, MOF and PANI/MOF composite were investigated by SEM and the results are presented in Figure 3.5(a, c and e), respectively. The SEM image of PANI depicted fibrous morphological structures along with a large number of interconnected tubules or agglomerated structures, which is in accordance with other reports [44, 45]. The fibrous structure may be due to the soft template-assisted growth of PANI [46]. EDS results of PANI (Figure 3.5(b)) showed the presence of Fe, Na, S

and Cl in the polymer backbone. These elements are due to oxidants and acidic medium used during synthesis. The MOF image depicted some irregular crystals with octahedral shapes confirming a low control on the crystal growth parameters [47]. The corresponding EDS results of MOF revealed the presence of Cu [47, 48]. The PANI/MOF composite also exhibited some finer morphological features compared to the neat PANI. In addition, there were some small nanorods observed in the case of PANI/MOF composite. It is also noticeable that the crystal structures of MOF are non-observable in the case of the composite. This result suggested wrapping of MOF by PANI. The PANI/MOF composite exhibited an increase in the percentage compositions of C and O with no trace of Cu detected on the surface of the polymer as an indicative of the wrapping of MOF by PANI.

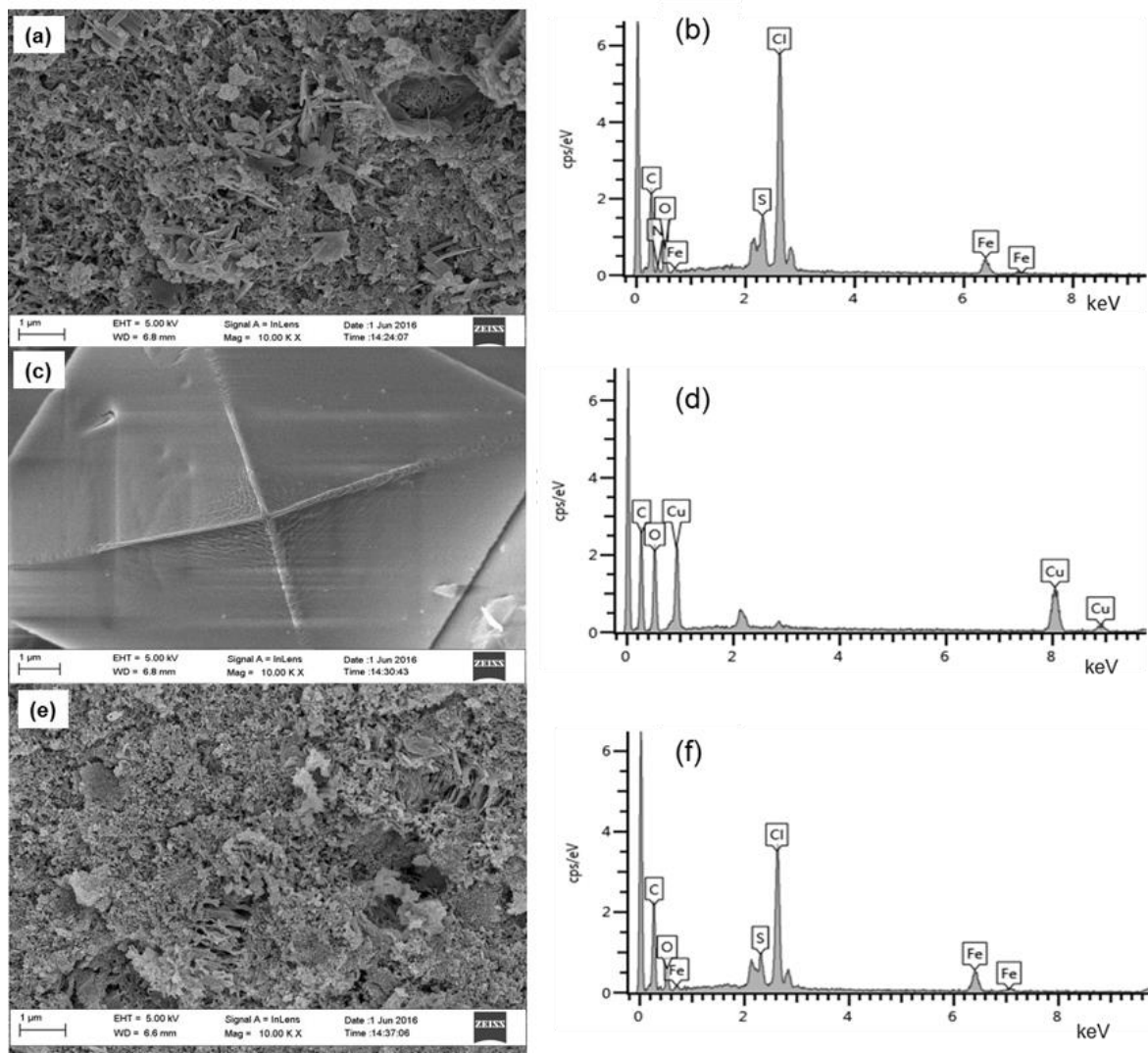


Figure 3.5: SEM images of (a) PANI, (c) MOF, (e) PANI/MOF composite and EDS spectra of (b) MOF, (d) PANI, (f) PANI/MOF composite.

Parts a–c of Figure 3.6 present the TEM images of PANI, MOF and PANI/MOF composite and inset images are the selected area electron diffraction (SAED) patterns used to determine the crystallinity of the samples. It can be seen that both PANI and MOF showed nanofibers/tubular structures (Figure 3.6 (a and b)). Upon composite formation, the morphology was relatively tubular but some microporous structures could also be noticed. This was attributed to the adsorption of aniline on the MOF template and its subsequent polymerisation. Furthermore, it is also noteworthy to mention that the fibrous structures of PANI are distracted when the composite is

formed. The SAED result of MOF showed clear ring patterns which suggested a crystalline structure [27]. Notably, the neat PANI exhibited a disordered structure, which indicated that the molecules are arranged to a certain definite position in the lattice. This is a typical amorphous structure of PANI [44, 49]. Figure 3.6(c) showed that the composite maintains an amorphous structure similar to PANI. Furthermore, it is also noticeable that the structural modification of PANI had been enhanced by MOF upon composite formation. This result is in good agreement with the XRD observations (see Figure 3.4). The elemental analysis of C and O in the composite were investigated using TEM coupled with EDX and the percentages are 74.6 and 5.02 for C and O respectively, as shown in Figure 3.6(d). The Cu content of MOF in the composite was detected. The presence of small peak of Ni (Figure 3.6(d)) is due to impurities trapped in the PANI backbone during synthesis process as well as Ni grid used during the TEM analysis.

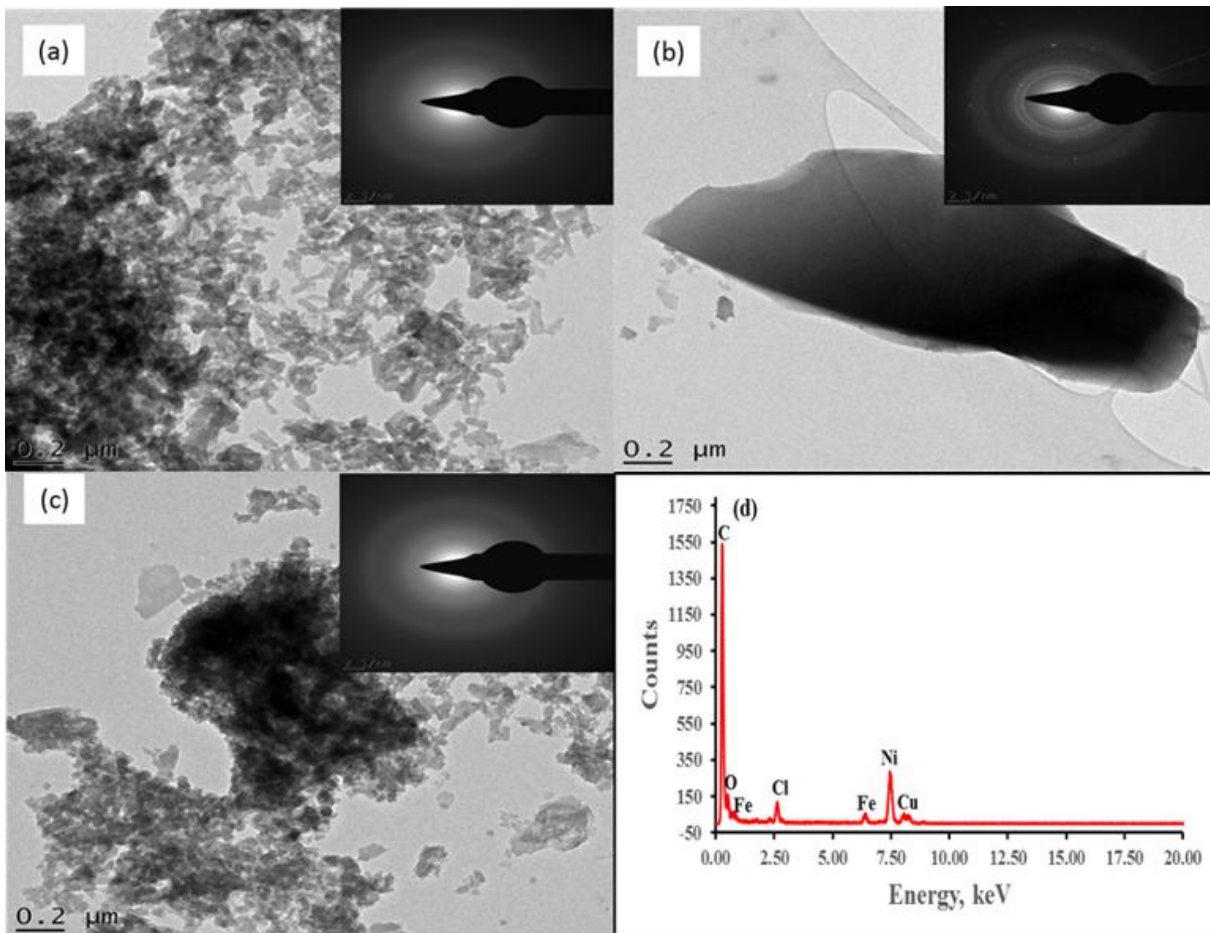


Figure 3.6: TEM images (a) MOF (b) PANI (c) PANI/MOF composite and (d) EDX spectrum of PANI/MOF composite. Inset: SAED images of various samples.

### 3.3.4. Thermogravimetric analysis

The TGA analysis can be used to determine the precise weight ratio of each component in a sample and the thermal stability of the composite. Furthermore, by comparing the TGA curve of each component separately to its curve in a composition material, we can also learn about the degree of interaction between the reacting species. The TGA thermograms of MOF, PANI and PANI/MOF composite, in comparison, analysed at a heating rate of 10 °C/min are presented in Figure 3.7. It can be seen that MOF exhibits two thermal degradation steps throughout the experimental temperature range. These two steps appear at about 100 and 350 °C. The thermal



degradation steps are normally attributed to the intrinsic thermal degradation characteristics of MOF which correspond to water and ethanol physisorbed in the framework of MOF, as well as the degradation of the organic linker and producing copper oxide [47, 48, 50, 51]. The neat PANI also shows a two-step weight loss from 100 to 450 °C due the release of moisture and the elimination of the doped acid bound to PANI chains as well as the decomposition of the pristine PANI backbone [44, 49]. For PANI/MOF composite, the lower rate of mass loss with increasing temperature may be due to the internal change in this material that is not accompanied by mass loss at elevated temperature. In addition, though the final degradation step occurred at about 350 °C for all the samples, the MOF sample exhibits a steeper weight loss as compared to both neat PANI and the composite. The slower, less steep degradation step in the case of the composite suggested a higher thermal stability due to the stabilizing effect of MOF and a changed morphology upon composite formation. Furthermore, an increased thermal stability may be due to a change in morphology upon addition of MOF in the composite as observed in the SEM results.

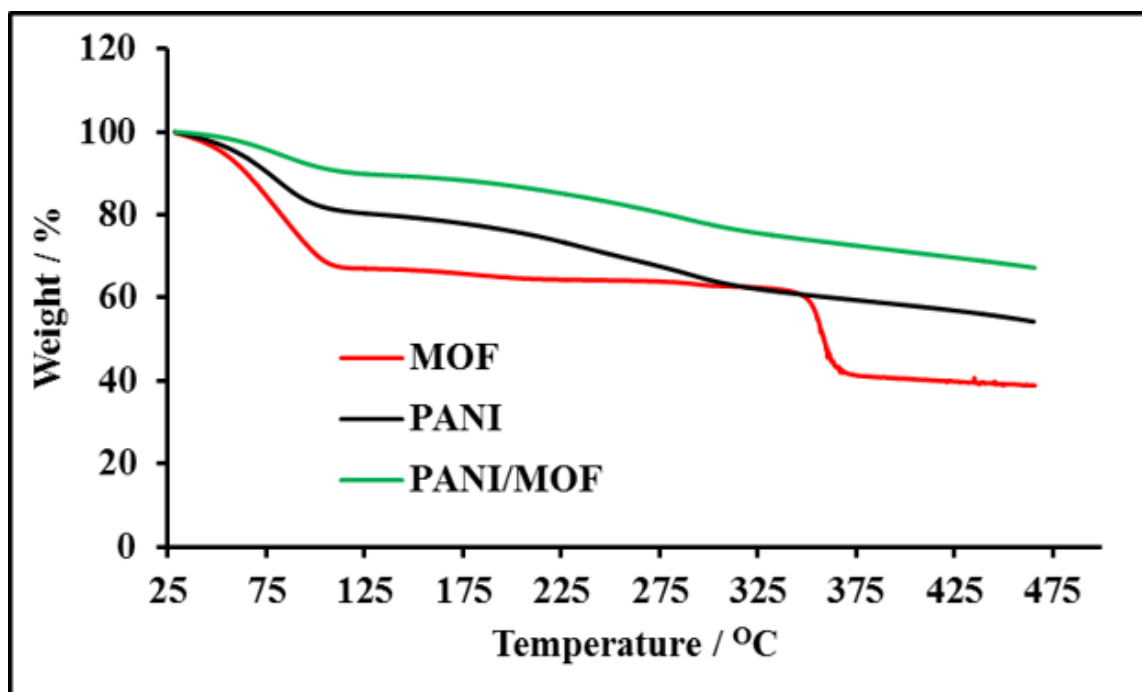


Figure 3.7: TGA curves of MOF, PANI and PANI/MOF composite.

### 3.3.5. Electrochemical Characterisations

Electrochemistry of functional species is one of the most prominent parameters for potential use as electrocatalysts for hydrogen production. In order to decide the possible use of any material, its electrochemical responses in a solution should be determined. Electrochemical characterizations of PANI, MOF and PANI/MOF composite were investigated using cyclic voltammetry (CV). Figure 3.8(a) showed typical current-potential curves of the gold electrode in 0.1 M TBAP/DMSO system of blank, MOF, PANI and PANI/MOF composite. It was noticeable that the Faradaic contributions (redox process) onto gold electrode (blank) was observed at around -0.58 V. This is a typical redox process of bare Au electrode [52]. However, there are two reduction processes observed for MOF. This could be related to the Cu deposition involving two successive one-electron process [53]. Nila and Gonzales [54] reported that the electrochemical reduction of  $\text{Cu}^{2+}$  in solution proceeds in two one electron reversible waves via a  $\text{Cu}^+$  intermediate, in which the stability of the intermediate was due to the presence of ions in the solution. The shift in potential was also observed and reported by Loera-Serna et al. [55] in LiCl solution indicating that the electrochemical processes of Cu during the direct sweep took place in the MOF. However, in this study, the reduction of  $\text{Cu}^{2+}$  to  $\text{Cu}^+$  occurs at more negative potential. This might be due to electrochemical properties of Au electrode in TBAP/DMSO system. On the other hand, PANI in the potential window of TBAP/DMSO electrolyte system showed a quasi-reversible processes. In addition, the voltammogram of PANI indicated a one redox couple which is an indication of the merging of three known oxidation states of PANI [56]. The redox couple observed at cathodic peak potential ( $E_{p,c}$ )  $\sim$  -0.64V and anodic peak potential ( $E_{p,a}$ )  $\sim$  -0.68V are due to polyleucoemeraldine radical cation, transformation of PANI from the reduced leucoemeraldine (LE) state to the partly oxidized emeraldine state (EM), and further oxidized to the pernigraniline (PE). Similar electrochemical characteristics of the synthesized PANI was reported by Genies et al. [57]. The increase in the cathodic current in CV of PANI/MOF composite encourages strong interaction between MOF and PANI, and therefore favours the uncoiling of PANI chains. In this uncoiled

conformation, the probability of moieties exposed to oxidation is more leading to higher Faradaic current [37]. The potential reduction of  $\text{Cu}^{2+}$  to  $\text{Cu}^+$  occurring in composite was *c.a.*  $-0.653$  V/Au electrode. Meanwhile, the reduction potential at around  $-1.59$  V in both PANI and composite was an illustration of redox process in PANI ring-based electron transfer characters. One of the important feature observed in the CV of the composite was the merging of new cathodic peak towards negative potential which was clearly visible on the square wave voltammogram (SWV) and the results are presented in Figure 3.8(b). The SWV was utilized as the electrochemical probe of the system due to its higher sensitivity Faradaic current [58]. The positive cathodic side was considered as it is the representative of hydrogen evolution prior evaluating the amount of current.

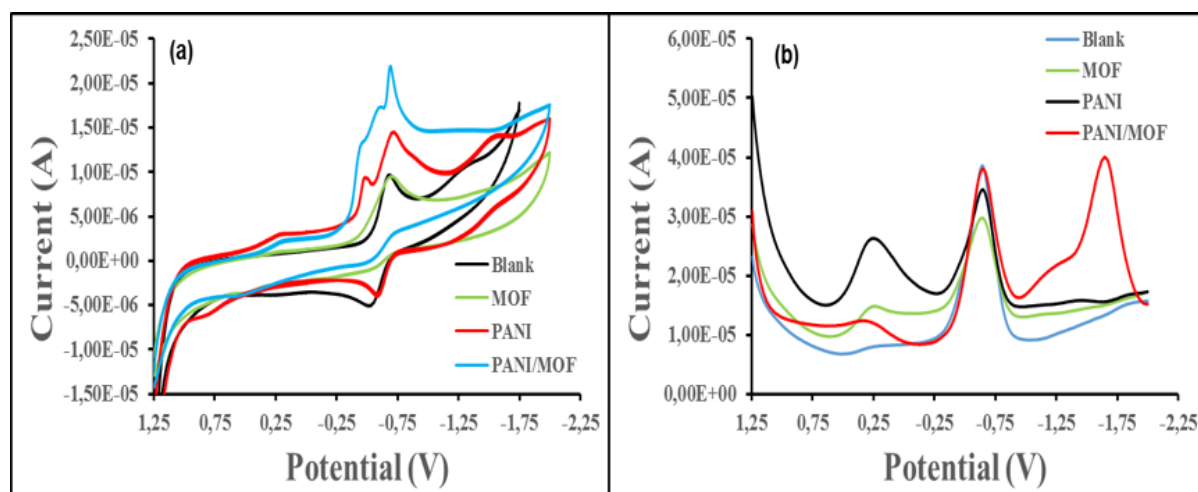


Figure 3.8: (a) CV and (b) SWV curves of MOF, PANI and PANI/MOF ( $\sim 3.0 \times 10^{-3}$  mol/L) in 0.1 M TBAP/DMSO electrolyte solution on Au electrode.

The influence of scan rate on the electrochemical response of MOF, PANI and PANI/MOF composite was accomplished in 0.1 M TBAP/DMSO system using Au working electrode. The multiscan voltammograms of the samples are shown in parts a-c of Figure 3.9, respectively. It was obvious that the current response increased with increasing scan rates. In Figure 3.9(c), the PANI/MOF composite showed enhancement of current response as compared to neat MOF and PANI. This indicated

that the PANI and MOF structures in the composite were conductive and diffusion of electrons along the polymer chain was taking place. All redox couples showed electrochemical quasi-reversible process with respect to change in peak potential ( $\Delta E_p$ ) and the ratio of anodic and cathodic peak current ( $I_{pa}/I_{pc}$ ) values. Unity of  $I_{pa}/I_{pc}$  ratios at all scan rates and the logarithm of the absolute value of the reductive peak current against the logarithm of the scan rate indicates diffusion controlled characters of the redox processes as shown in Figure 3.9(d).

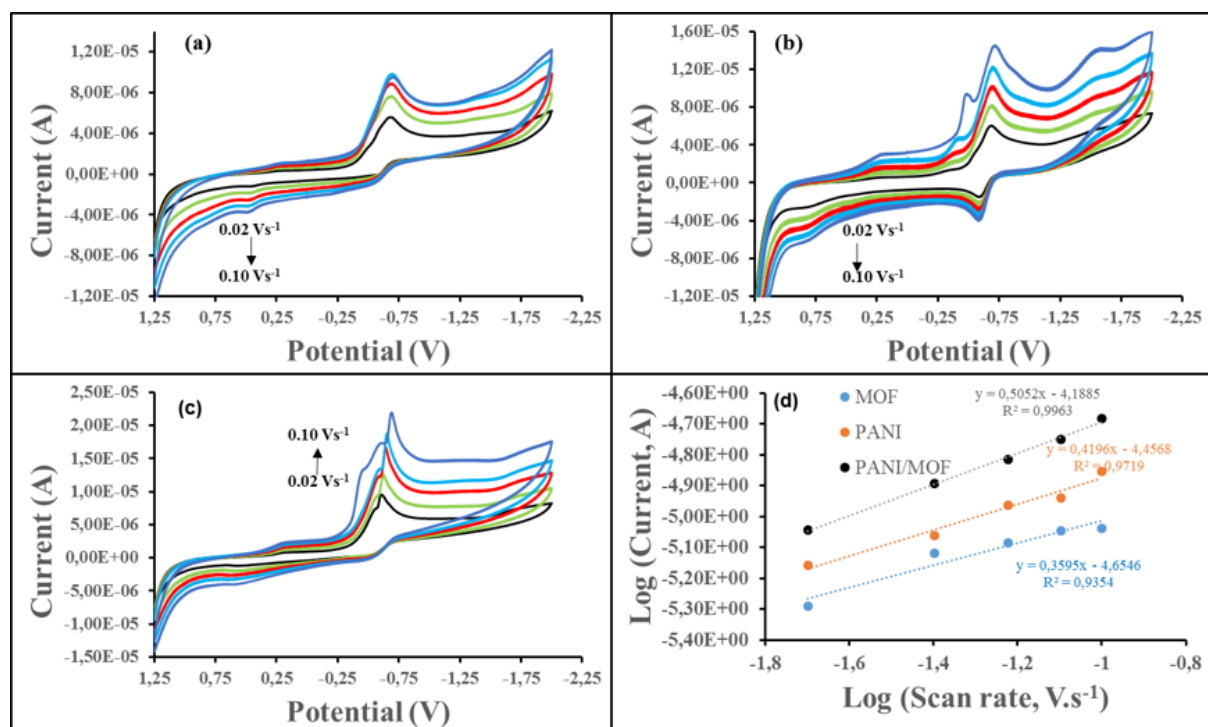


Figure 3.9: Voltammetric curves of (a) MOF (b) PANI (c) PANI/MOF composite ( $\sim 3.0 \times 10^{-3}$  mol/L) in 0.1 M TBAP/DMSO electrode system at different scan rate (0.02 – 0.10 Vs<sup>-1</sup>) and (d) The log-log plot of the absolute value of the peak current vs scan rate of MOF, PANI and PANI/MOF composite.

The peak current ( $I_p$ ) for diffusion-controlled electron-transfer process is given by Eq. (1) [59]:

$$I_p = nFA[\text{cat}](D)^{1/2}(Fv/RT)^{1/2} \quad (3.1)$$

where  $n$  is the number of electrons transferred,  $A$  is the area of the working electrode in  $\text{cm}^2$ ,  $F$  is Faraday's constant ( $96,485 \text{ C mol}^{-1}$ ),  $D$  is the diffusion coefficient,  $R$  is the gas constant ( $8.31451 \text{ J mol}^{-1} \text{ K}^{-1}$ ),  $T$  is the thermodynamic temperature (K),  $\nu$  is the scan rate and  $[\text{cat}]$  is the concentration of catalyst in  $\text{mol}\cdot\text{cm}^{-3}$ . Consistent with Eq. (1), Fig. 11 showed that the current increased linearly with increasing the square root of the scan rate,  $\nu^{1/2}$ . The  $D$  values were determined to be  $3.05 \times 10^{-7}$ ,  $2.40 \times 10^{-7}$  and  $7.34 \times 10^{-7} \text{ cm}^2\cdot\text{s}^{-1}$  for MOF, PANI and PANI/MOF composite, respectively. The significant value of the composite is approximately an order of magnitude faster than the neat PANI.

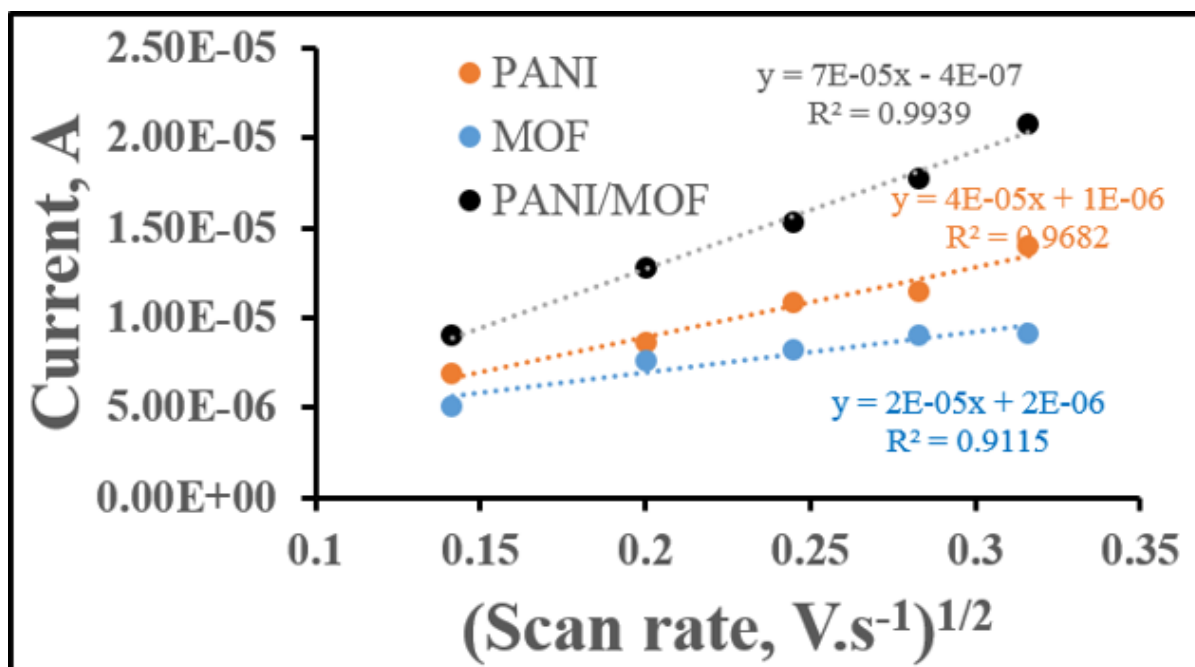


Figure 3.10: Peak current as a function of square root of scan rate on Au in 0.1 M DMSO/TBAP electrode system at various scan rate (0.02 – 0.10 Vs<sup>-1</sup>).

### 3.3.6. Hydrogen Studies

The electrocatalytic activity of the samples was evaluated using CV in 0.1 M TBAP/DMSO system as an electrolytic solution and  $\text{H}_2\text{SO}_4$  as  $\text{H}_2$  source and the results are presented in Figure 3.11(a). Upon addition of  $\text{H}_2\text{SO}_4$ , a wave catalytic near

the reduction potential was observed, which suggested that PANI, MOF and PANI/MOF composite are reducing  $\text{H}_2\text{SO}_4$  to  $\text{H}_2$ . The current intensities of the samples can be related to the amount of  $\text{H}_2$  produced. Therefore, the greater the current readings will result to a large quantity of  $\text{H}_2$  production. This observation confirmed that our samples possessed best electrocatalytic effect [60]. Furthermore, there was an intense increase in the current intensity of PANI/MOF composite at  $\sim -1.5$  V compared to both MOF and PANI. This result indicated that the PANI/MOF composite was more effective in producing maximum  $\text{H}_2$  in comparison to neat MOF and PANI. The different scan rate dependent studies were used to examine the electrochemical properties of the samples during electrocatalytic hydrogen evolution and the results are presented in Figure 3.11(b-d). Multiscan voltammogram of all the samples showed that there is an increase in the cathodic peak current with increasing the scan rate in acidic medium. From these results, it can be concluded that the enhancement of cathodic current of the samples showed suitability of the complexes as reasonable electrocatalysts for the HER application.

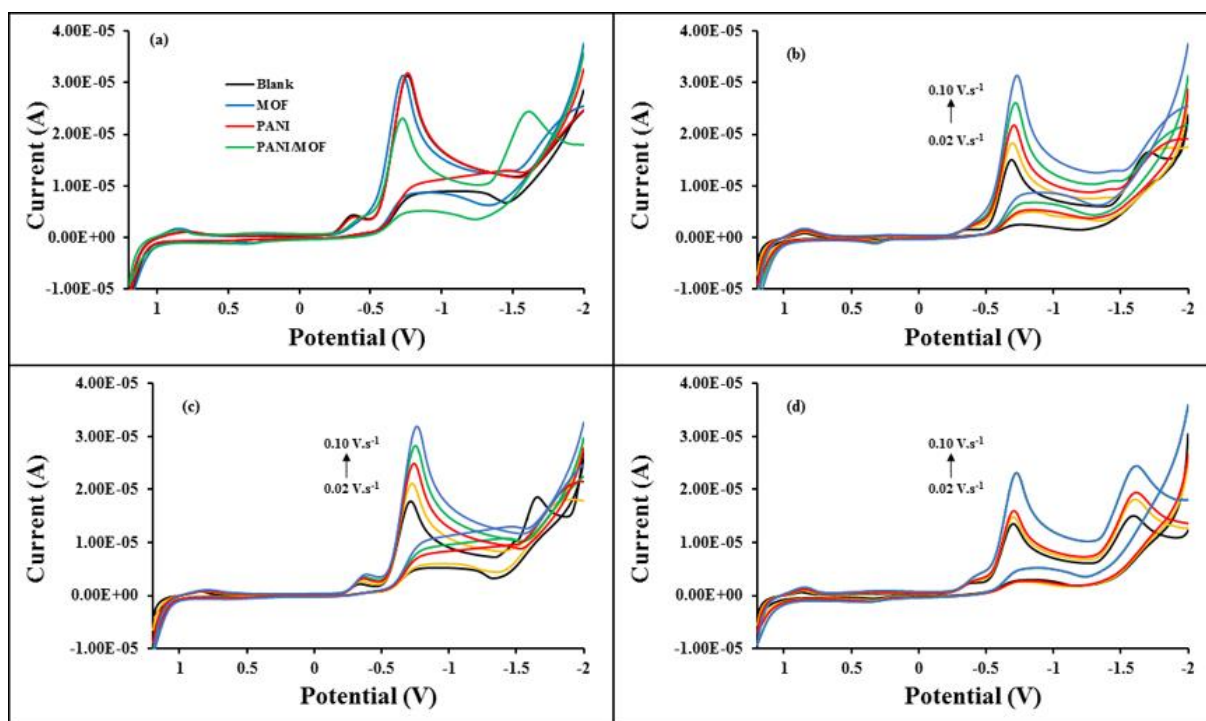


Figure 3.11: (a) CV curves of PANI, MOF and PANI/MOF composite ( $\sim 2.0 \times 10^{-4}$  mol/L) at  $0.10 \text{ V s}^{-1}$  (b) CV curves of (b) MOF (c) PANI and (d) PANI/MOF composite in the presence  $0.075 \text{ M H}_2\text{SO}_4$  at different scan rate on Au electrode in  $0.1 \text{ M TBAP/DMSO}$  electrode system.

Furthermore, CV of PANI, MOF and PANI/MOF composite in the presence of  $\text{H}_2$  source was performed at different  $\text{H}_2\text{SO}_4$  concentration ( $0.033 - 0.300 \text{ M}$ ) in  $0.1 \text{ M TBAP/DMSO}$  electrolytic system and the results are depicted in Figure 3.12(a-c). It is noticeable that the peak positions are independent of the  $\text{H}_2$  source concentration towards the more negative potential and high values of current. However, at low acid concentration, the peak current of catalytic wave in MOF and PANI/MOF composite increased linearly with the concentration, which indicated an enhancement in HER as shown in Figure 3.12(d) at fixed potential of  $-0.67 \text{ V}$ . Conversely, it was seen that there was a decrease in catalytic wave in the composite due to the material's ability to absorb hydrogen and the enhancement of hydrogen production was observed at  $-1.5 \text{ V}$ .

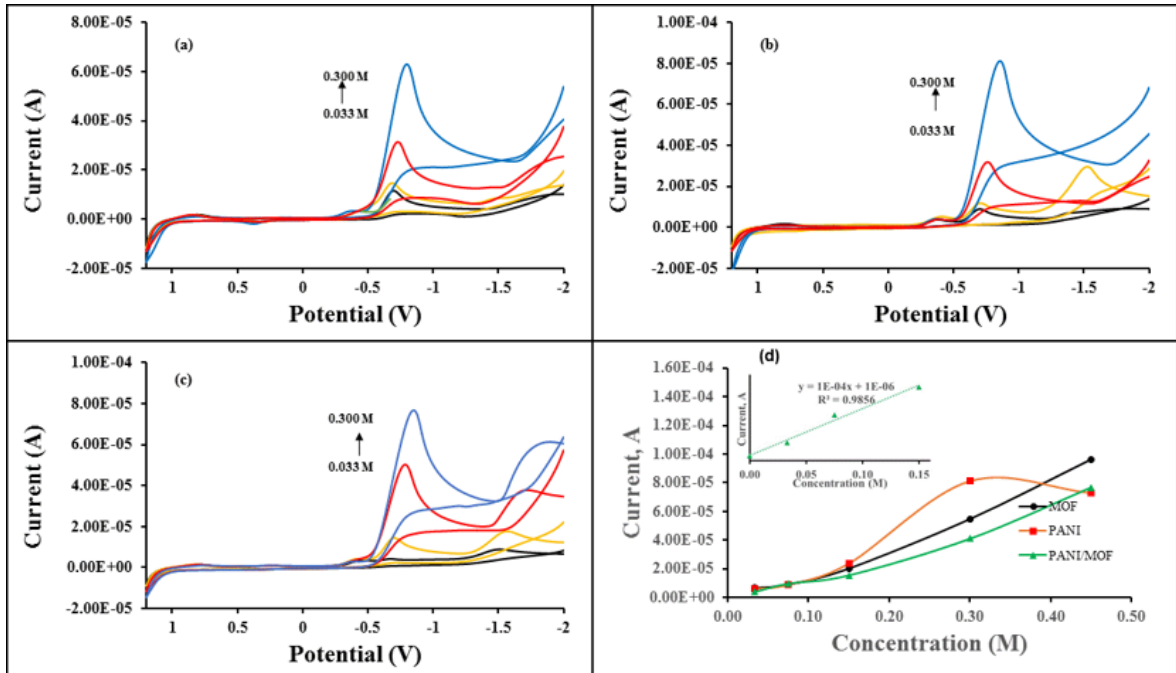
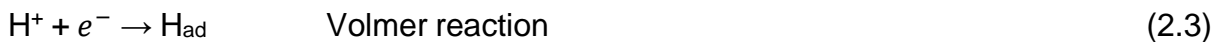


Figure 3.12: CV curves of (a) MOF (b) PANI and (c) PANI/MOF composite ( $\sim 2.0 \times 10^{-4}$  mol/L) in the presence 0.033 to 0.45 M  $\text{H}_2\text{SO}_4$ ; and (d) current as a function of  $\text{H}_2\text{SO}_4$  concentration of the electrocatalyst in 0.1 M TBAP/DMSO electrolyte solution on gold electrode at  $0.10 \text{ V} \cdot \text{s}^{-1}$  scan rate. Inset: Linear fitting at low concentration of composite.

The Tafel plot is used to get a better grasp on the kinetics of electrochemical reactions for HER [61]. The Tafel slope value gives an important information on the rate determining step in an electrochemical reaction. It is an inherent property of the electrode material. Furthermore, the overall electrocatalytic HER can also be explained by means of mechanism. In an acid medium, the HER pathway could proceed via three main steps [62, 63]:





It has been reported that for the HER on platinum electrode in acidic solutions, the reactions above show the Tafel slope values of 120 mV, 40 mV and 30 mV for the Volmer, the Heyrovsky and the Tafel, respectively [64, 65]. From these reactions, the HER process can either proceed by combination of Volmer-Heyrovsky or Volmer-Tafel mechanism.

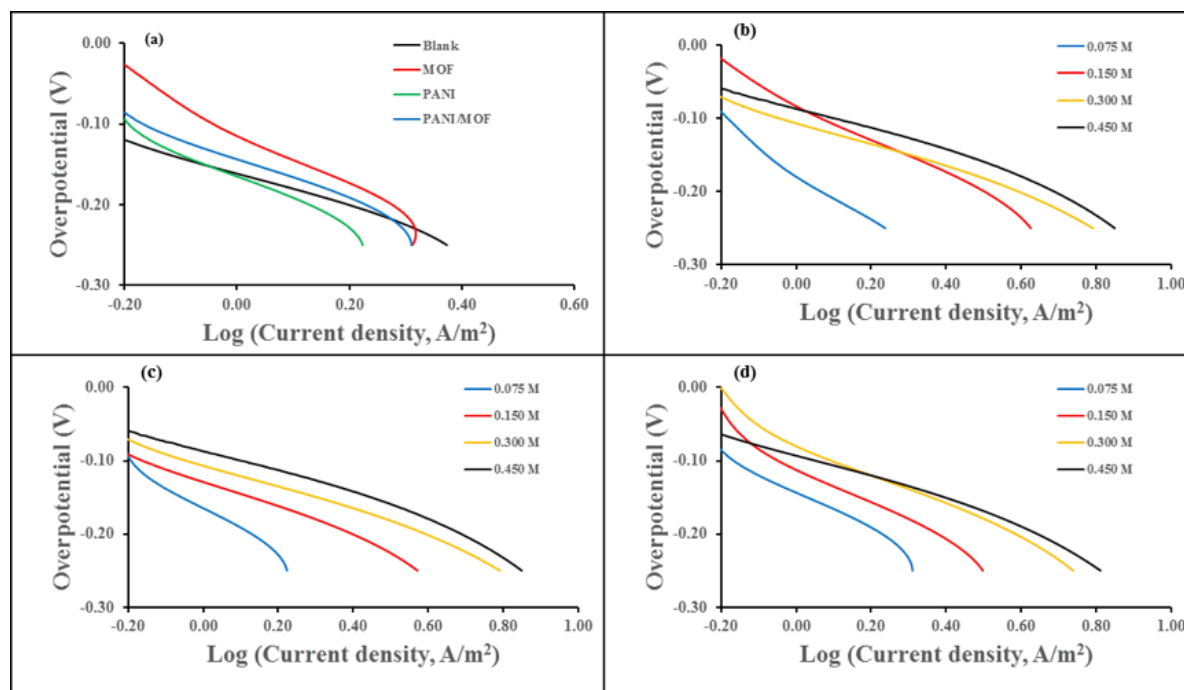


Figure 3.13: Tafel plots of (a) blank, PANI, MOF and PANI/MOF composite ( $\sim 2.0 \times 10^{-4}$  mol/L) in the presence 0.075 M  $\text{H}_2\text{SO}_4$  at  $0.10 \text{ Vs}^{-1}$  (b) MOF (c) PANI and (d) PANI/MOF composite in different concentrations of  $\text{H}_2\text{SO}_4$  and  $0.10 \text{ Vs}^{-1}$  scan rate on Au electrode in 0.1 M TBAP/DMSO electrode system.

The Tafel slopes estimated by linear fitting of the polarization curves ( $(\eta = b \log i + a)$ , where  $b$  is the Tafel slope and  $i$  is the current density) from Figure 3.13 are given in Table 1 as well as exchange current density ( $i_0$ ) and cathodic transfer coefficient ( $1 - \alpha$ ). The transfer coefficient was calculated using high overpotential region, where the Butler–Volmer equation simplifies to the Tafel equation, from the Tafel slope given by the relationship:

$$b = \frac{-2.303 RT}{(1-\alpha)F} \quad [3.2]$$

The HER exchange current densities ( $i_0$ ) for MOF, PANI and PANI/MOF composite were calculated from the Tafel plots by the extrapolation method with the abscissa ( $\log(i_0)$ ). The present study showed that the blank electrode gives the Tafel slopes of more than  $400 \text{ mV.dec}^{-1}$  at low concentrations. In the presence of MOF electrocatalyst, a decrease in Tafel slope values was noticed. Similar behavior was noticed with PANI and PANI/MOF composite as electrocatalysts at low concentrations. Upon increasing the concentration of the acid, the values of the slope decreased to less than  $200 \text{ mV.dec}^{-1}$ . This phenomenon is in agreement with the previous study [66], which suggested that the rate determining step of the HER may be Volmer reaction or the Volmer reaction coupled with one of the other two reactions [66, 67]. The charge-transfer coefficient values of the samples are close to 0.5. According to data presented in Table 1, the transfer coefficient decreased with increasing the acid concentration. The similar value of  $1-\alpha$  was documented to be 0.33 (or  $\alpha=0.67$ ) for Cu-Pt bimetallic nanoparticles supported metal organic framework-derived nanoporous carbon Cu-Pt-NPCC (Table 1) [6]. The values of the exchange current density increased with increasing the acid concentration for the electrode and the prepared samples. The exchange current density increased in an order of PANI/MOF >MOF >PANI at different concentrations. This confirmed that the presence of MOF improved the electron transfer process of PANI [68]. In addition, these current densities were also higher than the Ni-PANI [17] and Cu-Pt-NPCC [6] reported in the literature.

Table 3.1: Experimental values of Tafel slope, transfer coefficient  $1-\alpha$  and exchange current  $i_0$ , in the absence and presence of MOF, PANI and PANI/MOF composite.

Material	H <sub>2</sub> SO <sub>4</sub> (mol.L <sup>-1</sup> )	Slope ( <i>b</i> ) (V.dec <sup>-1</sup> )	- <i>b</i> (mV.dec <sup>-1</sup> )	1- $\alpha$	log <i>i</i> <sub>0</sub>	<i>i</i> <sub>0</sub> (A.m <sup>-2</sup> )
Blank	0.033	-0.4256	425.6	0.139	-0.15	0.709
	0.075	-0.2140	214.0	0.276	0.45	2.818
MOF	0.033	-0.2726	272.6	0.217	0.25	2.239
	0.075	-0.2778	277.8	0.212	0.40	2.512
PANI	0.033	-0.2567	256.7	0.230	0.30	2.000
	0.075	-0.2925	292.5	0.202	0.35	2.239
	0.150	-0.1766	176.6	0.0335	0.75	5.623
	0.300	-0.1570	157.0	0.377	0.90	7.943
	0.450	-0.1708	170.8	0.346	0.95	8.912
PANI/MOF	0.075	-0.2393	239.3	0.247	0.50	3.162
	0.150	-0.2263	226.3	0.261	0.80	6.310
	0.300	-0.1993	199.3	0.297	0.90	7.943
	0.450	-0.1682	168.2	0.352	1.00	10.00
Ni-PANI [17]	0.500	-0.1470	147.0	<sup>a</sup>	0.17	01.47
Cu-Pt-NPCC [6]	0.500	<sup>a</sup>	<sup>a</sup>	0.33	-2.62	0.002

<sup>a</sup>= no reported literature value

### 3.4. CONCLUSIONS

In summary, the hydrogen production material of PANI/MOF composite was synthesised by a novel and facile route. FTIR and Raman indicated successful synthesis of PANI/MOF composite. XRD showed some mixed amorphous and crystalline structure of PANI with no obvious change in the structure of the PANI/MOF composite. Both SEM and TEM morphologies showed successful incorporation of MOF into the polymer backbone with some wrapping by PANI. There was an improved thermal stability upon composite formation with MOF which is attributed to stabilizing effect of MOF.

Hydrogen studies of the composite evaluated using CV and Tafel plots indicated an intense cathodic peak upon addition of  $\text{H}_2\text{SO}_4$  suggesting that PANI/MOF composite has a greater potential to be used in HER application as it can easily generate and adsorb hydrogen through straight forward electrochemical process. This work demonstrated that the PANI/MOF composite is not only robust and stable but also produces considerable  $\text{H}_2$  gas. A remarkable hydrogen production observed was dictated by the identity of hydrogen source which opens new avenues for multi analyte investigations.

### 3.5. REFERENCES

- [1] Dresselhaus, M.S., Thomas, I.L. Overview alternative energy technologies. *Nature* 414 (2001) 332-337.
- [2] Safizadeh, F., Ghali, E., Houlachi, G. Electrocatalysis developments for hydrogen evolution reaction in alkaline solutions – a review. *International Journal of Hydrogen Energy* 40 (2015) 256-274.
- [3] Tang, J., Zhao, X., Zuo, Y., Ju, P., Tang, Y. Electrodeposited Pd-Ni-Mo film as a cathode material for hydrogen evolution reaction. *Electrochimica Acta* 174 (2015) 1041-1049.
- [4] Xie, Z., He, P., Du, L., Dong, F., Dai, K., Zhang, T. Comparison of four nickel-based electrodes for hydrogen evolution reaction. *Electrochimica Acta* 88 (2013) 390-394.
- [5] Cao, X., Han, Y., Gao, C., Xu, Y., Huang, X., Willander, M., Wang, N. Highly, catalytic active PtNiCu nanochains for hydrogen evolution reaction. *Nano Energy* 9 (2014) 301-308.
- [6] Mandegarzad, S., Raouf, J.B., Hosseini, S.R., Ojani, R. Cu-Pt bimetallic nanoparticles supported metal organic framework-derived nanoporous carbon as a catalyst for hydrogen evolution reaction: original. *Electrochimica Acta* 190 (2016) 729-736.
- [7] Ojani, R., Valiollahi, R., Raouf, J.B. Comparison between graphene supported Pt hollow nanospheres and graphene supported Pt solid nanoparticles for hydrogen evolution reaction. *Energy* 74 (2014) 871-876.
- [8] Malinsuskes, A. Electrocatalysis at conducting polymers. *Synthetic Metals* 170 (1999) 75-83.
- [9] Boeva, Z.A., Sergeev, V.G. Polyaniline: Synthesis, properties, and application. *Polymer Science Series* 56 (2014) 144-153.
- [10] Molapo, K.M., Ndangili, P.M., Ajayi, R.F., Mbambisa, G., Mailu, S.M., Njomo, N., Masikini, M., Baker, P., Iwouha, E.I. Electronics of conjugated polymers (I): polyaniline. *International Journal of Electrochemical Science* 7 (2012) 11859-11875.

- [11] Wang, H., Lin, J., Shen, Z.X. Polyaniline (PANI) based electrode materials for energy storage and conversion. *Journal of Science: Advanced Mater Devices* 1 (2016) 225-255.
- [12] Song, E., Choi, J.W. Conducting polyaniline nanowire and its applications in chemiresistive sensing. *Nanomaterials* 3 (2013) 498-523.
- [13] Densakulprasert, N., Wannatong, L., Chotpattananont, D., Hiamtup, P., Sirivat, A., Schwank, J. Electrical conductivity of polyaniline/zeolite nanocomposites and synergetic interaction with CO. *Material Science and Engineering B* 117 (2005) 276-282.
- [14] Wu, T.M., Lin, Y.W. Doped polyaniline/multi-walled carbon nanotube composites: Preparation, characterization and properties. *Polymer* 47 (2006) 3576-3582.
- [15] Neetika, G., Kumar, D., Tomar, S.K. Thermal behaviour of chemically synthesized polyanilines/polystyrene sulphonic acid composites. *International Journal of Materials and Chemistry* 2 (2012) 79-85.
- [16] Kickelbick, G. Concepts for the incorporation of inorganic building blocks into organic polymers on a nanoscale. *Progress in Polymer Science* 28 (2003) 83-114.
- [17] Corte, D.A.D., Torres, C., Correa, P.S., Reider, E.S., Malfatti, C.F. The hydrogen evolution reaction on nickel-polyaniline composite electrodes. *International Journal of Hydrogen Energy* 37 (2012) 3025-3032.
- [18] Ding, S., He, P., Feng, W., Li, L., Zhang, G., Chen, J., Dong, F., He, H. Novel molybdenum disulfide nanosheets-decorated polyaniline: Preparation, characterization and enhanced electrocatalytic activity for hydrogen evolution reaction. *Journal of Physical Chemistry and Solids* 91 (2016) 41-47.
- [19] Nandasiri, M.I., Jambovane, S.R., McGrail, B.P., Schaefer, H.T., Nune, S.K. Adsorption, separation, and catalytic properties of densified metal-organic frameworks. *Coordination Chemistry Reviews* 311 (2016) 38-52.
- [20] Guo, S., Zhu, Y., Yan, Y.Y., Min, Y.L., Fan, J.C., Xu, Q.J., Yun, H. (Metal-Organic Framework)-Polyaniline sandwich structure composites as novel

- hybrid electrode materials for high-performance supercapacitor. *Journal of Power Sources* 316 (2016) 176-182.
- [21] Bagheri, H., Javanmardi, H., Abbasi, A., Banihasheni, S. A metal organic framework-polyaniline nanocomposite as a fiber coating for solid phase microextraction. *Journal of Chromatography A* 1431 (2016) 27-35.
- [22] Furukawa, H., Cordova, K.E., O'Keeffe, M., Yaghi, O.M. The chemistry and applications of metal-organic frameworks. *Science* 341 (2013) DOI: 10.1126/science.1230444.
- [23] Song, Y.S., Yan, B., Chen, Z.X. Hydrothermal synthesis, crystal structure and luminescence of four novel metal-organic frameworks. *Journal of Solid State Chemistry* 179 (2006) 4037-4046.
- [24] David, T., Mathad, J.K., Padmavathi, T., Vanaja, A. Part-A: Synthesis of polyaniline and carboxylic acid functionalized SWCNT composites for electromagnetic interference shielding coatings. *Polymer* 55 (2014) 5665-5672.
- [25] Ke, F., Qiu, L.G., Yuan, Y.P., Peng, F.M., Jiang, X., Xie, A.J., Shen, Y.H., J.F. Zhu, J.F. Thiol-functionalization of metal-organic framework by a facile coordination-based postsynthetic strategy and enhanced removal of Hg<sup>2+</sup> from water. *Journal of Hazardous Materials* 196 (2011) 36-43.
- [26] Shao, W., Jamal, R., Xu, F., Ubul, A., Abdiryim, T. The effect of a small amount of water on the structure and electrochemical properties of solid-state polyaniline. *Materials* 5 (2012) 1811-1825.
- [27] Wang, F., Guo, H., Chai, Y., Li, Y., Liu, C. The controlled regulation of morphology and size of HKUST-1 by "coordination modulation method". *Microporous and Mesoporous Materials* 173 (2013) 181-188.
- [28] Abdolahi, A., Hamzah, E., Ibrahim, Z., Hashim, S. Synthesis of uniform polyaniline nanofibers through interfacial polymerisation. *Materials* 5 (2012) 1487-1494.
- [29] Ibrahim, M., Koglin, E. Spectroscopic study of polyaniline emeraldine base: modelling approach. *Acta Chimica Slovenica* 52 (2005)159-163.
- [30] Prestipino, C., Regli, L., Vitillo, J.G., Bonino, F., Damin, A., Lamberti, C., Zecchina, A., Solari, P.L., Kongshang, K.O., Bordiga, S. Local structure of

- framework Cu(II) in HKUST-1 metallorganic framework: Spectroscopic characterization upon activation and interaction with adsorbates. *Chemistry of Materials* 18 (2006) 1337-1346.
- [31] Todara, M., Alessi A., Sciortino, L., Angnello S, Cannas, M., Gelardi, F.M., Buscarino, G. Investigation by raman spectroscopy of the decomposition of HKUST-1 upon exposure to air. *Journal of Spectroscopy* (2006) Article ID 8074297 DOI:org/10.1155/2016/8074297.
- [32] Trchova, M., Moravkov, Z., Blaha, M., Stejskal, J. Raman spectroscopy of polyaniline and oligoaniline thin films. *Electrochimica Acta* 122 (2014) 28-38.
- [33] Grzeszczuk, M., Granska, A., Szostak, R. Raman spectroelectrochemistry of polyaniline synthesized using different electrolytic regimes-Multivariate analysis. *International Journal of Electrochemical Science* 8 (2013) 8951-8953.
- [34] Li, D., Kaner, R.B. Processable stabilizer-free polyaniline nanofiber aqueous colloids. *Chemical Communications* 51 (2005) 3286–3288.
- [35] Tao, S., Hong, B., Kerong, Z. An infrared and Raman spectroscopic study of polyanilines co-doped with metal ions and H<sup>+</sup>. *Spectrochimica Acta A* 66 (2007) 1364-1368.
- [36] Kulkarni, M., Kale, B., Apte, S., Naik, S., Mulik, U., Amalnerkar, D. Synthesis and characterization of polyaniline nanofibres by rapid liquid-liquid interfacial polymerisation method. *Chemistry & Chemical Technology* 5 (2011) 55-58.
- [37] Tharani, S., Vinayagam, S.C. Synthesis of novel cerium doped polyaniline multiwalled carbon nanotubes and their optical and electrochemical properties for supercapacitor applications. *International Journal of Advanced Research* 3 (2015) 810-822.
- [38] Abdulla, H.S, Abbo, A.I. Optical and electrical properties of thin films of polyaniline and polypyrrole. *International Journal of Electrochemical Science* 7 (2012) 10666-10678.
- [39] Sharma, S., Pollet, B.G. Support materials for PEMFC and DMFC electrocatalysts - A review. *Journal of Power Sources* 208 (2012) 96-119.



- [40] Osta, RE, Feyand, M., Stock, N., Millange, F., Walton, R.I. Crystallisation Kinetics of Metal Organic Frameworks From *in situ* Time-Resolved X-ray Diffraction. *Powder Diffraction* 28 (2013) s256.
- [41] Yang, Y., Wan, M. Chiral nanotubes of polyaniline synthesized by a template-free method. *Journal of Materials Chemistry* 12 (2002) 897-901.
- [42] Pouget, J.P., Jdzefowicszt, M.E., Epstein, A.J., Tang, X., MacDiarmid, A.G. X-ray structure of polyaniline. *Macromolecules* 24 (1991) 779-789.
- [43] Li, X.G., Lu, Q.F., Huang, M.R. Self-stabilized nanoparticles of intrinsically conducting copolymers from 5-sulfonic-2-anisidine. *Small* 4 (2008) 1201-1209.
- [44] Tamboli, M.S., Kulkarni, M.V., Patil, R.H., Gade, W.N., Navale, S.C., Kale, B.B. Nanowires of silver-polyaniline nanocomposite synthesized via *in situ* polymerisation and its novel functionality as an antibacterial agent. *Colloids and Surfaces B: Biointerfaces* 92 (2012) 35-41.
- [45] Parveen, N., Mahato, N., Ansari, M.O., Cho, M.H. Enhanced electrochemical behavior and hydrophobicity of crystalline polyaniline@graphene nanocomposite synthesized at elevated temperature. *Composite Part B* 87 (2016) 281-290.
- [46] Joshi, A., Bajaj, A., Singh, R., Anand, A., Alegaonkar, P.S., Datar, S. Processing of graphene nanoribbon based hybrid composite for electromagnetic shielding. *Composite Part B* 69 (2015) 472-477.
- [47] Raganati, F., Gagiulo, V., Ammendola, P., Alfe, M., Chirone, R. CO<sub>2</sub> capture of HKUST-1 in a sound assisted fluidized bed. *Chemical Engineering Journal* 239 (2014) 75-86.
- [48] Lin, K.S, Adhikari, A.K., Ku C.K., Chiang, CL., Kuo, H. Synthesis and characterization of porous HKUST-1 metal organic frameworks for hydrogen storage. *International Journal of Hydrogen Energy* 37 (2012) 13865-13871.
- [49] Boomi, P., Prabu, H.G., Mathiyarasu, J. Synthesis and characterization of polyaniline/Ag-Pt nanocomposite for improved antibacterial activity. *Colloid and Surfaces B* 103 (2013) 9-14.

- [50] Feng, Y., Jiang, H., Li, S., Wang, J., Jing, X., Wang, Y., Chen, M. Metal organic frameworks HKUST-1 for liquid-phase adsorption of uranium. *Colloid and Surfaces A* 431 (2013) 87-92.
- [51] Wang, X., Lu, X., Wu, L., Chen, J. 3D metal-organic framework as highly efficient biosensing platform for ultrasensitive and rapid detection of bisphenol A. *Biosensors & Bioelectronics* 65 (2015) 295-301.
- [52] Rahman, M.M., Jeon, I.C. Studies of electrochemical behavior of swnt-film electrodes. *Journal of the Brazilian Chemical Society* 18 (2007) 1150-1157.
- [53] Kim, K.J., Li, Y.J., Kreider, P.B., Chang, C.H., Wammenmacher, N., Thallapally, P.K., Ahn, H.G. High-rate synthesis of Cu-BTC metal-organic frameworks. *Chemical Communications* 49 (2013) 11518-11520.
- [54] Nila, C., González, I. Thermodynamics of Cu-H<sub>2</sub>SO<sub>4</sub>-Cl<sup>-</sup>-H<sub>2</sub>O and Cu-NH<sub>4</sub>Cl-H<sub>2</sub>O based on predominance-existence diagrams and Pourbaix-type diagrams. *Hydrometallurgy* 42 (1996) 63-82.
- [55] Loera-Serna, S., Oliver-Tolentino, M.A., López-Núñez, M.L., Santana-Cruz, A., Guzmán-Vargas, A., Cabrera-Sierra, R., Beltrán, H.I, Flores, J. Electrochemical behavior of [Cu<sub>3</sub>(BTC)<sub>2</sub>] metal-organic framework: The effect of the method of synthesis. *Journal of Alloys and Compounds* 540 (2012) 113-120.
- [56] Ngece, R.F., West, N., Ndangili, P.M., Olowu, R., Williams, A., Hendricks, N., Mailu, S., Baker, P., Iwuoha, E. A silver nanoparticle/poly (8-anilino-1-naphthalene sulphonic acid) bioelectrochemical biosensor system for the analytical determination of ethambutol. *International Journal of Electrochemical Science* 6 (2011) 1820-1834.
- [57] Geniès, E.M., Lapkowski, M., Penneau, J.F. Cyclic voltammetry of polyaniline: interpretation of the middle peak. *Journal of Electroanalytical Chemistry* 249 (2011) 97-107.
- [58] Dai, C., Song, P., Wadhawan, J.D., Fisher, A.C., Lawrence, N.S. Screen printed alizarin-based carbon electrodes: monitoring pH in unbuffered media. *Electroanalysis* 27 (2015) 917-923.
- [59] Portenkirchner, E., Schlager, S., Apaydin, D., Oppelt, K., Himmelsbach, M., Egbe, D.A.M., Neugebauer, H., Knör, G., Yoshida, T., Sariciftc, N.S. Using

- the alkynyl-substituted rhenium(I) complex (4,4'-bisphenyl-ethynyl-2,2'-bipyridyl)Re(Co)<sub>3</sub>Cl as catalyst for CO<sub>2</sub> reduction—synthesis, characterization, and application. *Electrocatalysis* 6 (2015) 185-197.
- [60] Leung, C.F., Chen, Y.Z., Yu, H.Q., Yiu, S.M., Ko, C.C., Lau, T.C. Electro- and photocatalytic hydrogen generation in acetonitrile and aqueous solutions by a cobalt macrocyclic Schiff-base complex. *International Journal of Hydrogen Energy* 36 (2011) 11640-11645.
- [61] Chen, J., Xia, G., Jiang, P., Yang, Y., Li, R., Shi, R., Su, J., Chen, Q. Active and durable hydrogen evolution reaction catalyst derived from Pd-doped metal-organic frameworks. *ACS Applied Material Interfaces* 8 (2016) 13378-13383.
- [62] Wu, C., Li, C., Yang, B., Zhou, S., Shi, D., Wang, Y., Yang, G., He, J., Shan, Y. Electrospun MnCo<sub>2</sub>O<sub>4</sub> nanofibers for efficient hydrogen evolution reaction. *Material Research Express* 3 (2016) 095018. doi.org/10.1088/2053-1591/3/9/095018.
- [63] Zhou, W., Jia, J., Lu, J., Yang, L., Hou, D., Li, G., Chen, S. Recent developments of carbon-based electrocatalysts for hydrogen evolution reaction. *Nano Energy* 28 (2016) 29-43.
- [64] Gao, M.R., Liang, J.X., Zheng, Y.R., Xu, Y.F., Jiang, J., Gao, Q., Li, J., Yu, S.H. An efficient molybdenum disulfide/cobalt diselenide hybrid catalyst for electrochemical hydrogen generation. *Nature Communications* 6 (2015) 5982-5988.
- [65] Tang, Q., Jiang, D. Mechanism of Hydrogen Evolution Reaction on 1T-MoS<sub>2</sub> from First Principles. *ACS Catalysis* 6 (2016) 4953-4961.
- [66] Bagotsky, V. S. Fundamentals of Electrochemistry. 2<sup>nd</sup> Ed., John Wiley & Sons, 2006.
- [67] Gileadi, E. Electrode Kinetics, for Chemists, Chemical Engineers, and Materials Scientist: VCH Publishers, Inc., 1993.
- [68] Ghiamata, Z., Ghaffarinejad, A., Faryadras, M., Abdolmaleki, A., Kazami, H. Synthesis of palladium-carbon nanotube-metal organic framework composite and its application as electrocatalyst for hydrogen production. *Journal of Nanostructure in Chemistry* 6 (2016) 299-308.

## CHAPTER FOUR

### ELECTROCATALYTIC HYDROGEN PRODUCTION PROPERTIES OF POLY(3-AMINOBENZOIC ACID) DOPED WITH METAL ORGANIC FRAMEWORKS

---

*This chapter has been published:*

*Kabelo E. Ramohlola, Milua Masikini, Siyabonga B. Mdluli, Gobeng R. Monama, Mpitloane J. Hato, Kerileng M. Molapo, Emmanuel I. Iwuoha, Kwena D. Modibane, Electrocatalytic hydrogen production properties of poly(3-aminobenzoic acid) doped with metal organic frameworks. International Journal of Electrochemical Science 12 (2017) 4292-4405.*

#### ABSTRACT

The design and development of inexpensive highly efficient electrocatalysts based on polymer organometallic composites for hydrogen production, underpins several emerging clean-energy technologies. In this work, for the first time, Poly(3-aminobenzoic acid) based metal organic framework (PABA/MOF) composite was synthesized by chemical oxidation of 3-aminobenzoic acid monomer in the presence of metal organic framework (MOF) content. Poly(3-amino benzoic acid) (PABA), MOF and PABA/MOF composite were characterised by ultraviolet visible (UV-vis) and fourier transform infrared (FTIR) spectroscopy, powder X-ray diffraction (XRD), thermogravimetric analysis (TGA), scanning electron microscope (SEM), transmission electron microscope (TEM), energy dispersive X-ray spectroscopy (EDS, EDX), selected area electron diffraction (SAED) and cyclic voltammetry (CV). Detailed structural and morphological characterisations established that PABA is wrapping MOF. Furthermore, spectroscopic analyses provided information that MOF was incorporated on the backbone of PABA as indicative of an easier path for the electron transport and plentiful active sites for the catalysis of hydrogen evolution reaction (HER) in acidic electrolyte. Experiments probing the electrochemical properties revealed that the composite was very stable and robust and had exceptionally properties. Significant HER was generated by the composite in dimethyl

sulfoxide/tetrabutylammonium perchlorate (DMSO/TBAP) supporting electrolyte in the presence of hydrogen source by applying a potential to the electrode.

**Keywords:** poly(3-aminobenzoic acid), metal organic frameworks, electrochemistry, hydrogen evolution reaction, Tafel plot.

## 4.1. INTRODUCTION

Polyaniline have been widely studied for electronic and optical applications due to its exceptional conducting, optical and mechanical properties [1, 2]. However, there is a limitation to the application of polyaniline due to its non-processibility which results from poor solubility in most organic solvents such as dimethylsulfoxide (DMSO), dimethylformamide (DMF) and N-methyl-2-pyrrolidone (NMP) [3, 4]. One of the methods to tackle the non-processibility of polyaniline is synthesising new aniline polymers from aniline monomer derivatives, thus functionalised aniline [5]. Sulfonated polyaniline has been dealt used with little attention paid on polyaniline with parent carboxylic acid group [6]. Amino benzoic acid (ABA), which differs with the positions (meta- (m), ortho- (o) and para- (p) of the carboxylic acid (COOH) and amine group (NH<sub>2</sub>) is one of aniline derivatives which is capable of forming conducting polymer containing electron-rich nitrogen atom and high electron density of carbonyl group [7, 8]. The amine and carboxylic group are easily polymerized and polymerisation can occur using the same radical mechanism as unsubstituted polyaniline.

Furthermore, the carboxylic acid group which is not altered during polymerisation reaction serves as a functional group that can be used as a matrix material to immobilize other substrates or form covalent bonds with other materials such as nanomaterials [9]. Recently, there have been an increased interest in applying polyaniline and its derivatives to fuel cells and photoelectrochemical cells [10, 11]. In fuel cells, it is expected that electrocatalyst materials exhibit the capability of sustaining high current densities with low overpotentials [13]. In particular, polyaniline has proved to be capable of activating the HER. In the current study, 3-aminobenzoic acid was selected as the starting monomer of the polymerisation for comparing the activities of these polymers as electrocatalyst. Carboxyl groups can be used to combine with the metal on MOF surface by a multi-bridging chelating coordination. MOF materials are constructed by joining metal-containing units (secondary building units (SBUs)) with organic linkers, using strong bonds (reticular synthesis) which gives the material the unique chemical properties such open crystalline frameworks with permanent porosity

[14, 15]. The synthesised PABA/MOF obtained by oxidative chemical polymerisation of amino benzoic acid monomer in the presence of MOF were characterised by FTIR, UV-visible spectra, SEM, TEM, EDS, EDX, TGA and SAED. The current study also aims to show the efforts in understanding the electrocatalysis mechanism of the HER over PABA, MOF and PABA/MOF composites.

## 4.2. EXPERIMENTAL SECTION

### 4.2.1. Materials

3-aminobenzoic acid monomer (ABA), copper nitrate trihydrate ( $\text{Cu}(\text{NO}_3)_3 \cdot 3\text{H}_2\text{O}$ ), trimesic acid ( $\text{H}_3\text{BTC}$ ) and tetrabutylammonium percholate (TBAP) were purchased from Sigma Aldrich, South Africa. Ammonium per sulfate (APS) and iron chloride ( $\text{FeCl}_3$ ) were purchased from Riedel-de Haen and Educhem, respectively. Absolute ethanol was purchased at Merck, South Africa. Hydrochloric acid (HCl), dimethyl sulfoxide (DMSO) and sulphuric acid ( $\text{H}_2\text{SO}_4$ ) were procured from Rochelle Chemicals.  $\text{H}_2\text{SO}_4$  standard solutions were made in DMSO solution with 0.1 M TBAP as a supporting electrolyte system unless otherwise stated. All measurements were carried out at  $22 \pm 2^\circ\text{C}$ .

### 4.2.2. Synthesis of PABA, MOF and PABA/MOF Composite

Poly(3-aminobenzoic acid)(PABA) was prepared by oxidation polymerisation of 3-amino benzoic acid (ABA) monomer according to a previously reported method[16]. The synthesis of Cu-trimesic MOF (HKUST-1) was based on a previously reported hydrothermal procedure [15] with a light amendments. Approximately, 1 g of the 3-aminobenzoic monomer and 3.6 wt.% MOF were dissolved in a solution of 10 ml HCl/100 ml distilled water in a 250 ml round-bottom flask. The solution was stirred for 30 minutes at  $50^\circ\text{C}$  where after 2.40 g of ammonium persulfate (APS),  $(\text{NH}_4)_2\text{S}_2\text{O}_8$ , and 1.88 g of  $\text{FeCl}_3$  were added respectively in the solution. The resulting mixture was stirred for another 3 hours at  $50^\circ\text{C}$  and the content of the reaction was placed in the

oven at 50 °C overnight to evaporate the solvents and remaining content was washed with ethanol and dried at 50 °C.

#### 4.2.3. Characterisation Techniques

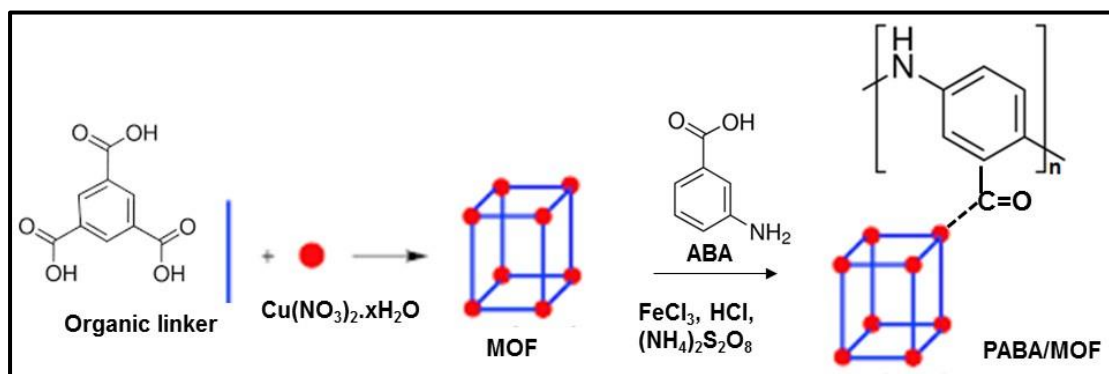
Absorbance spectra were recorded on a Varian Cary 300 UV-Vis-NIR spectrophotometer using 1 cm optical path length quartz cuvette. Morphological characterisations were performed using Auriga Field Emission Scanning Electron Microscope (FESEM) coupled with EDS detector for elemental analysis and transmission electron micrographs were collected using an FEI Tecnai G2 20 field-emission gun (FEG) TEM, operated in bright field mode at an accelerating voltage of 200 kV. Energy dispersive x-ray spectra were collected using an EDAX liquid nitrogen cooled Lithium doped Silicon detector. The thermal stability was studied by a thermogravimetric analyser (TGA Perkin-Elmer 4000). Samples ranging between 1 to 4 mg were heated from 30-500 °C at a heating rate of 20 °C/min under N<sub>2</sub> environment. The crystal structure of the PABA/MOF nanocomposite was analysed by using SAED and Phillips PW 1830 model XRD. The FTIR spectra were acquired on a Cary 600 series FTIR spectrometer (Agilent Technologies). The samples for FTIR measurement were prepared by grinding the dried sample powder mixed with potassium bromide (KBr) to a fine powder and then compressing under high pressure into thin pellets. Electrochemical measurements were performed using EPSILON electrochemical workstation performed in 10 ml of 0.1 M DMSO/TBAP electrolytic system. Prior to scans, the working electrode was polished with alumina paste, followed by washing with deionised water and rinsing with ethanol. The data was collected using a conventional three-electrode set-up with gold electrode (3 mm diameter, 0071 cm<sup>2</sup> area) as a working electrode, platinum wire as a counter electrode and Ag/AgCl wire as a reference electrode. Repetitive scanning of the solutions of the complexes MOF or MOF/PABA nanocomposites ( $\sim 2.0 \times 10^{-4}$  mol.L<sup>-1</sup>) was from -0.2 to 1.2 V at scan rate of 0.02-0.10 Vs<sup>-1</sup>. In HER experiments, different concentration of H<sub>2</sub>SO<sub>4</sub> were used as hydrogen source in DMSO/TBAP system.



## 4.3. RESULTS AND DISCUSSION

### 4.3.1. Synthesis

Scheme 1 shows the synthesis of PABA/MOF composite from the mixed solutions of 3-aminobenzoic acid and ammonium peroxydisulfate in the presence of MOF. The 3-aminobenzoic acid has an aromatic structure similar to aniline that can be polymerized to polyaniline by an oxidation reaction [17] and grow on the surface of MOF. In the reaction,  $(\text{NH}_4)_2\text{S}_2\text{O}_8$  is used as an oxidizing agent in a strongly acidic environment for the reaction. It was reported that introduction of  $(\text{NH}_4)_2\text{S}_2\text{O}_8$  solution into the aminobenzoic acid solution, free radicals as initiating agent produced by breaking peroxydisulfate can attract the activated hydrogen of amino group of aminobenzoic acid, resulted new free radical of aminobenzoic acid molecular [17,18].



Scheme 4.1: Synthesis of poly(aminobenzoic acid) based MOF composites through oxidation polymerisation of aminobenzoic monomer in the presence of MOF material.

The new free radical can attract aminobenzoic acid molecular, and then reacts with the initiating agent free radical for completing a substitution reaction on the aromatic ring by free radicals. This substitution product can be attracted and lengthened further by free radical of aminobenzoic acid molecular [17]. The product with higher molecular weight can be precipitated from reacting solution. Therefore, polymerisations of

lengthened chain can be ended, and formed PABA with carboxyl groups attached onto MOF surface as shown in Scheme 4.1.

### 4.3.2. Spectroscopic Characterisations

FTIR spectrum of synthesised composite with reference to PABA and MOF spectra is shown in Figure 4.1(a). It can be seen that the aminobenzoic acid has a sharp  $\nu(\text{N-H})$  bands located at around  $3500\sim 3300\text{ cm}^{-1}$  [19, 20] which was changed to broad bands after the polymerisation reaction. The band at  $1745\text{ cm}^{-1}$  is assigned to the  $\nu(\text{C=O})$  group of carboxylic acid [17] in both composite and PABA. The peak at  $1588\text{ cm}^{-1}$  is attributed to  $\text{COO}^-$  asymmetric stretch and medium band at  $1438\text{ cm}^{-1}$  due to  $-\text{COO}^-$  symmetric stretch of the carboxylate group. The FTIR spectra also show vibration bands at  $545$  and  $1256\text{ cm}^{-1}$  which are attributed to C-C and in-plane C-H bonding modes, respectively. Two bands at  $761$  and  $838\text{ cm}^{-1}$  are due to out-of phase C-H [21, 22].

The UV-visible absorption spectra of synthesised composite and PABA in DMSO solvent are shown in Figure 4.1(b). It is observed that all samples reveal a broad absorption band between  $300$  and  $600\text{ nm}$  which can be attributed to the  $\pi\text{-}\pi^*$  transition of the benzenoid rings and the exciton transition of the quinoid rings, respectively, for polymer and composite [19,23]. The slight bathochromic shift was observed for the composite compared with PABA due to the presence of MOF through carboxylate attachment, increase electron density of the polymer backbone. These observations were also demonstrated before when PABA incorporate with nanocomposite or materials [24].

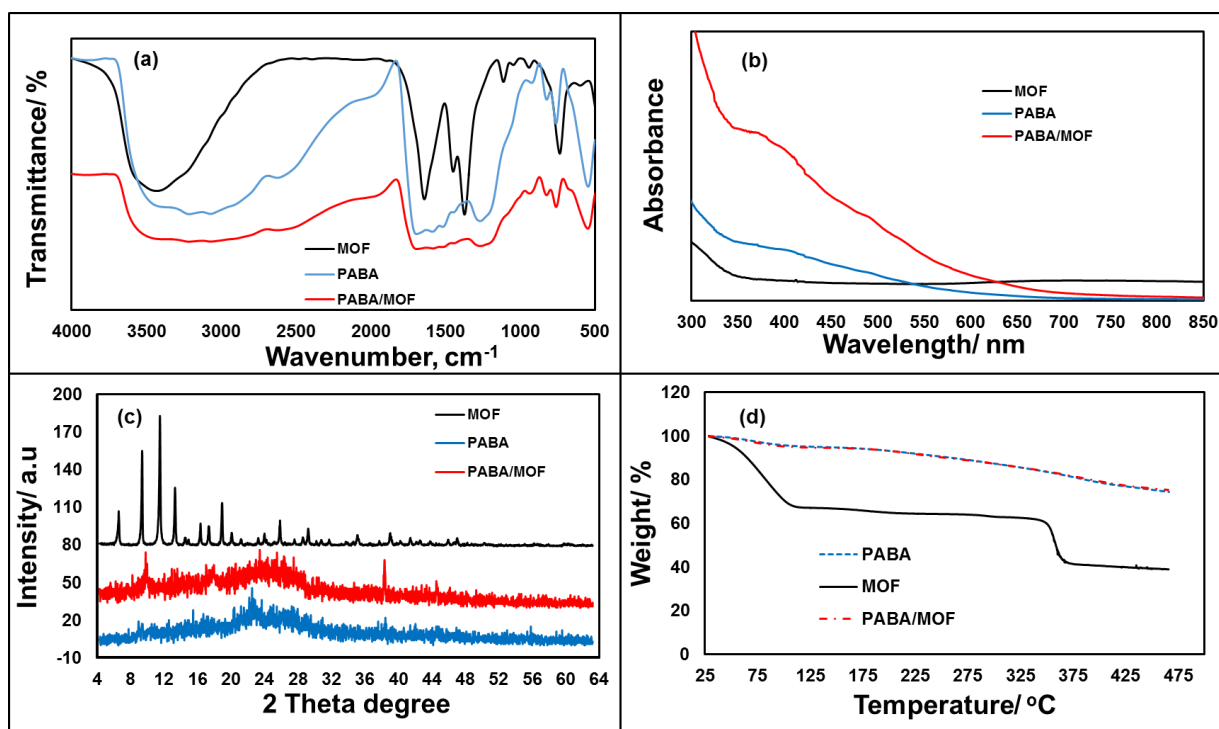


Figure 4. 1: (a) FTIR, (b) UV-vis spectra of PABA, MOF and PABA/MOF in DMSO, (c) XRD and TGA analysis of MOF, PABA and PABA/MOF.

The XRD patterns of PABA, MOF and PABA/MOF composite are shown in Figure 4.1(c). The MOF pattern show that the MOF phases are highly crystalline, which is an indication of micro-porous materials characteristics [25]. The XRD patterns of PABA show a broad peak at  $2\theta$  angle of  $25^\circ$  which indicate that synthesis of PABA was successful and it is also in accordance to the previous reported data on the XRD result of polyaniline [21]. In situ addition of MOF during polymerisation process resulted in decrease in the XRD intensities of PABA with appearance of new sharp peak at  $10^\circ$   $2\theta$  degrees which is an indicative that MOF is doped in PABA backbone to form a composite.

The thermal stability of the PABA, MOF, and PABA/MOF samples was investigated using TGA, as shown in Figure 4.1(d). The decomposition temperatures of the TGA curves indicate that MOF decomposes in two weight loss steps whereas PABA and its composite showed to be thermally stable. For MOF, the initial weight loss took place at 50– 100 °C is due to the loss of water bound molecules or moisture. The weight

loss for MOF at temperatures around 350 °C indicates a structural decomposition of the MOF framework as observed in Chapter three.

### **4.3.3. Morphological Characterisations**

Figure 4.2 shows the SEM images of (a) MOF, (c) PABA and (e) PABA/MOF and EDS elemental composition of (b) MOF, (d) PABA and (f) PABA/MOF samples. The SEM morphological images of MOF and PABA show a typically octahedral-shaped with smooth surfaces (Figure 4.2(a)) and hollow ball-like (Figure 4.2(c)), respectively. It is observed in Figure 4.2(e) that the morphology shows grain-like structures upon introduction of MOF on the polymer backbone as compared to spherical, granular and hollow ball-like for PABA (Figure 4.2(c)) [6, 19, 26-28]. The elemental composition of PABA/MOF composite from EDS (Figure 4.2(f)) showed an increase in the percentage compositions of C and O and there was no Cu metal of MOF detected on the surface of polymer as compared to the EDS of MOF (Figure 4.2(d)). From the SEM and EDS analysis, it can be deduced that PABA is wrapping around the MOF bundles as noncovalent attachment between PABA and MOF.

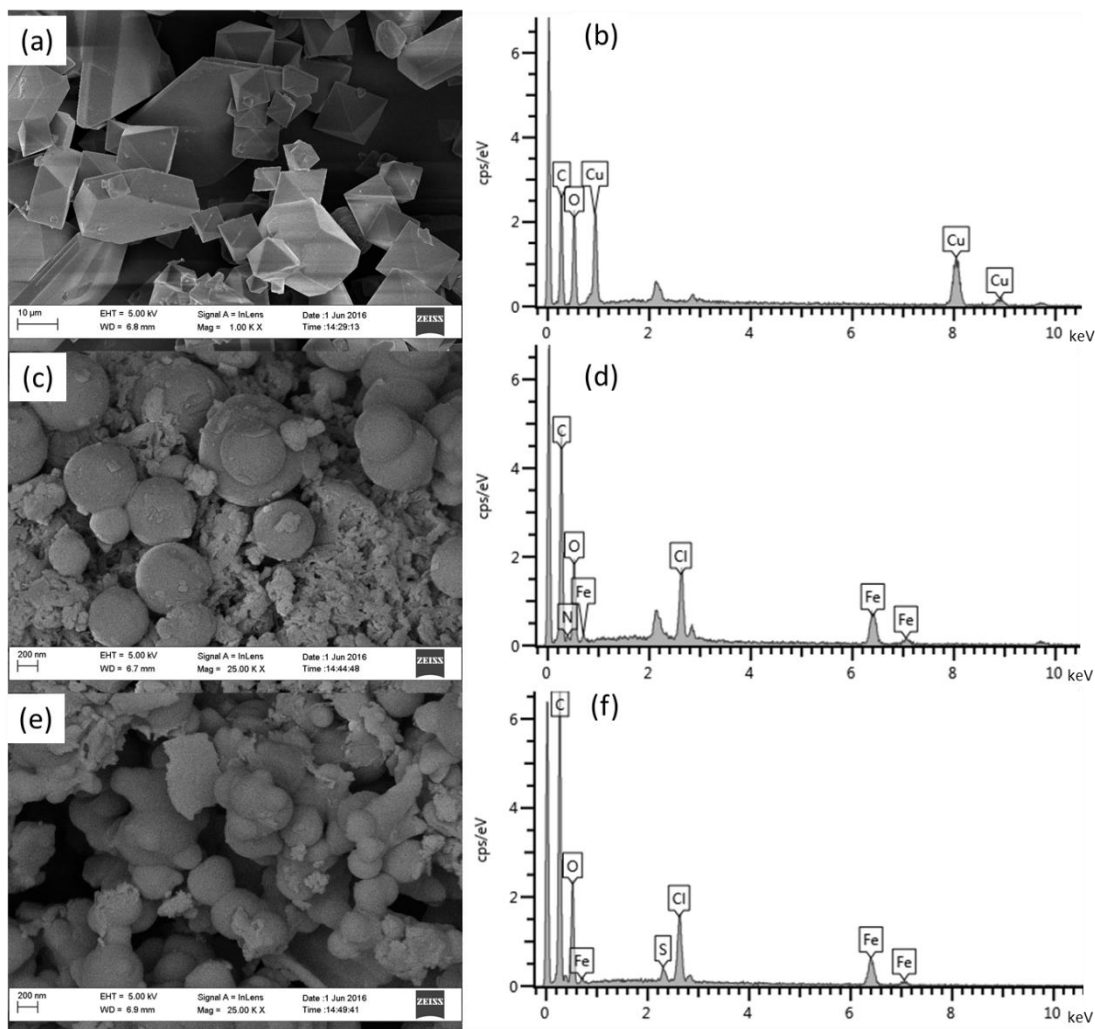


Figure 4.2: SEM image of (a) MOF, (c) PABA, (e) PABA/MOF composite and EDS spectrum of (b) MOF, (d) PABA, (f) PABA/MOF composite.

The TEM and SAED (inset) images for MOF, and PABA are shown in Figure 4.3(a) and (b) respectively. The MOF images show that the MOF phases are highly crystalline, which is an indication of micro-porous materials characteristics, as observed in Chapter three. The TEM image of PABA is in accordance to the previous reported data on the morphology of poly(3-aminobenzoic acid) [6]. The SAED inset image of PABA reveals a clear diffraction ring and spot of the polycrystalline characteristics. The PABA wrapping around MOF as an observation in SEM above (Figure 4.2(e)) was further confirmed by TEM image (Figure 4.3(c)) showing the presence of MOF covered

by polymer. The elemental analysis on TEM image using EDX (Figure 4.3(b)) showed an increase in carbon and oxygen content in the composite as compared to PABA. The enhanced atomic percentages are attributed to the organic linker of metal organic framework. The copper content of MOF was detected however it overlapped with the foreign species of the grid.

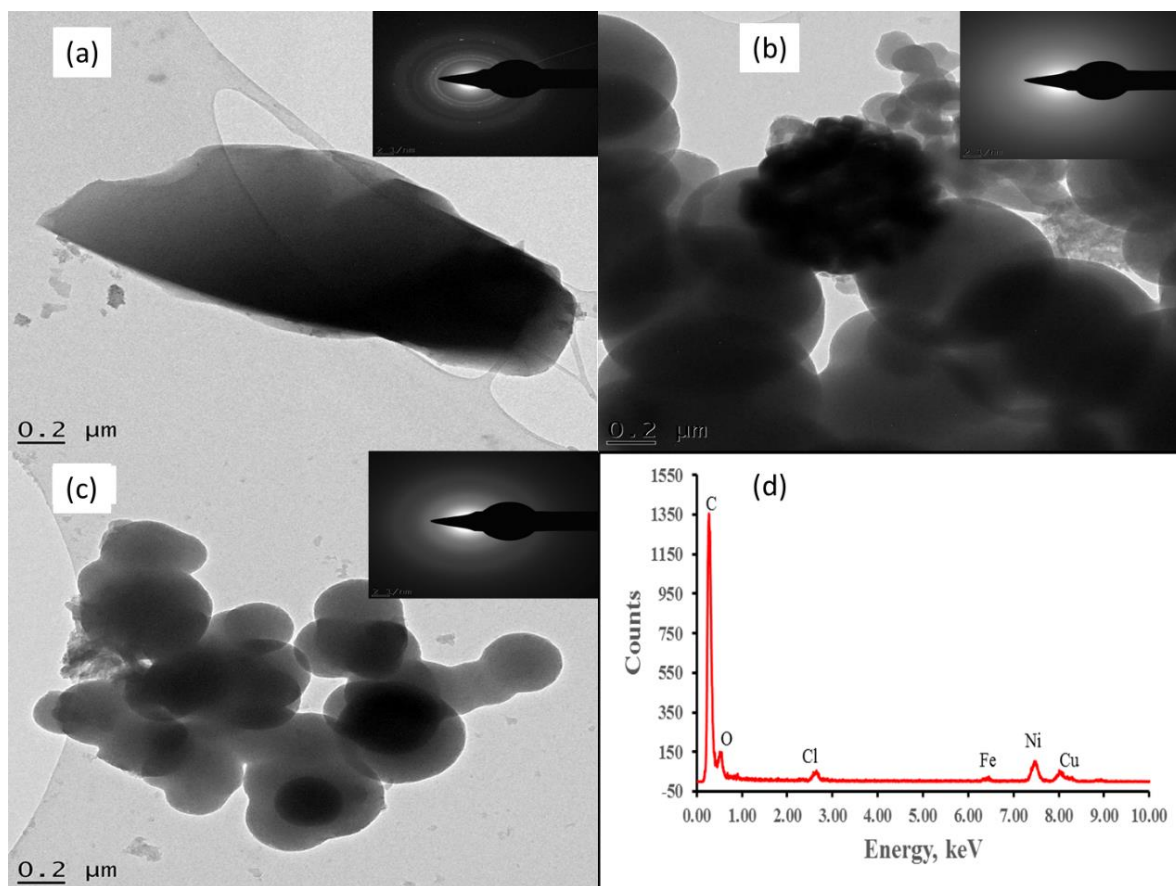


Figure 4.3: TEM images (a) MOF, (b) PABA, (c) PABA/MOF composite and (d) EDX spectrum of PABA/MOF composite. Inset: SAED image.

The inset SAED image (Figure 4.3(c)) showed that the composite maintains its amorphous structure of PABA. However, it has some slight spot where the d-spacing of the composite can be determined as indicative of modification of structural properties of the polymer with MOF and supported by the XRD (Figure 4.1(c)).

#### 4.3.4. Electrochemical Characterisations

Cyclic voltammetry characterisations of PABA and PABA/MOF were achieved by using a gold (Au) electrode in a 0.1 M TBAP/DMSO electrolyte at a scan rate of 0.1V/s and are recorded in Figure 4.4(a). The electrochemical properties of the materials was monitored by two ways, 1) change in current density at oxidation-reduction potential in relation to bare Au electrode and 2) appearance of new oxidation or/and reduction peaks or respective anodic or cathodic peaks. The voltammogram of a bare Au electrode showed a typical redox couple at  $E_{pc} \sim -0.6$  and  $E_{pa} \sim -0.8V$  which is due to migration of ion from the electrolyte solution to the Au electrode in order to maintain system equilibrium [29]. The voltammogram in the presence of PABA showed increase in current density as compared to the bare electrode. However, the presence of carboxylic group on the polymer backbone of PABA makes the voltammogram of PABA differs from the one of pure PANI, thus the three redox peaks which can be attributed to different oxidation state of PANI are not observed [30]. When MOF is introduced, there is a collapse of the oxidation and reduction peaks on the same region and an increase in cathodic peak intensity at lower potential which agree with the requirement of electrocatalyst [13]. The decrease in current density of the composite materials shows that during composite formation, the conductivity of PABA material was affected by incorporation of MOF.

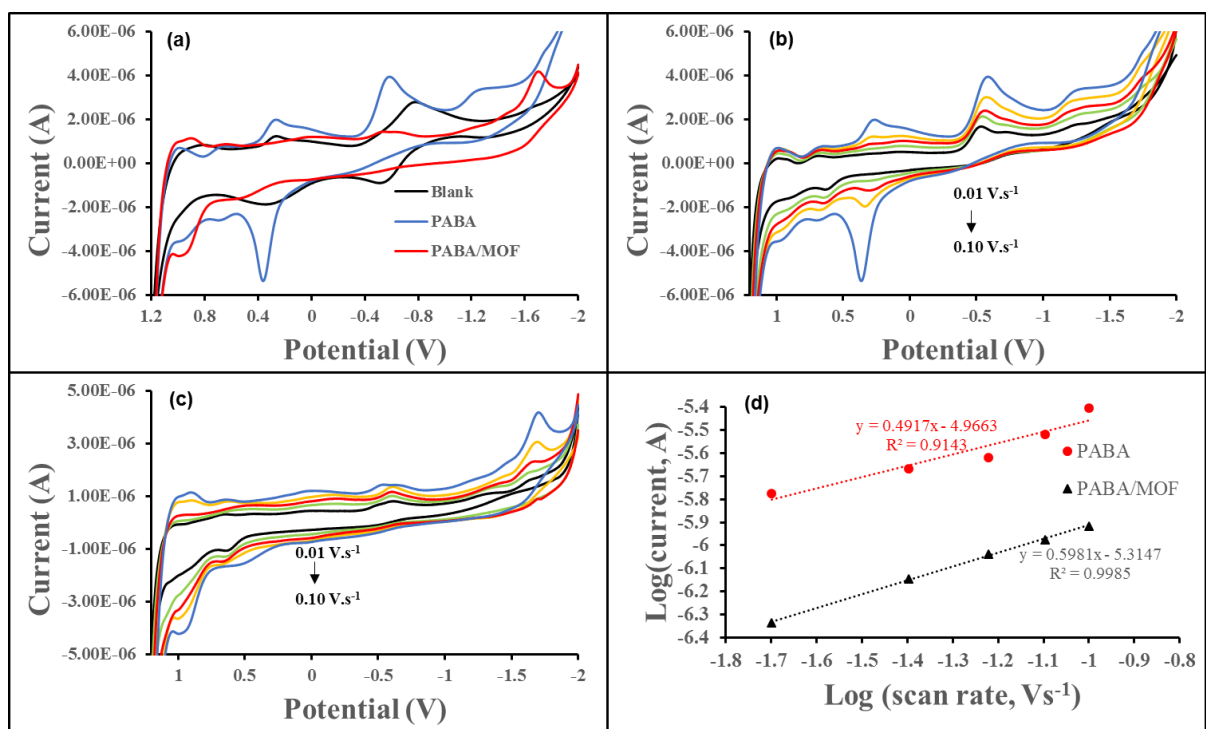


Figure 4.4: (a) CV results of PABA and PABA/MOF at 0.1 Vs<sup>-1</sup>; (b) and (c) CV of PABA and PABA/MOF at different scan rates (0.02- 0.10 Vs<sup>-1</sup>); and (d) The log-log plot of the absolute value of the peak current vs scan rate for the PABA and PABA/MOF materials at 0.02 to 0.1 Vs<sup>-1</sup> in 0.1 M DMSO/TBAP electrolyte solution on gold electrode.

The different scan rates dependent studies was used to examine the dynamic electrochemical properties of (b) PABA and (c) PABA/MOF during oxidation-reduction processes and are shown in Figure 4.4. The figures show that the current density of the materials increased with the increase scan rate with cathodic peak current shifting towards negative potential with increasing scan rate as indicative of quasi-reversible process [31]. The increase in peak current with increasing scan rates shows that there is an electric charge-transfer controlled process in all materials. Figure 4.4(d) shows the plot of the logarithm of the absolute value of the reductive peak current against the logarithm of the scan rate. The results show a linear relationship with a slope of 0.492 and 0.598 for PABA and PABA/MOF materials, respectively. These slope values are close to the expected value of 0.5 as indicative of semi-finite diffusion control [32]. The 0.5 slope shows that the peak current is directly proportional to the square root of the



scan rate [32]. The diffusion controlled process was also supported by current proportionality to square root of scan rate in the range of 0.02- 0.10 V/s for quasi-reversible couple as demonstrated in Figure 4.5.

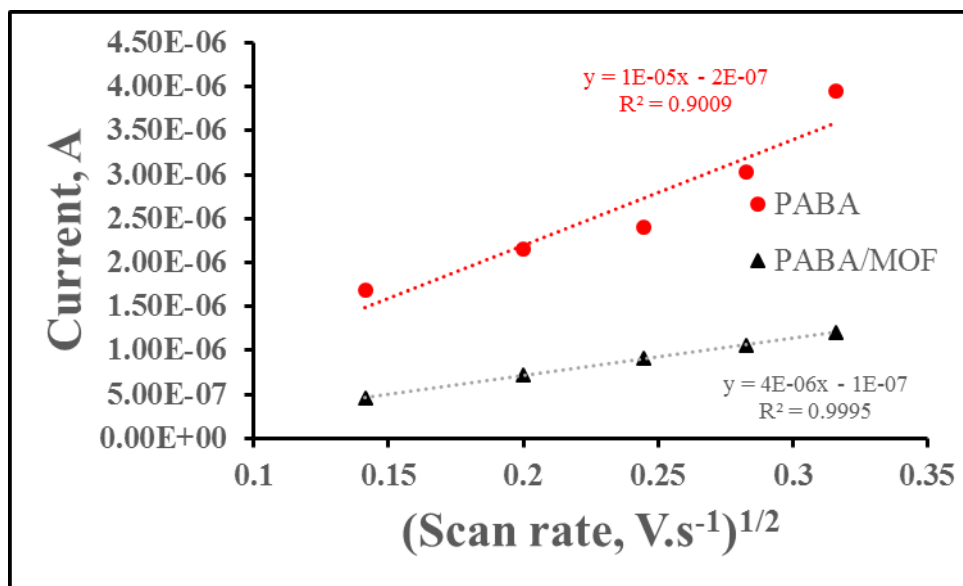


Figure 4.5: Peak current as a function of square root of scan rate on gold in 0.1 M DMSO/TBAP electrode system at different scan rate (0.02 – 0.10 Vs<sup>-1</sup>).

To accurately determine kinetic rate constants and other parameters, the diffusion coefficient,  $D$ , was determined for catalysts using cyclic voltammetry and following the Randles-Ševčík equation (Eq. 3.1) for a quasi-reversible system [31]:

$$I_p = (2.65 \times 10^5) n^{3/2} A C D^{1/2} \nu^{1/2} \quad (3.1)$$

where,  $n$  is the number of electrons transferred,  $A$  is the electrode area in cm<sup>2</sup>,  $D$  is the diffusion coefficient in cm<sup>2</sup> s<sup>-1</sup>,  $C$  is the bulk molar concentration of the electroactive species in mol.cm<sup>-3</sup> and  $\nu$  is scan rate is Vs<sup>-1</sup>. The diffusion coefficient was determined to be  $5.2 \times 10^{-7}$  and  $0.83 \times 10^{-7}$  cm<sup>2</sup> s<sup>-1</sup> for PABA and PABA/MOF composite, respectively. The value indicates that the movement of electrons along the polymer

chain was averagedly fast and agrees well with diffusion coefficient value reported for doped polyaniline [33].

#### 4.3.5. Hydrogen Evolution Reaction

Upon addition of sulphuric acid, two reduction peaks appeared within the potential window of DMSO (Figure 4.6(a)). An irreversible wave appeared between -0.40 and -0.90 V. This reductive wave is followed immediately by a large cathodic current that is assigned to the catalytic reduction of protons to dihydrogen. Notably, reductive wave had a corresponding oxidative wave on the positive potential sweep. For the catalytic wave at -1.80 V, it represents the evolution of hydrogen gas, an irreversible process. This irreversibility was attributed to the reduction being coupled to the complex accepting two protons from solution [34].

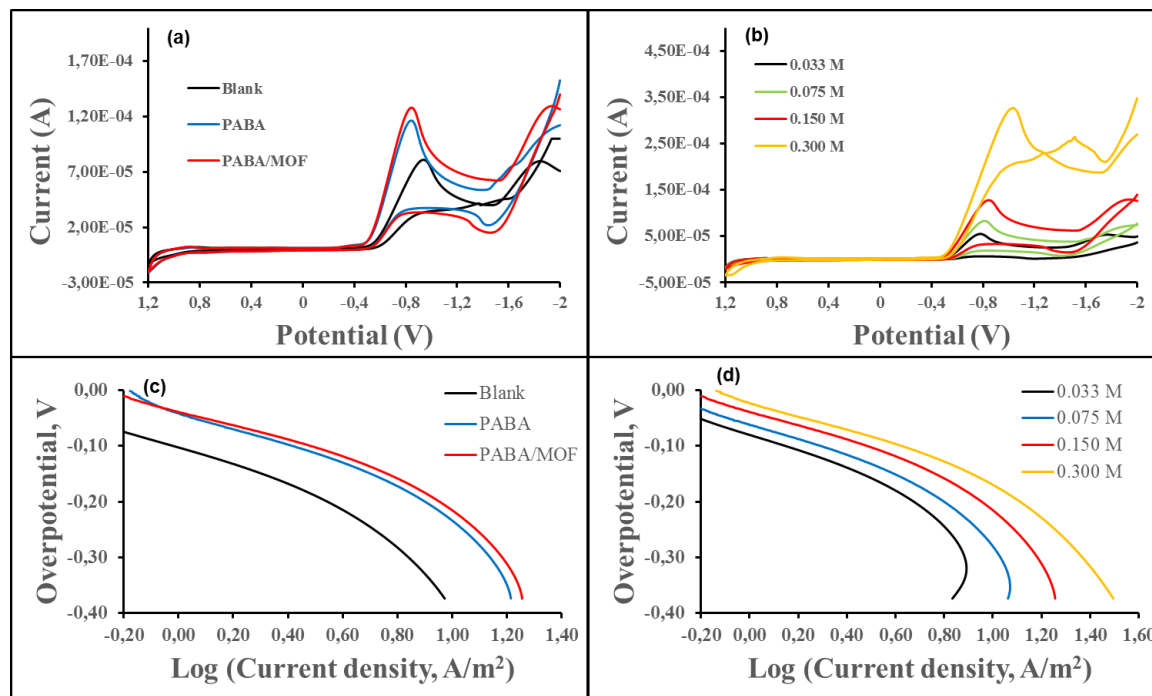


Figure 4.6: (a) CV and (c) Tafel plots of PABA and PABA/MOF in the presence 0.15 M H<sub>2</sub>SO<sub>4</sub>; (b) CV and (d) Tafel plots of PABA/MOF at 0.10 V s<sup>-1</sup> in the presence of different H<sub>2</sub>SO<sub>4</sub> concentration on gold electrode in 0.1 M DMSO/TBAP electrode system.

To determine the overpotential required to evolve hydrogen at the catalyst, a cyclic voltammogram was taken of a solution of sulphuric acid in DMSO using a gold electrode. The onset of cathodic current at gold in DMSO is -0.460 V in the presence of sulphuric acid (Figure 4.6(a), curve blank) as the control experiment to assure the catalyst was responsible for the currents observed. There was a small background current representing thermodynamically favourable, but kinetically hindered reduction of protons at the working electrode [35].

This is a good determination for the thermodynamic potential required for the hydrogen evolution reaction to proceed, as gold is known to evolve hydrogen from acidic solutions with minimal overpotential [36]. Using this value, it was estimated that the catalysts evolved hydrogen with an overpotential of approximately -0.405 V. In 0.15 M solution of sulphuric acid, the current at around -0.882 V was ~2 times less in the absence of PABA and PABA/MOF, than with it present.

To ascertain that proton reduction was the source of the catalytic current, cyclic voltammograms of catalyst were performed in the presence of increasing concentrations of sulphuric acid. Figure 4.6(b), there was reductive current observed in the presence of PABA/MOF using a gold (Au) electrode in a 0.1 M DMSO/TBAP electrolyte at a scan rate of 0.10 Vs<sup>-1</sup> for different acid concentrations. This supports that both reductive waves in the voltammogram above needed protons to proceed.

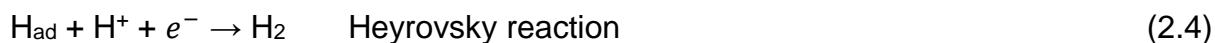
Tafel plots were recorded to determine the kinetic parameters in the absence and presence of PABA, and PABA/MOF that allow the evaluation of both exchange current density  $i_0$  and cathodic transfer coefficient  $1-\alpha$ . Crețu *et al.*; [36] and. Khanova and Krishtalik [37] have proved that on gold in sulphuric acid solution, Tafel plots present two distinct slopes at low and high overpotential corresponding to the HER controlled by desorption of the hydrogen atoms and charge transfer mechanism as a slow step of the cathodic process, respectively. Therefore, in order to determine kinetic parameters that characterise the charge transfer, Tafel slopes were plotted for a limiting domain of high overpotentials and presented in Figure 4.6(c) and (d). The

transfer coefficient  $1-\alpha$  was calculated using high overpotential region, where the Butler–Volmer equation simplifies to the Tafel equation, from the Tafel slope  $b$  given by relationship:

$$b = \frac{-2.303 RT}{(1-\alpha)F} \quad (3.2)$$

where  $R$  is the gas constant ( $8.31451 \text{ J mol}^{-1} \text{ K}^{-1}$ ),  $T$  - thermodynamic temperature (K),  $F$  – Faraday’s number ( $96,485 \text{ C mol}^{-1}$ ). The exchange currents  $i_0$  were evaluated from Tafel slope intersection with the abscissa ( $\log(i_0)$ ).

It was reported that the Tafel slope  $b$  is an important parameter as it can reveal the mechanisms of the HER in aqueous acid solutions which proceed in a series of three elementary reaction which comprises of two electrochemical steps and one chemical steps [38, 39]. The three elementary reaction steps as given in Chapter two (Eq. 2.3-2.5) in acidic medium are:



It was shown in Chapter two that the combination of steps (2.3 and 2.4) or (2.3 and 2.5) can lead to the production of molecular  $\text{H}_2$ . Kinetic models of the HER, under a specific set of conditions have shown that a slope of  $\sim 120 \text{ mV/dec}$  is indication of Volmer step, while a rate determining Heyrovsky or Tafel step should produce slopes between  $30\text{-}40 \text{ mV.dec}^{-1}$ . These values can be used as a guide in identifying HER mechanisms. The measured values slopes for the materials are listed in Table 4.1. Gold electrode exhibit the slope of  $106.2 \text{ mV.dec}^{-1}$  and  $167.4 \text{ mV.dec}^{-1}$  at  $0.300 \text{ M}$  and  $0.15 \text{ M H}_2\text{SO}_4$  concentrations, respectively which will be used as a control. Upon addition of PABA and PABA/MOF, at  $0.300 \text{ M H}_2\text{SO}_4$ , there is an increase in slope as compared to the Au electrode. This is in accordance with the reported results by

Zheng, *et. al.* [40] and Corte, *et. al.* [41]. The similar behaviour was observed in polyaniline nickel electrode (Ni-PANI, Table 1) with a slope of  $147 \text{ mV.dec}^{-1}$  in  $0.5 \text{ M H}_2\text{SO}_4$  [41]. At low concentration, the slope decreased with respect to Au electrode towards the Volmer slope,  $120 \text{ mV.dec}^{-1}$ . This shows that there is an adsorption of hydrogen proton on the surface of the materials and number of adsorption sites increases once the composites is formed since there is a further decrease in slope. According to the data presented in Table 1, it can be observed that in the absence and presence of PABA and PABA/MOF composite, the charge transfer coefficient  $1-\alpha$  decreases with decrease in concentration of  $\text{H}_2\text{SO}_4$ . To explain this phenomenon it is necessary to take into account that the charge transfer coefficient  $1-\alpha$  represents a measure of the activated complex coordinates at the metal – electrolyte solution interface [40, 41]. The lower the value of  $1-\alpha$ , the further is the reaction plane from the metal surface which was the case with the PABA/MOF composite. The low value of  $1-\alpha$  was documented to be 0.33 (or  $\alpha=0.67$ ) for Cu-Pt bimetallic nanoparticles supported metal organic framework-derived nanoporous carbon Cu-Pt-NPCC [42]. The resulting current densities ( $i_0$ ) from Tafel plots, confirmed the benefits of MOF incorporation on polymer for the HER (Table 1). The current density obtained for composite at  $0.300 \text{ M H}_2\text{SO}_4$  was ca. 2 and times higher than the current density observed on the control electrode. These current densities were also higher than the one Ni-PANI and Cu-Pt-NPCC (Table 1) reported before.

Table 4. 1: Experimental values of Tafel slope, transfer coefficient  $1-\alpha$  and exchange current  $i_0$ , in the absence and presence of PABA and PABA/MOF composite.

Material	H <sub>2</sub> SO <sub>4</sub> [mol/L]	Slope (b) [V.dec <sup>-1</sup> ]	-b [mV.dec <sup>-1</sup> ]	1- $\alpha$	log <i>i</i> <sub>0</sub>	<i>i</i> <sub>0</sub> [A.m <sup>-2</sup> ]
Blank	0.300	-0.1062	106.2	0.57	1.25	17.78
	0.150	-0.1674	167.4	0.35	0.98	09.55
PABA	0.300	-0.1237	123.7	0.48	1.45	28.18
	0.150	-0.1535	153.5	0.39	1.30	19.95
PABA/MOF	0.300	-0.1305	130.5	0.45	1.55	35.48
	0.150	-0.1355	135.5	0.44	1.35	22.39
	0.075	-0.1469	146.9	0.40	1.22	16.60
	0.033	-0.1602	160.2	0.37	1.10	12.60
Ni-PANI [41]	0.500	-0.1470	147.0	a	0.17	01.47
Cu-Pt-NPCC [42]	0.500	a	a	0.33	-2.62	0.002

#### 4.4. CONCLUSIONS

In summary, we demonstrated the preparation of novel poly(3-aminobenzoic acid)/metal organic framework composite through in situ polymerisation of 3-aminobenzoic acid (aniline derivative) in the presence of MOF. Structural and morphological characterisations using XRD, FTIR, TGA, SEM, TEM and SEAD confirmed successful formation of composite with PABA wrapping MOF. Significantly, the enhancement of HER generation is approximately an order of magnitude than that observed for traditional non-conducting metallopolymer. Furthermore, these PABA and its MOF composite merely require overpotentials as low as  $\sim -0.405$  V to attain current densities of  $\sim 0.8$  and  $1.5$  Am<sup>-2</sup> and show good long-term stability. The increased HER performance makes the PABA/MOF composite attractive for constructing HER based devices for hydrogen fuel cell applications. Despite the fact that PANI/MOF composite showed to be ideal HER electrocatalyst, there is need for introduction of novel composite for HER applications. To address this deficit in the

following chapter, MOF composites decorated with different weight percentage of PABA are explored.

#### 4.5. REFERENCES

- [1] Bhadra, S., Khastgir, D., Singha, N.K., Lee, J.H. Progress in preparation, processing and applications of polyaniline. *Progress in Polymer Science* 34 (2009) 783-810.
- [2] Stejskal, J., Sapurina, I., Trchova, M. Polyaniline nanostructures and role of oligomers in their formation. *Progress in Polymer Science* 35 (2010) 1420-1481.
- [3] Bilal, S., Gul, S., Holze, R, Shah, A-H.A. An impressive emulsion polymerisation route for the synthesis of highly soluble and conducting polyaniline salts. *Synthetic Metals* 206 (2015) 131–144.
- [4] Abdolahi, A., Hamzah, E., Ibrahim, Z., Hashim, S. Synthesis of uniform polyaniline nanofibers through interfacial polymerisation. *Materials* 5 (2012) 1487-1494.
- [5] Kamaraj, K., Karpakam, V., Sathiyarayanan, S., Ventakachari, G. Electrosynthesis of poly(aniline-co-m-amino benzoic acid) for corrosion protection of steel. *Materials Chemistry and Physics* 122 (2010) 123-128.
- [6] Sophia, I.A., Gopu, G., Vedhi, C. Synthesis and characterisation of poly anthranilic acid metal nanocomposite. *Open Journal of Synthesis Theory and Applications* 1 (2012) 1-8.
- [7] Sangeetha, R.S.D., Arasu, P.T., Kumar, G.H., Bella, R.S.D. Study on dissociation of amini benzoic acid isomers in dimethyl formamide and polyethylene glycol<sub>200</sub>. *International Journal of ChemTech Research* 6 (2014) 5335-5341.
- [8] Thiemann, C., Brett, C.M.A. Electrosynthesis and properties of conducting polymers derived from aminobenzoic acids and from aminobenzoic acids and aniline. *Synthetic Metals* 123 (2001) 1-9.
- [9] Netsuwan, P., Chaisu, W., Phanichphant, S., Sriwichai, S. Nanocomposite thin film of poly(3-aminobenzoic acid) and multiwalled carbon nanotubes fabricated through electrochemical method. *Advances in Materials Science and Engineering* 1 (2014) 1-6.



- [10] Chen, Z., Xu, L., Li, W., Waje, M., Yan, Y. Polyaniline nanofibre supported platinum nanoelectrocatalysts for direct methanol fuel cells. *Nanotechnology* 17 (2006) 5254-5259.
- [11] Liu, J., Lu, S., Liang, X., Gan, Q., Wang, Y., Li, H. Photoelectrocatalytic oxidation of ascorbic acid and electrocatalytic reduction of dioxygen by polyaniline films for renewable energy conversion. *Journal of Electroanalytical Chemistry* 764 (2016) 15–22.
- [12] Zeng, M., Li, Y. Recent advances in heterogeneous electrocatalysts for the hydrogen evolution reaction. *Journal of Materials Chemistry A* 3 (2015) 14942-14962.
- [13] Vargas-Uscategui, A., Mosquera, E., Chornik, B., Cifuentes, L. Electrocatalysis of the hydrogen evolution reaction by rhenium oxides electrodeposited by pulsed-current. *Electrochimica Acta* 178 (2015) 739-747.
- [14] Hosseini, H., Ahmar, H., Dehghani, Bagheri, A., Tadjarodi, A., Fakhari, A.R. A novel electrochemical sensor based on metal-organic framework for electrocatalytic oxidation of L-cysteine *Biosensors and Bioelectronics* 42 (203) 426-429.
- [15] Ke, F., Qiu, L.G., Yuan, Y.P., Peng, F.M., Jiang, X., Xie, A.J., Shen, Y.H., Zhu, J.F. Thiol-functionalization of metal-organic framework by a facile coordination-based postsynthetic strategy and enhanced removal of Hg<sup>2+</sup> from water. *Journal of Hazardous Materials* 196 (2011) 36-43.
- [16] David, T., Mathad, J.K., Padmavathi, T., Vanaja, A. Part-A: Synthesis of polyaniline and carboxylic acid functionalized SWCNT composites for electromagnetic interference shielding coatings. *Polymer* 55 (2014) 5665-5672.
- [17] Patra, S., Munichandraiah, N. Insoluble poly (anthranilic acid) confined in Nafion membrane by chemical and electrochemical polymerisation of anthranilic acid. *Synthetic Metals* 150 (2005) 285-290.
- [18] Wen, P., Wang, X. Synthesis and Visible Photocatalytic Activities of Poly(aminobenzoic acid)/TiO<sub>2</sub> Nanocomposites. *Journal of Nanomaterials* (2013) doi:10.1155/2013/795652.

- [19] Zare, E.N., Lakouraj, M.M., Moosavi, E. Poly (3-aminobenzoic acid) @MWCNTs hybrid conducting nanocomposite: preparation, characterisation, and application as a coating for copper corrosion protection. *Composite Interfaces* (2016) doi:10.1080/09276440.2016.1156366.
- [20] Sharifirad, M., Kiani, F., Koohyar, F. Glassy carbon electrode modified by Poly(m-aminobenzoic acid)/nano SiO<sub>2</sub> film and electrical and electrochemical properties. *European Online Journal of Natural and Social Sciences* 2 (2013) 366-378.
- [21] Mostafaei, A., Zolriasatein, A. Synthesis and characterisation of conducting polyaniline nanocomposites containing ZnO nanorods. *Progress in Natural Science: Materials International* (2012) 273-280.
- [22] Benyoucef, A., Huerta, F., Va'zquez, J.L., Morallon, E. Synthesis and in situ FTIRS characterisation of conducting polymers obtained from aminobenzoic acid isomers at platinum electrodes. *European Polymer Journal* 41 (2005) 843–852.
- [23] Dash, M.P., Tripathy, M., Sasmal, A., Mohanty, G.C., Nayak, P.L. Poly(anthranilic acid)/multi-walled carbon nanotube composites: spectral, morphological, and electrical properties. *Journal of Material Science* 45 (2010) 3858-3865.
- [24] Golshaei, R., Guler, Z., Ünsal, C., Sarac, A.S. In situ spectroscopic and electrochemical impedance study of gold/poly (anthranilic acid) core/shell nanoparticles. *European Polymer Journal* 66 (2015) 502-512.
- [25] Lin, K.S., Adhikari, A.K., Ku, C.N., Chiang, C.L., Kou, H. Synthesis and characterisation of porous HKUST-1 metal organic frameworks for hydrogen storage. *International Journal of Hydrogen Energy* 37 (2012) 13865-13871.
- [26] Mildan, E., Gulfen, M., Equilibrium, kinetics, and thermodynamics of Pd(II) adsorption onto poly(m-aminobenzoic acid) chelating polymer. *Journal of Applied Polymer Science* (2015) 1-10.
- [27] Ranganathan, S., Raju, P., Arunachalam, V., Krishnamoorthy, G., Ramadoss, M., Arumainathan, S., Vengidusamy, N. Poly(anthranilic acid) Microspheres:

- Synthesis, Characterisation and their Electrocatalytic Properties. *Bulletin of the Korean Chemical Society* 33 (2012) 1919-1924.
- [28] Singh, A.K., Joshi, L., Prakash, R., Kaneto, K. Influence of Synthesis Conditions on Electronic and Junction Properties of Poly(anthranilic acid)–Clay Nanocomposites with Aluminum. *Japanese Journal of Applied Physics* 49 (2010) 1-7.
- [29] Rahman, M.M., Jeon, I.C. Studies of electrochemical behavior of swnt-film electrodes. *Journal of the Brazilian Chemical Society* 18 (2007) 1150-1157.
- [30] Giray, D., Balkan, T., Dietzel, B., Sarac, A.S. Electrochemical impedance study on nanofibers of poly(m-anthranilic acid)/polyacrylonitrile blends. *European Polymer Journal* 49 (2013) 2645–2653.
- [31] Yang, j., Gunasekaran, S. Electrochemically reduced graphene oxide sheets for use in high performance supercapacitors. *Carbon* 51 (2013) 36-44.
- [32] Tucceri, R. A review about the charge conduction process at poly(o-aminophenol) film electrodes. *The Open Physical Chemistry Journal* 4 (2010) 62-77.
- [33] Iwuoha, E.I., de Villaverde, D.S., Garcia, N.P., Smyth, M.R., Pingarron, J.M. Reactivities of organic phase biosensors, 2. The amperometric behaviour of horseradish peroxidase immobilised on a platinum electrode modified with an electrosynthetic polyaniline film. *Biosensors Bioelectronics* 12 (1997) 749-761.
- [34] Guin, P.S., Das, S., Mandal, P.C. Electrochemical reduction of quinones in different media: A review. *International Journal of Electrochemistry* (2011) doi: 10.4061/2011/816202.
- [35] Lever, A.B.P. The phthalocyanines—molecules of enduring value; a two-dimensional analysis of redox potentials. *Journal of Porphyrins and Phthalocyanines* 3 (1999) 488-499.
- [36] Cretu, R., Kellenberger, A., Medeleanu, M., Vaszilcsin, N. Cathodic hydrogen evolution reaction on gold catalyzed by proton-carriers. *International Journal of Electrochemical Science* 9 (2014) 4465-4477.

- [37] Khanova, A.K., Krishtalik, L.I. Kinetics of the hydrogen evolution reaction on gold electrode. A new case of the barrierless discharge. *Journal of Electroanalytical Chemistry* 660 (2011) 224-229.
- [38] Conway, B.E. Electrochemical proton transfer and cathodic hydrogen evolution. *Science Progress* 71 (1987) 479-509.
- [39] Zheng, Y., Jiao, Y., Jaroniec, M., Qiao, S.Z. Advancing the electrochemistry of the hydrogen-evolution reaction through combining experiment and theory. *Angewandte Chemie International Edition* 54 (2015) 52-65.
- [40] Zheng, Z., Li, N., Wang, C.Q., Li, D.Y., Zhu, Y.M., Wu, G. Ni–CeO<sub>2</sub> composite cathode material for hydrogen evolution reaction in alkaline electrolyte. *International Journal of the Hydrogen Energy* 37 (2012) 13921-13932.
- [41] Corte, D.A.D., Torres, C., Correa, P.S., Rieder, E.S., F. Malfatti, C. The hydrogen evolution reaction on nickel-polyaniline composite electrodes. *International Journal of the Hydrogen Energy* 37 (2012) 3025-3032.
- [42] Mandegarzad, S., Raof, J.B., S. R. Hosseini, S.R., Ojani, R. Cu-Pt bimetallic nanoparticles supported metal organic framework-derived nanoporous carbon as a catalyst for hydrogen evolution reaction. *Electrochimica Acta* 190 (2016) 729-736.

## CHAPTER FIVE

### ELECTROCATALYTIC HYDROGEN EVOLUTION REACTION OF METAL ORGANIC FRAMEWORKS DECORATED WITH POLY (3-AMINOBENZOIC ACID)

---

*This chapter has been submitted for publication:*

*Kabelo E. Ramohlola, Milua Masikini, Siyabonga B. Mdluli, Gobeng R. Monama, Mpitloane J. Hato, Kerileng M. Molapo, Emmanuel I. Iwuoha, Kwena D. Modibane. Electrocatalytic Hydrogen Evolution Reaction of Metal Organic Frameworks decorated with poly (3-aminobenzoic acid). Electrochimica Acta.*

#### ABSTRACT

Advanced materials for hydrogen evolution reaction are central to the area of renewable energy. Here, we developed a solvothermal synthesis of metal organic framework (MOF) nanoparticles decorated with poly (3-aminobenzoic acid) (PABA) referred as MOF-3.6wt.-%-PABA and MOF-5wt.-%-PABA composites. The parent material (MOF) and composites were characterised by ultraviolet visible (UV-vis) and Fourier transform infrared (FTIR) spectroscopy, powder X-ray diffraction (XRD), thermogravimetric analysis (TGA), scanning electron microscope (SEM), transmission electron microscope (TEM), energy dispersive X-ray spectroscopy (EDS, EDX), selected area electron diffraction (SAED) and cyclic voltammetry (CV). Detailed structural and morphological characterisations established that PABA interacts with MOF on the external surface as observed by appearance of rough surface of the composites. The XRD and SAED showed that MOF and composites are crystalline and the presence of PABA did not alter the crystallinity of the material. Experiments probing the thermal, electrochemical and photophysical properties revealed that the composites were very stable and robust and had exceptionally properties. Significant hydrogen evolution reaction (HER) using CV and Tafel plots, was generated by MOF and composites in dimethyl sulfoxide/tetrabutylammonium perchlorate (DMSO/TBAP) supporting electrolyte in the presence of hydrogen source by applying a negative potential to the electrode.

**Keywords:** Metal organic frameworks, poly(3-amino benzoic acid), electrochemistry, electrocatalytic hydrogen evolution reaction, Tafel plots

## 5.1. INTRODUCTION

As described in Chapter two that metal organic frameworks are highly crystalline, nanoporous materials consisting of metal ions connected to a multifunctional organic linker/ligand to form a three dimensional structure with a high surface area, high pore volume and chemical tenability [1-3]. These properties make MOF a good candidate in various applications such as gas storage, catalysis and sensors [4-7]. Little attention has been paid in electrochemical hydrogen evolution reaction (HER) using MOFs it has low electrical conductivity. This is due to insulating characters of organic linkers which form part of MOF structures and poor overlap between the  $\pi$  orbitals and the d orbitals of the metal ions [8].

It is well documented that advanced catalyst for HER should reduce the overpotential, and consequently increase the efficiency of this important electrochemical process [9-11]. The most effective HER electrocatalysts are Pt group metals [12], however, their widespread practical utilization has been hampered by high cost and low abundance [13]. Even though MOFs have low electrical conductivity, their high surface areas and high volume of porosity provide additional advantage towards electrocatalytic reactions [13]. Approaches to increase conductivity of MOF have been previously reported [14]. These include incorporation of carboxylic, sulfonic and phosphoric acid species as channel-accessible functionalities on framework linkers and physical introduction of proton donor or carriers into the pores of already synthesized framework structure [14].

In this study, we present a new route of increasing the conductivity of a material by formation of a hybrid composite to be a suitable electrocatalyst for HER. The hybrid is formed between MOF and poly(3-amino benzoic acid) polymer using solvothermal route because this method provides precise control over the size, shape distribution, well-crystalline nanoparticles, efficient synthesis conditions and ability to control the morphology of the material as compared to other methods [1]. Polyaniline and its derivatives have been studied widely for various electrochemical applications due to their exceptional properties such as ease of synthesis, low cost and environmental stability [15-17]. The interaction between MOF and the polymer can occur either by strong covalent, electrostatic interaction,  $\pi$ - $\pi^*$  stacking or hydrogen bonding [18, 19]. These interactions can change the surface morphologies of MOF material, giving new shapes and even highly crystal structures. Interactions between poly(3- amino benzoic

acid)(PABA) and MOF in this work were obtained by in situ solvothermal preparation of MOF in the presence of PABA with different weight percentages and confirmed by XRD, TGA, FTIR, UV-vis, SEM, TEM, EDS, EDX and SAED. The HER studies were evaluated using CV and Tafel plots.

## 5.2. EXPERIMENTAL SECTION

### 5.2.1. Materials

3-aminobenzoic acid monomer (ABA), copper nitrate trihydrate ( $\text{Cu}(\text{NO}_3)_2 \cdot 3\text{H}_2\text{O}$ ), trimesic acid ( $\text{H}_3\text{BTC}$ ) and tetrabutylammonium percholate (TBAP) were purchased from Sigma Aldrich, South Africa. Ammonium per sulfate (APS) and iron chloride ( $\text{FeCl}_3$ ) were purchased from Riedel-de Haen and Educhem, respectively. Absolute ethanol was purchased at Merck, South Africa and hydrochloric acid (HCl), dimethyl sulfoxide (DMSO) and sulphuric acid ( $\text{H}_2\text{SO}_4$ ) were procured from Rochelle Chemicals. Aniline was distilled before use and the rest of the reagents were used without further purification.  $\text{H}_2\text{SO}_4$  standard solutions were made in DMSO solution with 0.1 M TBAP as a supporting electrolyte system unless otherwise stated. All measurements were carried out at  $22 \pm 2^\circ\text{C}$ .

### 5.2.2. Synthesis of PABA, MOF and MOF/PABA composite

Poly(3-aminobenzoic acid) (PABA) was prepared by oxidation polymerisation of 3-aminobenzoic acid monomer according to a previously reported method [20]. The synthesis of Cu-trimesic MOF (HKUST-1) was based on a previously reported hydrothermal procedure [21]. MOF/PABA composites were synthesised by in situ hydrothermal synthesis of MOF in the presence of 3.6 wt. % and 5.0 wt. % PABA, respectively. Benzene-1,3,5-tricarboxylic acid was dissolved in 10 ml ethanol and  $\text{Cu}(\text{NO}_3)_2 \cdot 3\text{H}_2\text{O}$  was dissolved in 10 ml distilled water in the presence of PABA. The two solutions were mixed, stirred for 30 minutes and consequently the mixture was transferred into a Teflon-lined stainless autoclave, sealed and heated at  $120^\circ\text{C}$  for 36 hours to yield MOF/PABA composites. Finally, the product was filtered, washed with ethanol/distilled water solution and dried at  $50^\circ\text{C}$  for overnight.



### 5.2.3. Material Characterisations

The characterisation measurements used in this section were as described in Chapter four.

## 5.3. RESULTS AND DISCUSSION

### 5.3.1. Spectroscopic Characterisations

FTIR spectra of MOF and MOF/PABA composites (Figure 5.1(a)) reveal a broad peak at 3000-3400  $\text{cm}^{-1}$  which is attributed to the OH bond stretching/ moisture trapped inside the framework of MOF materials [22]. For neat MOF, the peaks at 1643, 1461 and 1374  $\text{cm}^{-1}$  correspond to the C=O symmetrical and asymmetrical modes and also a bridging bidentate coordination of the carboxylate group in the organic linker [22, 23]. Introduction of PABA alters the characteristic peaks of MOF. It is also noticeable that there is an increase in aromaticity of the samples and new peaks developed upon introduction of PABA. These new peaks appear at approximately 1548 and 1627  $\text{cm}^{-1}$  are associated to C-C stretching of the benzenoid and quinoid rings of the PABA, respectively. The bands at 1272 and 1778  $\text{cm}^{-1}$  are attributed to C-O and C=O vibrations of the carboxylic acid functional group of PABA, respectively. It is also noteworthy to mention that the absorption band at 1094  $\text{cm}^{-1}$  attributed to the C-O stretching mode of C-OH group in the case of MOF disappeared upon introduction of PABA indicating a successful synthesis of MOF/PABA composite. The UV-vis results of MOF and MOF/PABA composites in DMSO solvent (partially soluble) are shown in Figure 5.1(b). It has been reported that MOF exhibits two absorption bands, thus ligand-to-metal charge transfer (LMCT) with an edge around 280 nm and the d-d transition of the  $\text{Cu}^{2+}$  around 750 nm [24]. However, the two absorption bands associated to LMCT and d-d transitions are not clear in the UV-vis results of MOF and its composites due to insolubility of MOF in most organic solvent [24]. When PABA is introduced, there is an increase in the absorbance of the materials as a result of an improved solubility in DMSO as depicted in Figure 1b. In addition, there is an appearance of a new band around 450 nm which is attributed to  $\pi$ - $\pi^*$  transition of PABA as indicative of polymer incorporated on the MOF surface [16].

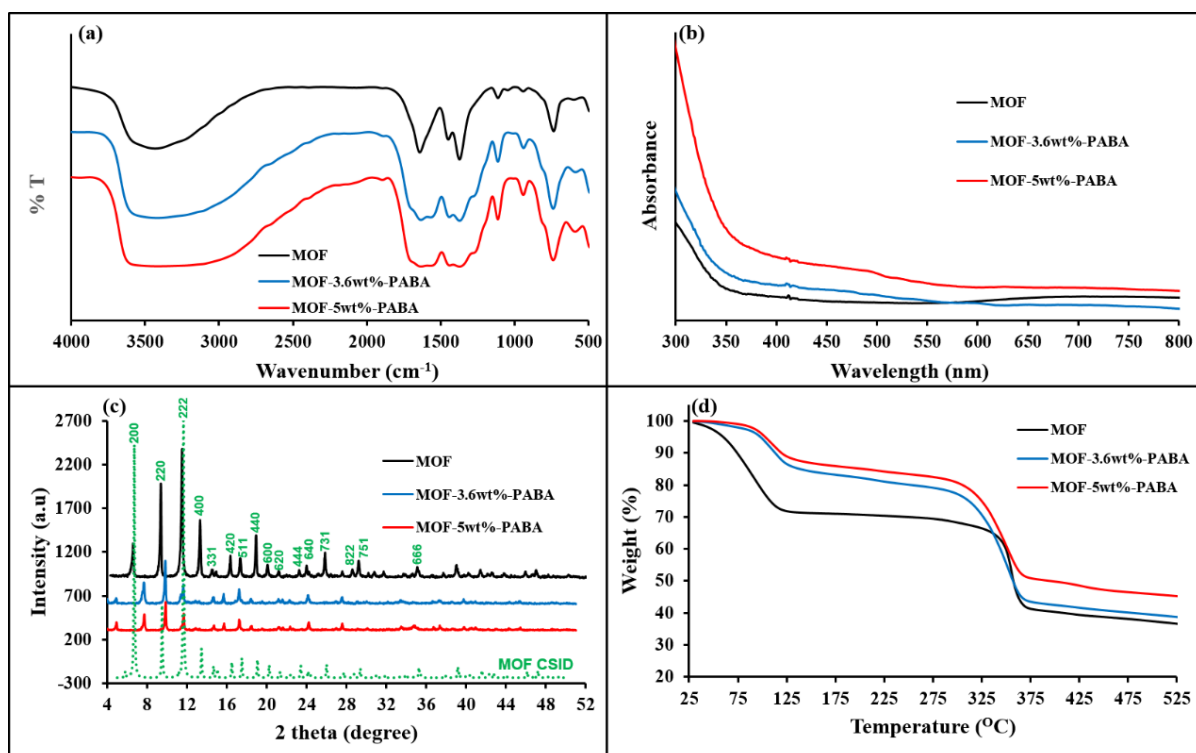


Figure 5.1: (a) FTIR, (b) UV-vis spectra of MOF and MOF/PABA composites in DMSO, (c) XRD and (d) TGA analysis of MOF and MOF/PABA composites.

In order to substantiate the purity of the synthetic MOF, XRD analysis was carried out. Figure 5.1(c) gives the XRD patterns of MOF and MOF/PABA composites. It can be noticed that MOF exhibits cubic crystal structure diffraction patterns identical to those of the simulated one (MOF crystal structural information data (CSID)), indicating that the structure of HKUST-1 was well preserved and the MOF was a pure powder [3, 25]. Addendum to this, these patterns show that MOF phases are highly crystalline, which is an indication of microporous structure [25]. The observed main peaks relating to reflection planes are indexed at  $2\theta$  degree = 6.68, 9.42, 11.62, 13.27 and 18.85 correspond to (200), (220), (222), (400), and (440) planes, respectively [25]. The intensive peaks of Figure 1c appearing at lower  $2\theta$  degree are characteristics of microporous material which possessed numerous tiny pores or cavities. Upon composite formation, it can be seen that the crystallinity of MOF was maintained as indicated by a numerous number of sharp peaks. Nonetheless, there is a slight shift in XRD patterns of the composites to a lower  $2\theta$  values. This observation suggests that there was an interaction between MOF and PABA. The composites showed some

additional small diffraction peaks at around  $2\theta = 21^\circ$ , which correspond to (100) plane of the polymer [16]. Furthermore, MOF-3.6wt%-PABA showed a small sharp peak at around  $2\theta = 32^\circ$  ascribed to the Fe impurity of oxidant used in the synthesis. It is very surprising that this peak disappeared with increasing the loading of PABA in to the MOF. This observation may suggest a strong interaction between MOF and PABA, which resulted in a decrease in the presence of impurities [16].

TGA analysis can be used to determine the precise weight ratio of each component in a sample and the thermal stability of the composite. Furthermore, by comparing the TGA curve of each component separately to its curve in a composition material, we can also learn about the degree of interaction between the reacting species. The TGA curves of MOF and MOF/PABA composites, in comparison, analysed at a heating rate of  $10^\circ\text{C}/\text{min}$  are presented in Figure 5.1(d). It can be seen that MOF and its composites exhibit two similar thermal degradation steps throughout the experimental temperature range. These two degradation steps appear at around  $100$  and  $325^\circ\text{C}$ . These thermal degradation steps are normally attributed to the intrinsic thermal degradation characteristics of MOF which correspond to water and ethanol physisorbed in the framework of MOF, by losing its organic linker molecules and producing copper oxide [25 - 29]. The TGA of MOF displays an overall weight loss of 60%, while both MOF-3.6wt%-PABA and MOF-5wt%-PABA composites showed overall weight losses of 58 and 50%, respectively. At the initial period the weight loss is due to the evaporation of water and organic linker molecules. For MOF/PABA composites, the lower rate of mass loss with increasing temperature may be due to the internal change in this material that is not accompanied by mass loss at elevated temperatures. Addition of PABA in the MOF increases the thermal stability of the composites. This observation maybe due to a strong interaction between MOF and PABA. In addition, though the final degradation step occurs at about  $325^\circ\text{C}$  for all the samples, the MOF sample exhibits a steeper weight loss as compared to composites. The slower, less steep degradation step of the composites suggests higher thermal stability due to the stabilizing effect of PABA. In addition, increasing the loading of PABA in the composite resulted with more of PABA on the surface of MOF as observed in SEM images which resulted in a change in morphology.

### 5.3.2. Morphological Characterisations

The FE-SEM microphotographs (Figure 5.2) were used to investigate the morphologies and microstructures of MOF and MOF/PABA composites. As shown in Figure 5.2(a), and also in Chapter three and four, MOF shows typical irregular crystals with octahedral shapes confirming a low control on the crystal growth parameters [25, 28] and its corresponding EDS (Figure 5.2(b)) reveals the presences of C-, O- and Cu-atoms in the MOF structure. The inset image (Figure 5.2(a)) shows that MOF crystal have smooth surfaces, this tells that hydrothermal synthesis gives pure, highly crystalline MOF materials. The SEM images of MOF/PABA composites (Figure 5.2(c and e)) show similar octahedral shapes with the presence of spherical crystals which can be attributed to morphologies of PABA. Magnification of the octahedral crystals (inset images in Figure 5.2(c and e)) of MOF/PABA composites showed that after introduction of PABA the surfaces of the crystals develops rough surfaces which can be due to interaction of MOF and PABA. Clear demonstration of rough surfaces is observed when the PABA amount is increased in which the inset image (Figure 5.2(e)) shows the interconnecting structures of polymer on the surfaces of MOF. This shows that there is a surface interaction between MOF and PABA materials. EDS analyses (Figure 5.2(d and f)) result also revealed the presence of copper, carbon and oxygen. Furthermore, the EDS analysis of MOF-3.6wt.-%-PABA showed the presence of iron (Fe) which is due to oxidant used during synthesis of PABA.

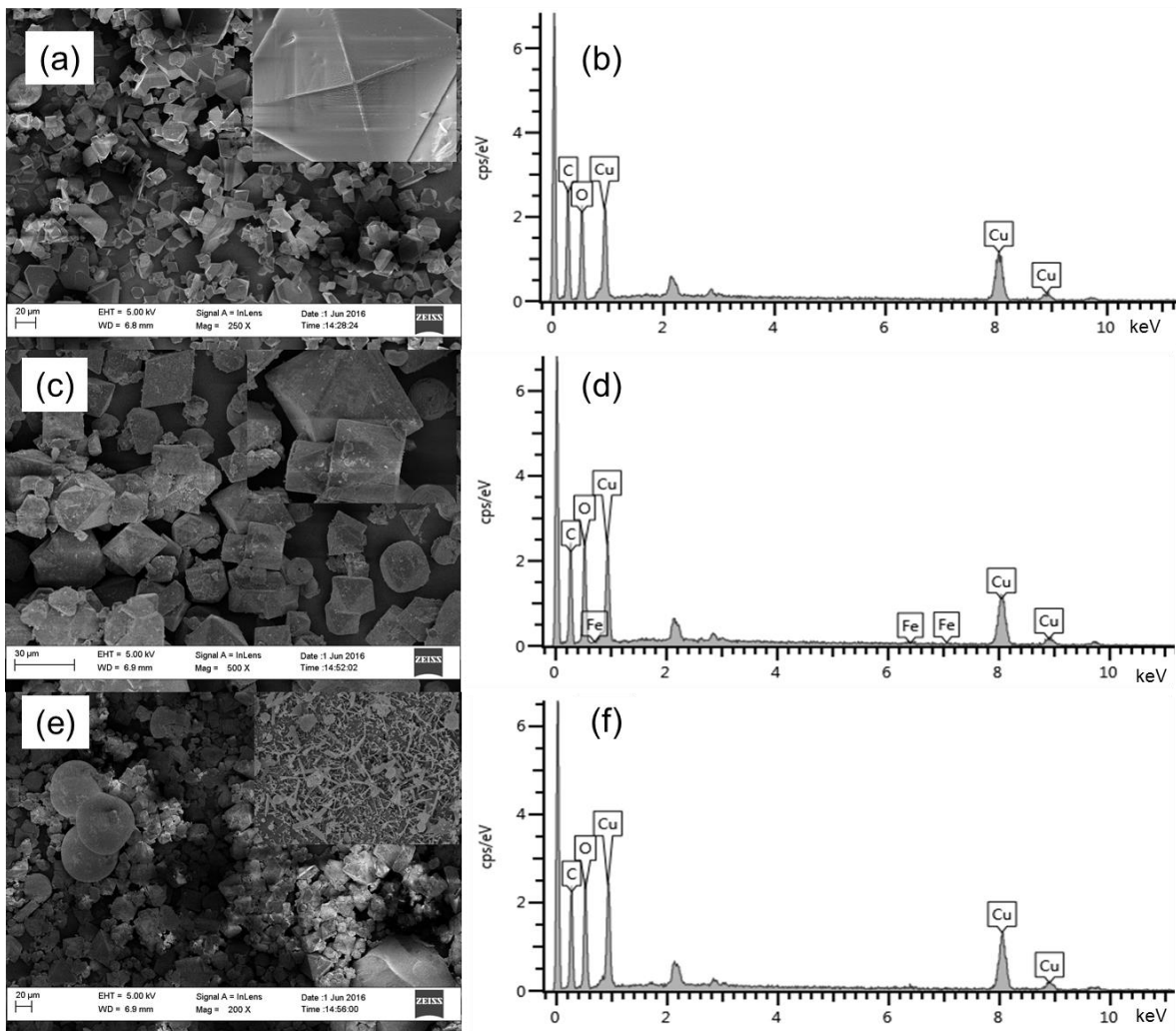


Figure 5.2: SEM image of (a) parent MOF, (c) MOF-3.6wt.-%-PABA (e) MOF-5wt.-%-PABA composites (inset : magnification on the crystal structure to view the surface of the crystal) and EDS spectrum of (b) MOF, (d) MOF-3.6wt.-%-PABA, (f) MOF-5wt.-%-PABA composites.

TEM images of MOF and MOF/PABA composites are shown in Figure 5.3(a, c and e) and inset images are the selected area electron diffraction (SAED) patterns used to determine the crystallinity of the materials. Figure 5.3(a) exhibits the TEM images of MOF with microporous structures. The SAED image of MOF shows clear ring patterns indicating a highly crystalline MOF material [25]. The EDX results (Figure 3b) showed the presence of Cu-, C- and O- atoms and is consistent with the EDS results of MOF presented in Figure 5.2(b). TEM images of MOF/PABA composites (Figure 5.3(c and e)) shows the dispersion of PABA on the microstructures of MOF materials. The dispersion of PABA had no effect on the crystallinity as ring patterns can be clearly

observed on the inset SAED results; however the rings were not as clear as observed on the SAED results of pure MOF. This is in agreement with the XRD results of parent material and composites as shown in XRD patterns in Figure 5.1(c). EDX results of composites also shown the presence of Cu-, C- and O- atoms and are shown in Figure 3(d and f). The presence of small peaks (Figure 3(f)) and Ni (Figure 5.3(d and f)) are due to impurities trapped in the PABA backbone from synthetic conditions and Ni grid used during analysis. Intensive study of EDX results of parent MOF and its MOF/PABA composites shows that there is an increase of carbon counts when PABA is introduced as an indicative of composite formation.

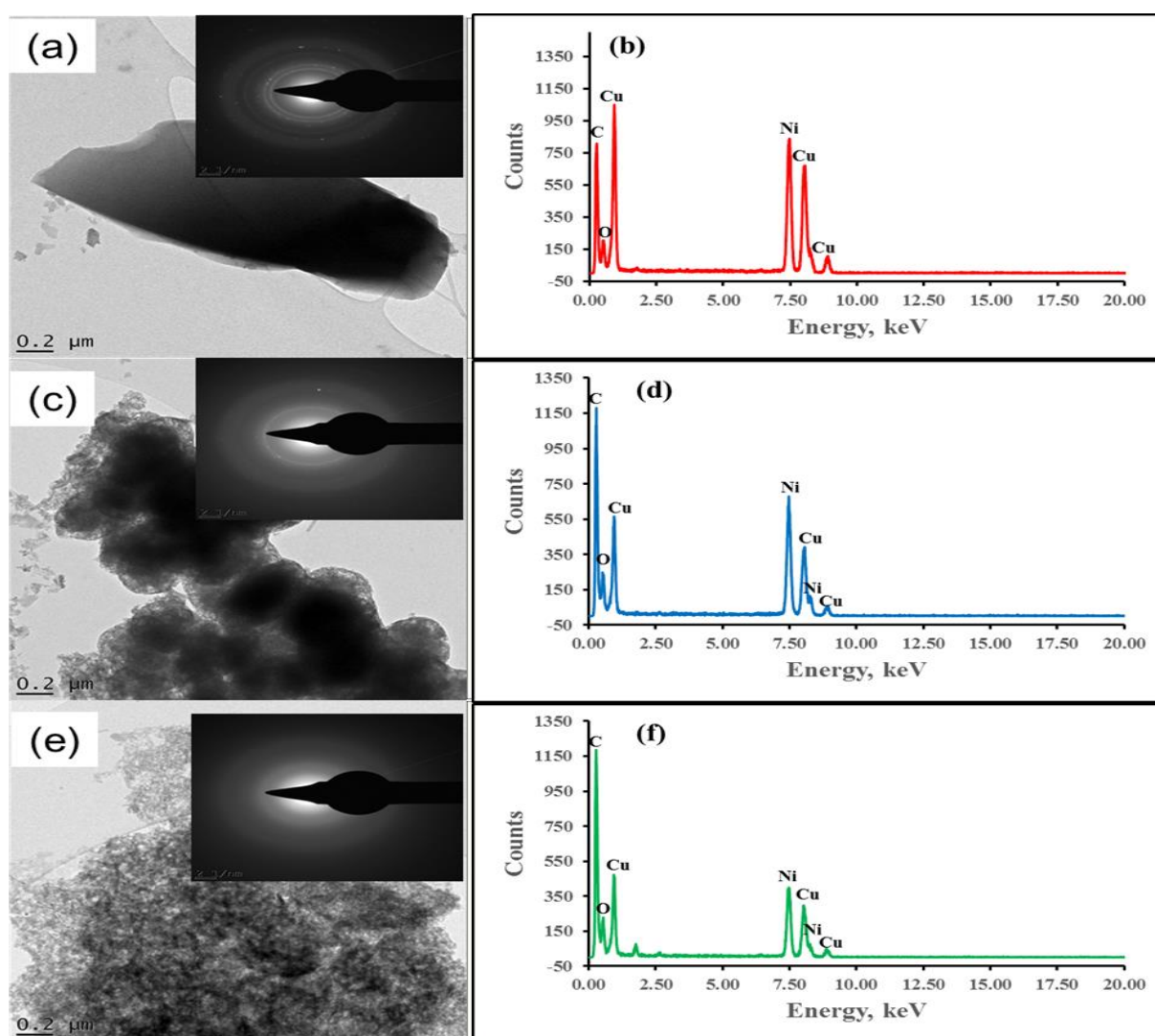


Figure 5.3: TEM image of (a) parent MOF, (c) MOF-3.6wt.%-PABA (e) MOF-5wt.%-PABA composites (inset : SAED images) and EDX spectrum of (b) MOF, (d) MOF-3.6wt.%-PABA, (f) MOF-5wt.%-PABA composites.

### 5.3.3. Electrochemical Characterisations

Cyclic voltammetry was conducted using gold electrode and 0.1 M TBAP/DMSO electrolyte to determine the redox potential and electrochemical behaviour of MOF and MOF/PABA composites. Cyclic voltammograms of all materials are represented in Figure 5.4. Cyclic voltammogram of MOF (blue) and MOF-5wt.%-PABA (green) showed similar redox behaviour as compared to MOF-3.6wt.%-PABA (red) in which both redox peaks cannot deduced in reference to gold electrode. The reason for this disappearance was due to the weak interaction between MOF and PABA when 3.6wt%-PABA was added as well as the presence of the impurities as observed in structural analyses. This observation resulted in a decrease in the conductivity of the composite formed. For both MOF and MOF-5wt.%-PABA, clear redox peaks are observed at  $E_{p,c} \sim -0.20$  V which is due to reduction reaction of  $[\text{Cu}_3(\text{BTC})_2 \rightarrow \text{Cu}_3(\text{BTC})_2^-]$  and at  $E_{p,a} \sim -0.40$  V attributed to reverse oxidation reaction of  $[\text{Cu}_3(\text{BTC})_2^- \rightarrow \text{Cu}_3(\text{BTC})_2]$  [29]. The difference between voltammogram of MOF and MOF-5wt.%-PABA is that for the composite, there is an increase in the current densities which tells that the presence of PABA in the composite have an effects in the electrochemical behaviour of MOF. The different scan rates dependent studies was used to examine the electrochemical properties of the materials and are shown in Figure 5.4(b-d). For all the materials, the anodic-cathodic wave separations increased with increasing scan rates which in an evident of diffusion-controlled reactions on the surface of the materials [30]. Multiscan voltammogram of MOF-3.6wt.%-PABA (Figure 4(c)) shows double redox reversible peaks at  $E_{p,c} \sim -0.80$  V and  $E_{p,a} \sim -0.60$  V which is attributed to gold electrode and second redox couple at  $E_{p,c} \sim 0.30$  V and  $E_{p,a} \sim -0.40$  V which is due to diffusion of electrons from PABA to MOF material.

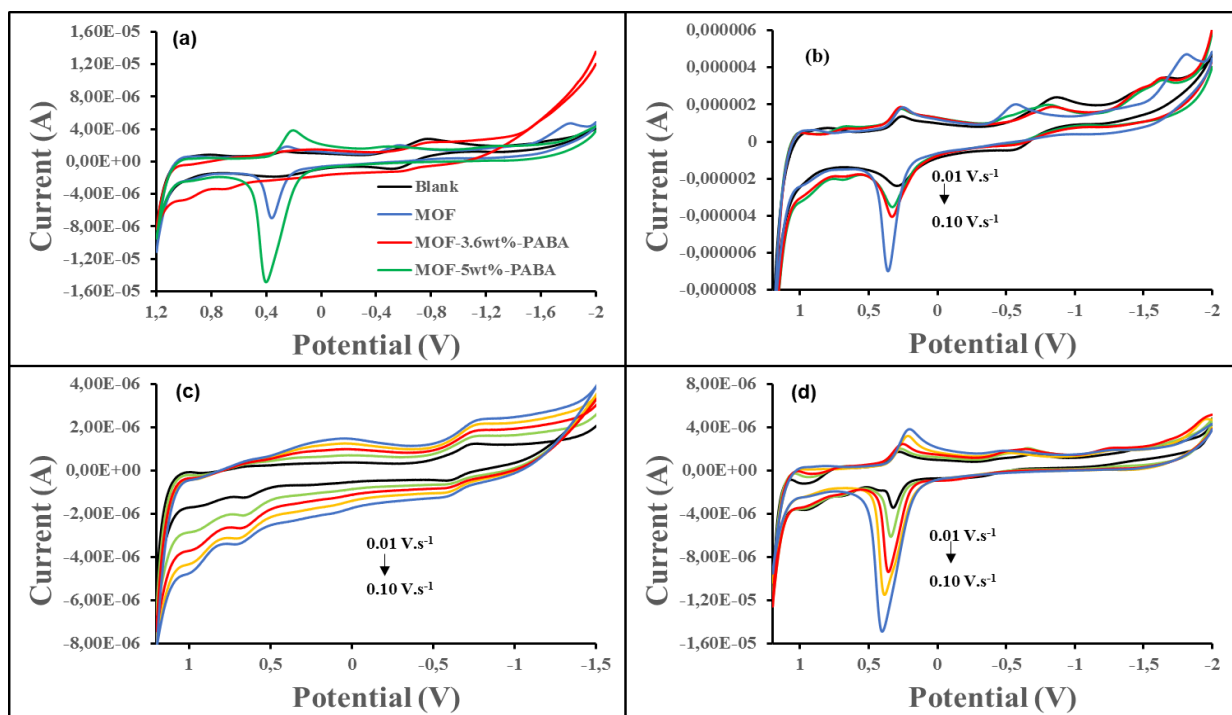


Figure 5.4: (a) CV results of blank, MOF and MOF-PABA at  $0.1 \text{ Vs}^{-1}$ ; (b) and (c) CV of MOF and MOF-3.6wt%-PABA and (d) MOF-5wt%-PABA at different scan rates ( $0.02$ - $0.10 \text{ Vs}^{-1}$ ) in  $0.1 \text{ M DMSO/TBAP}$  electrolyte solution on gold electrode.

To examine the diffusion control characters of the materials, the plot of the logarithm of the current against the logarithm of the scan rate was constructed for each material and represented in Figure 5.5(a). The linear relationship was observed for all materials which shows that MOF and MOF/PABA composites exhibit the characteristics of a response due to diffusion transport of electron. The slopes between  $0.4$ - $0.5$  is an indicative of a diffusion control and the diffusion processes were supported by linear relationship of reductive peak current versus square root of scan rate plot as demonstrated in Figure 5.5(b) which is a evident of semi-definite diffusion control mass transport [30, 31].



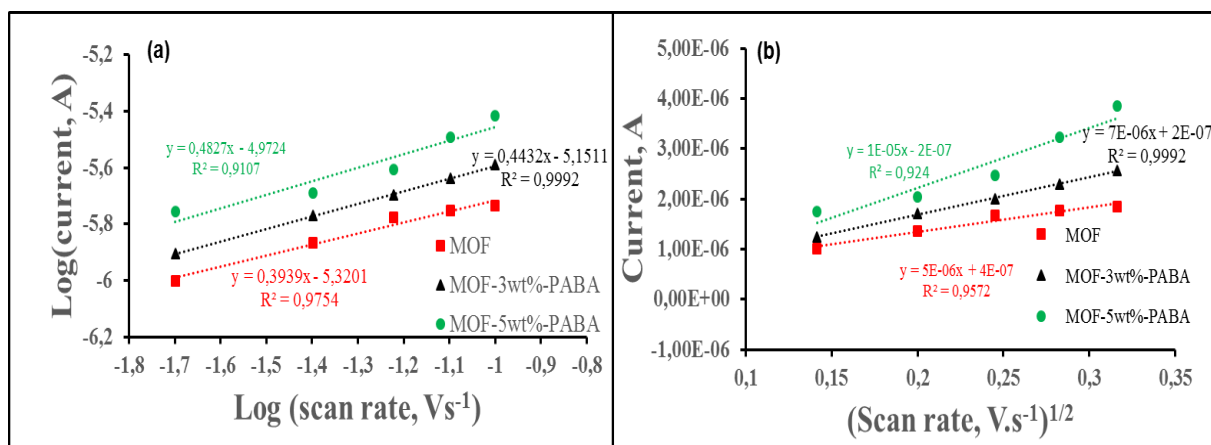


Figure 5.5: (a) The log-log plot of the absolute value of the peak current vs scan rate and (b) Peak current as a function of square root of scan rate for s<sup>-1</sup> for MOF, MOF-3.6wt%-PABA and MOF-5wt%-PABA composites in 0.1 M DMSO/TBAP electrode system at different scan rate (0.02 – 0.10 Vs<sup>-1</sup>).

The diffusion coefficient,  $D$ , was determined for catalysts using cyclic voltammetry and following the Randles-Ševčík equation (Eq. 3.1) for a quasi-reversible system [32]:

$$I_p = (2.65 \times 10^5) n^{3/2} A C D^{1/2} \nu^{1/2} \quad (3.1)$$

where,  $n$  is the number of electrons transferred,  $A$  is the electrode area in cm<sup>2</sup>,  $D$  is the diffusion coefficient in cm<sup>2</sup> s<sup>-1</sup>,  $C$  is the bulk molar concentration of the electroactive species in mol.cm<sup>-3</sup> and  $\nu$  is scan rate is Vs<sup>-1</sup>. The diffusion coefficients were determined to be  $2.53 \times 10^{-6}$  and  $4.96 \times 10^{-6}$  and  $10.1 \times 10^{-6}$  m<sup>2</sup> s<sup>-1</sup> for MOF, MOF-3.6wt%-PABA and MOF-5wt%-PABA composites, respectively.

### 5.3.4. Hydrogen Studies

Electrocatalytic studies of MOF and MOF/PABA composites were performed in TBAP/DMSO electrolyte with sulphuric acid, H<sub>2</sub>SO<sub>4</sub> as a proton source and the results are shown in Figure 5.6. As shown in Figure 5.6(a), H<sub>2</sub>SO<sub>4</sub> gives hydrogen reduction peak around -1.0 V in absence of catalysts which indicates the ability of Au electrode to adsorb some of the proton. Upon addition of MOF, there was an increase in the current density at the very same region. Voltammetric response of MOF-3.6wt%-PABA upon addition of acid shown similar response with less current response as

compared to MOF. This is in accordance with the voltammogram in absence of a proton source where reduction and oxidation peaks were not observed. Voltammetric responses of MOF-5wt%-PABA for electrocatalytic HER are similar to those of MOF and MOF-3.6wt%-PABA, however the reduction wave shifted to more negative potentials which is one requirement of an electrocatalyst for HER [9,10]. Cyclic voltammogram of the materials in the presence of proton source was performed at different sulphuric acid concentration and represented in Figure 5.6(b-d). For all materials, at the similar cathodic peak region, there was an increase in current density with increase in acid concentration which is an evident that proton reduction is a source of catalytic current.

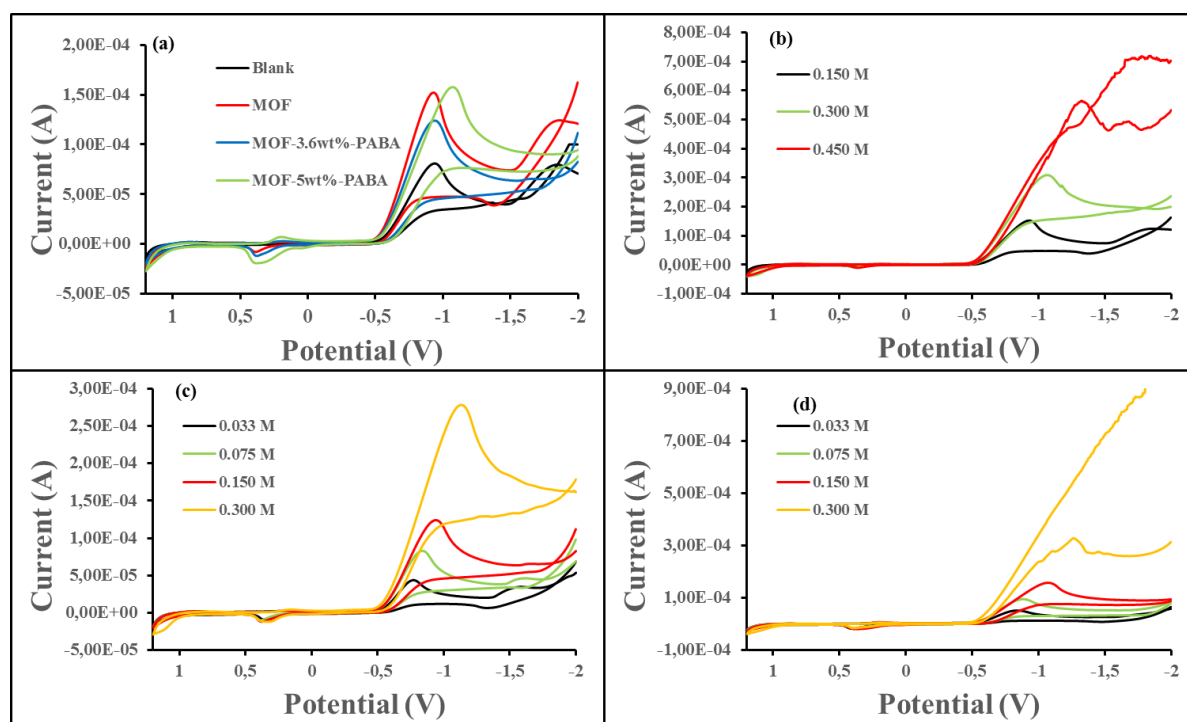


Figure 5.6: (a) CV results of blank, MOF and MOF-PABA; and (b) MOF, (c) MOF-3.6wt%-PABA and (d) MOF-5wt%-PABA at 0.10 Vs<sup>-1</sup> in the presence of different H<sub>2</sub>SO<sub>4</sub> concentration on gold electrode in 0.1 M DMSO/TBAP electrode system.

It is well known that in certain cases Tafel slopes can serve as indicator of the rate determining step in the HER and illustrate the existence of other kinetical effects [33]. Figure 5.7 shows Tafel plots (V versus log *i*<sub>0</sub> plots) for blank electrode, MOF, MOF-3.6wt%-PABA and MOF-5wt%-PABA materials which reveal the kinetics of HER process. The HER process are demonstrated in Chapter two and four that there are

three major reaction steps, thus discharge step (Volmer reaction), electrochemical discharge (Heyrovsky reaction) and combination step of adsorbed hydrogen (Tafel reaction) in acid solution [33-37].

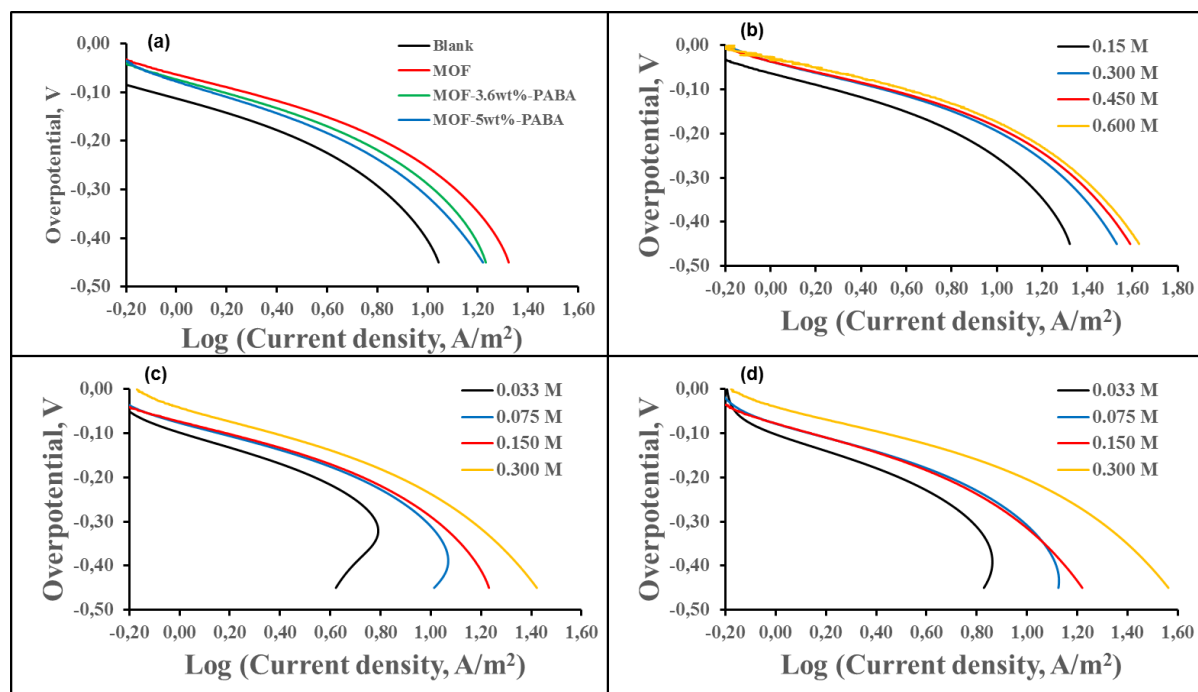


Figure 5.7: (a) Tafel plots of blank, MOF and MOF-PABA; and (b) MOF, (c) MOF-3.6wt%-PABA and (d) MOF-5wt%-PABA at  $0.10 \text{ Vs}^{-1}$  in the presence of different  $\text{H}_2\text{SO}_4$  concentration on gold electrode in  $0.1 \text{ M DMSO/TBAP}$  electrode system.

The Tafel slopes estimated by linear fitting of the polarization curves ( $\eta = b \log i + a$ ), where  $b$  is the Tafel slope and  $i$  is the current density) from Figure 5.7 are tabulated in Table 5.1 as well as exchange current density ( $i_0$ ) and cathodic transfer coefficient ( $1-\alpha$ ). The transfer coefficient  $1-\alpha$  was calculated using high overpotential region, where the Butler–Volmer equation simplifies to the Tafel equation, from the Tafel slope  $b$  given by relationship:

$$b = \frac{-2.303 RT}{(1-\alpha)F} \quad (3.2)$$

where  $R$  is the gas constant ( $8.31451 \text{ J mol}^{-1} \text{ K}^{-1}$ ),  $T$  - thermodynamic temperature (K),  $F$  – Faraday’s number ( $96,485 \text{ C mol}^{-1}$ ). The HER exchange current densities ( $i_0$ ) for MOF and MOF/PABA composites were calculated from the Tafel plots by the

extrapolation method with the abscissa ( $\log(i_0)$ ). The present study showed that the blank electrode gives Tafel slopes of  $167.4 \text{ mV.dec}^{-1}$  and  $106.2 \text{ mV.dec}^{-1}$  at the acid concentration of  $0.15 \text{ M}$  and  $0.30 \text{ M}$ , respectively. At the very same concentrations, MOF gave slopes of  $149.0$  and  $142.2 \text{ mV.dec}^{-1}$ . Furthermore, MOF-3.6wt.-%-PABA and MOF-5wt.-%-PABA composites gave Tafel slopes of  $164.5$  and  $166.7 \text{ mV.dec}^{-1}$  as well as  $179.2$  and  $153.5 \text{ mV.dec}^{-1}$  at the same acid conditions. It was reported that Tafel slopes in the ranges of  $105\text{-}150 \text{ mV.dec}^{-1}$  may be explained on the basis of a Volmer rate determining step for the HER [38]. However, the presence of the PABA on the MOF surface results in an increase in the Tafel slope value. This phenomenon that the materials shows a high Tafel slope value is in good agreement with other research [39]. It has been seen that when the charge-transfer coefficient is  $0.5$ , the rate determining step is the Volmer reaction or the Volmer reaction coupled with one of other two reactions [38]. As listed in Table 5.1, the charge-transfer coefficients are all close to  $0.5$ . Thus, the rate determining step of HER on the studied MOF, and MOF/PABA composites may be the Volmer reaction or the Volmer reaction coupled with one of other two reactions [38, 40]. The increase in charge-transfer coefficient of the composites was due electron conductivity of the PABA polymer [41]. In addition, the increase was primarily ascribed to the effective electron transport channels of the polymer and the increase of electro-chemically accessible surface area in nanocomposite materials, which was advantageous to facilitate the charge transfer at catalyst/electrolyte interface [41, 42]. The values of exchange current density,  $i_0$  increase with increase in acid concentrations for electrode and prepared materials. The exchange current density increases in an order of blank electrode >MOF >MOF-3.6wt.-%-PABA >MOF-5wt.-%-PABA at different concentration. This confirms that the presence of PABA improves the electron transfer process of MOF [42].

Table 5. 1: Experimental values of Tafel slope, transfer coefficient  $1-\alpha$  and exchange current  $i_o$ , in the absence and presence of MOF and MOF/PABA composites.

Material	H <sub>2</sub> SO <sub>4</sub> [mol/L]	Slope (b) [V.dec <sup>-1</sup> ]	-b [mV.dec <sup>-1</sup> ]	1- $\alpha$	log <i>i</i> <sub>o</sub>	<i>i</i> <sub>o</sub> [A.m <sup>-2</sup> ]
Blank	0.300	-0.1062	106.2	0.557	1.25	17.78
	0.150	-0.1674	167.4	0.353	0.98	09.55
MOF	0.300	-0.1422	142.2	0.416	1.60	39.81
	0.150	-0.1490	149.0	0.397	1.40	25.12
MOF-3wt%- PABA	0.300	-0.1667	166.7	0.355	1.50	31.62
	0.150	-0.1645	164.5	0.360	1.30	19.95
	0.075	-0.1784	178.4	0.332	1.20	15.85
	0.033	-0.2007	200.7	0.295	1.00	10.00
MOF-5wt%- PABA	0.300	-0.1535	153.5	0.385	1.70	50.12
	0.150	-0.1792	179.2	0.330	1.30	19.95
	0.075	-0.1645	164.5	0.360	1.20	15.85
	0.033	-0.2003	200.3	0.295	1.00	10.00

#### 5.4. CONCLUSIONS

In this chapter, highly active MOF/PABA composites for the HER were prepared through in situ solvothermal synthesis of MOF in the presence of 5 and 3.6wt.-%-PABA polymers. Formation of composites were confirmed by UV-vis, FTIR, XRD, TGA, SEM, TEM and CV. The influences of PABA on the morphological and structural properties of MOF surface, as well as resulting electro-catalytic activity in hydrogen evolution were systematically investigated. It was seen that the presence of PABA on the MOF surface can significantly increase electrochemical properties of MOF. The increase in the PABA loading resulted with increase in electro-catalytic activity composite. This observed tional roles of incorporated PABA on the MOF surface is as result of possible synergetic effects between PABA particles and the MOF matrix, leading to a facilitation of H<sub>ads</sub> migration. Furthermore, the rate determining step of HER on the studied MOF, and MOF/PABA composites was determined using Tafel slope and charge-transfer

coefficients and it may be the Volmer reaction or the Volmer reaction coupled with one of other two reactions.

## 5.5. REFERENCES

- [1] Alhamami, M., Doan, H., Cheng, C.H. A review on breathing behaviour of metal-organic frameworks (MOFs) for gas adsorption. *Materials* 7 (2014) 3198-3250.
- [2] Srimuk, P., Luanwuthu, S., Krittayavathanon, A., Sawangphruk, M. Solid-type supercapacitor of reduced graphene oxide-metal organic framework composite coated on carbon fibre paper. *Electrochimica Acta* 157 (2015) 69-77.
- [3] Osta, R.E., Feyand, M., Stock, N., Millange, F., Walton, R.I., Crystallisation kinetics of metal organic frameworks from in situ time-resolved X-ray diffraction. *Powder Diffraction* 28 (2013) s256-s275.
- [4] Sun, L.B., Li, J.R., Park, J., Zhou, H.C. Cooperative template-directed assembly of mesoporous metal-organic frameworks. *Journal of the American Chemical Society* 134 (2012) 126-129.
- [5] Dikio, E.D., Farah, A.M. Synthesis, characterization and comparative study of copper and zinc metal organic frameworks. *Chemical Science Transactions* 2 (2013) 1386-1394.
- [6] Kurmoo, M. Magnetic metal-organic frameworks. *Chemical Society Reviews* 38 (2009) 1353-1379.
- [7] Yu, Y., Ren, Y., Shen, W., Deng, H and Gao, Z. Applications of metal-organic frameworks as stationary phases in chromatography. *Trends in Analytical chemistry* 50 (2013) 33-41.
- [8] Talin, A.A., Centrone, A., Ford, A.C., Foster, M.E., Stavila, V., Haney, P., Kinney, R.A., Szalai, V., Gabaly, F.E., Yoon, H.P., Leonard, F., Allendorf, M.D. Tunable electrical conductivity in metal-organic framework thin-film devices. *Science* 343 (2014) 66-69.
- [9] Zhou, J., Caban-Acevedo, M., Liang, H., Samad, L., Ding, Q., Fu, Y., Li, M., Jin, S. High-performance electrocatalysis for hydrogen evolution reaction using Se-doped pyrite-phase nickel diphosphide nanostructures. *ACS Catalysis* 5 (2015) 6355-6361.
- [10] Zheng, Y., Jiao, Y., Li, L.H., Xing, T., Chen, Y., Jaroniec, M., Qiao, S.Z. Toward design of synergistically active carbon-based catalysts for electrocatalytic hydrogen evolution. *ACS Nano* 8 (2014) 5290-5296.

- [11] Liu, Q., Tian, J., Cui, W., Jiang, P., Cheng, N., Asiri, A.M., Sun, X. Carbon nanotubes decorated with CoP nanocrystals: A highly active non-noble-metal nanohybrid electrocatalyst for hydrogen evolution. *Angewandte Chemie* 126 (2014) 6828-6832.
- [12] Walter, M. G., Warren, E. L., McKone, J. R., Boettcher, S. W., Mi, Q., Santori, E. A., Lewis, N. S. Solar Water Splitting Cells. *Chemical Reviews* 110 (2010) 6446- 6473.
- [13] Qin, J.S., Du, D.Y., Guan, W., Bo, X.J., Li, Y.F., Guo, L.P., Su, Z.M., Wang, Y.Y., Lan, Y.Q., Zhou, H.C. Ultrastable polymolybdate-based metal-organic frameworks as highly active electrocatalysts for hydrogen generation from water. *Journal of the American Chemical Society* 137 (2015) 7169-7177.
- [14] Jeong, N.C., Samanta, B., Lee, C.Y., Farha, O.K., Hupp, J.T. Coordination-chemistry control of proton conductivity in the iconic metal-organic framework HKUST-1. *Journal of the American Chemical Society* 134 (2012) 51-54.
- [15] Ciric-Marjanovic, G., Dragicevic, L., Milojevic, M., Mojovic, M., Mentus, S., Dojcinovic, B., Marjanovic, B., Stejskal, J. Synthesis and characterization of self-assembled polyaniline nanotubes/silica nanocomposites. *The Journal of Physical Chemistry B* 113 (2009) 7116-7127.
- [16] Du, X.S., Xiao, M., Meng, Y.Z. Facile synthesis of highly conductive polyaniline/graphite nanocomposites. *European Polymer Journal* 40 (2004) 1489–1493.
- [17] Dong, H., Prasad, S., Nyame, V., Jones, W.E. Submicrometer conducting polyaniline tubes prepared from polymer fiber templates. *Chemistry of Materials* 16 (2004) 371-373.
- [18] Radtke, M., McMillan, D.G.G., Schroter, B., Hoppener, S., Dietzek, B., Schubert, U.S., Ignaszak, A. The effect of 3-amino benzoic acid linker and the reversal of donor-acceptor pairs on the electrochemical performance and stability of covalently bonded poly(pyrrole) nanotubes. *Polymer* 77 (2015) 289-296.
- [19] Zhao, Y., Tang, G.S., Yu, Z.Z., Qi, J.S. The effect of graphite oxide on the thermoelectric properties of polyaniline. *Carbon* 50 (2012) 3064-3073.
- [20] David, T., Mathad, J.K., Padmavathi, T., Vanaja, A. Part-A: Synthesis of polyaniline and carboxylic acid functionalized SWCNT composites for electromagnetic interference shielding coatings. *Polymer* 55 (2014) 5665-5672.



- [21] Ke, F., Qiu, L.G., Yuan, Y.P., Peng, F.M., Jiang, X., Xie, A.J., Shen, Y.H., Zhu, J.F. Thiol-functionalization of metal-organic framework by a facile coordination-based postsynthetic strategy and enhanced removal of Hg<sup>2+</sup> from water. *Journal of Hazardous Materials* 196 (2011) 36-43.
- [22] Azad, F.N., Ghaedi, M., Dashtian, K., Hajati, S., Pazeshkpour, V. Ultrasonically assisted hydrothermal synthesis of activated carbon-HKUST-1-MOF hybrid for efficient simultaneous ultrasound-assisted removal of ternary organic dyes and antibacterial investigation: Taguchi optimization. *Ultrasonics Sonochemistry* 31 (2016) 383-393.
- [23] Zhu, C., Zhang, Z., Wang, B., Chen, Y., Wang, H., Chen, X., Zhang, H., Sun, N., Wei, W., Sun, Y. Synthesis of HKUST-1/MCF compositing materials for CO<sub>2</sub> adsorption. *Microporous and Mesoporous* 226 (2016) 476-481.
- [24] Wang, H., Zhu, W., Li, J., Tian, T., Lan, Y., Gao, N., Wang, C., Zhang, M., Faul, C.F.J., Li, G. Helically structured metal organic frameworks fabricated by using supramolecular assemblies as templates. *Chemical Science* 6 (2015) 1910-1916.
- [25] Wang, X., Lu, X., Wu, L., Chen, J. 3D metal-organic framework as highly efficient biosensing platform for ultrasensitive and rapid detection of bisphenol A. *Biosensors and Bioelectronic* 65 (2015) 295-301.
- [26] Lin, K.S., Adhikari, A.K., Ku, C.K., Chiang, C.L., Kuo, H. Synthesis and characterization of porous HKUST-1 metal organic frameworks for hydrogen storage. *International Journal of Hydrogen Energy* 37 (2012) 13865-13871.
- [27] Feng, Y., Jiang, H., Li, S., Wang, J., Jing, X., Wang, Y., Chen, M. Metal organic frameworks HKUST-1 for liquid-phase adsorption of uranium. *Colloids and Surfaces A: Physicochem. Eng. Aspects* 431 (2013) 87-92.
- [28] Raganati, F., Gagiulo, V., Ammendola, P., Alfe, M., Chirone, R. CO<sub>2</sub> capture of HKUST-1 in a sound assisted fluidized bed. *Chemical Engineering Journal* 239 (2014) 75-86.
- [29] Fleker, O., Borenstein, A., Lavi, R., Benesvy, L., Ruthstein, S., Aurbach, D. Preparation and properties of metal organic framework/activated carbon composite materials. *Langmuir* 32 (2016) 4935-4944.
- [30] Raina, S., Kang, W.P., Davidson, J.L. Nanodiamond film with 'ridge' surface profile for chemical sensing. *Diamond and Related Materials* 17 (2008) 896-899.

- [31] Tucceri, R. A review about the charge conduction process at poly(o-aminophenol) film electrodes. *The Open Physical Chemistry Journal* 4 (2010) 62-77.
- [32] Yang, j., Gunasekaran, S. Electrochemically reduced graphene oxide sheets for use in high performance supercapacitors. *Carbon* 51 (2013) 36-44.
- [33] Chen, J., Xia, G., Jiang, P., Yang, Y., Li, R., Shi, R., Su, J., Chen, Q. Active and durable hydrogen evolution reaction catalyst derived from Pd-doped metal-organic frameworks. *ACS Applied Materials & Interfaces* 8 (2016) 13378-13383.
- [34] Wu, C., Li, C., Yang, B., Zhou, S., Shi, D., Wang, Y., Yang, G., He, J., Shan, Y. Electrospun MnCo<sub>2</sub>O<sub>4</sub> nanofibers for efficient hydrogen evolution reaction. *Materials Research Express* 3 (2016) 095018.
- [35] Zhou, W., Jia, J., Lu, J., Yang, L., Hou, D., Li, G., Chen, S. Recent developments of carbon-based electrocatalysts for hydrogen evolution reaction. *Nano Energy* 28 (2016) 29-43.
- [36] Gao, M.R., Liang, J.X., Zheng, Y.R., Xu, Y.F., Jiang, J., Gao, Q., Li, J., Yu, S.H. An efficient molybdenum disulfide/cobalt diselenide hybrid catalyst for electrochemical hydrogen generation. *Nature Communications* 6 (2015) 5982-5988.
- [37] Tang, Q., Jiang, D. Mechanism of Hydrogen Evolution Reaction on 1T-MoS<sub>2</sub> from First Principles. *ACS Catalysis* 6 (2016) 4953-4961.
- [38] Morozan, A., Goellner, V., Nedellec, Y., Hannauer, J., Jaouen, F. Effect of the transition metal on metal-nitrogen-carbon catalysts for the hydrogen evolution reaction. *Journal of the Electrochemical Society* 162 (2015) 719-726.
- [39] Kubisztal, J., Budniok, A., Lasia, A. Study of the hydrogen evolution reaction on nickel-based composite coatings containing molybdenum powder. *International Journal of Hydrogen Energy* 32 (2007) 1211-1218.
- [40] Jaksic, J.M., Vojnovic, M.V, Krstajic, N.V. Kinetic analysis of hydrogen evolution at Ni-Mo alloy electrodes. *Electrochimica Acta* 45 (2000) 4151-4158.
- [41] Ding, S., He, P., Feng, W., Li, L., Zhang, G., Chen, J., Dong, F., He, H. Novel molybdenum disulfide nanosheets-decorated polyaniline: Preparation, characterization and enhanced electrocatalytic activity for hydrogen evolution reaction. *Journal of Physics and Chemistry of Solids* 91 (2016) 41-47.

- [42] Ghiamata, Z., Ghaffarinejad, A., Faryadras, M., Abdolmaleki, A., Kazami, H. Synthesis of palladium-carbon nanotube-metal organic framework composite and its application as electrocatalyst for hydrogen production. *Journal of Nanostructure in Chemistry* 6 (2016) 299-308.

## CHAPTER SIX:

### GENERAL DISCUSSION, CONCLUSIONS AND RECOMMENDATIONS

---

#### 6.1. GENERAL DISCUSSION AND CONCLUSIONS

This chapter deals with conclusions of the results presented in the study and make further recommendations for future electrocatalysts research. This study has been directed towards the development of organic-inorganic hybrid materials based on polyaniline and its derivative poly (3-aminobenzoic acid) and metal organic framework. The overall goal of this thesis was to develop the most optimal, efficient and viable novel electrocatalyst nanocomposite in order to increase the scope of these polymer and MOF materials for application in different areas such as; electrocatalyst, hydrogen storage material and in the development of hydrogen fuel cell devices in the future. The electrocatalyst materials studied were identified and chosen on the basis of the excellent properties they offer. For example polyaniline and its derivative polymers exhibit optical and electrical materials properties of semiconductors or metals, whilst retaining attractive mechanical properties and processing advantages of organic polymers. They also exhibit favourable electrochemical redox properties such as being able to undergo electron transfer reactions at potentials that are accessible. MOF compounds offer remarkable photophysical and optical spectroscopic properties, when compared to the porous materials due to their exceptional properties such as high surface area and their porous structure.

The work was outlined into six chapters. Chapter one (introduction) and Chapter two (literature review) based on the background of Hydrogen technology. Furthermore, polyaniline and MOF material science, and techniques used for characterisation of materials were presented in Chapter two.

The first approach was taken in Chapter three involves synthesis of polyaniline doped with metal organic framework composite referred as PANI/MOF. Formation of polyaniline was obtained through oxidative chemical polymerisation process in the presence of ammonium disulfate and  $\text{FeCl}_3$  oxidants. MOF was prepared using solvothermal method to obtain highly crystalline material. PANI/MOF composite was

achieved by in situ oxidative chemical polymerisation of aniline in the presence of MOF. Structural and morphological characterisations using FTIR, Raman, XRD, SEM and TEM confirmed the successful preparation of PANI/MOF and showed that MOF is wrapped by the polymer. Hydrogen studies was evaluated using CV and SWV, in which an intense cathodic peak was observed upon addition of H<sub>2</sub>SO<sub>4</sub>. It showed that PANI/MOF hybrid composite has great potential to be used in hydrogen evolution reaction applications as it can easily generate and adsorb hydrogen through straight forward electrochemical process. It has been demonstrated that the PANI/MOF composite is not only robust and stable but also produces considerable H<sub>2</sub> gas. Remarkably, the observed hydrogen generation is dictated by the identity of hydrogen source which opens new avenues for multi analyte investigation.

The second approach taken in Chapter four involved preparation of a substituted polyaniline as it was reported that poor processibility and insolubility of polyaniline can be addressed by forming a polyaniline derivative, thus functionalized polyaniline. 3-amino benzoic acid was used in preparation of polyaniline derivative, poly(3-aminobenzoic acid) referred as PABA in this study. The 3-amino benzoic acid monomer have a similar structure as aniline, hence polymerisation follows the same mechanism as for aniline monomer. As compared to polyaniline, poly (3-aminobenzoic acid) gave spherical, granular structures unlike fiber rod-like structures of polyaniline. This tells that the presence of carboxylic group on the polymer backbone have an effect on the morphologies of a material. PABA has poor conductivities as compared to PANI and in order to increase the conductivity of PABA, incorporation of MOF was done through doping method as achieved in the case of PANI. Likewise, spectroscopic, microscopic, physical and electrochemical characterisation confirmed preparation of a novel PABA/MOF hybrid material. Electrocatalytic hydrogen generation of these hybrid material was investigated and results showed that introduction of MOF increased the current density at hydrogen evolution overpotential. The catalytic effect of PABA and PABA/MOF composites on HER was studied using exchange current density and charge transfer coefficient determined by the Tafel slope method. A drastic increase in catalytic H<sub>2</sub> evolution was observed in PABA and composite. Moreover, they merely require overpotentials as low as  $\sim -0.405$  V to attain current densities of  $\sim 0.8$  and  $1.5 \text{ Am}^{-2}$  and show good long-term stability. All these characteristics meet requirements for HER electrocatalysts for hydrogen fuel cell. The

improved catalytic activity observed in this work can be attributed to the following factors (i) increase in electron density of the polymer by introduction of MOF, which allows efficient electron transfer between the electron rich edges and the electrode and (ii) presence of Cu atom, which plays a crucial role in catalyzing the electrochemical HER (iii) improvement of photophysical and electrochemical properties of the PABA and PABA/MOF composite, which substantially improves the charge transfer kinetics of HER. We have demonstrated that the HER performance of PABA and PABA/MOF composite varies significantly with incorporation of MOF. The polymerisation method reported here for PABA/MOF material is scalable and can be extended to obtain other MOF based catalysts with different MOF loading and therefore represents an important development toward HER and other energy conversion technologies.

Final approach was taken in Chapter five whereby a novel metal organic framework decorated with poly(3-aminobenzoic acid) was developed towards electrocatalytic hydrogen production studies. Highly active MOF/PABA composites for the HER were prepared through in situ solvothermal synthesis of MOF in the presence of PABA. The influences of PABA with different loading amount on the morphology and crystalline structure of MOF surface, as well as resulting electro-catalytic activity in hydrogen evolution were systematically investigated. The presence of PABA on the MOF surface can significantly increase the HER exchange current density, and reduce the electrochemical reaction resistance. The electro-catalytic activity of the MOF-5wt.-%-PABA composite is higher than that of the MOF and MOF-3.6wt.-%-PABA composite. The observed promotional roles of incorporated PABA is ascribed to possible synergetic effects between PABA particles and the MOF matrix, leading to a facilitation of  $H_{ads}$  migration. Furthermore, the Tafel slope and charge-transfer coefficients showed that the rate determining step of HER on the studied MOF, and MOF/PABA composites may be the Volmer reaction or the Volmer reaction coupled with one of other two reactions.

These demonstrated that the PANI/MOF, PABA/MOF and MOF/PABA nanocomposites are suitable materials for electrocatalytic hydrogen production and storage for hydrogen fuel applications. Since, there is involvement of hydrogen evolution reaction which undergoes in the different HER mechanisms, Volmer reaction or the Volmer reaction coupled with one of other two reactions. These mechanisms

illustrate that the hydrogen gas may be produced in acidic condition followed by adsorption of hydrogen atoms by the composite material as part of hydrogen storage.

## 6.2. RECOMMENDATIONS FOR FUTURE WORK

Further improvement of the electrocatalyst materials will aid towards an increase of hydrogen productivity and efficiency. An important milestone in the work was to develop other alternative electrocatalyst which are to MOF material as HER material. It was clear from the work that the HER responses obtained in neat PANI and PABA were significantly low when compared to the lead PANI/MOF and PABA/MOF composites. Furthermore, since the PANI and PABA in the conventional solvents such DMSO or DMF showed to be insoluble and partially soluble, respectively. Thus it would be useful to consider other solvents that can be used for homogeneous HER applications.

Moreover, low HER responses of PANI and PABA have also been attributed to instability of the radical cations produced during HER experiment in acidic condition, two alternatives can potentially be explored in the future to improve the HER response. The first is consider alkaline solution as the alternative solvents for HER studies. The second strategy is to investigate the HER of PANI/MOF and PABA/MOF films on interdigitated electrodes in the future through electrochemical polymerisation as heterogeneous HER studies. This is because the results showed that the cross reaction between the PANI/MOF and PABA/MOF radicals and the electrolytic solution is an important contributing process which influences the HER performance as reflected in the scan rate dependent studies. In-depth studies of the effect of increased amount of MOF on PANI and PABA up until they have the same proportion on the catalytic activity of the material will also help in understand the role of MOF on the polymers matrix.

The MOF/PABA composites showed good HER performance however quantification of the amount of hydrogen produced will be important. This can be achieved by coupling CV experiments with gas chromatography or mass spectroscopy to form a hyphenated instrument that can reveal the amount of gases in the HER. Furthermore,

the effect of varying the amount of PABA up to 50% weight percentage while MOF remains fixed on the catalytic performance of the material will be of a good use to reveal the role of polymer on the MOF surface. The alternative method, it is to consider the post-synthetic route of polymer and MOF where MOF and polymer may be directly mixed to form a composite. The Photo-catalytic hydrogen evolution studies of these material is an alternative route to be employed in future study the HER. Furthermore, it will be noteworthy to consider coupling photo-and-electro-catalytic hydrogen evolution studies in future.



## Appendix 1(a)

### Hato, Mpitloane

---

**From:** satoru@kanagawa-iri.jp  
**Sent:** 13 March 2017 10:34 AM  
**To:** Mpitloane Hato; Hato, Mpitloane  
**Cc:** Satoru Kaneko; Paolo Mele; David Hui; 土屋哲男; 田中勝久; 遠藤民生  
**Subject:** message for Suzuki book authors about reproduction permissions  
**Attachments:** Permission Request Form.doc

Dear Prof. Hato,

Thanks a lot for your nice contribution to the book in honour of Prof. Suzuki.

This message is to inform you about one important duty required by Springer before publication of your chapter.

**\*permission for reproduction of figures\***

This is very important question: the figure in your chapter are original or reproduced from literature papers or books?  
If they are original, it is OK, but please confirm it to us.

If you used figures (original or partially modified) from literature papers or books, you are expected to request permissions to reproduce ALL copyrighted figures.

Please note that you have to do this work by yourself. The editors of Suzuki Springer book cannot act on your behalf.

So, you should kindly request two kind of permission for each figure:

A) request of permission to publishers (for example Nature, Springer, IoP, Elsevier etc.)

B) request of permission to one of authors of the paper where the figure was published (request to corresponding author is enough)

Request to authors can be done by e-mail sending the permission request form of Springer attached to this email.

Request to publisher can be usually done using web sites of the publishers and usually involves the use of Rightlinks.

Some publishers, like IoP, have not rightslink system and direct request to editorial office must be done.

Please start this work ASAP because submission of reproduction permissions is required together with chapter book file.

After obtaining the permissions, please send a copy to us because must be submitted to Springer together with your chapter.

If there is any doubt about copyright permissions, please contact us.

The permissions should be sent to

Paolo Mele pmele@mmm.muroran-it.ac.jp

Satoru Kaneko satoru@kanagawa-iri.jp

Best regards

☞Editors

Dr. Satoru Kaneko, Kanagawa Industrial Technology Center, Japan.

Prof. Paolo Mele, Muroran Institute of Technology, Hokkaido, Japan

Prof. David Hui, University of New Orleans, U.S.A.

Dr. Tetsuo Tsuchiya, AIST, Japan.

Prof. Katsuhisa Tanaka, Kyoto University, Japan.

Prof. Masahiro Yoshimura, National Cheng Kung University, Taiwan.

Prof. Tamio Endo, Gifu University, Japan.

## Appendix 1(b)

### Consent to Publish

Series Title:

Published under the imprint

**Springer**

---

**Title of Book/Volume/Conference:** Organic Synthesis of Carbon Related Materials: Polymers, Carbon Nanocomposites, Graphene

**Editor(s) name(s):** Satoru Kaneko, Paolo Mele, David Hui, Tetsuo Tsuchiya, Katsuhisa Tanaka, Masahiro Yoshimura, & Tamio Endo

**Title of Contribution:** Electrocatalytic Hydrogen Production Properties of Polyaniline doped with Metal Organic Frameworks

**Author(s) full name(s):** Kabelo E. Ramohlola\*, Milua Masikini†, Siyabonga B. Mdluli†, Gobeng R. Monama\*, Mpitloane J. Hato\*, Kerileng M. Molapo†, Emmanuel I. Iwuoha†, Kwena D. Modibane\*

**Corresponding Author's name, address, affiliation and e-mail:** Mpitloane Joseph Hato, Kwena Desmond Modibane

\*Department of Chemistry, School of Physical and Mineral Sciences, University of Limpopo (Turfloop), Polokwane, Sovenga 0727, South Africa

†SensorLab, Chemistry Department, University of the Western Cape, Cape Town, South Africa,

E-mail(s): Mpitloane.Hato@ul.ac.za; kwena.modibane@ul.ac.za

When Author is more than one person the expression "Author" as used in this agreement will apply collectively unless otherwise indicated.

#### § 1 Rights Granted

Author hereby grants and assigns to **Springer International Publishing AG** (hereinafter called Publisher) the exclusive, sole, permanent, world-wide, transferable, sub-licensable and unlimited right to reproduce, publish, distribute, transmit, make available or otherwise communicate to the public, translate, publicly perform, archive, store, lease or lend and sell the Contribution or parts thereof individually or together with other works in any language, in all revisions and versions (including soft cover, book club and collected editions, anthologies, advance printing, reprints or print to order, microfilm editions, audiograms and videograms), in all forms and media of expression including in electronic form (including offline and online use, push or pull technologies, use in databases and data networks (e.g. the Internet) for display, print and storing on any and all stationary or portable end-user devices, e.g. text readers, audio, video or interactive devices, and for use in multimedia or interactive versions as well as for the display or transmission of the Contribution or parts thereof in data networks or search engines, and posting the Contribution on social media accounts closely related to the Work), in whole, in part or in abridged form, in each case as now known or developed in the future, including the right to grant further time-limited or permanent rights. Publisher especially has the right to permit others to use individual illustrations, tables or text quotations and may use the Contribution for advertising purposes. For the purposes of use in electronic forms, Publisher may adjust the Contribution to the respective form of use and include links (e.g. frames or inline-links) or otherwise combine it with other works and/or remove links or combinations with other works provided in the Contribution. For the avoidance of doubt, all provisions of this contract apply regardless of whether the Contribution and/or the Work itself constitutes a database under applicable copyright laws or not.

The copyright in the Contribution shall be vested in the name of Publisher. Author has asserted his/her right(s) to be identified as the originator of this Contribution in all editions and versions of the Work and parts thereof, published in all forms and media. Publisher may take, either in its own name or in that of Author, any necessary steps to protect the rights granted under this Agreement against infringement by third parties. It will have a

## Appendix 2 (a)

Dear Mr. Ramohlola,

You have been listed as a Co-Author of the following submission:

Journal: Composites Part B

Title: Polyaniline-metal organic framework nanocomposite as an efficient electrocatalyst for hydrogen evolution reaction

Corresponding Author: Mpitloane Hato

Co-Authors: Kabelo Edmond Ramohlola, Gobeng Release Monama, Kwena Desmond Modibane, Milua Masikini, Kerileng Mildred Molapo, Siyabonga Beizel Mdluli, Emmanuel Iwuoha

Mpitloane Hato submitted this manuscript via Elsevier's online submission system, EVISE®. If you are not already registered in EVISE®, please take a moment to set up an author account by navigating to

[http://www.evise.com/evise/faces/pages/navigation/NavController.jsp?JRNL\\_ACR=JCOMB](http://www.evise.com/evise/faces/pages/navigation/NavController.jsp?JRNL_ACR=JCOMB)

If you already have an ORCID, we invite you to link it to this submission. If the submission is accepted, your ORCID will be transferred to ScienceDirect and CrossRef and published with the manuscript.

To link an existing ORCID to this submission, or sign up for an ORCID if you do not already have one, please click the following link: [Link ORCID](#)

What is ORCID?

ORCID is an open, non-profit, community-based effort to create and maintain a registry of unique researcher identifiers and a transparent method of linking research activities and outputs to these identifiers.

More information on ORCID can be found on the ORCID website, <http://www.ORCID.org>, or on our ORCID help page:

[http://help.elsevier.com/app/answers/detail/a\\_id/2210/p/7923](http://help.elsevier.com/app/answers/detail/a_id/2210/p/7923)

If you did not co-author this submission, please contact the Corresponding Author directly at [mpitloane.hato@ul.ac.za](mailto:mpitloane.hato@ul.ac.za).

Thank you,  
Composites Part B

This message was sent automatically. Please do not reply

## Appendix 2 (b)

From: Composites Part B [mailto:[EviseSupport@elsevier.com](mailto:EviseSupport@elsevier.com)]  
Sent: 28 May 2017 05:09 PM  
To: Hato, Mpitloane  
Subject: Received revision JCOMB\_2017\_851\_R1

*This message was sent automatically. Please do not reply.*

Ref: JCOMB\_2017\_851\_R1  
Title: Polyaniline-metal organic framework nanocomposite as an efficient electrocatalyst for hydrogen evolution reaction  
Journal: Composites Part B

Dear Dr. Hato,

Thank you for submitting your revised manuscript for consideration for publication in Composites Part B. Your revision was received in good order.

To track the status of your manuscript, please log into EVISE® [http://www.evise.com/evise/faces/pages/navigation/NavController.jsp?JRNL\\_ACR=JCOMB](http://www.evise.com/evise/faces/pages/navigation/NavController.jsp?JRNL_ACR=JCOMB) and locate the submission under the header 'My Submissions with Journal' on your 'My Author Tasks' view.

We appreciate your submitting your revision to this journal.

Kind regards,

Composites Part B

Have questions or need assistance?

For further assistance, please visit our [Customer Support](#) site. Here you can search for solutions on a range of topics, find answers to frequently asked questions, and learn more about EVISE® via interactive tutorials. You can also talk 24/5 to our customer support team by phone and 24/7 by live chat and email.

---

Copyright © 2017 Elsevier B.V. | [Privacy Policy](#)

Elsevier B.V., Radarweg 29, 1043 NX Amsterdam, The Netherlands, Reg. No. 33156677.

DISCLAIMER \*\*\* This message and any attachments are confidential and intended solely for the addressee. The following link will display the full disclaimer: <http://www.ul.ac.za/disclaimer.jpg> \*\*\*

## Appendix 3

*Int. J. Electrochem. Sci.*, 12 (2017) 4392 – 4405, doi: 10.20964/2017.05.58

---

**International Journal of  
ELECTROCHEMICAL  
SCIENCE**  
[www.electrochemsci.org](http://www.electrochemsci.org)

---

### **Electrocatalytic Hydrogen Production Properties of Poly(3-aminobenzoic acid) doped with Metal Organic Frameworks**

*Kabelo E. Ramohlola<sup>1</sup>, Milua Masikini<sup>2</sup>, Siyabonga B. Mdluli<sup>2</sup>, Gobeng R. Monama<sup>1</sup>, Mpitloane J. Hato<sup>1</sup>, Kerileng M. Molapo<sup>2</sup>, Emmanuel I. Iwuoha<sup>2</sup>, Kwena D. Modibane<sup>1,\*</sup>*

<sup>1</sup> Department of Chemistry, School of Physical and Mineral Science, University of Limpopo, Polokwane, Sovenga 0727 South Africa

<sup>2</sup> SensorLab, Chemistry Department, University of the Western Cape, Cape Town, South Africa

\*E-mail: [kwena.modibane@ul.ac.za](mailto:kwena.modibane@ul.ac.za)

*Received:* 30 November 2016 / *Accepted:* 14 February 2017 / *Published:* 12 April 2017

---

The design and development of inexpensive highly efficient electrocatalysts based on polymer organometallic composites for hydrogen production, underpins several emerging clean-energy technologies. In this work, for the first time, Poly(3-aminobenzoic acid) based metal organic framework (PABA/MOF) composite was synthesized by chemical oxidation of 3-aminobenzoic acid monomer in the presence of metal organic framework (MOF) content. Poly(3-amino benzoic acid) (PABA), MOF and PABA/MOF composite were characterized by ultraviolet visible (UV-vis) and fourier transform infrared (FTIR) spectroscopy, powder X-ray diffraction (XRD), thermal gravimetric analysis (TGA), scanning electron microscope (SEM), transmission electron microscope (TEM), energy dispersive X-ray spectroscopy (EDS, EDX), selected area electron diffraction (SAED) and cyclic voltammetry (CV). Detailed structural and morphological characterizations established that PABA is wrapping MOF. Furthermore, spectroscopic analyses provided information that MOF was incorporated on the backbone of PABA as indicative of an easier path for the electron transport and plentiful active sites for the catalysis of hydrogen evolution reaction (HER) in acidic electrolyte. Experiments probing the electrochemical properties revealed that the composite was very stable and robust and had exceptionally properties. Significant HER was generated by the composite in dimethyl sulfoxide/tetrabutylammonium perchlorate (DMSO/TBAP) supporting electrolyte in the presence of hydrogen source by applying a potential to the electrode.

---

**Keywords:** poly(3-aminobenzoic acid), metal organic frameworks, electrochemistry, hydrogen evolution reaction, Tafel plot.

---

## Appendix 4 (a)

Dear Mr. Kabelo Ramohlola,

You have been listed as a Co-Author of the following submission:

Journal: Electrochimica Acta

Corresponding Author: Kwena Modibane

Co-Authors: Kabelo E Ramohlola, BSc Honours; Milua Masikini, PhD; Siyabonga B Mdluli, BSc Honours; Gabong R Monama, BSc Honours; Mpitloane J Hato, PhD; Kerileng M Molapo, PhD; Emmanuel I Iwuoha, PhD;

Title: Electrocatalytic Hydrogen Evolution Reaction of Metal Organic Frameworks decorated with poly (3-aminobenzoic acid)

If you did not co-author this submission, please contact the Corresponding Author of this submission at [kwena.modibane@ul.ac.za](mailto:kwena.modibane@ul.ac.za); [dezzkwena@gmail.com](mailto:dezzkwena@gmail.com); do not follow the link below.

An Open Researcher and Contributor ID (ORCID) is a unique digital identifier to which you can link your published articles and other professional activities, providing a single record of all your research.

We would like to invite you to link your ORCID ID to this submission. If the submission is accepted, your ORCID ID will be linked to the final published article and transferred to CrossRef. Your ORCID account will also be updated.

To do this, visit our dedicated page in EES. There you can link to an existing ORCID ID or register for one and link the submission to it:

<http://ees.elsevier.com/electacta/l.asp?i=762360&l=R2NGDI4V>

More information on ORCID can be found on the ORCID website,

<http://www.ORCID.org>, or on our help page:

[http://help.elsevier.com/app/answers/detail/a\\_id/2210/p/7923](http://help.elsevier.com/app/answers/detail/a_id/2210/p/7923)

Like other Publishers, Elsevier supports ORCID - an open, non-profit, community based effort - and has adapted its submission system to enable authors and co-authors to connect their submissions to their unique ORCID IDs.

Thank you,

Electrochimica Acta

## Appendix 4 (b)

From: eesserver@eesmail.elsevier.com [mailto:eesserver@eesmail.elsevier.com]

Sent: 10 February 2017 04:39 PM

To: Modibane, Kwena; dezzkwena@gmail.com

Subject: Submission Confirmation for EO16-3434R1

Ms. Ref. No.: EO16-3434R1

Title: Electrocatalytic Hydrogen Evolution Reaction of Metal Organic Frameworks decorated with poly (3-aminobenzoic acid) *Electrochimica Acta*

Dear Desmond,

Your revised manuscript was received for reconsideration for publication in *Electrochimica Acta*.

You may check the status of your manuscript by logging onto the Elsevier Editorial System as an Author at <https://ees.elsevier.com/electacta/>.

Your username is: kwena.modibane@ul.ac.za If you need to retrieve password details, please go to: [http://ees.elsevier.com/electacta/automail\\_query.asp](http://ees.elsevier.com/electacta/automail_query.asp)

Kind regards,

Elsevier Editorial System

*Electrochimica Acta*